

**EFFECTS OF VARIATION OF URANIUM ENRICHMENT  
ON NUCLEAR SUBMARINE REACTOR DESIGN**

by

**Thomas Dominic Ippolito Jr.**

**B.S.N.E., University of Lowell, Lowell, Massachusetts  
(1987)**

**SUBMITTED IN PARTIAL FULFILLMENT  
OF THE REQUIREMENTS FOR THE  
DEGREE OF MASTER OF  
SCIENCE**

at the  
**MASSACHUSETTS INSTITUTE OF TECHNOLOGY  
May, 1990**

© Massachusetts Institute of Technology 1990

Signature of Author

*Thomas D. Ippolito Jr.*  
Department of Nuclear Engineering, May, 1990

Certified by

*David D. Lanning*  
Professor David D. Lanning, Thesis Cosupervisor

Certified by

*Marvin M. Miller*  
Dr. Marvin M. Miller, Thesis Cosupervisor

Accepted by

*A. F. Henry*  
Professor Allan F. Henry,  
Chairman, Committee on Graduate Students

MASSACHUSETTS INSTITUTE  
OF TECHNOLOGY

NOV 13 1990

LIBRARIES ARCHIVES

# Effects of Variation of Uranium Enrichment on Nuclear Submarine Reactor Design

by

Thomas D. Ippolito Jr.

Submitted to the Department of Nuclear Engineering on May 18, 1990, in partial fulfillment of the requirements for the degree of Master of Science.

## Abstract

Certain design tradeoffs exist between the use of highly-enriched uranium (HEU) versus the use of low enriched uranium (LEU) as a nuclear submarine reactor fuel with regard to such factors as core life and size, total power, and reactor safety. To evaluate these tradeoffs, three 50MWt reactor designs using uranium fuel enriched to 7%, 20% and 97.3% respectively are compared. The 7% and 20% designs are assumed to be fueled with uranium dioxide ( $UO_2$ ) fuel in a "caramel configuration", while the 97.3% design is assumed to be of the dispersion type. (The designs are modeled using the EPRI-Cell computer code on the IBM 3033 at the Argonne National Laboratory. Access to this facility from a DEC VT-100 terminal at M.I.T. was through the TYMNET Public Network System). It was concluded that the 20% enriched core could be designed to have the same lifetime (1200 full power days) as the 97.3% enriched core. The 7% enriched core could not maintain criticality for this period. However, a core life of 600 full power days could be attained. The 7% and 20% cores are both larger than the 97.3% core. However, the use of an integral design rather than a loop-type design could compensate for the larger core size.

Thesis Cosupervisor: David D. Lanning  
Title: Professor of Nuclear Engineering

Thesis Cosupervisor: Marvin M. Miller  
Title: Senior Research Scientist

## Table of Contents

	<u>Page</u>
Abstract	2
List of Figures	6
List of Tables	8
Acknowledgements	9
Disclaimer	10
Chapter 1. Introduction	11
1.1 Conventional Vs. Nuclear Propulsion	12
1.2 Submarine Pressurized Water Reactor Nuclear Power Plant	15
1.3 Design Criteria and Objectives	17
1.4 Selection of Reactor Design Limits	23
Chapter 2. Fuel Type Considerations	29
2.1 Nuclear Fuel Considerations	30
2.1.1 Fuel Selection Criteria	31
2.1.2 Review of Fuels Considered	33
2.1.2.1 Metallic Uranium Fuel	34
2.1.2.2 Metallic Uranium Rich Alloy Fuels	37
2.1.2.3 Uranium Aluminide - Aluminum Dispersion Fuel	41
2.1.2.4 Uranium Silicide - Aluminum Dispersion Fuel	42
2.1.2.5 Uranium Oxide - Aluminum Dispersion Fuel	43
2.1.2.6 Uranium Carbide and Uranium Nitride Fuels	45
2.1.2.7 Uranium Dioxide Fuel	46
2.2 Cladding Material Considerations	47
2.2.1 Cladding Material Selection Criteria	49
2.2.2 Selection of Cladding Material	51
2.3 Burnable Poison Material	55
2.4 Reactor Coolant	59
2.5 Summary of Selected Materials	59
Chapter 3. Fuel Element Design	61
3.1 Fuel Plate Design	62
3.3.1 LEU Fuel Plate: $\text{UO}_2$ - Caramel Fuel	63
3.3.2 HEU Fuel Plate: $\text{UO}_2$ - Zircaloy Cermet	65

3.2 Fuel Element Design	71
Chapter 4. Analytic Methods	79
4.1 Reactor Physics Analysis	82
4.1.1 The EPRI-Cell Code	92
4.1.2 Reactor Core Model	97
4.1.2.1 Fuel Cell Model	99
4.1.2.2 Treatment of Extra Regions	103
4.1.2.3 Treatment of Burnable Poison Lump	106
4.1.2.4 Fuel Meat Material Volume Fractions	107
4.1.2.5 Number Densities	111
4.1.2.6 Simplified Overall Core Model	116
4.1.3 Reactor Core Design Procedure	122
4.1.4 Whole Core Materials Calculations	126
4.1.5 Safety Analysis	128
4.2 Thermal-Hydraulic Analysis	130
Chapter 5. Results of the Analysis	138
5.1 Excess Reactivity Curves	138
5.2 Potential for Excess Reactivity Curve Shape Adjustment	147
5.3 Mechanical Burnup Results	148
5.4 Reactor Safety Coefficients	151
5.5 Reactor Core Volume and Power Density Results	151
5.6 Thermal Hydraulic Results	155
5.7 Whole Core Materials	157
5.8 Correction for Coolant Water Number Density Error	164
Chapter 6. Conclusion and Recommendation	177
6.1 Conclusion	177
6.2 Recommendations	179
References	181

<b>Appendix A. Non-Proliferation Treaty and Foreign Nuclear Objectives</b>	<b>187</b>
<b>Appendix B. Nuclear Materials Criticality</b>	<b>191</b>
<b>Appendix C. Reactivity Considerations</b>	<b>194</b>
<b>Appendix D. Fuel Burnup Considerations</b>	<b>196</b>
<b>Appendix E. EPRI-Cell Input/Output Description</b>	<b>198</b>
<b>E.1 Input Description</b>	<b>198</b>
<b>E.2 Variables Used in the Calculations of this Study</b>	<b>205</b>
<b>E.3 EPRI-Cell Output Description and Interpretation</b>	<b>213</b>
<b>E.4 Sample EPRI-Cell Output File</b>	<b>214</b>
<b>Appendix F. Detailed Summary of Calculated Results</b>	<b>251</b>
<b>Appendix G. Improved Reflector Savings Calculation Method</b>	<b>256</b>

## List of Figures

<u>Figure</u>		<u>Page</u>
1.1	Typical PWR plant.	18
1.2	Typical nuclear submarine propulsion system.	19
1.3	Technicatome's integrated PWR which powers France's SSNs.	20
2.1	Correlation between fission gas release and fuel center temperature for UO <sub>2</sub> fuels.	48
3.1	Caramel fuel plate.	64
3.2	Cermet fuel plate.	66
3.3	Partial estimate of burnup Vs. UO <sub>2</sub> volume fraction.	68
3.4	Schematic cross-sections of cermet dispersion systems.	70
3.5	Thick plate fuel element design.	73
3.6	Assemblage of reactor fuel elements.	73
3.7	Fuel element design window.	75
4.1	Interdependence of reactor design parameters.	85
4.2	Design space.	86
4.3a	Design variations for reactor core (1).	90
4.3b	Design variations for reactor cores (2,3,4,5).	91
4.4	EPRI-Cell data flow.	95
4.5	EPRI-Cell 3-D slab.	96
4.6	Fuel cell for reactor core (1).	100
4.7	Fuel cell for reactor cores (2,3,4,5).	101
4.8	Fuel element extra water.	105
4.9	Thermal flux distribution for reflected reactor.	118
4.10	Design procedure for reactor core (1).	123
4.11	Design procedure for reactor cores (2,3,4,5).	124
4.12	Fuel plate temperature profiles.	132
5.1	Reactor core (1), k-eff Vs. time.	141
5.2	Reactor core (2), k-eff Vs. time.	142
5.3	Reactor core (3), k-eff Vs. time.	143
5.4	Reactor core (4), k-eff Vs. time.	144
5.5	Reactor core (5), k-eff Vs. time.	145
5.6	Effects of gadolinia distribution on k-eff Vs. time.	146
5.7	Reactor core fuel element grids.	154

5.8	Reactor core (1), plutonium Vs. time.	159
5.9	Reactor core (2), plutonium Vs. time.	160
5.10	Reactor core (3), plutonium Vs. time.	161
5.11	Reactor core (4), plutonium Vs. time.	162
5.12	Reactor core (5), plutonium Vs. time.	163
B.1	Reflected critical masses of uranium and plutonium Vs. isotopic mix.	193

## **List of Tables**

<b><u>Table</u></b>		<b><u>Page</u></b>
1.1	Submarine Power Requirements at 2670 tons displacement.	14
1.2	Design choices and limits for comparative core neutron analysis studies.	28
2.1	Uranium bearing compounds.	35
2.2	Uranium rich alloys.	36
2.3	Possible cladding materials.	52
2.4	Zircaloy alloy series.	54
2.5	Reactivity control materials.	57
2.6	Isotopes of gadolinium.	58
2.7	Some properties of gadolinium.	58
2.8	Important physics properties of H <sub>2</sub> O.	60
3.1	Feasible dimensions of various parts of the caramel fuel plate.	65
3.2	Fuel element characteristics.	78
4.1	Reactor designs.	80
4.2	Reactor design data.	81
4.3	Energy break points.	94
4.4	EPRI-Cell input variables for reactor design.	98
5.1	Core burnup data.	150
5.2	Safety coefficients of reactivity.	150
5.3	Core dimensions and power densities.	152
5.4	Thermal-hydraulic data.	156
5.5	Core materials data.	158
5.6	Approximate correction factors.	176

## **Acknowledgments**

The author wishes to express his thanks to Dr. Marvin M. Miller who, through the sponsorship of the MIT Center for International Studies, provided him with the opportunity to participate in this study and who also provided valuable guidance throughout its duration.

He also thanks Professor David D. Lanning for his expert advice, guidance and instruction with the many aspects and technical details of nuclear reactor design and analysis encountered in this study.

A word of appreciation goes to Professor Ronald G. Ballinger with whom the author consulted regarding the prolonged irradiation performance of the various nuclear fuels considered.

Special thanks to Dr. Rachel Morton for her invaluable assistance with setting up the computer link from MIT to Argonne National Laboratory.

The author expresses his sincere appreciation to Dr. William Woodruff of the Engineering Staff of Argonne National Laboratory for his guidance with the use of the EPRI-Cell code and his many suggestions for the application of EPRI-Cell to the reactor physics problems encountered. Dr. Woodruff also provided much assistance with the IBM Job Control Language needed to run EPRI-Cell. Also, thanks go to Fran Carneghi of Argonne's Computing Services Division for her administration of the computer account set up to conduct this study.

The author must also thank those who provided him with much encouragement and emotional support through this thesis and his three years at MIT; his father, mother and grandmothers, and of course his brother and sisters.

Finally, the author must give thanks to,

- the one who allowed him to come to MIT;
- the one who provided him with endless motivation;
- the one who was with him through the many sleepless nights spent running EPRI-Cell, making figures and writing this thesis;
- the one who made this thesis happen;
  
- the Eternal God of Heaven.

## **Disclaimer**

**This study does not involve in any way, the use of classified material; rather, it is derived from material that is published in the open literature.**

## **CHAPTER 1**

### **Introduction**

**This study was motivated by the planned acquisition of nuclear powered attack submarines (SSNs)<sup>†</sup> by three non-nuclear weapons states (NNWS) India, Brazil and Canada. There is concern that possession of SSNs by NNWS states might facilitate the proliferation of nuclear weapons by providing either; (1) the opportunity for diversion of the fissile material used as fuel, or (2) a rationale for the development of indigenous uranium enrichment capability.**

**U.S. and British nuclear submarine reactors are fueled with very highly enriched uranium; typically 97.3% in the U.S. case.[1] France, however, has deployed SSNs fueled with low enriched uranium (LEU); typically less than 10%.[2] (By convention, weapons-grade uranium (WGU), highly enriched uranium (HEU) and low enriched uranium (LEU) are defined to be uranium which has a U<sup>235</sup> content of greater than 90%, greater than 20 % and less than 20% respectively.) Since the critical mass increases rapidly below 20%, LEU is considered to be less of a proliferation concern than HEU, although more plutonium is produced in an LEU fueled reactor. For this reason, it is generally easier to purchase LEU on the international market, reducing the argument for the need to develop indigenous enrichment capability. Relevant here is the fact that more than half of the separative work of the enrichment process required to produce HEU has been done in producing LEU.[3]**

**† As distinguished from SSBNs which are both nuclear powered and are also armed with nuclear-tipped ballistic missiles.**

The purpose of this study is to assess the tradeoffs involved in the use of HEU Vs. LEU as an SSN reactor fuel, with regard to such factors as core life, core size, and reactor safety. This has been accomplished by modeling one HEU and an two LEU reactor cores for comparison.

### 1.1 Conventional Vs. Nuclear Propulsion

Drag power requirements for a submarine are related to its velocity by the following correlated equation.[4]

$$P = 0.06977 C_d V^{2/3} v^3 \quad (1.1)$$

where,

$P$  = propulsive power (MW)

$C_d$  = drag coefficient

$V$  = volume displacement ( $m^3$ )

$v$  = forward speed (knots)

For a submarine such as the French-designed Rubis of 2385tons (2385m<sup>3</sup>) displacement while surfaced and 2670tons (2670m<sup>3</sup>) submerged displacement, the estimated shaft power for varying forward velocities as calculated by Equation 1, are presented in Table 1.[5] These figures represent a combined propeller/transmission system efficiency of about 75%. These powers are calculated for a minimum drag coefficient of ( $C_d \approx 0.025$ ). However, for a submarine with a drag coefficient of 0.035, which is not unusual depending on the general condition of the hull, the drag power

requirement can increase by as much as 40%.[4]. One should note the propulsive power increases with the cube of the forward velocity.

The Rubis can be considered to be an intermediate size submarine whose volume displacement and total power requirements will serve as a design basis. Submarine submerged volume displacements range from the 1070tons (1070m<sup>3</sup>) West German Vastergotland class diesel powered submarine or SSK, to the 8400tons (8400m<sup>3</sup>) of the British SSN, HMS Resolution.[6]

Naval submarines must be able to take evasive action requiring high speeds of 25-30 knots or greater. Since an SSK runs submerged on electricity produced by diesel generators and stored in batteries, this can only be achieved for a short period of time; typically 1 hour maximum. This is due to the tremendous propulsive power requirements which rapidly deplete the batteries.[5] SSKs can maintain an average speed of about 13 knots submerged.[6] The higher the average speed, the higher the "indiscretion rate" or the percentage of time that the submarine must surface to snorkel. In doing so, an SSK is highly vulnerable to radar detection, visual detection and attack by surface ships, aircraft and other submarines.

By contrast, most SSNs can maintain an average speed of 25-35 knots without approaching the surface. SSNs have an underwater endurance which is limited only by the endurance of the crew. The SSN can thus make high-speed, long distance undetected transits from one part of the world to another. Only SSNs are capable of traveling under the Polar Ice Cap, through the Northwest Passage and into the Arctic Ocean.

**Table 1.1 Submarine power requirements at 2670 tons displacement  
[adapted from Reference E]**

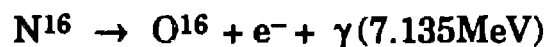
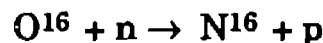
<b>Forward Speed (knots)</b>	<b>Propulsive Power(MW)</b>	<b>Hotel Power(MW)</b>	<b>Total Power(MW)</b>
0	0	0.150	0.150
2	0.004	0.150	0.154
4	0.029	0.150	0.179
6	0.096	0.150	0.246
8	0.229	0.150	0.379
10	0.448	0.150	0.598
12	0.773	0.150	0.923
.	.	.	.
.	.	.	.
20	3.581	0.150	3.731
25	6.994	0.150	7.144
30	12.085	0.150	12.235
33.2	16.350	0.150	16.500
35	19.191	0.150	19.341

By consequence, an SSN is a vehicle of maneuver since it's capabilities and relative invulnerability provide much greater operating flexibility, enabling it to redeploy quickly and often, in the wake of changing tactical requirements. Clearly SSNs are more desirable as a military platform than SSKs. However, they cost much more than SSKs. especially if one takes into account the need for more sophisticated training and support.

## 1.2 Submarine Pressurized Water Reactor Nuclear Power Plant

Nuclear submarine propulsion systems generally consist of a small (relative to commercial power reactors) pressurized light water (PWR) reactor. A typical pressurized water reactor plant is shown in Figure 1.1. Light water of the primary loop at approximately 15MPa is circulated through the core and exits as nearly saturated water. Reactor inlet and outlet temperatures are roughly 290°C and 320°C respectively.[7] The nearly saturated outlet water enters a heat exchanger or steam generator where heat is transferred to a cooler secondary loop with inlet and saturated outlet temperatures of roughly 225°C and 285°C respectively.[7] Secondary loop pressure is 7MPa which produces a steam quality of about 15%. The steam is then used to drive a turbine which may be mechanically connected to either a gearbox in which the shaft rotation speed is reduced and used to drive the boat propeller directly, or to an electric generator for propulsion through an electric motor, Figure 1.2.

As water flows through the core and is exposed to a neutron flux, the following reaction takes place,



Submarine personnel in contact with any portion of the primary loop during reactor operation could receive a significant gamma radiation dose. Thus the submarine nuclear power plant consists of two basic sections.

- 1) A shielded radioactive compartment containing the reactor, a pressurizer, a steam generator and a primary coolant pump.
- 2) A nonradioactive machinery compartment containing the steam turbines, drive train and condensers.

The steam generator serves as a barrier preventing radioactivity from leaving the shielded compartment. It should also be noted that since  $N^{16}$  has a half life of 7.13s, personnel can enter the shielded compartment roughly one minute after reactor shutdown.

During the lifetime of the reactor the fission products are prevented from escaping to the environment by a total of five separate barriers. First, the metallurgy of the fuel is optimized to retain the fission products within the matrix of the fuel itself. Secondly, the individual fuel elements are hermetically sealed in metal tubes or sandwiched between metal plates known as cladding. Thirdly, the fuel in its entirety is encased in a high-integrity reactor pressure vessel. Fourthly, the nuclear propulsion system is contained in an airlock compartment within the submarine. Finally, the pressure hull of the submarine itself serves as the fifth boundary to the outside environment.

Due to volume and weight constraints in submarine design, the former which is more constraining, it is desirable to keep the power plant as small and compact as possible. Since shielding accounts for a large percentage of total plant weight, it is especially desirable to keep the reactor core and steam generator as small and compact as possible. This can be better accomplished if the components in the shielded compartment are constructed using an integral design such as that developed by the French

firm, Technicatome, and employed in all of France's SSNs, Figure 1.3. In this design, the reactor, steam generator, and primary coolant pump are integrated into one steam producing unit eliminating component separation and the large diameter interconnecting primary loop piping.

### **1.3 Design Criteria and Objectives**

The following criteria have been employed in the nuclear reactor designs of this study.

- 1) The over-all core design study can be simplified with a one-dimensional neutronics calculation of the fuel assembly for the comparative purposes of this project. The EPRI-Cell Code (see Appendix E.), which computes the space, energy, and burnup dependence of the neutron spectrum within light water reactor fuel cells and which has been modified by Argonne National Laboratory for use on plate-type research reactor fuels, is used for this purpose.[9]
  
- 2) For this study the thermal-hydraulic parameters of fuel temperatures and required flow rates are assumed not to be limiting within the simplifications which are discussed in Section 1.4 and the fuel element design presented in Chapter 3. This judgement is based on review of operating experiences with the chosen mechanical arrangement of the fuel design (i.e. the Engineering Test Reactor, ETR, of the National Reactor Testing Station operated by Idaho National Engineering Laboratory)

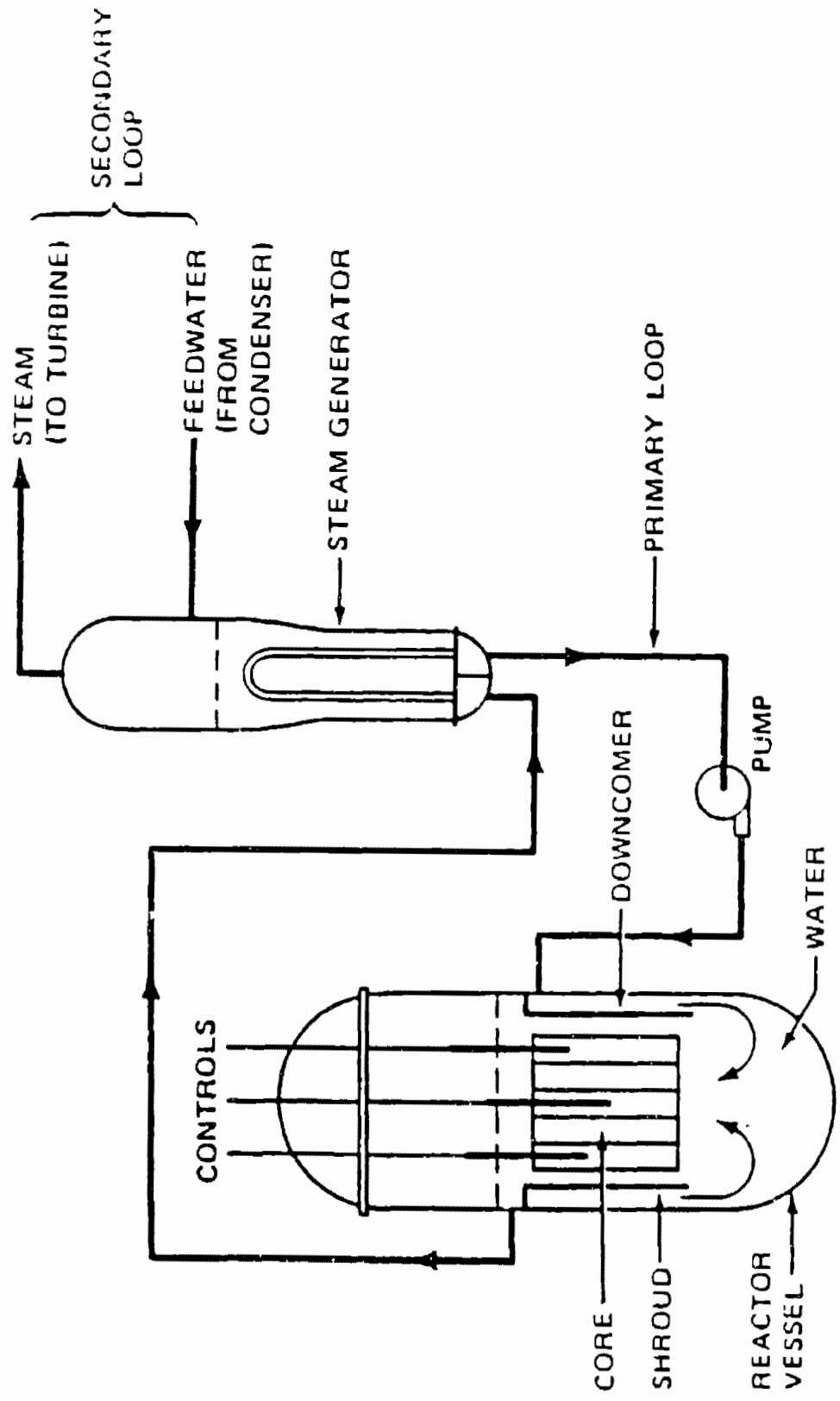


**Figure 1.1.** Typical PWR plant.



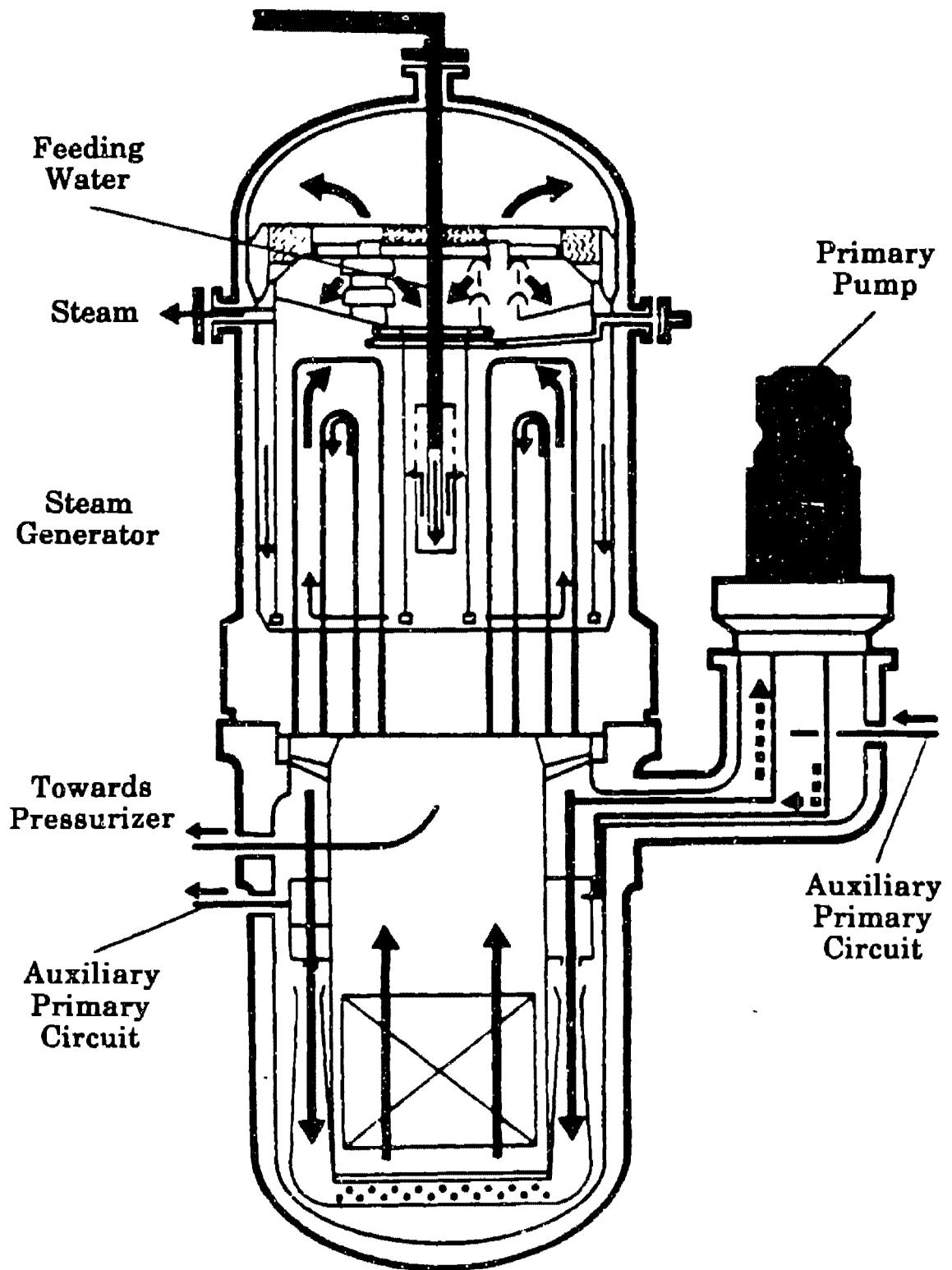


**Figure 1.3.** Technicatome's integrated PWR which powers France's SSNs.[8]

- 3) It was assumed that no shuffling of the fuel elements would take place in order to extend fuel burnup. At the end of core life, fuel elements near the center of the core are depleted more than those in the outer region of the core. In a fuel shuffling operation, some of the fuel elements near the outer regions of the core are switched with fuel elements near the core center. Consequently the total available reactivity of the core is increased. Reactivity is defined in Appendix C. Fuel burnup is discussed in Appendix D.
- 4) To conserve space, the reactor cores and components of Figure 1.1 were assumed to be constructed using the integral design of Figure 1.3 thus permitting the use of a larger reactor core. This applies to both the LEU and HEU reactors designs.

The objectives of the present calculations are to provide:

- 1) Comparisons of reactor core sizes for uranium enrichments of 7%, 20% and 97.3% with varying amounts and distributions of burnable poison, gadolinium oxide ( $Gd_2O_3$ ). A burnable poison is a neutron absorbing material placed in certain locations of a fuel element in order to reduce the excessive neutron multiplication at the beginning-of-life, (BOC), of the reactor core. As the fuel fissions, the gadolinium (Gd) also burns out, thus providing a longer core refueling interval.

- 2) Estimates of the safety parameters such as the Doppler, void and temperature coefficients of reactivity as a function of enrichment and quantity of burnable poison,  $Gd_2O_3$ , present in the reactor.
- 3) Fuel burnup information and plutonium buildup in the LEU cores at comparable powers and operating cycles.

These results can be used as a basis for deciding if selected cases should be calculated in more detail, including distributed burnable poison and/or enrichment for power flattening and better burnup; control movement reactivity and power peaking effects, and thermal-hydraulic considerations. Power flattening involves the reduction of the peaking factor which is described in Section 1.4.

Upon reaching the above outlined objectives, conclusions can be drawn about the effects, if any, of using LEU as a fuel instead of HEU, on submarine design and operation. For example, if the LEU cores were found to be significantly larger than the HEU core for a given reactor power, a larger hull may be needed for the LEU fueled submarine compared to the HEU fueled submarine. Based on the discussion of Section 1.2, this will reduce the submarines maximum forward velocity. Also, if the unshuffled LEU core lifetimes are shorter than that of the unshuffled HEU core (the HEU core lifetime may, in some cases, be as long as the submarine lifetime), the submarine must return to port for fuel shuffling or refueling. These are major operations that for many submarine designs require cutting open the hull, thus increasing the time the submarine will be out of service. Submarine designers have generally avoided the use of

hatches due to sealing problems at large depths.[10] However, the French Rubis does use large hatches to refuel.

#### **1.4 Selection of Reactor Design Limits**

In order for an SSN with a submerged volume displacement similar to that of the Rubis to attain forward velocities of 25-35 knots, a reactor power output of approximately 50 MWth is required. This is based on a typical PWR plant thermodynamic efficiency of 33%, which yields a shaft power of 16.35MWe. As shown in Table 1.1, this corresponds to a forward velocity of 33.2 knots. For the unfavorable hull conditions described earlier, Equation 1 yields a maximum forward velocity of 29.6 knots, considering the propeller /transmission efficiency. As a result of these considerations, this study focuses on SSN reactors of 50MWth power output.

For this study uranium dioxide,  $UO_2$ , was selected as the fuel and Zircaloy was selected as the cladding material for reasons that will be discussed in depth in Chapter 2. Use of HEU permits a smaller concentration or volume fraction of fuel in the fuel elements of a given dimension than does use of LEU. In the HEU case the volume unoccupied by fuel is occupied by zircaloy. Since  $UO_2$  is a ceramic of poor thermal conductivity and zircaloy has a relatively high thermal conductivity, the HEU fuel elements can be operated with a higher average volumetric heat generation rate or average power density ( $q'''_{ave}$ ). This is because the effective thermal conductivity of the mixture of  $UO_2$  and zircaloy present in the HEU fuel elements is higher than that of the  $UO_2$  present in the LEU fuel elements. Based on a review of the operating experiences of existing HEU and LEU reactors, the maximum power density for the HEU reactor to

be analyzed here was set at 1000kW/l and for the LEU reactors was set at about 100kW/l. The 93% enriched, UO<sub>2</sub> fueled Advanced Test Reactor at the National Reactor Testing Station operated by Idaho National Engineering Laboratory has a maximum operating power density of about 2600kW/l.[11] Commercial PWRs fueled with LEU of about 3% average enrichment, operate with a maximum power density of about 250kW/l. To be conservative, the maximum power densities to be applied to these calculations were reduced. For each reactor design to be considered for this study, a minimum average power density limit ( $q'''_{ave}$ ) was set at 50kW/l in order to ensure the ability of the reactor to produce steam. The average power density in a commercial BWR is about 56kW/l.

Another important design parameter that was estimated for purposes of this study is the ratio of the maximum heat generation rate to the average heat generation rate or more simply, the power peaking factor ( $\Omega$ ).

$$\Omega = \frac{q'''_{max}}{q'''_{ave}} \quad (1.2)$$

For a typical unreflected cylindrical reactor (bare reactor)  $\Omega$  is approximately 3.6. However for a reflected cylindrical reactor,  $\Omega$  is reduced to about 2.5.[7] The reactor designs considered here are assumed reflected by a layer of light water. It is possible to further reduce the peaking factor by a non-uniform distribution of burnable poison, however this has not been investigated in this study.

In this study, LEU reactor cores with uranium enrichments of 7% and 20%, and an HEU core of 97.3% uranium enrichment were modeled. An enrichment value of 97.3% was selected since U.S. and British SSNs are

fueled with uranium of this enrichment. U.S. SSN reactor cores are reported to have refueling intervals greater than 12 years, while future designs are aimed at refueling intervals approaching 20 years, or the service lifetime of the submarine.[2] Thus for the HEU core to be analyzed in this study, the design operating lifetime without fuel shuffling or refueling, was set at 20 years. These refueling intervals are based on a submarine service time of 240 days per year at sea while operating at an average of 25% of full power, or 60 full power days per year (60 FPD/Y). As deduced from Equation 1, this represents about 63% of the maximum velocity.

$$(\text{Percent of maximum velocity}) = (0.25)^{1/3} = 0.63 \quad (1.3)$$

It is known that the French designed Rubis is fueled with uranium of three different enrichments whose average is less than 10%.[10] The value of 7% was selected since the French have reported detailed designs of "Caramel" fuel for research reactors with 7% enrichment.[12] This fuel element design is discussed in detail in Chapter 3. It was not possible to attain a refueling interval of 20 years for a 50MW reactor core fueled with uranium of 10% enrichment or less without increasing the size of the core and prohibitively lowering the average volumetric heat generation rate ( $q'''_{ave}$ ). Too low a value of  $q'''$  will result in an insufficient coolant temperature rise in the core. Thus a refueling interval of 10 years was selected as a design parameter for the 7% enriched LEU core. With fuel shuffling, however, the operating lifetime of this core can be increased.

Newer U.S. SSN reactor core designs are being developed with refueling intervals approaching 20 years and other nations seeking SSNs may desire a similar capability. Our aim was to determine the possible effects or

differences in submarine design and operation between submarines fueled with HEU and those fueled with LEU. Thus an LEU core also with a refueling interval of 20 years needed to be modeled. As a result, feasibility calculations were done for a reactor core of 20 year operating life and fueled with uranium enriched to 20%.

Throughout a reactor core lifetime (beginning-of-life(BOL) - end-of-life (EOL)) the total available reactivity swings from some maximum design value to some minimum design value at which the reactor can no longer operate. The maximum design value is determined by the total possible negative reactivity that can be inserted by control rods. The minimum design value is set at some point above zero reactivity in order to compensate for the buildup to some maximum value, of the neutron absorbing isotope  $Xe^{137}$  upon shutdown of the reactor. This isotope results from the decay of certain fission products. The maximum and minimum design reactivity values that have been conservatively estimated based on consideration of existing reactors, corresponds to values of  $k_{eff} = 1.24$  and  $k_{eff} = 1.04$  respectively. The terms reactivity and  $k_{eff}$  are defined in Appendix C.

During the operating lifetime of a reactor core, the maximum permissible materials-limited fuel burnup may be reached before the minimum design reactivity value. At this point, structural integrity of the fuel element may not be assured if the fission process were allowed to continue. This results from fission gas pressure buildup (i.e., some fission products are gases) and irradiation damage to the fuel matrix. For the fuel element design used in the LEU cases, the materials-limited fuel burnup limit is estimated to be 60,000MWd/T.[13] The burnup limit for the fuel element design used in the HEU case will be further discussed in Chapter 5.

neutronics data provided by the EPRI-Cell code, it will be possible to calculate with accuracy sufficient for this study, the information outlined in Section 1.3.

The design choices and assumed limits are summarized in Table 1.2.

**Table 1.2** Design choices and limits for comparative core neutron analysis studies.

1) Total reactor power MWth	50	50
2) Power density limit kW/liter ( $q'''_{ave}$ )	100	1000
3) Minimum power density kW/liter ( $q'''_{ave}$ )	50	50
4) Mechanical limit on burnup MWd/T	≈ 60,000 (See Figure 3.3)	
5) Desired years of operation without refueling at 60 full power days/year (60 F.P.D./yr)	≈ 10 years	≈ 20 years
6) Control rod reactivity worth	$k_{eff}(\max) \approx 1.24$ $k_{eff}(\min) \approx 1.04$ (For Xe override)	
7) Peaking Factor	≈ 2.5	≈ 2.5
8) Height to radius ratio of USS Savannah reactor	= 2.5 [14]	

## **CHAPTER 2**

### **Materials Considerations**

Nuclear reactor fuel elements consist of a system of interacting materials that includes the fuel material, clad material and in most cases a reactivity control material (i.e., burnable poison). For the optimum performance required of an SSN reactor as described in Chapter 1, small size, high power density and maximum refueling lifetime, this system of materials must allow good neutron economy, maximum fuel burnup, and corrosion resistance. This system must attain these goals while subject to the environment encountered in the PWR core described in Section 1.2 which includes high neutron fluxes (at high energies) as well as high operating temperatures, system pressures, thermal gradients and heat fluxes. Also of great importance is the chemical compatibility of the fuel element materials with respect to each other and to the reactor coolant (i.e., H<sub>2</sub>O). This system of materials must also be capable of withstanding transient and off-normal conditions without failure and must retain coolable geometry during accident conditions such as a LOCA (loss-of-cooling-accident) or LOFA (loss-of-flow-accident).

A fuel element composed of a given set of materials may meet a given set of performance objectives for a given set of reactor operating conditions. However, the fuel element may be entirely inadequate when exposed to a different reactor environment. For example, a particular fuel element may perform satisfactorily in a low temperature research reactor used for the production of neutrons but may melt or rapidly corrode when exposed to the relatively high operating temperatures of a central station power generating reactor or an SSN propulsion reactor. This fuel element may be

even less attractive for use or in a reactor cooled with a fluid other than H<sub>2</sub>O. The final materials selection process is more or less a compromise between the various in-reactor operating properties and characteristics of the fuel element materials that results in a combination that most closely meets the performance objectives.

The same performance objectives and reactor operating environment mentioned above must be considered for the determination of the size and shape of the fuel elements and the thickness of the cladding. This will be discussed in detail in Chapter 3.

## **2.1 Nuclear Fuel Considerations**

The central and most important constituent of a nuclear reactor is the fuel material in which energy is produced from the nuclear fission process. In most cases, the operating lifetime of the fuel element is limited by the fuel material. For a reactor fueled with HEU, the operating lifetime of the fuel element is often limited by the mechanical behavior of the fuel when irradiated in the reactor environment. For the reactor fueled with LEU, the lifetime is often limited by the available reactivity supplied by the fuel elements. The reactivity limitation of LEU fuel results from two effects; the concentration of fissile material may be low compared to the HEU case, and use of LEU results in the addition of neutron absorbing U<sup>238</sup> (i.e., negative reactivity).

### **2.1.1 Fuel Selection Criteria**

**The fuel material must be carefully chosen in order for the fuel element to meet the SSN reactor fuel element design objectives of maximum burnup, maximum operating lifetime, corrosion resistance and ability to withstand credible accident conditions. In the following section, the required fuel material characteristics that permit the fuel element to meet these objectives have been summarized.**

- 1) In order to produce the reactor coolant outlet temperature of 320°C necessary for the production of steam, high fuel temperatures are required. Thus the melting point of the fuel must be sufficiently above the maximum normal operating temperature of the fuel element to provide a safety margin in the event of an accident that raises the fuel element temperature. The combination of fuel conductivity and melting point must be compatible to allow for this temperature margin. The maximum fuel temperature calculation method and associated assumptions are discussed in Section 4.2.**
  
- 2) The fuel material should have only one crystal structure within the operating temperature range of the reactor (i.e., room temperature to maximum operating temperature). Changes in crystal structure are usually accompanied by a volume change that can damage the fuel element.**

- 3) To preserve fuel element integrity during the attainable lifetime of the fuel element (based on fuel mechanical behavior fuel material or available reactivity in the fuel elements), the fuel material should be chemically and metallurgically inert with respect to the reactor coolant and fuel element cladding.**
  
- 4) In order to conserve reactivity, the nonfissionable constituent of the fuel material should have a relatively low macroscopic neutron absorption cross-section ( $\Sigma_a$ ).**
  
- 5) The fuel must exhibit good irradiation behavior. When uranium or plutonium atoms fission, they produce a wide range of fission products. Among them, are the noble gases xenon and krypton which are produced in approximately 30% of all fissions. Xenon is also produced by the decay of other fission products or precursors such as iodine. These gases can remain in the fuel and form bubbles which cause the fuel to swell or the gases can diffuse to the surface and contact the cladding. In either case, the cladding is subject to a pressure which rises steadily with fuel burnup. At the limit, the internal fission gas pressure will exceed the coolant pressure and cause the cladding to fail. Hence fission gas behavior is a major factor with regard to the selection of a particular reactor fuel. The ideal fuel material retains fission gases within its structure and resists swelling.**

6) The fuel material should permit maximum uranium loading per unit volume of fuel. An enrichment limit imposed on the uranium fuel produces two effects which must be considered. Lowering the uranium enrichment results in the addition of  $U^{238}$  which reduces the reactivity of the fuel element even if the amount of  $U^{235}$  can be kept the same. Further, the added  $U^{238}$  reduces the allowable loading or concentration of  $U^{235}$  in the reactor fuel elements. For many reactor fuel element designs, use of LEU will sufficiently lower the initial reactivity so as to render the use of the fuel element impractical. This will be discussed further in Chapter 3. It should be noted that there are three ways to regain reactivity lost by the use of LEU: (1) the use of higher uranium-loading fuel, (2) the use of a higher performance reflector material, and (3) increase the core size. Of course a combination of these approaches can be used.[12.]

### **2.1.2 Review of the Fuels Considered for this Study**

Generally, the many proven nuclear fuels in existence today consist of a fissile material which is mixed with a fertile material or diluent. In this case, and as stated earlier, the fissile material is  $U^{235}$ , and the fertile material is  $U^{238}$ . This fissile/fertile mixture is almost always combined with some other element or elements in the form of a compound, alloy or mixture. As a result, nuclear fuels may be grouped into three different classes: metallic, ceramic and dispersion types; some examples of which are considered in the proceeding discussion.

The following section reviews the fuel types that have been considered for use as an SSN reactor fuel both in the past and for the purposes of this study. The ceramic and metallic compounds of uranium that were considered are listed in Table 2.1. The alloys of uranium that were considered for use as nuclear fuels are listed in Table 2.2. These tables are by no means exhaustive.

### **2.1.2.1 Metallic Uranium Fuel**

The ideal uranium fuel is the metal itself since it has the highest uranium mass density or uranium loading possible, ( $18.9 \text{ g/cm}^3$ ). Its high thermal conductivity of  $35 \text{ W/m}\cdot\text{K}$  allows a fuel maximum temperature on the order of  $500^\circ\text{C}$  for the fuel element designs considered for this study. This offsets the relatively low melting point ( $1130^\circ\text{C}$ ) of uranium metal. Other fuel types such as ceramic oxides may require maximum fuel temperatures approaching  $1000^\circ\text{C}$  in order to achieve the necessary heat flux required to produce a coolant outlet temperature of  $320^\circ\text{C}$ .

A major drawback to the use of uranium metal is that it has three crystalline structures that are stable in the range of fuel temperatures that can be encountered in the reactor. This includes the normal operating temperature range and temperature increases that can occur in transient or accident conditions. Uranium metal undergoes a phase change at  $661^\circ\text{C}$  from alpha-uranium to beta-uranium and at  $769^\circ\text{C}$  from beta-uranium to gamma-uranium. Alpha-uranium has an orthorhombic crystal structure; beta-uranium a tetragonal crystal structure and gamma-uranium a body-centered-cubic crystal structure. A volume increase accompanies the

**Table 2.1. Uranium bearing compounds.**

Uranium Bearing Compound	Melting Point (°C)	Density (g/cm <sup>3</sup> )	Uranium Density (g/cm <sup>3</sup> )	Uranium Mass Fraction (wt%) (For 100% enriched)	Thermal Conductivity (W/m·°K)	Thermal Microscopic Absorption Cross-Section of Second Element, $\sigma_a$ (barns)	Thermal Macroscopic Absorption Cross-Section of Second Element, $\Sigma_a$ (cm <sup>-1</sup> )
U	1133	18.9	18.9	100	35.0 (at 400°C)	—	—
UAl <sub>2</sub>	1590	8.1	6.6	81.5		0.23	0.086
UAl <sub>3</sub>	1350	6.7	5.0	74.6		0.23	0.098
UAl <sub>4</sub>	730	6.0	4.1	68.3		0.23	0.106
UC	2500	13.6	13.0	95.6	21.6 (to 1000°C)	0.0032	0.00048
UC <sub>2</sub>	≈2500	12.9	10.6	82.4	35.0 (to 1000°C)	0.0032	0.00802
UN	2630	14.3	13.5	94.4	20.0 (at 1000°C)	1.88	0.535
UO <sub>2</sub>	2875	10.96	9.7	88.2	3.5 (at 600°C)	0.00027	0.00010
U <sub>3</sub> O <sub>8</sub>	—	8.4	7.1	84.5		0.00027	0.00011
U <sub>3</sub> Si	930	15.6	14.91	95.6	20.0 (to 1000°C)	0.16	0.037
U <sub>3</sub> Si <sub>2</sub>	1665	12.2	11.3	92.6		0.16	0.038

**Table 2.2. Uranium rich alloys.**

Uranium Bearing Alloy	Melting Point (°C)	Density (g/cm <sup>3</sup> )	Uranium Density (g/cm <sup>3</sup> )	Uranium Mass Fraction (wt%)	Thermal Conductivity (W/m-°K)	Thermal Microscopic Absorption Cross-Section of Second Element, $\sigma_a$ (barns)	Thermal Macroscopic Absorption Cross-Section of Second Element, $\Sigma_a$ (cm <sup>-1</sup> )
U-10wt%Mo	1150	17.33	15.67	90	29	2.5	0.257
U-10wt%Nb	1300 (Solidus)	16.68	15.12	90		1.1	0.133
U-10wt%Zr	1135 (Solidus)	15.76	14.25	90		0.18	0.027
U-75wt%Al	1105 (Solidus)	3.93	1.35	35		0.23	0.132

change from alpha-uranium to beta-uranium and from beta-uranium to gamma-uranium. The volume increase from alpha-uranium to beta-uranium is about 1%.[17] Thus, a reactor temperature excursion can result in a uranium phase transition accompanied by a fuel volume increase, thereby potentially rupturing the fuel element cladding.

Since metallic uranium oxidizes readily upon contact with high temperature water, the consequences of cladding rupture in a metallic uranium fueled water cooled reactor are serious. Cladding rupture permits fuel/water contact that results in rapid oxidation of the fuel which causes further cladding rupture. Exposure to 300°C water for a few hours would completely destroy the fuel element.[18]

Uranium metal also exhibits severe swelling under prolonged irradiation due to fission gas. Thus the attainable fuel burnup is greatly limited. In light of this and the above considerations, metallic uranium is

not a satisfactory fuel for use in the power producing PWRs considered for this study.

### **2.1.2.2 Metallic Uranium Rich Alloy Fuels**

Various properties of metallic uranium can be improved by the addition of non fissionable elements as a minor constituent. Alloying additions that have been used in the past and that have been considered for this study are molybdenum, niobium, zirconium and aluminum. As with metallic uranium, uranium rich alloy fuels offer the desirable properties of high thermal conductivity and high uranium loading. The general purposes and specific goals of these alloying additions are summarized below.

- 1) To stabilize the gamma phase from 769°C down to room temperature: Alloying additions of about ten weight percent (10wt%) molybdenum, zirconium or niobium can suppress the formation of beta and then alpha uranium at room temperature. These elements when added to molten uranium, result in the retention of the gamma phase when the uranium is quenched to room temperature. This eliminates the phase change related volume increases in the fuel upon heat up of the fuel element during reactor transients.
- 2) To raise the alpha/beta transformation temperature in cases where the gamma phase is not stabilized to room temperature: It should be noted that for relatively low temperature applications (i.e., below the beta/gamma transition temperature), alpha-uranium can be

**used where the alpha/beta transformation temperature has been raised by alloying additions.**

- 3) To improve low and high temperature mechanical properties: For example, the alloying additions mentioned above increase the yield strength which increases the resistance to fission gas swelling.**
- 4) To form higher melting point uranium compounds: Molybdenum, niobium and zirconium additions raise the melting point of metallic uranium.**
- 5) To improve corrosion resistance: Although uranium rich alloy fuels are more resistance to high temperature aqueous corrosion than metallic uranium, uranium rich alloy fuels oxidize fairly readily in high temperature water. Thus the consequences of cladding failure remain serious if metallic uranium rich alloys are to be used in a water cooled reactor.**

**Uranium-molybdenum alloys, at temperatures up to 650°C, have been used in the Dounreay and Enrico Fermi fast reactors with 9wt% and 10wt% molybdenum respectively. The later offers a uranium loading of 15.6g/cm<sup>3</sup>. However, these fuel elements were limited to a burnup of 2at% due to the accompanying excessive fission gas induced swelling that occurs at temperatures greater than approximately 400°C. Since metallic uranium rich alloys as employed in the chosen fuel element design require a maximum operating fuel temperature of about 500°C, this fuel is**

incapable of meeting the performance objectives of the SSN reactor designs considered in this study.[12]

A disadvantage to the use of molybdenum is that it has a relatively high macroscopic neutron absorption cross-section ( $\Sigma_a$ ) of  $160 \text{ cm}^{-1}$ , (see Table 2.4), that may sufficiently lower the available reactivity of a fuel element using LEU so as to prohibit its use in a modern SSN reactor core.

The uranium-niobium and uranium-zirconium alloys described in Table 2.2 provide uranium loadings of  $16.68 \text{ g/cm}^3$  and  $15.76 \text{ g/cm}^3$  respectively. As with uranium-molybdenum alloys, fission gas swelling at 2-4at% burnup are prohibitively high at temperatures greater than  $400^\circ\text{C}$ . Thus these fuels are also incapable of meeting the performance objectives of a modern SSN reactor. It should be noted that at lower temperatures uranium-molybdenum alloys are more resistant to swelling than uranium-niobium and uranium-zirconium alloys.

As in the case of molybdenum, niobium has a relatively high  $\Sigma_a$  ( $60 \text{ cm}^{-1}$ ) and will also lower the reactivity of a fuel element using LEU. Zirconium, however has the advantages of a relatively small  $\Sigma_a$  ( $9.8 \text{ cm}^{-1}$ ) high melting point ( $1845^\circ\text{C}$ ), excellent ductility and good resistance to aqueous corrosion. It is interesting to note that uranium-zirconium alloy fuels were used in the early nuclear submarine program.[16] At that time submarines did not require the refueling lifetimes of modern SSNs.

Although uranium rich alloy fuels appear to be unsuitable for use in the plate type fuel elements considered for this study, they can be used in rod type fuel elements where there exists a sufficiently large gap between the outer fuel surface and the cladding inner surface to accommodate the excessive swelling. During operation, fission gas swelling increases the original fuel volume by roughly 20% at which the fuel contacts the cladding.

At this point, sufficient numbers of fission gas bubbles present on the fuel grain boundaries link together to form a continuous path which allows for fission gas release and prevents additional swelling. The released gasses collect in a plenum or void element at the top of each fuel element.

A large fuel/cladding gap requires a highly conducting medium such as liquid sodium in order to prevent excessive fuel temperatures. Due to the violent sodium/water reaction that will occur in the event of cladding rupture, water can not be used as the reactor coolant. Thus the reactor must be cooled by liquid sodium. In the 1950s U.S. Navy Admiral Hyman Rickover prevented the liquid metal cooled reactor (LMR) from being implemented on U.S. submarines because of concerns of the possibility of sea water contacting the sodium coolant.

Uranium-aluminum alloy fuels clad in aluminum have been used extensively in research reactors. The uranium loading must be less than 35wt% uranium in the fuel material. Above this 35wt% limit it is extremely difficult to maintain the specified homogeneity of the uranium throughout the fuel material that is required to prevent hot spots.[15] With the densities of metallic uranium and aluminum taken as 18.8g/cm<sup>3</sup> and 2.7g/cm<sup>3</sup> respectively the following equation [12.],

$$\frac{M_U}{V_{meat}} = \frac{\rho_U}{1 + \frac{\rho_U}{\rho_{Al}} \left( \frac{100}{wt\%U} - 1 \right)} \quad (2.1)$$

yields a uranium loading of 1.35g/cm<sup>3</sup> at 35wt%U. This is insufficient to provide the reactivity required for a modern SSN reactor.

### **2.1.2.3 Uranium Aluminide - Aluminum Dispersion Fuel ( $UAl_x - Al$ )**

Dispersion type fuels are two phase alloys consisting of a fissile isotope bearing material that is uniformly dispersed in a matrix of nonfissile material or diluent. These fuels are usually prepared by powder metallurgy, a process in which fine powders of the fissile phase and nonfissile phase are mixed, compacted, sintered, and rolled to form a continuous fuel material. The dispersion technique offers the following advantages when the diluent predominates in volume.

- 1) Damage to the fuel material due to fission fragments is localized to the each fuel particle and the region immediately surrounding it.[17]
- 2) The potential for reaction between the fuel and the coolant is essentially eliminated in the event of cladding rupture. Only particles on the surface of the fuel material can be exposed to the coolant.[17]
- 3) The path for heat flow from the fissile particles is through a highly conducting metallic nonfissile medium which lowers the required operating fuel temperature.

The uranium bearing intermetallic compounds formed by uranium and aluminum,  $UAl_2$ ,  $UAl_3$  and  $UAl_4$ , can be dispersed in a continuous matrix of aluminum to form uranium aluminide - aluminum ( $UAl_x - Al$ ) dispersion type fuel. This fuel has been used extensively in research reactors not intended for power generation. Thus they can operate at a

relatively low temperature. Since aluminum metal melts at 660°C, a temperature which can easily be exceeded during transient or accident conditions, it should not be used as a fuel matrix or cladding material for PWR operating conditions.

Uranium aluminide - aluminum dispersion type fuel is used in the Advanced Test Reactor operated by the Idaho National Engineering Laboratory with an average uranium loading in the fuel plates of 42wt% uranium or about 60wt%  $UAl_x$ . As calculated from Equation 1.2, this corresponds to a uranium loading of about 2.0g/cm<sup>3</sup>. [12.] It has been estimated that a uranium loading of 2.6g/cm<sup>3</sup> could be achieved with this type of fuel. [12] This fuel loading is not sufficient to provide adequate reactivity for the LEU fuel elements of this study.

#### **2.1.2.4 Uranium Silicide - Aluminum Dispersion Fuel**

Another more promising fuel type is uranium silicide which has been used to form a dispersion with aluminum. The uranium silicide compounds of interest are  $U_3Si$  which has a uranium density of 14.91g/cm<sup>3</sup> and  $U_3Si_2$  which has a uranium density of 11.3g/cm<sup>3</sup>.  $U_3Si_2$  has a moderately high melting point of 1665°C while  $U_3Si$  has a melting point of 930°C.  $U_3Si_2$  was shown to more stable under irradiation than  $U_3Si$ . [17]

Uranium silicide - aluminum dispersion type fuels ( $U_3Si_x$  - Al) offer higher uranium loadings than the  $UAl_x$  - Al dispersion type fuels. Fuel elements containing  $U_3Si_x$  - Al dispersion type fuel of up to 45 volume percent (45Vol%)  $U_3Si_x$ , corresponds to a uranium loading of 4.75g/cm<sup>3</sup>, have been successfully irradiated in the Oak Ridge Research Reactor (ORR) with maximum fuel temperatures of approximately 130°C. [17] Also, it has

been reported that  $U_3Si_x$  - Al dispersion type fuels with a uranium loading of  $6g/cm^3$  have been irradiated to a burnup of 50at%.[21] However, this was done with fuel maximum operating temperatures at about low temperature. At the operating temperatures of  $500^\circ C$  or greater required for a power producing reactor, uranium silicide fuels exhibit excessive swelling under irradiation. Furthermore, uranium silicide fuel undergoes rapid and gross swelling at fuel temperatures in excess of  $900^\circ C$ . Such fuel temperatures can be reached quickly during a LOCA.[18] Thus, uranium silicide dispersion type fuels are also not suitable for use in the power producing reactors needed by SSNs.

### 2.1.2.5 Uranium Oxide - Aluminum Dispersion Fuel

Another dispersion type fuel that is used in research reactors is uranium oxide ( $U_3O_8$ ), a ceramic fuel which is dispersed in aluminum and clad in aluminum. This is used as a fuel in the High Flux Isotope Reactor (HFIR) operated by Oak Ridge National Laboratory. This type of fuel has performed successfully in HFIR fuel elements up to a uranium loading of 35wt% uranium (40wt%  $U_3O_8$ ). Furthermore, at that time, as part of development tests for  $U_3O_8$  - Al dispersion type fuel, samples were made, and irradiated, evaluated, and deemed satisfactory up to a maximum loading of 42wt% uranium (50wt%  $U_3O_8$ ) in the fuel material. [12] With the densities of the  $U_3O_8$  compound and aluminum taken as  $8.4g/cm^3$  and  $2.7g/cm^3$  respectively, Equation 1.2,

$$\frac{M_{U_3O_8}}{V_{meat}} = \frac{\rho_{U_3O_8}}{1 + \frac{\rho_{U_3O_8}}{\rho_{Al}} \left( \frac{100}{wt\%U_3O_8} - 1 \right)} \quad (2.2)$$

yields a  $U_3O_8$  compound loading of  $2.04\text{g/cm}^3$  for 50wt%  $U_3O_8$ . Since the uranium mass fraction in  $U_3O_8$  is 84.5% as listed in Table 2.1, the uranium loading is  $1.73\text{g/cm}^3$ . It has been estimated, however, that  $U_3O_8$  - Al dispersion type fuels with a uranium loading of 2.8 to  $3.7\text{g/cm}^3$  could be fabricated.[12] Based on atomic geometry considerations, a uranium loading of about  $3.6$  -  $3.7\text{g/cm}^3$  (about 80wt%  $U_3O_8$ ) is thought to be the theoretical limit at which the continuous aluminum phase can be maintained. This is required in order to facilitate heat removal from the fuel element through the highly conducting continuous aluminum matrix.[12] Higher uranium loadings than those mentioned above are required for SSN reactor fuel elements.

A major drawback to the use of  $U_3O_8$  fuel is that it reverts to  $UO_2$  at approximately  $1200^\circ\text{C}$ . This is known as the thermite reaction. With the concentration of the poorly conducting ceramic  $U_3O_8$  approaching 80wt% in the fuel material,  $1200^\circ\text{C}$  can easily be reached during transient or accident conditions. When a higher oxide such as  $UO_3$  or  $U_3O_8$ , is reduced, the conversion to  $UO_2$  is accompanied by a relatively large decrease in specific volume (50% for  $UO_3$  and 32% for  $U_3O_8$ ). The specific volume change can result in fracture and size reduction of the higher oxide particles which can destroy the fuel element.[17] As a result  $U_3O_8$  - Al dispersion type fuel can not be used in the PWR reactor designs considered for this study.

### **2.1.2.6 Uranium Carbide and Uranium Nitride Fuels**

Uranium forms two carbides which are of practical interest as reactor fuels, uranium carbide, UC, and uranium dicarbide, UC<sub>2</sub>. UC melts at 2780°C and UC<sub>2</sub> at 2720°C. Basically, uranium carbides have two desirable properties: (1) these compounds provide relatively high uranium loadings of 13.0g/cm<sup>3</sup> and 10.6g/cm<sup>3</sup> for UC and UC<sub>2</sub> respectively, (2) the thermal conductivity of these compounds are relatively high, 21.6W-m/°K for UC and 35W-m/°K for UC<sub>2</sub>.

Uranium nitride fuel UN has a uranium loading of 13.5g/cm<sup>3</sup> and has a melting point of 2630°C and also has a relatively high thermal conductivity. These properties lead to high available reactivity and to lower thermal gradients in the fuel elements.

Uranium carbide and uranium nitride fuels exhibit excessive swelling upon irradiation due to fission gas retention. This is due to the high densities of carbide and nitride fuels in which the volatile fission products are less mobile than in the other fuel types listed in Tables 2.1 and 2.2.[16] Fission gas induced swelling in these fuels is greater than that of UO<sub>2</sub> by a factor of two.[16] Thus the allowable burnup is limited in order to prevent excessive strain on the cladding.

As with metallic uranium fuel and uranium rich alloy fuels, the chemical reactivity of UC, UC<sub>2</sub> and UN with water and the resulting release of oxidizing gases make these fuels unsuitable for use in the power producing PWR cores required by SSNs. As stated earlier, contact with water will occur in the event of cladding rupture.

It should be noted that these fuels are best suited for the liquid sodium cooled reactor described in Section 2.1.2.2. where excessive swelling can be accommodated and the fuel/water reaction is eliminated.

### **2.1.2.7 Uranium Dioxide Fuel**

Uranium dioxide, a ceramic fuel, is the most commonly used nuclear fuel today. It has a fabrication density of  $10.3\text{g/cm}^3$ , (95% of its theoretical density), and offers a relatively high uranium loading of about  $9.1\text{g/cm}^3$ . This combined with the low macroscopic neutron absorption cross-section ( $\Sigma_a$ ) of oxygen in this fuel ( $0.00054\text{cm}^{-1}$ ), facilitates the use of LEU. Thus  $\text{UO}_2$  has strong non-proliferation characteristics. Uranium dioxide also exhibits chemical inertness and has excellent resistance to corrosion when exposed to high temperature and pressure water.

Use of  $\text{UO}_2$  necessitates a high maximum operating fuel temperature due to its poor thermal conductivity. However, since  $\text{UO}_2$  has a high melting point of  $2875^\circ\text{C}$ , fuel melting is unlikely except in severe accident situations. A disadvantage to a high fuel temperature and fuel element temperature gradient is that during accident conditions such as a LOCA or a LOFA, the cladding temperature will rise faster than in the case of a lower operating fuel temperature. Thus the available time before emergency core cooling action must be effective is decreased. As stated earlier, zircaloy is the chosen cladding material. It has a melting point of approximately  $1852^\circ\text{C}$  but reacts with water at about  $1200^\circ\text{C}$  releasing explosive hydrogen gas.

As the operating temperature of  $\text{UO}_2$  fueled elements is increased, the rate of fission gas release also increases. This will exert pressure on the

inner surface of the cladding which will cause some swelling. Rod type fuel elements used in commercial reactors are constructed with a plenum at the top of each fuel rod where released fission gasses collect. In these fuel rods, there is no fuel/cladding bond, thus allowing fission gasses to reach this plenum via the gap. Figure 2.1 shows the percentage of fission gasses released as a function of temperature. Although  $UO_2$  exhibits some fission gas swelling it is considered to be one of the most stable under irradiation and fission gas swelling resistant fuels available.

Despite these limitations caused by poor thermal conductivity and fission gas swelling,  $UO_2$  is considered to be the fuel best suited for use in the SSN PWR reactor design of this study. Furthermore, much operating experience has been gained through the years with  $UO_2$  fuel clad in zircaloy by its use in commercial PWRs and to a lesser extent in research reactors.

## **2.2 Cladding Material Considerations**

In nearly all reactors, the fuel is covered with a protective material or cladding which prevents the release of radioactive fission products from the fuel surface to the coolant channel. The cladding also prevents corrosion of the fuel and acts to retain the original shape of the fuel material during the operating life time of the fuel element. The cladding must remain intact both throughout the operation of the reactor and following removal of the fuel element from the reactor core.

In high fuel burnup power producing reactors, the cladding must resist swelling due to internal pressure buildup caused by fission gasses. Typical design limits are 1% cladding strain in commercial reactors. In

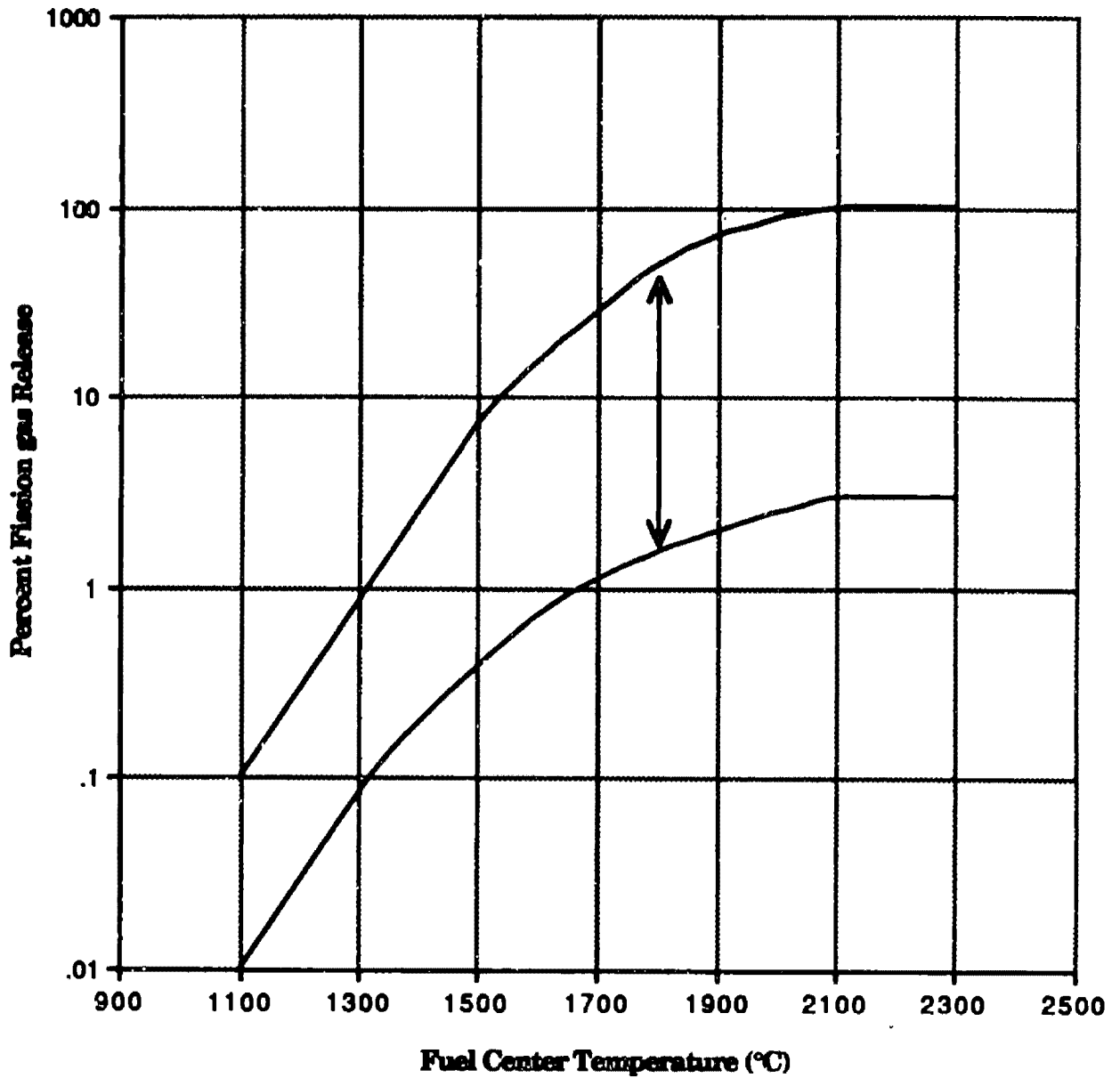


**Figure 2.1.** Correlation between fission gas release and fuel center temperature for  $UO_2$  fuels.[22]

the case of weak or defective cladding, fission gas pressure can result in failure of the cladding.

### **2.2.1 Clad Material Selection Criteria**

A variety of materials exist that have been used or could possibly be used as a nuclear fuel cladding material, the most common of which are listed in Table 2.3 along with some important properties. None of these materials or any other material satisfies all the requirements for an ideal cladding. However, the material best suited for this purpose is the one that forms the best compromise between the conflicting specifications for an ideal cladding in a particular reactor environment. The characteristics of the ideal cladding material are summarized below.

- 1) **Low macroscopic neutron absorption cross-section ( $\Sigma_a$ , cm<sup>-1</sup>):**  
Since cladding materials add negative reactivity to the reactor, it is desirable for  $\Sigma_a(\text{clad})$  to be as low as possible.
- 2) **High thermal conductivity (k, W/m-°C):** A high value for k for the cladding material decreases the thermal resistance between the fuel material and coolant. This decreases the maximum fuel element center-line temperature needed to yield the heat transfer rate that produces the desired reactor power level.
- 3) **High melting point:** Almost all materials that have been used as nuclear fuel cladding materials have a lower melting point than UO<sub>2</sub> (~2800°C). During normal operation, the average

temperature of the fuel in a power producing PWR is about 1000°C and the average temperature of the cladding is about 380°C. If a loss-of-flow-accident were to occur, in a brief time period, the temperature profile through the fuel/cladding system would flatten which can possibly result in melting of the cladding. Thus a cladding material with a high melting point increases the safety margin for the reactor.

- 4) The material should have good irradiation stability (i.e., the material should be resistant to irradiation induced swelling and growth). Swelling is a change in shape and volume while growth is a change in shape with no change in volume. Poor irradiation behavior can distort the shape of the fuel elements.
- 5) Low coefficient of thermal expansion( $\alpha$ ,  $\text{cm}/^\circ\text{C}$ ): This is for reasons similar to that stated in item (4).
- 6) The ideal nuclear fuel cladding material should have the conflicting properties of high strength and ductility. Most high strength materials are also brittle and thus are subject to catastrophic failure when their yield strength ( $\sigma_y$ ) is exceeded.
- 7) The cladding material should be resistant to corrosion as influenced by contact with fuel material and coolant water at high temperatures. Some of the more volatile fission products such as iodine and cesium migrate to the cooler regions of the fuel element (i.e., the region in contact or closest to the cladding)

where they may induce stress corrosion cracking or other degrading phenomena. Also, in PWRs, excessive hydrogen concentrations in the coolant water can react with some potential cladding materials to form hydrides. Hydrides are very brittle materials which can result in cladding failure if formed in high stresses regions.

## 2.2.2 Selection of Cladding Material

The material with the lowest macroscopic neutron absorption cross-section ( $\Sigma_a$ ), and best combination of the ideal mechanical properties described in the above discussion is zircaloy. It has a  $\Sigma_a$  of  $10.7\text{cm}^{-1}$ , has good high temperature strength, is ductile, has a relatively high thermal conductivity of  $21\text{W}\cdot\text{m}^{-1}\cdot\text{K}$ , and a high melting point of  $1852^\circ\text{C}$ . Note that temperature of zircaloy in a PWR system must remain below  $1200^\circ\text{C}$  at which the following exothermic reaction can occur,



which results in the liberation of explosive hydrogen gas.

Magnesium and aluminum also have a low  $\Sigma_a$  of  $2.59\text{cm}^{-1}$  and  $13.8\text{cm}^{-1}$  respectively. However, magnesium is highly reactive to high temperature high pressure water and both have relatively low melting points of  $648.8^\circ\text{C}$  and  $660.4^\circ\text{C}$  respectively. Thus, they are excluded from consideration. Stainless steel type 304 possesses excellent strength up to  $\approx 600^\circ\text{C}$ , is quite ductile, and has excellent corrosion resistance but its high  $\Sigma_a$  of  $258\text{cm}^{-1}$  makes it less attractive for use in compact military reactors where good

**Table 2.3. Possible cladding materials.**

<b>Material</b>	<b>Atomic Weight</b>	<b>Density (g/cm<sup>3</sup>)</b>	<b>Thermal Conductivity (W/m-°K)</b>	<b>Melting Point (°C)</b>	<b>Thermal Microscopic Absorption Cross-Section, <math>\sigma_a</math> (barns)</b>	<b>Thermal Macroscopic Absorption Cross-Section, <math>\Sigma_a</math> (cm<sup>-1</sup>)</b>
<b>Magnesium</b>	<b>24.3</b>	<b>1.74</b>	<b>149</b>	<b>648.8</b>	<b>0.06</b>	<b>2.59</b>
<b>Zirconium</b>	<b>91.2</b>	<b>6.44</b>	<b>21</b>	<b>1852±2</b>	<b>0.18</b>	<b>9.8</b>
<b>Zircaloy - 4</b>	<b>91.2</b>	<b>6.50</b>	<b>21</b>	<b>-1850</b>	<b>0.26</b>	<b>10.7</b>
<b>Aluminum</b>	<b>27.0</b>	<b>2.7</b>	<b>231</b>	<b>660.4</b>	<b>0.23</b>	<b>13.8</b>
<b>Niobium</b>	<b>92.9</b>	<b>8.4</b>	<b>58</b>	<b>2468±10</b>	<b>1.1</b>	<b>60.0</b>
<b>Molybdenum</b>	<b>95.9</b>	<b>10.2</b>	<b>126</b>	<b>2617</b>	<b>2.5</b>	<b>160.0</b>
<b>Iron</b>	<b>55.8</b>	<b>7.86</b>	<b>55</b>	<b>1535</b>	<b>2.6</b>	<b>221.0</b>
<b>Stainless Steel (304)</b>	<b>55.3</b>	<b>7.92</b>	<b>55</b>	<b>-1535</b>	<b>3.0</b>	<b>258.0</b>
<b>Vanadium</b>	<b>50.9</b>	<b>5.96</b>	<b>33</b>	<b>1890±10</b>	<b>5.1</b>	<b>360.0</b>
<b>Nickel</b>	<b>58.7</b>	<b>8.9</b>	<b>66</b>	<b>1453</b>	<b>4.6</b>	<b>422.0</b>
<b>Cobalt</b>	<b>58.9</b>	<b>8.92</b>	<b>67</b>	<b>1495</b>	<b>37.0</b>	<b>3380.0</b>

neutron economy is necessary.[16]

Although unalloyed zirconium (zirconium metal) has a lower  $\Sigma_a$  ( $9.8\text{cm}^{-1}$ ) than zircaloy ( $10.7\text{cm}^{-1}$ ), it is not suitable as a cladding material since it exhibits the following problems.

- 1) **Inadequate corrosion resistance:** Normal oxide films that form on the cladding surface fall off easily resulting in continuous unchecked corrosion. This occurs rapidly in water over  $300^\circ\text{C}$ . [22]
- 2) **Insufficient high temperature strength:** This requires a thicker clad which results in more material in the core and hence increased neutron losses.
- 3) **Pure zirconium is susceptible to hydrogen absorption and subsequent embrittlement.** Excessive hydrogen in PWR coolant water is absorbed by zirconium to form zirconium hydride; a brittle compound. If this occurs in high stress areas, cladding failure can result.

To combat these problems, a series of zirconium alloys which are listed in Table 2.4 and known as the zircaloys were developed in the late 1950s. Zircaloys are roughly 98% zirconium with minor additions of Tin (Sn), Iron (Fe), Chromium (Cr) and Nickel (Ni) not necessarily including all. Tin additions improve the adherence of the oxide film which acts as a protective layer to slow further corrosion, however, some corrosion will continue to

**Table 2.4. Zircaloy alloy series.**

<b>Alloy Designation</b>	<b>Normal Percentages by Weight</b>			
	<b>Sn</b>	<b>Fe</b>	<b>Cr</b>	<b>Ni</b>
<b>Zircaloy - 1</b>	2.5	—	—	—
<b>Zircaloy - 2</b>	(1.4-1.6)	(0.14-0.16)	(0.10-0.12)	0.05
<b>Zircaloy - 2 (Ni - Free)</b>	(1.4-1.6)	(0.14-0.16)	(0.10-0.12)	0.007max
<b>Zircaloy - 3A (Discontinued)</b>	0.25	0.25	—	—
<b>Zircaloy - 4</b>	(1.4-1.6)	(0.18-0.20)	(0.10-0.12)	0.007max

occur. Additions of Fe, Ni and Cr, as used in the alloy zircaloy - 2, collectively act to greatly improve the general corrosion behavior of zirconium. Nickel, however, has the adverse effect of promoting hydrogen absorption which leads to the formation of brittle zirconium hydrides. To improve this, zircaloy - 4 has a lower Ni concentration. The decrease in Ni is offset by an increase in Fe to maintain the same level of high temperature strength and corrosion resistance.

It should also be noted that zirconium and the zircaloys have a hexagonal close packed crystal structure. As a result these materials exhibit anisotropic thermal expansion, irradiation induced growth and tensile strength. Thermal expansion is maximum parallel to the basal planes of the hexagon while irradiation induced growth and tensile strength are maximum perpendicular to the basal planes or parallel to the

**C - axis. Such complications can be overcome with proper fabrication techniques and orientation of the hexagonal crystal structure.[22]**

### **2.3 Burnable Poison Material**

**As a means of controlling excess reactivity at the beginning-of-cycle (B.O.C.) and to provide a means for power shaping and optimum core burnup, commercial LWRs employ a control material or burnable poison. These are solid neutron absorbing materials that are placed in selected fuel elements of the reactor. As they are subject to neutron irradiation, the absorber material is gradually depleted, thus matching, ideally, the depletion of the fissile material. Table 2.5 lists some of these materials, along with their microscopic neutron capture cross-sections ( $\sigma_\gamma$ ), that have been or could be used as reactivity control materials; not necessarily as a burnable poison in a PWR.**

**Gadolinia ( $Gd_2O_3$ ) is a ceramic, which unlike other compounds listed in Table 2.5 can be readily mixed as a solid solution with ceramic  $UO_2$  fuel where it becomes an integral part of the fuel element.[23] It does not have to be lumped into separate fuel elements, thus eliminating the need for special absorber hardware or control rods. Consequently, there is no reduction in the number of fuel elements in the core. The high thermal cross-section of  $Gd_2O_3$ , due mostly to its odd-A isotopes  $Gd^{155}$  and  $Gd^{157}$ , results in a more complete burnout of the poison toward the end-of-cycle (E.O.C.) yielding better neutron economy and hence a higher fuel utilization. Table 2.6 lists the isotopes of gadolinium and their neutron absorption cross-sections. Table 2.7 lists the important properties of**

gadolinium. With proper design and distribution of  $Gd_2O_3$  throughout the reactor core, flatter power distributions and low neutron leakage can be achieved. A flatter power distribution results in a reduction of the reactor power peaking factor which also results in better fuel utilization.

Additional advantages to the use of  $Gd_2O_3$  as a solid solution with  $UO_2$  are no displacement of water and little displacement of the fuel.

There are two potential disadvantages to the use of  $Gd_2O_3$ . Although  $Gd_2O_3$  is physically compatible with  $UO_2$ , the thermal conductivity and the melting point of the fuel material is lowered with its addition to  $UO_2$ . [19] However, for the reactor designs and fuel elements considered for this study, this is not a problem. It was stated earlier that maximum uranium fuel temperature heat would be encountered in the  $UO_2$  fuel elements considered for this study is  $975^\circ C$  and that the melting point of  $UO_2$  is  $2875^\circ C$ . Thus there is a wide margin to accommodate these undesirable effects and gadolinium has been chosen for this study.

It should be noted that for the 20% and 97.3% enriched reactor designs,  $Gd_2O_3$  is lumped into separate plates for reasons that will be discussed in detail in Chapter 5. In the 7% enriched reactor design, the  $Gd_2O_3$  is uniformly distributed throughout the reactor fuel elements.

**Table 2.5. Reactivity control materials.**

<b>Compound</b>	<b>Controlling Element</b>	<b>Thermal Macroscopic Absorption Cross-Section, <math>\Sigma_a</math> (cm<sup>-1</sup>)</b>
<b>B<sub>4</sub>C</b>	<b>B</b>	<b>759</b>
<b>HfC</b>	<b>Hf</b>	<b>102</b>
<b>B<sub>2</sub>O<sub>3</sub></b>	<b>B</b>	<b>759</b>
<b>Gd<sub>2</sub>O<sub>3</sub></b>	<b>Gd</b>	<b>49000</b>
<b>Eu<sub>2</sub>O<sub>3</sub></b>	<b>Eu</b>	<b>4600</b>
<b>HfO<sub>2</sub></b>	<b>Hf</b>	<b>102</b>
<b>H<sub>3</sub>BO<sub>3</sub></b>	<b>B</b>	<b>759</b>
<b>Er<sub>2</sub>O<sub>3</sub></b>	<b>Er</b>	<b>162</b>
<b>Ag-In-Cd</b>	<b>Ag</b> <b>In</b> <b>Cd</b>	<b>63.6</b> <b>193.5</b> <b>2450</b>

**Table 2.6. Isotopes of gadolinium.**

<b>Gadolinium Isotope</b>	<b>Isotopic Abundance (a/o)</b>	<b>Atomic Weight</b>	<b>Thermal Microscopic Absorption Cross-Section, (<math>\sigma_a</math>) barns</b>
154	2.18	153.921	80
155	14.80	154.923	6100
156	20.47	155.922	2
157	15.65	156.922	255000
158	24.84	157.924	2.4
160	21.86	159.921	0.8

**Table 2.7. Some properties of gadolinium.**

<b>Density (g/cm<sup>3</sup>)</b>	7.64
<b>Melting Point (C)</b>	2347
<b>Atomic mass</b>	362.5
<b>Gadolinium mass fraction</b>	86.8%
<b>Thermal Macroscopic Absorption Cross-Section, <math>\Sigma_a</math> (cm<sup>-1</sup>)</b>	49000

## **2.4 Reactor Coolant**

**As stated in Chapter 1, H<sub>2</sub>O is the coolant material by choice of the SSN reactor type, the PWR. Water serves two functions in this reactor. It acts as a reactor coolant and as a neutron moderator which slows down neutrons to thermal energies (-0.025eV) at which most fission occur. Each fission releases an average of 2.4 neutrons with an average energy of about 2MeV.**

**With regard to reactor operation and control, water has two opposing effects. Its neutron moderating characteristics contribute positive reactivity to the reactor, while its neutron absorption characteristics contribute negative reactivity to the reactor. The degree to which each of these characteristics, relative to each other, effect core reactivity, depends on the ratio of fuel element material to coolant water present in the core. These effects are of dire importance to reactor operation and safety and will be discussed further in Chapter 3. Table 2.8 summarizes the important physics properties of H<sub>2</sub>O.**

## **2.5 Summary of Selected Materials**

**From the discussion of this chapter, our SSN reactors will consist of an arrangement of UO<sub>2</sub> fuel at some enrichment level, zircaloy - 4 cladding and structural material, Gd<sub>2</sub>O<sub>3</sub> burnable poison material and H<sub>2</sub>O coolant. The remainder of this study will consist of determining the quantity, distribution and arrangement of these materials that will result in the optimum utilization of 7%, 20% and 97.3% enriched uranium.**

**Table 2.8. Important physics properties of H<sub>2</sub>O.**

Density (g/cm <sup>3</sup> )	0.726(305°C)
$\sigma_a$ (H) (barns)	0.00027
$\sigma_a$ (O) (barns)	0.332
$\Sigma_a$ (H <sub>2</sub> O) (cm <sup>-1</sup> )	0.022
$\Sigma_s$ (H <sub>2</sub> O) (cm <sup>-1</sup> )	1.64
Atomic weight	18.0153
$\xi$ (2MeV - 0.025eV) (Number of collisions to thermalize)	19.6
$\xi\Sigma_s$ (Slowing down power)	1.5
$\xi\Sigma_s/\Sigma_a$ (Moderating Ratio)	70
$\rho$ (305°C)(kg/m <sup>3</sup> )	740
$c_p$ (305°C)(J/kJ.°K)	5.7
$k_w$ (305°C)(W/m.°K)	0.56
$\mu_w$ (305°C)(μPa.s)	$92 \times 10^{-6}$

## **CHAPTER 3**

### **Fuel Element Design**

At this point, the reader should be reminded that a reactor core is assembled from a number of fuel elements or assemblies, each of which contains a number of fuel rods or fuel plates. In order to maintain fuel plate position and maintain coolant channel width, the fuel element must contain side plates in addition to fuel plates. Rod type fuel elements or assemblies must contain spacers to maintain rod position.

The general functions and purposes of solid nuclear reactor fuel plates or rods are to maintain a permanent space location of the fissile material in the reactor core, retain fission products and fissile material, resist volume changes due to internal or external stresses (i.e., fission gas pressure) and provide for the optimum transfer of heat with minimal thermal gradients. As discussed in the previous chapter, the reactor design objectives of safety, small size, high power density and maximum refueling lifetime are mainly influenced by the materials of which the fuel plates are composed. However, the design of the fuel plate and the fuel element also has some effect on the ability of the reactor to meet these objectives by influencing neutron economy, ability to remove heat from the reactor, attainable fuel burnup, and ability to withstand transient and off-normal conditions, and in the PWR case, the void coefficient of reactivity (see Figure 3.7 and Appendix C).

Very crudely, reactor core design involves the solution to two problems: that of maintaining controlled criticality in order to produce fission energy; and that of removing the heat released in an orderly, useful fashion. In relatively low-temperature low-power systems, fuel plate and fuel element

design geometry is determined primarily by physics considerations since heat removal is not the major concern. In continuous operation high power reactors, especially those that must operate at high temperatures, fuel element design geometry is determined primarily by heat removal or thermal hydraulics considerations. Since the reactor designs considered for this study are high power density, relatively high temperature power producing reactors, fuel element designs with a high surface to fuel volume ratio should be employed. Of the two basic power reactor fuel element types, those using clad fuel rods and clad fuel plates, plates offer the highest surface to volume ratio. Thus plate type fuel elements have been selected for this study.

### **3.1 Fuel Plate Design**

The structure of the fuel plate (i.e., cladding and fuel material) has a direct influence on the ability of the reactor core in question to obtain high fuel burnup and thus a long refueling lifetime. For the fuel plates considered for this study, the volume of the fuel plates, excluding that of the cladding, is not completely occupied by fuel material. The remaining volume is occupied by plate structural material, which is used to form structures that are more resistant to fission gas swelling with respect to fuel plates occupied by fuel material only. For the LEU case, a fuel structure known as caramel type fuel has been employed. For the HEU reactor cores considered for this study, a lower fuel volume fraction is required in the fuel plates than for the fuel plates of the LEU fueled reactor cores. This lower fuel volume fraction enables the use of a structure known

as a cermet that is highly resistant to fission gas swelling enabling high fuel burnup.

### **3.1.1 LEU Fuel Plate: UO<sub>2</sub> Caramel Fuel**

In recent years, the French have utilized 7% enriched UO<sub>2</sub> caramel type fuel in the Osiris reactor which is located at the Saclay Nuclear Research Center in France. A description of these fuel plates and fuel element has been published by the French as a part of the studies for conversion of research reactor fuels from HEU to LEU.[12] It should be noted that fuel plates similar to the French caramel fuel plates have been used in the Shippingport reactor core II.[18]

The caramel fuel plate used in the Osiris reactor takes the form of two thin sheets of zircaloy cladding enclosing a regular array of rectangular UO<sub>2</sub> platelets or caramels which are separated by small pieces of zircaloy, Figure 3.1.[12] This type of design allows a UO<sub>2</sub> fuel burnup of approximately 60,000MWd/T.[13] Zircaloy separators which are each bonded to the inner surfaces of both zircaloy cladding plates provide an added restraining effect against fission gas swelling. Regular research reactor fuel plates are composed

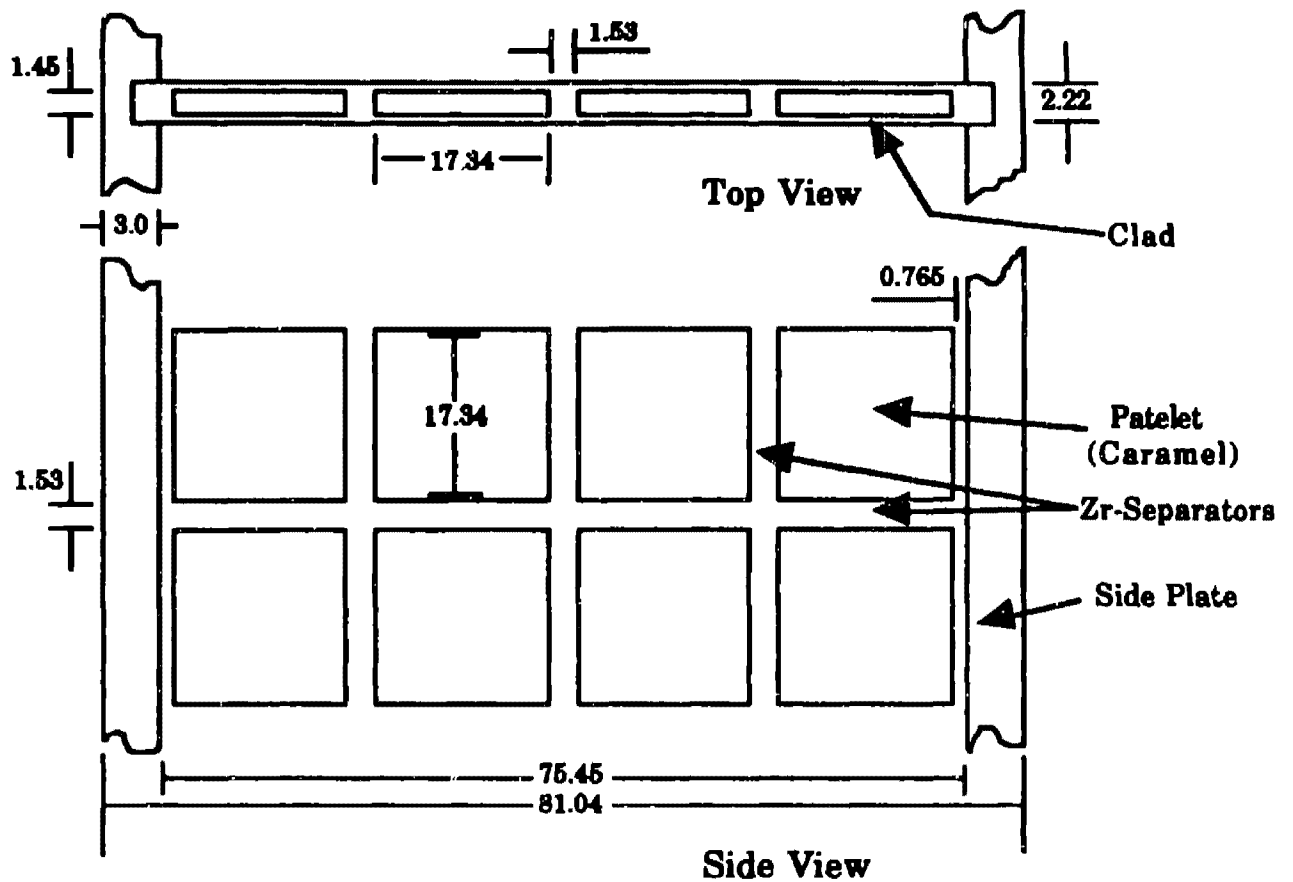


**Figure 3.1. Caramel fuel plate.**

of a continuous sheet of fuel material and consequently are more susceptible to swelling. The platelet and spacer dimensions of the caramel type fuel plate used in the Osiris reactor were employed in the 7% enriched case. For the 20% enriched case, the volume fraction of fuel in the plates was reduced in order to lower core reactivity (see Figure 3.7 which illustrates the fuel element design space). Thus the dimensions of the platelets were reduced while the dimensions of the zircaloy separators were increased. Table 3.1 lists the range of dimensions of the caramel fuel plate structure that have been successfully tested. The dimensions of the platelets and zircaloy spacers used for each LEU fuel plate are listed in Table 3.2.

**Table 3.1 Feasible dimensions of various parts of the caramel fuel plate.[12]**

<b>Dimension</b>	<b>Length (mm)</b>	<b>Width (mm)</b>	<b>Thickness (mm)</b>
<b>Plate</b>	<b>12 - 26</b>	<b>12 - 26</b>	<b>1.4 - 4.0</b>
<b>Platelet</b>	<b>600 - 1800</b>	<b>65 - 200</b>	<b>2.2 - 5.0</b>
<b>Assembly</b>	<b>600 - 1800</b>	<b>65 - 200</b>	<b>—</b>

The caramel fuel plate is well suited for the direct integration of the burnable poison gadolinium oxide with the UO<sub>2</sub> fuel platelets.

Experimental irradiation of caramel type fuel plates containing mixed Gd<sub>2</sub>O<sub>3</sub>-UO<sub>2</sub> oxide has already shown satisfactory behavior.[12]

### **3.1.2 HEU Fuel Plate: UO<sub>2</sub> - Zircaloy Cermet**

It was stated in section 3.1, that the caramel fuel design increased the allowable fuel burnup by increasing the ability of the cladding to resist swelling due to internal fission gas pressure. The cermet fuel design provides cladding restraint as well as providing the fuel with tremendous structural strength, enabling the fuel element to resist fission gas swelling to high fuel burnups. Cermets are dispersions of ceramic fuel particles within a metal matrix. As a result their properties fall between those of metals and ceramics. The value of each property is affected by the relative proportion of the ceramic to the metal. Cermets can be used in fuel elements where the required fuel volume fraction is roughly 50% or less which is true for the HEU fuel plates considered for this study.[20] Figure 3.2 illustrates the cermet fuel plate used in the thick plate HEU reactor

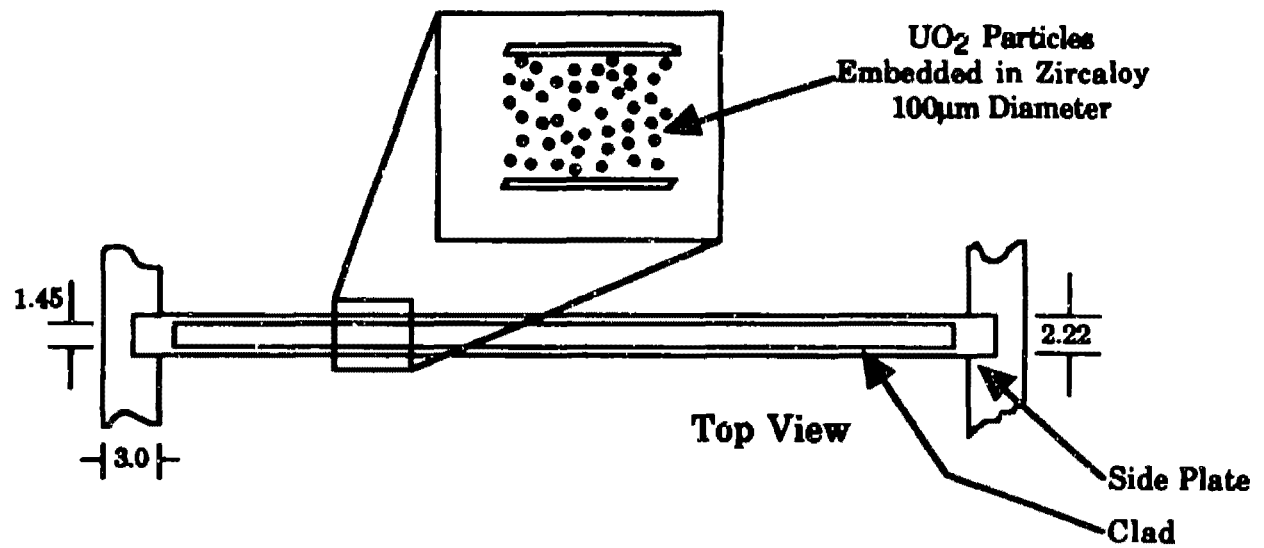


**Figure 3.2. Cermet fuel plate.**

core. Thinner cermet type fuel plates were used to model two other reactor cores as discussed in Section 3.2. Cermet type fuels are also highly corrosion resistant since in the event of cladding failure; only those particles near the inside surface of the cladding will be in contact with the reactor coolant.

The most common example of a cermet is  $UO_2$  dispersed in a stainless steel matrix material. In the proceeding sections, irradiation tests that have been performed on these cermets will be cited. However, stainless steel is not an ideal matrix material, since it has a relatively high macroscopic neutron absorption cross-section ( $\Sigma_a$ ) of  $258cm^{-1}$ . The relatively large volume fraction of the stainless steel results in large parasitic neutron losses. The characteristics of the ideal cladding material described in Section 2.2.1 also apply to the ideal matrix material. As a result, it was reasonably assumed that zircaloy-4, the material selected for use as a cladding, could replace the volume occupied by the stainless steel in the cited tests without reducing the attainable fuel burnup.[10] Since the large volume of matrix or structural material present in cermet type fuels,

regardless of the particular material, will always result in parasitic neutron losses, cermets have been studied primarily for military reactors rather than for commercial type reactors using approximately 3% enriched  $\text{UO}_2$ . [16] As stated earlier, most military reactors have employed HEU. Thus neutron economy was not of concern as it is in LEU commercial reactors.

The attainable fuel burnup of a cermet fuel is directly related to the volume fraction of structural material present in the fuel plate. As the volume fraction of the structural material is increased the attainable fuel burnup also increases. The following irradiation tests were used to obtain a reasonable estimate of attainable fuel burnup as a function of  $\text{UO}_2$  volume fraction in the fuel. This partial estimate is illustrated in Figure 3.3.

- 1) Frost(1964) tested cermets containing 55 wt% (50vol%)  $\text{UO}_2$  in stainless steel. The specimens survived, irradiations at surface temperatures of 625°C to a burnup of 10% without failure.[3]
- 2) A specimen containing 26wt% (21vol.%)  $\text{UO}_2$  survived irradiation to a burnup of 70at% of the uranium at fuel temperatures of about 550°C without failure (Richt and Shaffer, 1963).[3]

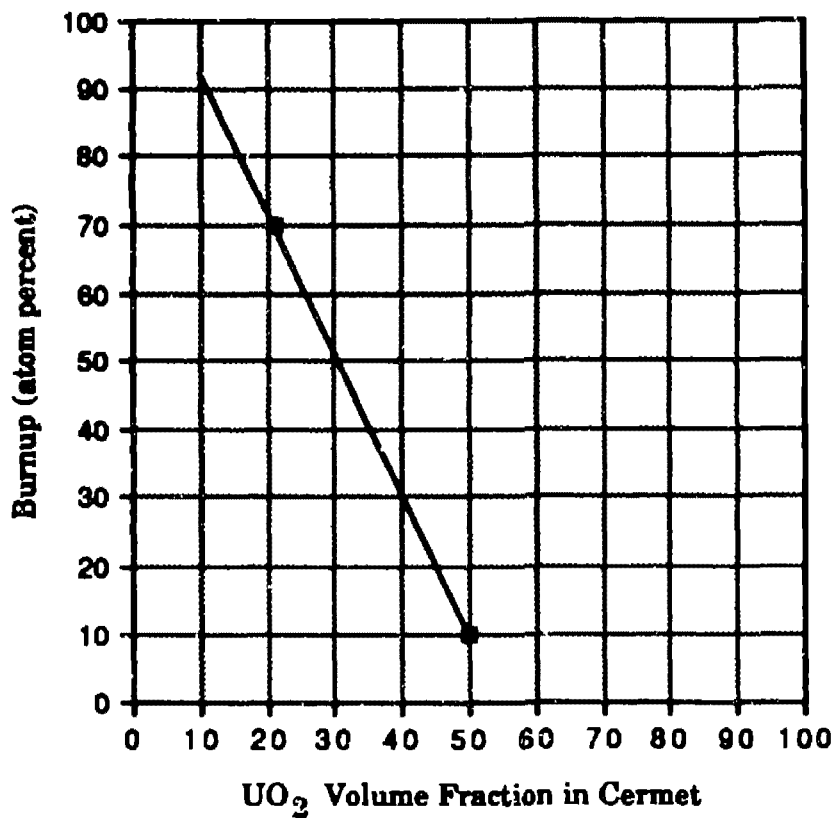


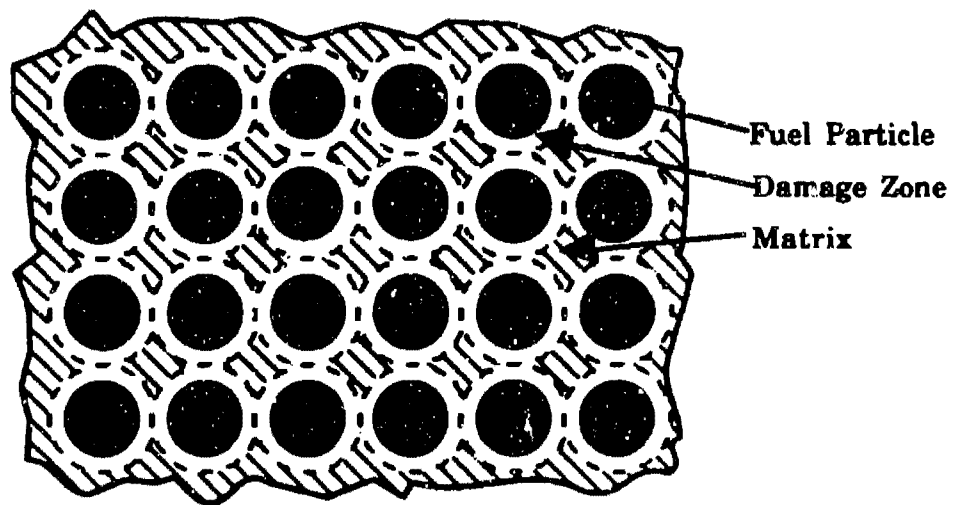
**Figure 3.3. Partial estimate of burnup Vs. UO<sub>2</sub> volume fraction.**

The design objectives to be achieved by an ideal cermet dispersion system are summarized as follows,

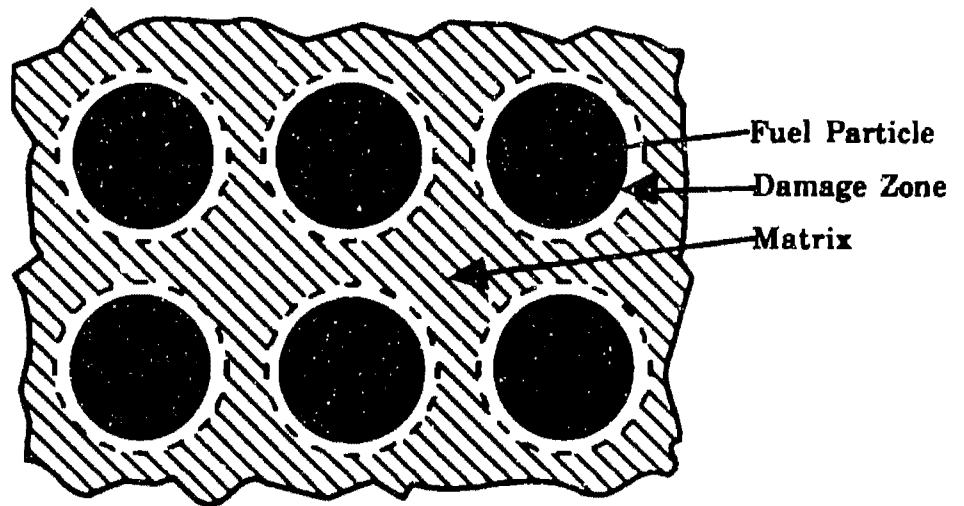
- 1) Dispersed particle size large compared to the fission product range.
- 2) A continuous phase of matrix metal of maximum possible volume fraction.
- 3) Uniform dispersion of particles in a real matrix.

As a cermet fuel element is irradiated, damage to the fuel structure is caused by a combination of the static and dynamic effects of the fission products. At low fuel burnups the major damaging effect is due primarily to the dynamic properties of the fission fragments (i.e., fission product recoil in the matrix). At high fuel burnups where higher concentrations of fission products are approached the major damaging effect is due to the static properties of the fission products (i.e., fission gas pressure).

In order to combat damage due the dynamic properties of fission fragments, fuel particle diameter in a properly designed cermet should be large compared to the range of the fission fragments. Thus fission products released from the fuel during reactor operation are confined to narrow regions or damage zones surrounding the fuel particles, while most damage is concentrated in the fuel particles. Thus an undamaged fission product free region of matrix metal exists around around each zone of damage which surrounds each fuel particle. This objective cannot be achieved in a homogeneous fissile metal or two phase alloy systems where both the fuel bearing compound and matrix may contain fissile atoms. For a given volume fraction of fuel, the volume of damaged matrix is proportional to the surface area of the particles. Thus the fraction of the matrix subject to recoil damage can be minimized by the use of smooth, spherical particles as large as can be tolerated. Most fuels designed to take advantage of the cermet dispersion principle have particles of a least 100 $\mu$ m diameter.[20] Schematic cross sections of cermet dispersant systems are shown in Figure 3.4. The dispersed particles are assumed to be spheres in a cubically close-packed array. Two particle sizes are shown with a spherical zone of damaged matrix metal surrounding each particle. Figure 3.4a illustrates a poorly designed cermet where damage zones



a



b

**Figure 3.4.** Schematic cross-sections of cermet dispersion systems.

overlap. Figure 3.4b illustrates a properly designed cermet where damage zones do not overlap. Thus a continuous web of undamaged matrix material exists in the fuel plate providing good internal strength.

With increased fuel burnup, irradiation induced swelling arises due to growth of the  $UO_2$  particles. This is caused by the static accumulation of fission products and the partial escape of fission gases from the  $UO_2$  fuel. The later effect is the most significant. A gas filled void is created around

the fuel particles which pressurizes the matrix shell causing it to expand as a thick-walled vessel under pressure. Thus, the matrix swelling that can be allowed will determine the maximum fuel burnup. Swelling limits are determined on the basis of allowable dimensional changes or a maximum strain based on reduced ductility limit of the neutron embrittled matrix.[18] In effect, the matrix material acts as the structural material in the fuel element. The cermet of Figure 3.4b is more resistant to swelling than the cermet of Figure 3.4a due to its continuous web of undamaged matrix material.

In order for the design principles described above to be effective, the particles must be uniformly dispersed throughout a matrix that predominates in volume.[20] If the particles are not uniformly dispersed some fission product damage zones will overlap thus weakening the matrix. If the fuel material predominates in volume, it remains possible to design a cermet system in which fission product damage zones do not overlap. However, in this case the structural strength of the matrix material is significantly reduced and the susceptibility to swelling approaches that of a plate type fuel element utilizing a continuous sheet of  $UO_2$  fuel.

## **3.2 Fuel Element Design**

Reactor cores fueled with 7%, 20% and 97.3% enriched uranium were modeled using fuel element designs adopted from the original caramel fuel element design of the Osiris reactor. Its geometry is similar to that of current UAI MTR-type fuel elements used in some research reactors.

**Figure 3.5 illustrates the 17 plate caramel fuel element used in the 7% enriched core. Figure 3.6 shows how these fuel elements fit together as building blocks to form a reactor core. As in the case of the Osiris reactor and many other research reactors using plate type fuel, the intra-element spacing is set at 1mm.**

**In order to facilitate the reactor core modeling process the following modifications were made to the original caramel fuel element,**

- 1) Fuel element end spacings were decreased in order that the intra-element gap and the end-spacing of two adjacent fuel elements will equal the width of a water channel.**
  
- 2) To allow for a square lattice pitch, the width of the fuel plates was increased.**

**These modifications were applied to identical fuel element geometries used for the reactors fueled with 20% enriched caramel type fuel and 97.3% enriched cermet type fuel respectively.**

**For the HEU case, due to high reactor power density and thus relatively high fuel temperatures, two additional reactor cores were modeled consisting of thinner ATR-type fuel plates (Advanced Test Reactor operated by the Idaho National Engineering Laboratory). Use of a thinner plate in the high power density core will reduce the relatively high fuel centerline temperature by increasing the heat transfer area. The thin plate HEU reactor cases are described below,**

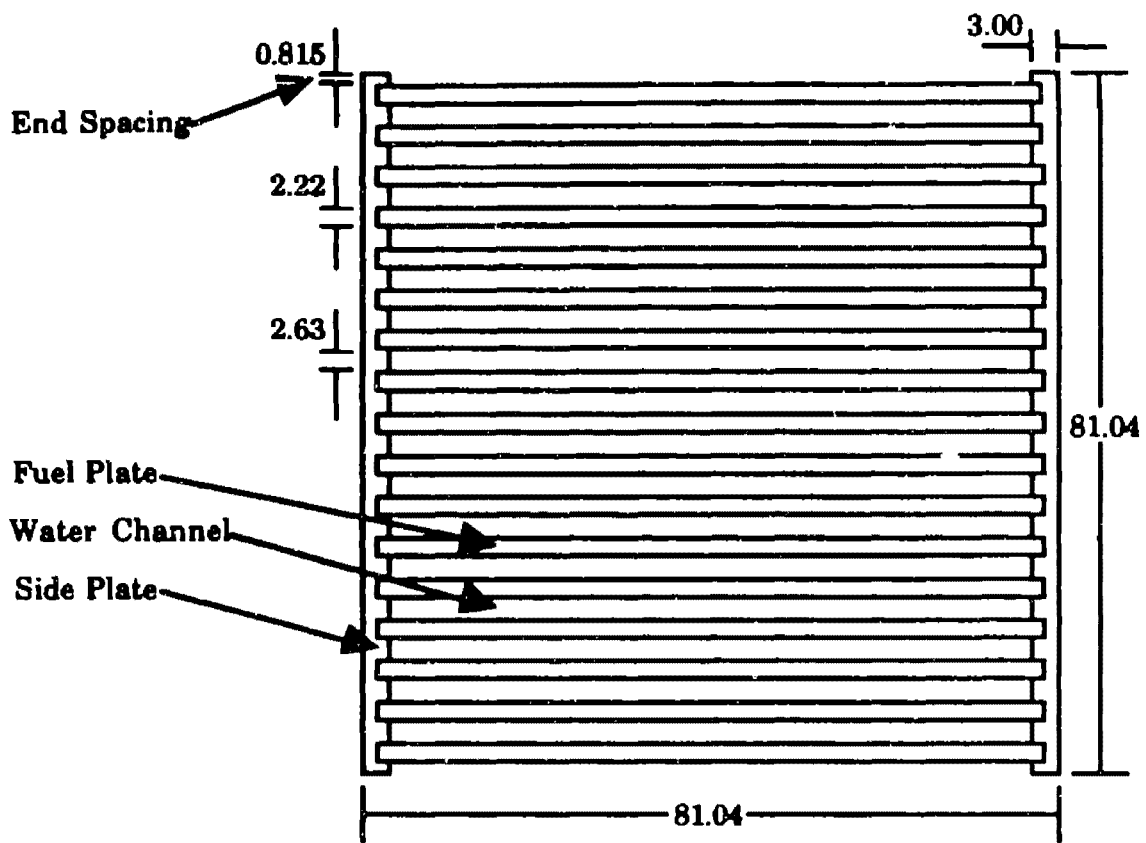


**Figure 3.5.** Thick plate fuel element design.

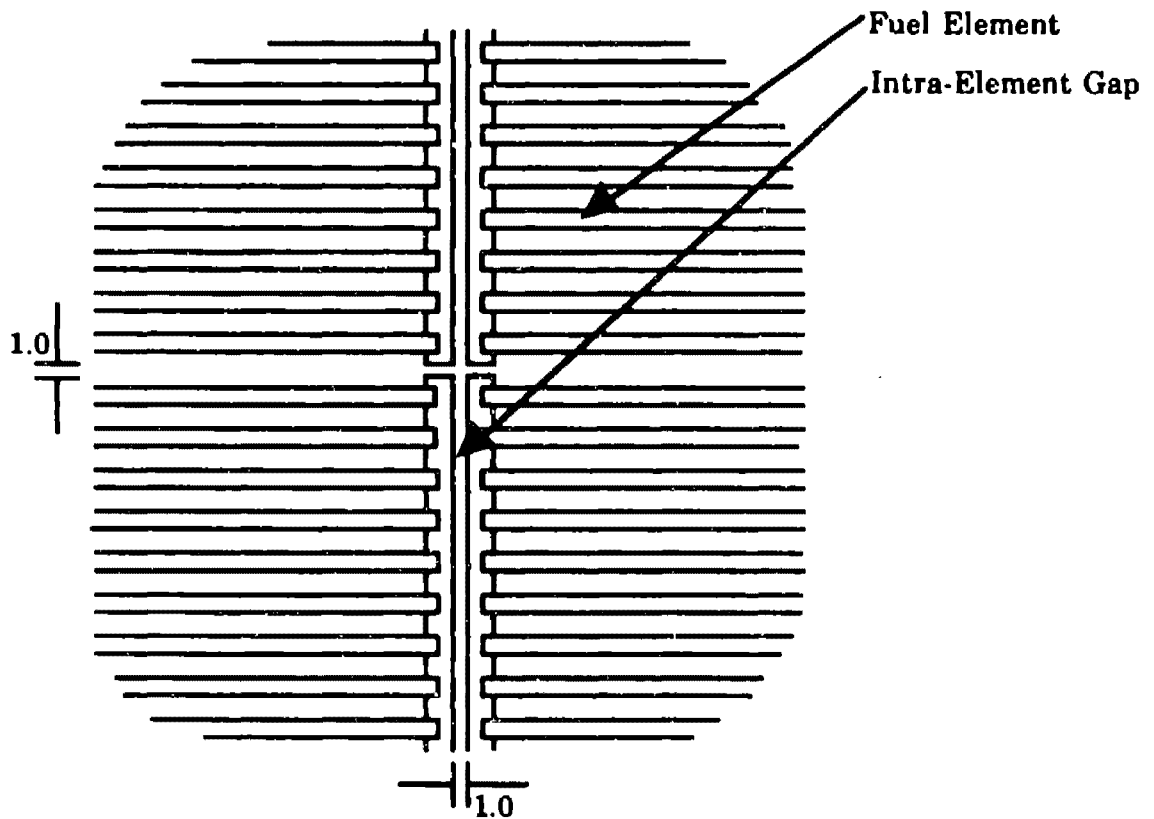


**Figure 3.6.** Assemblage of reactor fuel elements.

- 1) In the first thin plate reactor core, the coolant channel thickness (2.63mm) remained as it is in thick plate fuel element design of Figure 3.5, increasing the water/metal ratio.
- 2) In the second thin plate reactor core, the coolant channel thickness was also decreased in order that the water/metal ratio remain the same.

The modifications that were applied to the thick plate fuel elements described above were also applied to the thin plate fuel elements. Also, the number of fuel plates in the thin plate fuel element designs were increased in order that the thin plate fuel element lattice dimensions be close to the thick plate fuel element lattice dimensions. Use of larger fuel elements reduces the ratio of structural material (i.e., side plates) to fuel material in the core and thus decreases parasitic neutron losses. All relevant dimensions for the five reactor cores considered for this study are summarized in Table 3.2.

As stated earlier, the design of a reactor fuel element is a balance between neutronics considerations and thermal hydraulic considerations, where for the high power density, relatively high temperature reactor, thermal-hydraulics considerations dominate. Figure 3.7 illustrates the design space in which neutronic and thermal hydraulics are compatible. If the fuel plate thickness (i.e., thin plate thickness) is assumed to be constant, a water/metal ratio exceeding  $r_{\max}$  results in a positive void coefficient of reactivity or the overmoderation of the reactor. Also, increasing the water/metal ratio also reduces the heat transfer area to the

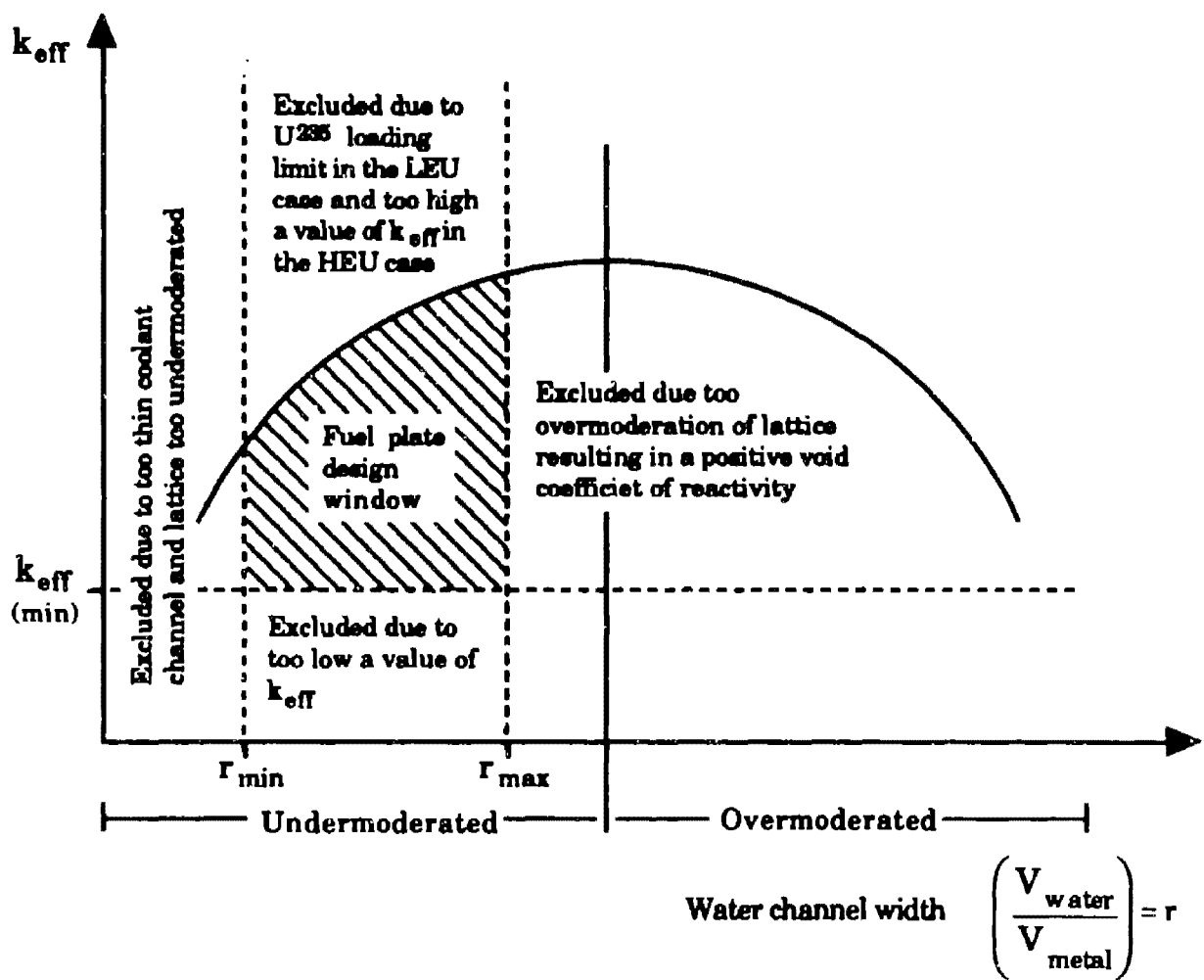


Figure 3.7. Fuel element design window.

coolant. In Figure 3.7, the design space is not extended to the boundary between the undermoderated and overmoderated reactors since reactors that are undermoderated and close to this boundary can become overmoderated in the event of a sudden coolant temperature decrease. A water/metal ratio below  $r_{\min}$  is excluded since the thermal hydraulic wetted perimeter becomes too large requiring excessive pumping power. Also in this case  $k_{eff}$  can be significantly reduced due to too low neutron moderation. The above considerations apply to the design of thin plate HEU reactor case 1.

**For the second thin plate HEU reactor case, plate and coolant channel dimensions were decreased in similar proportions resulting in a constant water/metal ratio. This, however, increases the homogeneity of the reactor core and reduces  $k_{eff}$ . This can be compensated for by increasing the  $UO_2$  volume fraction in the cermet fuel. A disadvantage to decreasing the coolant channel thickness, as stated earlier, is the increase in the wetted perimeter which increases required pumping power. Thin fuel plates provide the advantage of increased heat transfer area and thus lower fuel centerline temperatures. However factors exist which prohibit fuel plates from being made extremely thin. Some of these are listed below**

- 1) The ratio of cladding to core becomes larger as the fuel plate thickness decreases, leading to larger parasitic neutron losses.**
- 2) Thin elements have less rigidity and are more difficult to support. They are also more prone to damage resulting from coolant flow induced vibrations.**
- 3) Coolant passages become smaller, leading to greater possibility of obstruction of the passage, greater pressure drops and greater pumping power.**

**These considerations as illustrated by Figure 3.7 form the basis for the reactor designs which will be discussed in the proceeding chapters.**

**Chapters 1, 2 and 3 have covered the selection of the reactor operating conditions and limits, materials and fuel element design. Chapter 4 will**

**cover the methods used to design and analyse each reactor core considered while Chapter 5 presents the results of the analysis.**

**Table 3.2. Fuel element characteristics.**

	(Caramel Type) Thick Plate Regular channel	(ATR Type) Thin Plate Thin channel	
<b><u>PLATE</u></b>			
Plate thickness(mm)	2.220	1.270	1.270
Water Channel(mm)	2.630	1.372	1.120
Cladding material	Zircaloy-4	Zircaloy-4	Zircaloy-4
Cladding thickness(mm)	0.385	0.385	0.385
<b><u>FISSILE PART</u></b>			
Fuel Material	UO <sub>2</sub> /Zircaloy-4	UO <sub>2</sub> /Zircaloy-4	UO <sub>2</sub> /Zircaloy-4
Enrichment	7% - 97.3%	97.3%	97.3%
UO <sub>2</sub> density(g/cm <sup>3</sup> )	10.3	10.3	10.3
Thickness(mm)	1.45	0.5	0.5
Active width(mm)	75.45	74.90	74.26
Platelet(caramel)(mm)	17.34	N.A.	N.A.
Spacing between platelets(mm)		1.53	N.A. N.A.
<b><u>SIDE PLATES</u></b>			
Material	Zircaloy-4	Zircaloy-4	Zircaloy-4
Thickness(mm)	3.0	3.0	3.0
Width(mm)	81.04	80.90	80.26
<b><u>FUEL ELEMENT</u></b>			
Number of plates per element	17	31	35
Cross-section(mm)	(81.04x81.04)	(80.90x80.90)	(80.26x80.26)
Lattice pitch(mm)	(82.04x82.04)	(81.90x81.90)	(81.26x81.26)

\* N.A. - Not Applicable

## **CHAPTER 4**

### **Analytical Methods**

In Chapter 1, certain operating characteristics and design specifications for a modern SSN reactor were selected as derived from the performance requirements of a modern SSN. Chapter 2 outlined the basis for which the reactor fuel, cladding, coolant and reactivity control material (burnable poison) were selected in order to meet the required reactor operating characteristics and design specifications. Chapter 3 described the reactor fuel element designs chosen for this study, which are constructed based on the required reactor operating characteristics selected in Chapter 1. This present chapter is divided into two sections which cover the reactor physics and the thermal hydraulic analysis methods used in this study. However, as stated in Chapter 1, thermal-hydraulics considerations are assumed not to be limiting for the reactor designs modeled in this study. Thus the design effort focuses on the reactor physics (i.e., the adjustment of the reactor design to satisfy all relevant reactor physics criteria). Following the reactor physics analysis, a simplified thermal-hydraulic analysis is however included to verify that fuel element temperatures are within acceptable bounds and that the required coolant flow rates needed to remove heat are practical. All analytical methods employed in this study are covered in this chapter.

Table 4.1 summarizes the reactor designs considered for this study. Three reactor cores fueled with 7%, 20%, and 97.3% enriched uranium are considered. For the HEU case (97.3%), two additional reactor core designs are considered which use fuel containing thinner plates. As stated in Chapter 3, a thinner fuel plate reduces the required fuel center-line

**Table 4.1. Reactor designs.**

<b>Design</b>	<b>Enrichment</b>	<b>Fuel Type</b>	<b>Fuel Element Design</b>
<b>Core 1</b>	<b>7%</b>	<b>Caramel</b>	<b>Thick Plate/Thick Channel</b>
<b>Core 2</b>	<b>20%</b>	<b>Caramel</b>	<b>Thick Plate/Thick Channel</b>
<b>Core 3</b>	<b>97.3%</b>	<b>Cermet</b>	<b>Thick Plate/Thick Channel</b>
<b>Core 4</b>	<b>97.3%</b>	<b>Cermet</b>	<b>Thin Plate/Thick Channel</b>
<b>Core 5</b>	<b>97.3%</b>	<b>Cermet</b>	<b>Thin Plate/Thin Channel</b>

operating temperature. For one thin plate design, the coolant channel thickness is reduced in order to examine the effect of water/metal ratio on reactor physics and safety parameters.

Table 4.2 summarizes the design specifications and operating limits that have thus far been selected for each reactor core listed in Table 4.1.

**Table 4.2. Reactor design data.**

<b>Design Parameter</b>	<b>Symbol</b>	<b>Status</b>	<b>Constraint</b>
Total Core Power	Q	Known	50MWth Fixed
Maximum Power Density	$q'''_{max}$	Unknown	$q'''_{max} \leq 100\text{kW/L}$ (7%, 20% Cases) $q'''_{max} \leq 1000\text{kW/L}$ (97.3% Case)
Average Power Density	$q'''_{ave,r}$	Unknown	$q'''_{ave,r} \geq 50\text{kW/L}$
Power Peaking Factor	$\Omega_T$	Known	2.5
Operating Lifetime	$\Delta t$	Known	600FPD (7% case) 1200 FPD (20%, 97.3% cases)
Enrichment	e	Known	7%, 20%, 97.3%
Number Densities ( $\text{UO}_2$ , $\text{Gd}_2\text{O}_3$ )	N	Unknown (7% case) Known (20%, 97.3% cases)	—
Volume Percents ( $\text{UO}_2$ , $\text{Gd}_2\text{O}_3$ , Zr-4)	Vol%	Known (7% case) Unknown (20%, 97.3% cases)	85% - 50% (7%, 20% Cases) $\leq 50\%$ (97.3% Case)
Core Radius	R	Unknown	H/R = 2.5
Core Height	H	Unknown	H/R = 2.5
Buckling	$B^2$	Unknown	—
Control Swing	$\Delta k_{eff}$	Unknown	1.04 - 1.24
$k_{eff} = f(t)$	$k_{eff}(t)$	Unknown	—
Burnup	BU	Unknown	$\leq 60000\text{MWd/T}$ (7%, 20% Cases) See Figure 3.3 (97.3% case)

## **4.1 Reactor Physics Analysis**

For the comparative purposes of this study, a simplified one-dimensional steady-state overall core reactor physics calculation is used to model the reactor cores listed in Table 4.1. With this model, the spatial dependence of neutron flux and fuel depletion (burnup) are neglected. (The consumption of fuel is treated as constant in all locations of the reactor core. In an actual reactor, the neutron flux is greatest in the center of the core. Thus fuel depletion is also greatest in the center.) This model also does not simulate the effects of control rod motion or startup, shutdown and transient behavior.

For the one-dimensional overall core model the entire reactor core is characterized by each reactor physics parameter employed. For this analysis, these parameters are,

- 1) Uranium enrichment ( $e$ ).
- 2) Relative proportions or volume percents of  $\text{UO}_2$  fuel, Zr-4 structural material and  $\text{Gd}_2\text{O}_3$  burnable poison in the fuel meat  $\text{Vol}\%_m(\text{UO}_2, \text{Zr-4}, \text{Gd}_2\text{O}_3)$ . The subscript ( $m$ ) refers to the volume fraction of the particular material in the fuel meat. (Note that volume percents are denoted by  $\text{Vol}\%_x(I)$  while a volume fractions are denoted by  $\text{Vol}_x(I)$ . The subscript,  $x$ , designates the volume of concern and  $I$  refers to the material.
- 3) Total operating power ( $Q$ ).

- 4) Power density ( $q'''_{ave,r}$ ) where the subscript (r) refers to the reflected reactor. A subscript (u) designates an unreflected reactor core. The specification of  $q'''_{ave,r}$  sets the reactor core volume (V) by the following equation,

$$q'''_{ave,r} = \frac{Q}{V_{core}} \quad (4.1)$$

From the volume  $V_{core}$ , the geometric buckling ( $B^2$ ) or neutron leakage term is determined. Thus  $q'''_{ave,r}$  and  $B^2$  are directly dependent and will be considered as one design variable  $q'''_{ave,r} \setminus B^2$  for purposes of this study.

- 5) Refueling interval ( $t_{rf}$ ).
- 6) Fuel depletion or burnup (BU).
- 7) The neutron multiplication,  $k_{eff} = f(t)$ , over the reactor refueling lifetime.
- 8) The control swing or range of values of  $k_{eff}$  over the refueling lifetime of the reactor ( $\Delta k_{eff}$ ).

With items 1 through 8, all important information about the steady state operation of a nuclear reactor can be determined. A three-dimensional steady state analysis can provide space dependent burnup data and hence, a better estimate of the end-of-cycle core materials inventory. It would also

provide a more accurate estimation of  $k_{\text{eff}} = f(t)$  and  $\Delta k_{\text{eff}}$ . However, as stated in Chapter 1, it was decided that such refinement is unnecessary for the comparative purposes of this study.

Figure 4.1 illustrates the relationship and interdependence of each of these parameters which together describe the operating reactor system. A certain percentage of the composition of this system is fuel material and a certain percentage is non fuel material. The fuel is consumed in a nuclear reaction to produce power for an operating time, after which the fuel has reached a burnup level (i.e., a certain percentage of fuel has been consumed). At any particular time during the operating time span the system has excess reactivity or excess capability to sustain the power producing reaction. This excess capability changes over the operating time. The range of excess reactivity over the operating time determines the amount of control capability that must be provided to this system. Some of this capability is supplied the burnable poison ( $\text{Gd}_2\text{O}_3$ ), a non fuel material. An increase in the volume of control material in the system is accompanied by a decrease in the volume of fuel material in the system. Thus as shown by this figure, a change in any one of these parameters affects all the other parameters, and thus the overall operation of the reactor system.

In Figure 4.1, to the left of the dashed line are the reactor physics parameters that have been fixed according to the discussion of Chapter 1. To the right of the dashed line are the reactor physics parameters which have not been fixed but are variable. These variable parameters are interdependent and are constrained by the limits specified in Table 4.2. Thus the design window shown in Figure 4.2 for a reactor core of fixed total operating power ( $Q$ ), uranium enrichment ( $e$ ), and refueling lifetime ( $t_{\text{rf}}$ ) is formed.

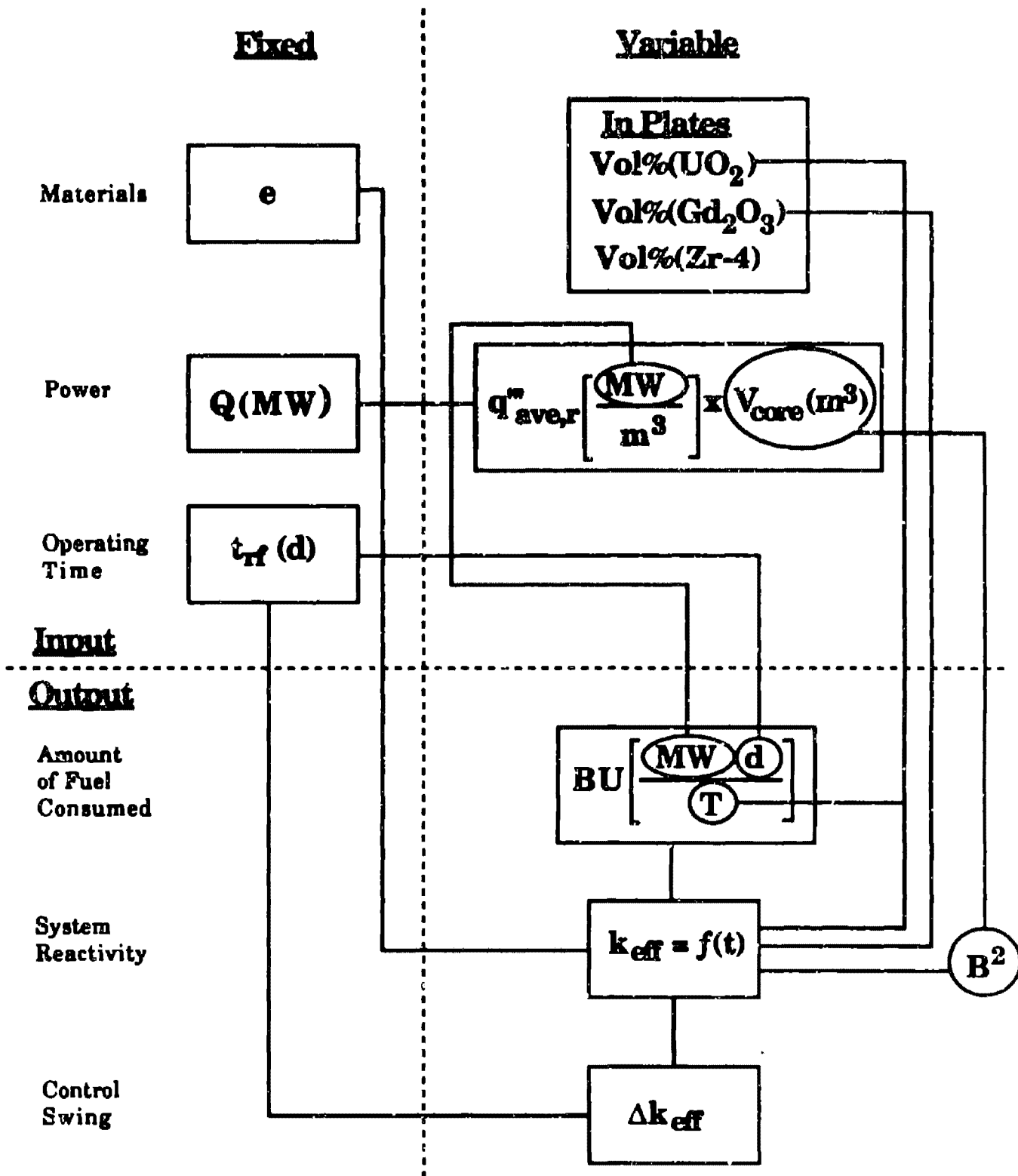


Figure 4.1. Interdependence of reactor design parameters.

Design space for reactor core of fixed  
 Uranium enrichment ( $e$ ),  
 Refueling time ( $t_{rf}$ ),  
 Total power ( $Q$ )

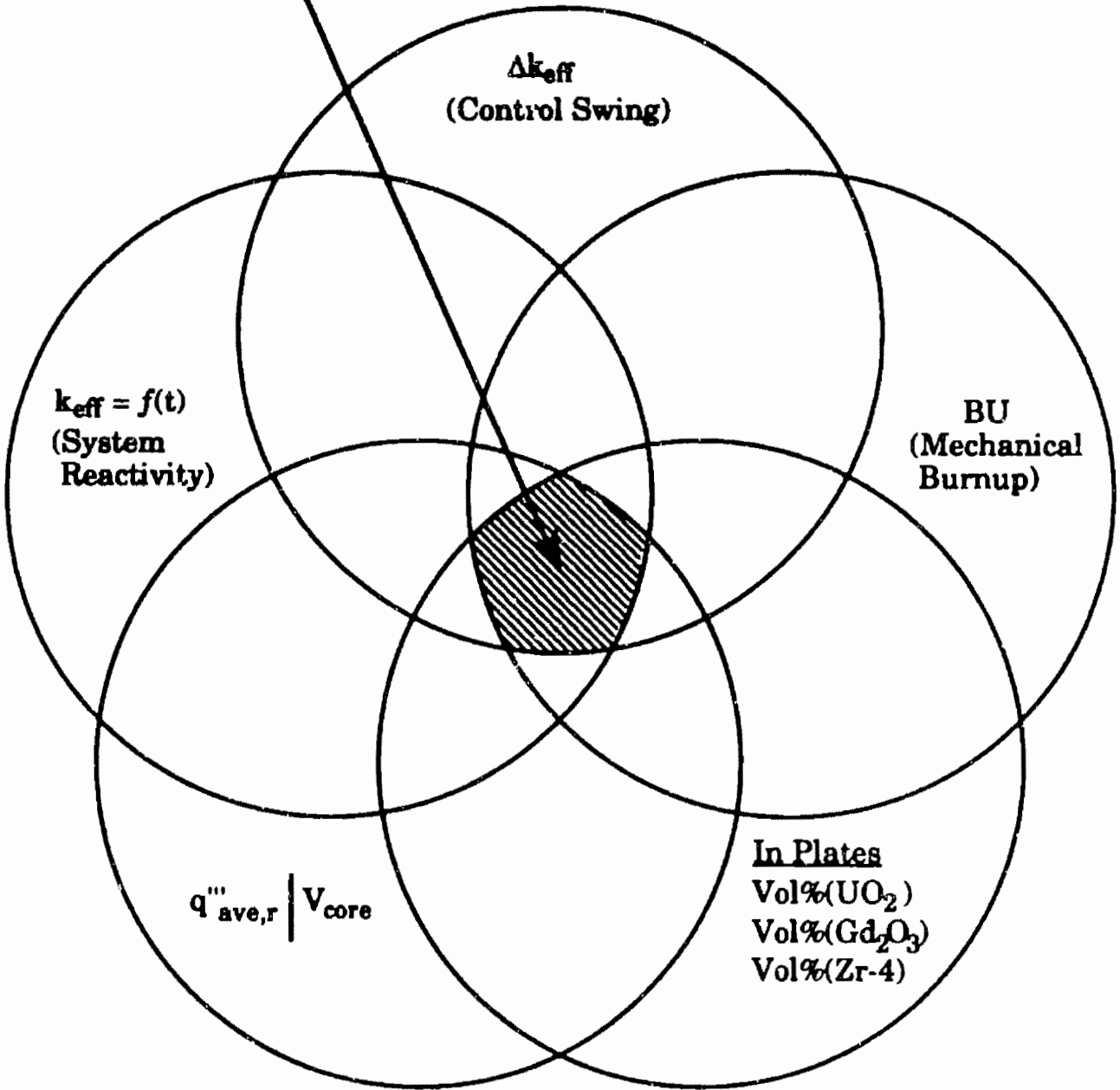


Figure 4.2. Design space.

In this figure each circle represents all possible values of each variable parameter. The design space or region of overlap of the circles represents the acceptable range of values of each variable parameter in combination with the range of acceptable values of the other variable parameters. Thus each reactor core must be designed in order that the value of each of these parameters lie in the design space. One can see by inspection of Figures 4.1 and 4.2 that the one-dimensional calculation used for this study requires iteration in order to adjust the reactor physics design parameters to lie in the design space.

To perform these iterative 1-D calculations the EPRI-Cell code is employed.[9] As shown in Figure 4.1, the parameters above the horizontal dashed line are required as input to EPRI-Cell while the parameters below the dashed line are produced in the EPRI-Cell output. Thus the values for  $q'''_{ave,r}/B^2$  and  $Vol\%_m(UO_2, Zr-4, Gd_2O_3)$  are varied in the EPRI-Cell input to cause the values of  $BU$ ,  $k_{eff} = f(t)$  and  $\Delta k_{eff}$  to satisfy the constraints listed in Table 4.2. At this point the value of  $q'''_{ave,r}/B^2$ ,  $Vol\%_m(UO_2, Zr-4, Gd_2O_3)$ ,  $BU$ ,  $k_{eff}$  and  $\Delta k_{eff}$  will simultaneously lie in the design space of Figure 4.2.

For each core design, Figure 4.3 illustrates the variable input design parameters (physical reactor design adjustments) of  $q'''_{ave,r}/B^2$  and  $Vol\%_m(UO_2, Zr-4, Gd_2O_3)$  with regard to the complete core system. The variable input design parameters (physical characteristics which are variable) are contained in circles while the physical characteristics which are constant (physical characteristics which are not design variables) are contained in rectangles. The physical basis for the variable input parameters  $q'''_{ave,r}/B^2$  and  $Vol\%_m(UO_2, Zr-4, Gd_2O_3)$  for each reactor core design is discussed below.

## Core (1)

For reactor core design 1 which utilizes 7% enriched caramel type fuel, it is desirable for the  $\text{UO}_2$  volume percent in the fuel meat to be as large as possible in order to maximize available reactivity. Thus for this core, the  $\text{UO}_2/\text{Zr-4}$  volume percent ratio in the fuel meat is fixed at what it is in the original caramel fuel design. Note that the Zr-4 structural material in the fuel meat is structural material as described in Chapter 3. Also, for this LEU design, the reactivity control material ( $\text{Gd}_2\text{O}_3$ ) is mixed directly with the  $\text{UO}_2$  fuel material. Thus the variable input design parameters as illustrated by Figure 4.3a are,

- 1) ratio of volume percents of  $\text{UO}_2/\text{Gd}_2\text{O}_3$ ,  $\text{Vol}\%_f(\text{UO}_2, \text{Gd}_2\text{O}_3)$  within the fuel (i.e., the original dimensions of the fuel platelets of the caramel fuel design); [The subscript (f) refers to the volume percent of the particular material in the fuel (i.e., in this case the fuel material is a mixture of  $\text{UO}_2$  and  $\text{Gd}_2\text{O}_3$ .)]
  
- 2) the values of  $q'''_{\text{ave},r} \backslash B^2$  which are varied by a changes in the core volume ( $V_{\text{core}}$ ). [Note that with each change in the core volume, the height to radius ratio is constant as stated in table 4.2. This is discussed in detail in section 4.1.2.6.]

These parameters are adjusted in the EPRI-Cell input to cause the values of  $\text{BU}$ ,  $k_{\text{eff}} = f(t)$  and  $\Delta k_{\text{eff}}$  to satisfy the constraints listed in Table 4.2.

### Cores (2,3,4,5)

For reactor core designs 2,3,4 and 5, the  $\text{UO}_2$  volume percent in the fuel plate must be lower than that of core 1 in order to reduce excess reactivity to a controllable level. Thus for this core, the  $\text{UO}_2/\text{Zr-4}$  volume percent ratio in the fuel meat is a variable input design parameter. As discussed in Chapter 3, a lumped gadolinia distribution was employed for these cores. For these cores the thickness of the  $\text{Gd}_2\text{O}_3$  plate lump was varied. Note that as the lump thickness decreases, the thickness of the cladding which covers the lump must increase proportionally. This is discussed in detail in Section 4.1.2.3. Thus the variable input design parameters for these cores, as illustrated by Figure 4.3b are,

- 1) ratio of volume percent of  $\text{UO}_2/\text{Zr-4}$ ,  $\text{Vol}\%_m(\text{UO}_2, \text{Zr-4})$  within the fuel plates. For the 20% enriched case, this is the ratio of the volume of the fuel platelets to the volume occupied by the zircaloy spacers. [For the 97.3% enriched cases, this is the ratio of fuel particle volume to the volume of the cermet matrix material. This is discussed in detail in Section 4.1.2.4.]
- 2) the thickness of the  $\text{Gd}_2\text{O}_3$  plate lump,  $\text{Vol}\%(\text{Gd}_2\text{O}_3)$ . A change in the thickness of this lump changes the relative proportions of  $\text{Gd}_2\text{O}_3$  to the  $\text{UO}_2$  and Zr-4 in the fuel meat.
- 3) the values of  $q'''_{ave,r}/B^2$  which are varied by a changes in  $V_{core}$ .

These parameters are adjusted in the EPRI-Cell input to cause the values of  $\text{BU}$ ,  $k_{eff} = f(t)$  and  $\Delta k_{eff}$  to satisfy the constraints listed in Table 4.2.

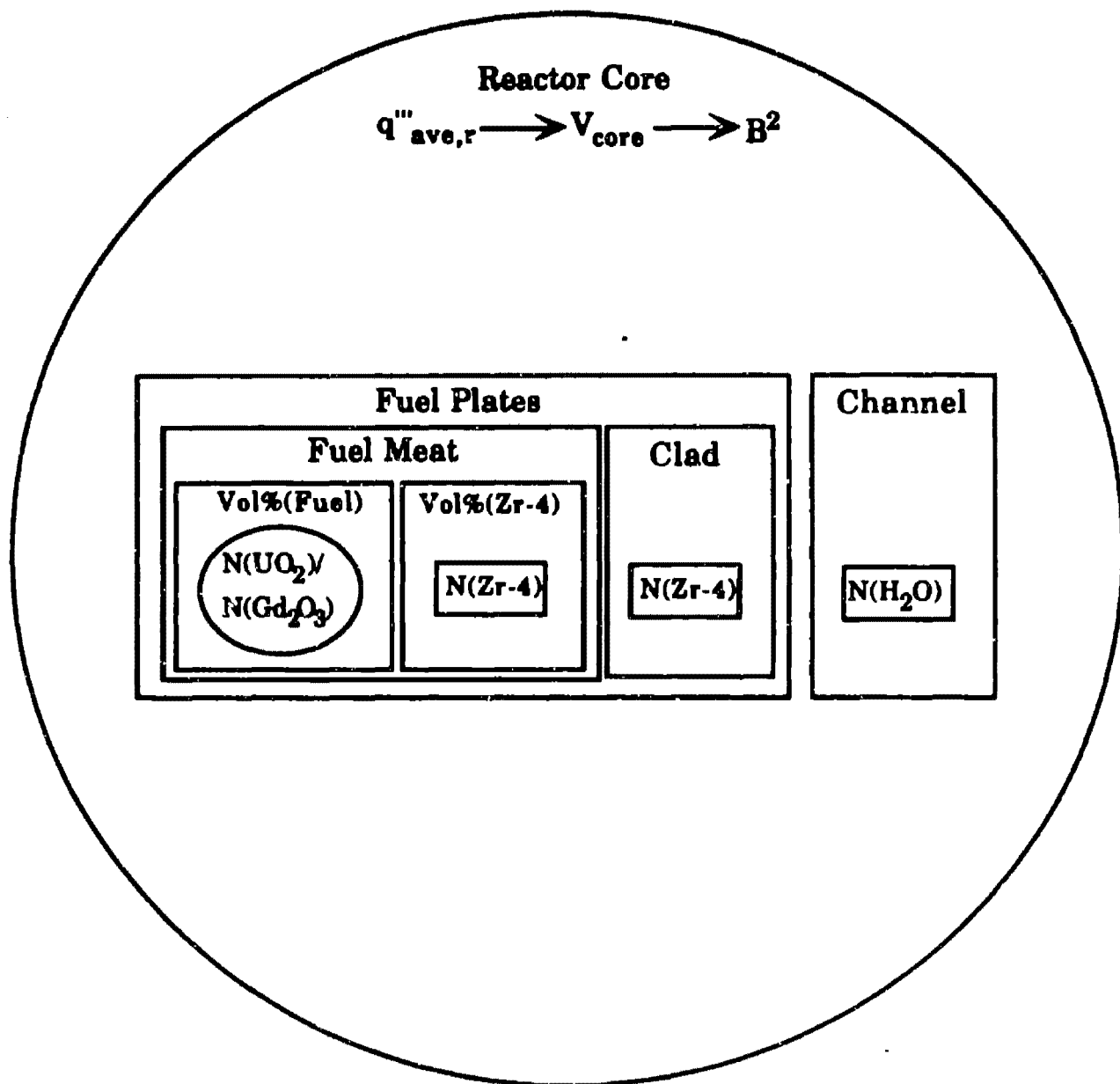


**Figure 4.3a.** Design variations for reactor core (1).

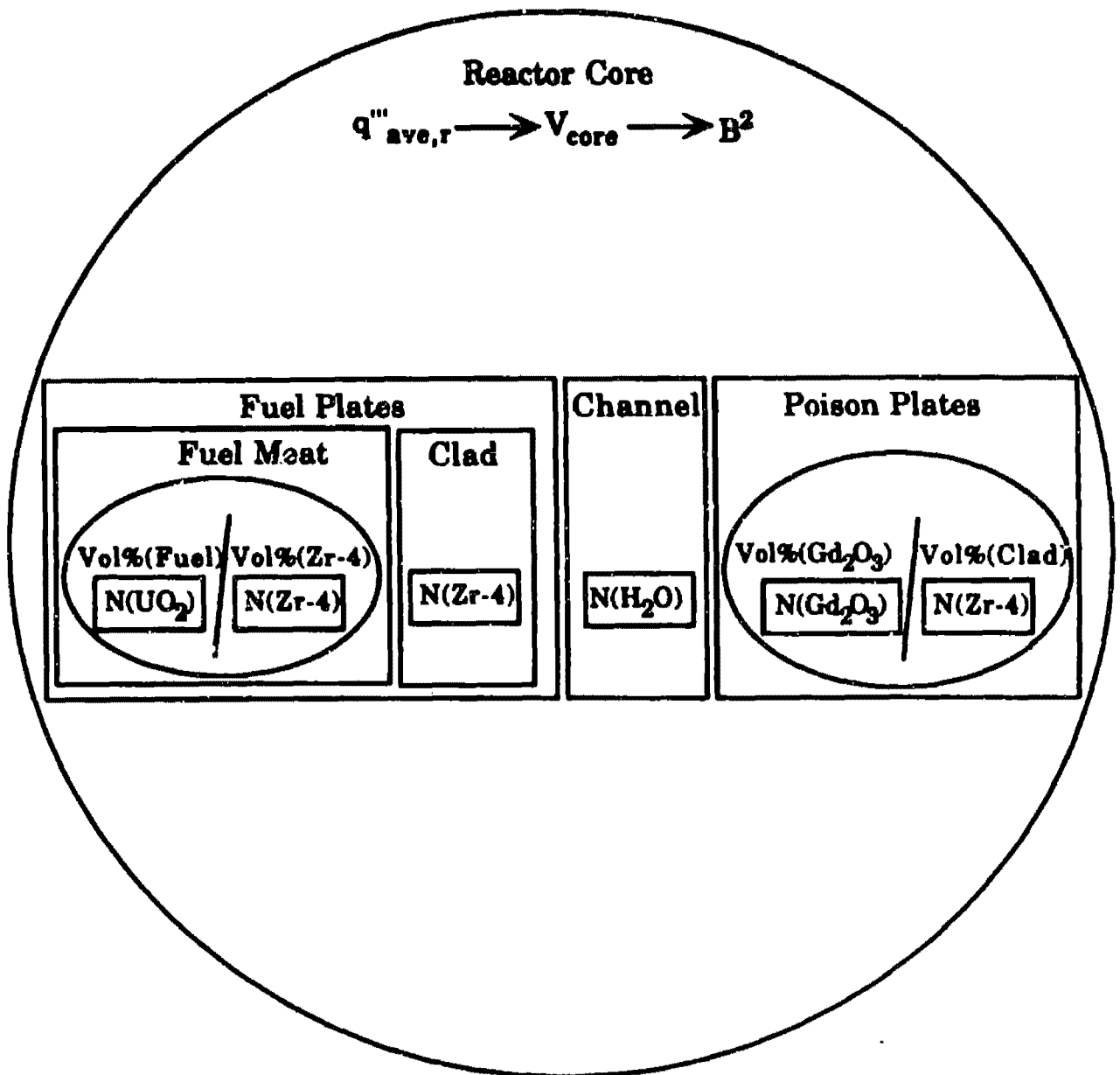


**Figure 4.3b.** Design variations for reactor cores (2,3,4,5).

Sections 4.4.1. - 4.1.4. describe the methods used to model the reactor cores of Table 4.1 using the EPRI-Cell code.

#### **4.1.1 The EPRI-Cell Code**

A sophisticated computer code with the capabilities to solve a complicated problem can sometimes hinder the rapid completion of the calculations at hand. Such was the case with the computer code (EPRI-Cell) chosen as the analytical tool for this study. Much time and effort was devoted to the successful implementation and utilization of this code. This would not have been possible without the aid of the administrative and engineering staff of Argonne National Laboratory.

The EPRI-Cell code was run on Argonne's IBM 3033 computer system and was accessed from M.I.T. via the TYMNET public network system with a DEC-VT100 computer terminal and a Quibe modem. The TYMNET public network system is a system of interconnected communications processors, called nodes, which transmit and receive computer data. It offers local telephone access in hundreds of metropolitan areas around the United States. Once a TYMNET connection was established with the IBM 3033, user interface was accomplished using the OBS WYLBUR operating system. OBS WYLBUR was selected above other available operating systems since it permits on-line file viewing of lengthy EPRI-Cell output data files. Thus the costly and lengthy process of having each output file printed out and mailed to M.I.T. for data examination was eliminated. In order to greatly reduce computer usage costs, the IBM 3033 was used in the cheaper batch mode rather than in the interactive mode. OBS WYLBUR was used to set up batch files containing installation-dependant IBM Job

Control Language (JCL) and accompanying EPRI-Cell input data. Job Control Language controls the data input process to EPRI-Cell and the data output process from EPRI-Cell to appropriate memory locations and retrieval queues. In order to further reduce computer usage costs, each batch job was submitted and run during night and weekend hours and specified as a low priority job. Low priority specification, at times, resulted in significant time intervals between data submission and output file retrieval. Charges per CPU hour were prohibitively high for full priority batch jobs regardless of the time period in which they were submitted.

As stated in Section 1.3, EPRI-Cell computes the space, energy, and burnup dependence of the neutron spectrum in light water reactor fuel cells. Its output consists mainly of broad group, macroscopic, exposure dependent cross-sections for subsequent input into multidimensional transport theory codes or diffusion theory codes such as DIF3D or REBUS-3 (this is discussed further in Section 6.2). EPRI-Cell combines a GAM resonance treatment in the fast and epithermal energy ranges with a THERMOS, heterogeneous integral-transport treatment in the thermal energy range. The original GAM and THERMOS codes have been modified for use in EPRI-Cell; these modifications are fully described in the EPRI-Cell users manual. The GAM and THERMOS cross-section libraries consist of 68 and 35 energy groups respectively. These cross-section sets are collapsed by EPRI-Cell into 1, 2, 3, 4 or 5 energy groups, according to the specification of the user. The broad-group energy break points used by EPRI-Cell are listed in Table 4.3.

A modified version of CINDER, which is a general 'point' program that evaluates the time dependent concentrations of coupled nuclides following irradiation in a specified time-dependent flux, is incorporated into the

**Table 4.3. Energy break points.[9]**

<b>Number of Broad Groups</b> <b>Lower Energy of Group</b>	<b>5</b>	<b>4</b>	<b>3</b>	<b>2</b>
<b>1</b>	<b>0.821 MeV</b>	<b>0.821 MeV</b>	<b>5.53 keV</b>	<b>0.625 eV</b>
<b>2</b>	<b>5.53 keV</b>	<b>5.53 keV</b>	<b>0.625 eV</b>	<b>0.0</b>
<b>3</b>	<b>1.855 keV</b>	<b>0.625 eV</b>	<b>0.0</b>	<b>—</b>
<b>4</b>	<b>0.625 eV</b>	<b>0.0</b>	<b>—</b>	<b>—</b>
<b>5</b>	<b>0.0</b>	<b>—</b>	<b>—</b>	<b>—</b>

EPRI-Cell package. The modifications made to the CINDER program are also fully described in the EPRI-Cell user manual, Reference [9]. Built into CINDER, are depletion chains which are distinguished from fission chains for the fission products. These chains include fuel and transuranic isotopes as well as burnable poisons. The 21 depletion chains contain 116 linear nuclides: 27 distinct heavy elements and 19 burnable poisons. The 69 fission chains of CINDER contain 367 linear nuclides with 179 distinct fission products. The number of depletion calculations performed and timesteps between each is specified by the user (See Appendix E).

Figure 4.4 illustrates the general flow of data during an EPRI-Cell depletion run. The output of each iteration is processed into ECDATA files with later entries overriding earlier values.

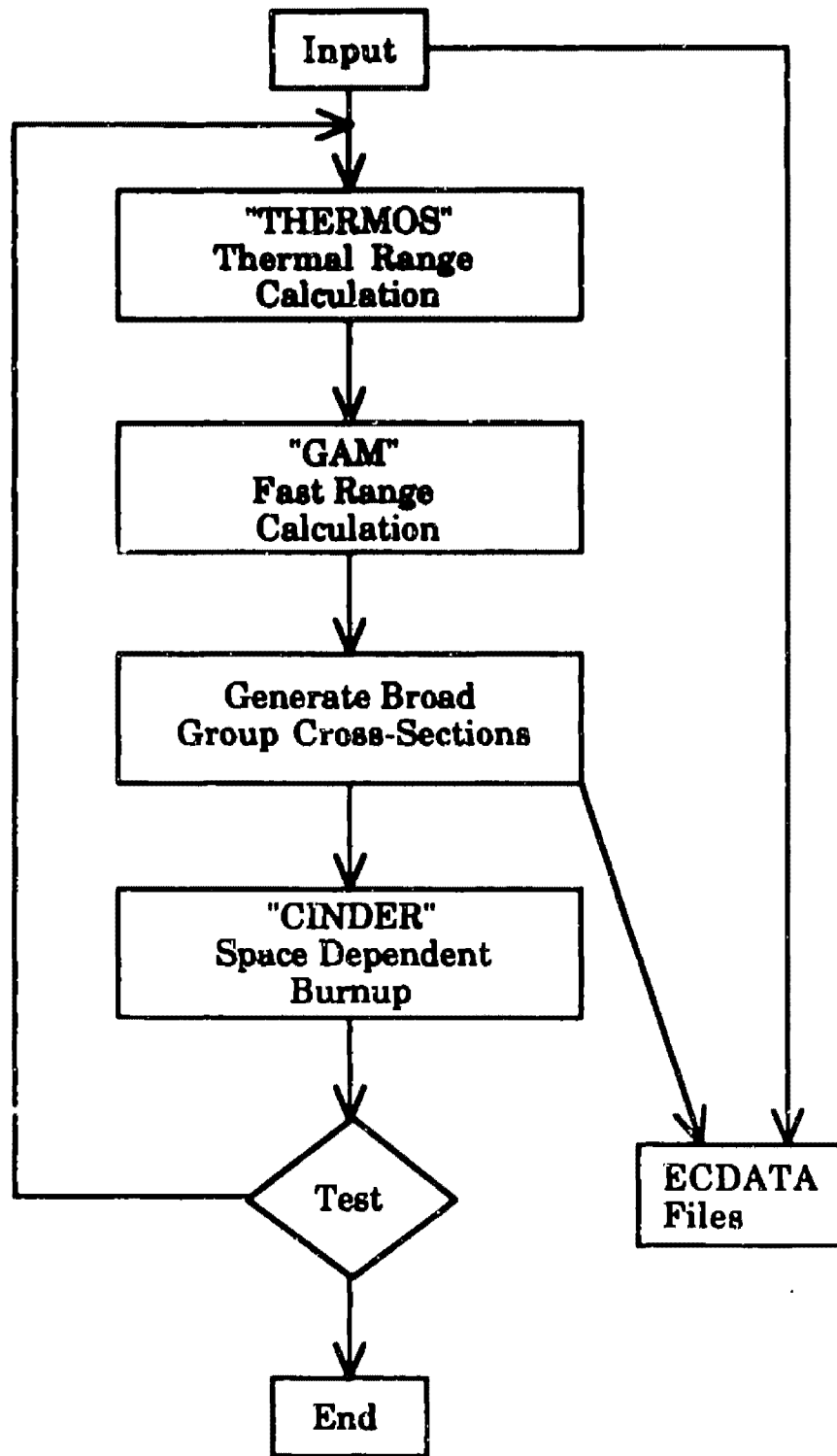


**Figure 4.4. EPRI-Cell data flow.[9]**



Each zone in the fuel cell can represent fuel, cladding, coolant channels, burnable poison or any other material component of the fuel element in question. EPRI-Cell breaks each zone into compositions and requires input specifying the volume percent of each material composition in each zone and the number density of each nuclide in each composition. EPRI-Cell has the capability to treat 20 compositions and 35 nuclides.

The EPRI-Cell code was used to mock up the reactor cores of this study with one-dimensional calculations. In general, one-dimensional calculations performed on high power density reactor cores are used only for preliminary or survey type analysis.[12] Since the objectives of these calculations are only to provide an estimate of reactor core size, refueling lifetime, reactivity coefficients, and plutonium buildup for comparative purposes, one-dimensional calculations were deemed appropriate. Other reactor design considerations such as spatially dependant burnup, control element motion and startup, shutdown and transient behavior have been neglected for the comparative purposes of this study. Possibilities for further, more detailed analysis are discussed in Chapter 6.

#### **4.1.2 Reactor Core Model**

This section describes the methods used to model the reactor cores considered for this study which are summarized in Table 4.1. Also described in this section are the methods used to calculate the values of the particular EPRI-Cell input parameters listed in Table 4.4 which represent the reactor core design variables described in Figures 4.1 and 4.2. Each calculation is based on the fixed and variable input data listed in Table 4.2

**Table 4.4. EPRI-Cell input variables used for reactor design.**

<b>Input Parameter</b>	<b>Design Specification</b>	<b>Symbol</b>
<b>POWR</b>	<b>Power Density</b>	$q'''_{ave,r}$
<b>BUCLNG</b>	<b>Geometric Buckling</b>	$B^2$
<b>PUREDND</b>	<b>Number Densities</b>	<b>N(Nuclide)</b>
<b>VOIFRC</b>	<b>Volume Fractions</b>	<b>Vol%(Composition)</b>
<b>ZONECT</b>	<b>Zone Thickness</b>	$t_x$

and also the fuel element design dimensions of Table 3.2 and materials data presented in Chapter 2.

All EPRI-Cell input parameters not used as reactor design variables are discussed in detail in Appendix E which provides the following information,

- 1) An input description as presented by the EPRI-Cell user's manual.
- 2) A discussion of the particular input parameters and associated input data needed to perform the desired reactor design calculations.
- 3) A description and interpretation of the EPRI-Cell output.

- 4) The first and second depletion timesteps of the reactor core 3 EPRI-Cell output file.

#### 4.1.2.1 Fuel Cell Treatment

A description of the fuel cells used to model each reactor core is provided in this section. The geometry or thickness of each zone in each fuel cell is specified in the EPRI-Cell input file by the parameter ZONECT.

##### Core (1)

As discussed earlier, for this core which is fueled with 7% enriched uranium, a uniform burnable poison distribution was employed. A lumped gadolinia distribution was not required for this enrichment as will be discussed in Chapter 5.

Figure 4.6 illustrates the fuel cell considered this core. It consists of fuel, cladding, and coolant water zones with planes of symmetry occurring in the center of each fuel plate and coolant water channel. Consequently, the zone thicknesses which must be specified by ZONECT in order to model this fuel cell, are the half thickness of the fuel meat, the cladding thickness and the half thickness of the water channel. As illustrated in Figure 4.5, this cell is treated as infinite in the Y-direction and also in the Z-direction (extending into and out of the page).

Each zone contains material compositions which in turn are composed of nuclides. The fuel zone consists of the compositions  $\text{UO}_2\text{-Gd}_2\text{O}_3$  and zircaloy-4 structural material. The  $\text{UO}_2\text{-Gd}_2\text{O}_3$  composition is a mixture of  $\text{UO}_2$  and  $\text{Gd}_2\text{O}_3$ , where  $\text{Gd}_2\text{O}_3$ , as stated in Section 2.3, can be mixed directly with  $\text{UO}_2$ . The cladding and water zones consist of the

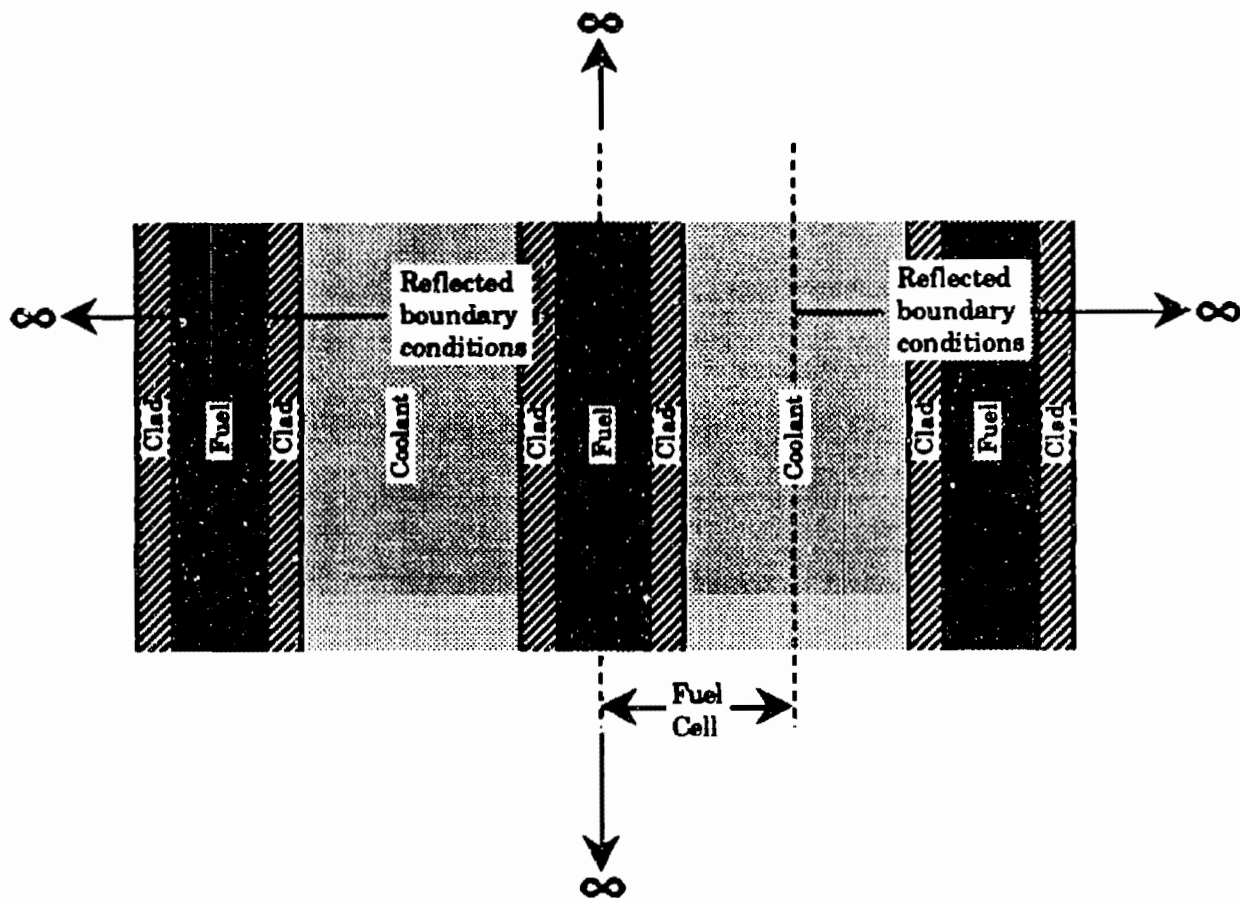


**Figure 4.6.** Fuel cell for reactor core (1).

compositions zircaloy-4 and  $H_2O$  respectively.

The  $UO_2$ - $Gd_2O_3$  composition (mixture) contains the nuclides  $U^{235}$ ,  $U^{238}$ ,  $O$ ,  $Gd^{155}$  and  $Gd^{157}$ . The other gadolinium isotopes,  $Gd^{154}$ ,  $Gd^{156}$ ,  $Gd^{158}$  and  $Gd^{160}$  are treated by the modeler as void. Upon specification of the isotope  $Gd^{155}$ , EPRI-Cell automatically initializes  $Gd^{154}$ ,  $Gd^{156}$  and  $Gd^{158}$  in the naturally occurring proportions. This is discussed in Appendix E. The zircaloy-4 composition present in the fuel zones and cladding zones is treated as a single nuclide by EPRI-Cell. Thus this zone contains the nuclide Zr-4. The composition  $H_2O$  contains the nuclides H and O.

### Cores (2.3.4.5.)

For reactor core designs 2,3,4 and 5, a lumped gadolinia distribution was employed in order to take advantage of self shielding effects in the gadolinia. As will be discussed further in Chapter 5, this prevents the rapid depletion of gadolinia near B.O.C., thus providing reactivity control towards E.O.C. Unlumped gadolinia depletes faster than the uranium fuel since it has a larger absorption cross-section. For these designs, the gadolinia was lumped into fuel plate locations and clad with Zr-4. This requires an expanded fuel cell model.

Calculations were performed with burnable poison plates occurring at every fourth and sixth plate location as illustrated by Figures 4.7a and 4.7b. As will be discussed in Chapter 5, the reactor core with burnable poison plates distributed every sixth plate exhibited a lower control swing,  $\Delta k_{\text{eff}}$ . For these designs, the fuel element is modeled with four zone types, fuel, cladding, coolant and burnable poison zones. The planes of symmetry for this fuel cell occur in the center of the burnable poison zones and the center of the middle fuel plate or zone with respect to the burnable poison zones. However, the fuel cells shown in Figures 4.7a and 4.7b contain three planes of symmetry and not two as in the case of Figure 4.6. This was done in order to verify, using the corresponding EPRI-Cell output, that the code was performing a symmetric depletion calculation about the center planes of symmetry. In other words, to verify the reflection of boundary conditions across the symmetry planes.

In this case, the fuel zone consists of the compositions,  $\text{UO}_2$  and zircaloy-4 structural material. The  $\text{UO}_2$  consists of the nuclides  $\text{U}^{235}$ ,  $\text{U}^{238}$  and O. No  $\text{Gd}_2\text{O}_3$  is present since it is lumped into a solid sheets occupying fuel plate locations. The zircaloy-4 in the fuel and cladding zones is treated

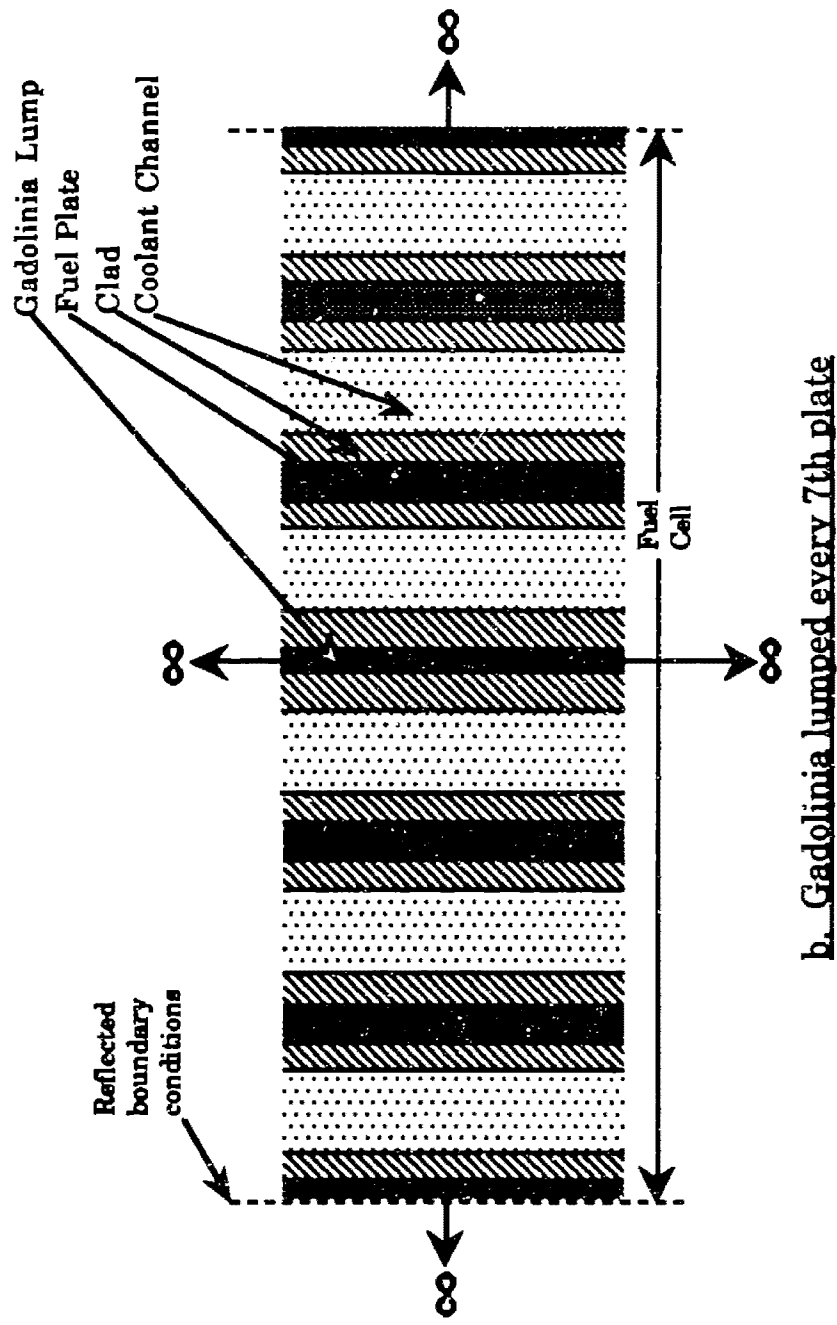
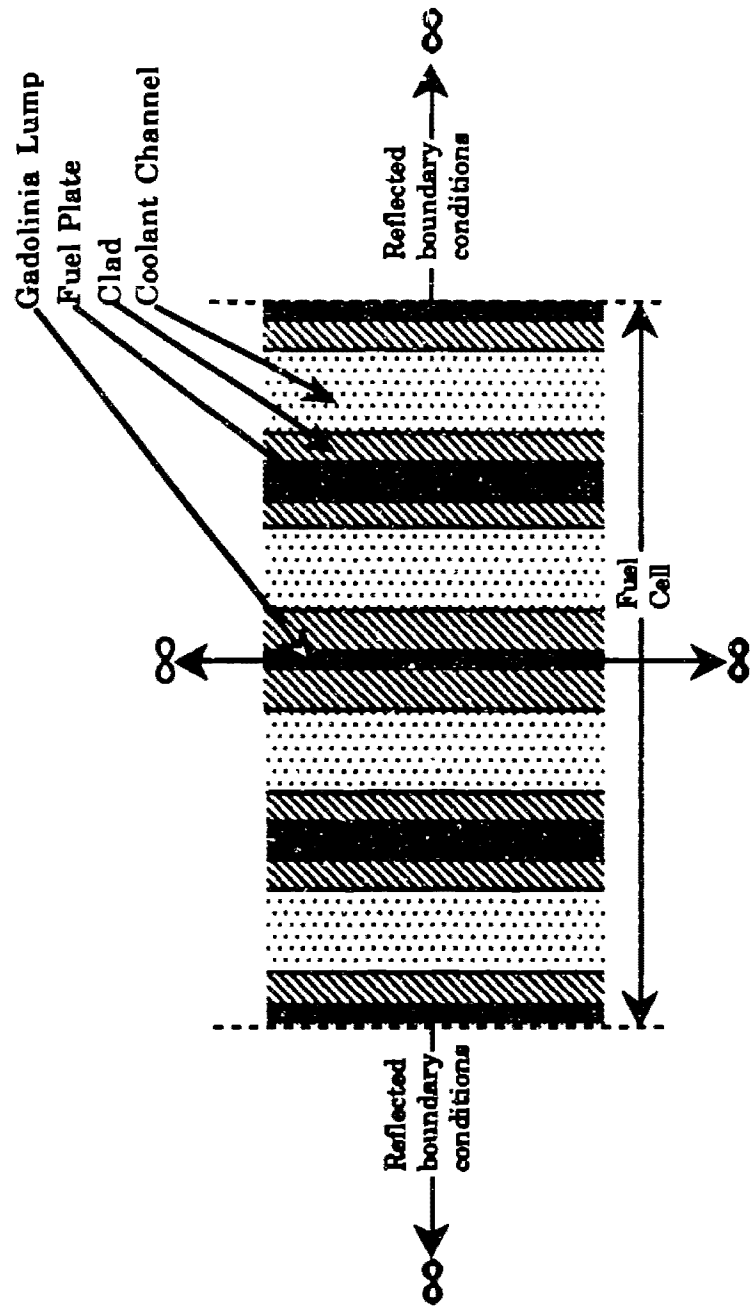


Figure 4.7. Fuel cell for reactor cores (2,3,4,5).

as in the above case (core 1). Also, the water zone is treated as in the above case. The burnable poison zone consists of the composition  $Gd_2O_3$  which in turn consists of the nuclides  $Gd^{157}$ ,  $Gd^{155}$  and O. The remaining gadolinium isotopes are treated as in the above case.

It must be noted that for EPRI-Cell calculation involving a change in the fuel zone or plate thickness, the input parameters  $Res(2, J)$  and  $Res(3, J)$  must be recalculated. These parameters are described in Appendix E.

#### 4.1.2.2 Treatment of Extra Regions

In order to more accurately model the neutronics properties of the reactor fuel elements considered here, the reactivity effects of the zircaloy-4 side plates and a portion of the intra-element gap water must be taken into account. Together, the side plates and the intra element gap comprise 8.53%, 8.55%, and 8.61% of the total core volume for the thick plate/thick channel, thin plate/thick channel and thin plate/thin channel reactor designs respectively. To model the extra zircaloy-4 of the side plates, the total cross-sectional area of the side plates of each fuel element design was divided by the total wetted perimeter of the fuel plates in a fuel element and added to the actual cladding zone thickness. This effective cladding zone thickness (effective thickness with regard to neutronics considerations) is used in the EPRI-Cell input. The modified cladding zone thickness is given by,

$$t'_c = \frac{S_e t_g}{N_f w_p} + t_c \quad (4.2)$$

where,

$s_e$  = Fuel element pitch

$t_s$  = Side plate thickness.

$N_f$  = Number of fuel plates in the fuel element

$w_p$  = Width of fuel plate or coolant channel (distance between the side plates of a fuel element)

$t_c$  = Actual cladding thickness

$t'_c$  = Modified cladding zone thickness

In Figure 4.8 the portion of intra-element gap water represented by area A is treated as part of a coolant channel. The thickness of area A plus the thickness of both adjacent fuel element end spacings is equal to the thickness of a coolant channel. The reactivity effects of the extra fuel element water represented by area B can be approximately accounted for by dividing its cross sectional area among the fuel element water channel zones and uniformly increasing the water channel zone thickness. The modified water channel zone thickness is given by,

$$t'_w = \frac{2[s_l(t_g + t_s) - s_e t_s]}{N_f w_p} + t_w \quad (4.3)$$

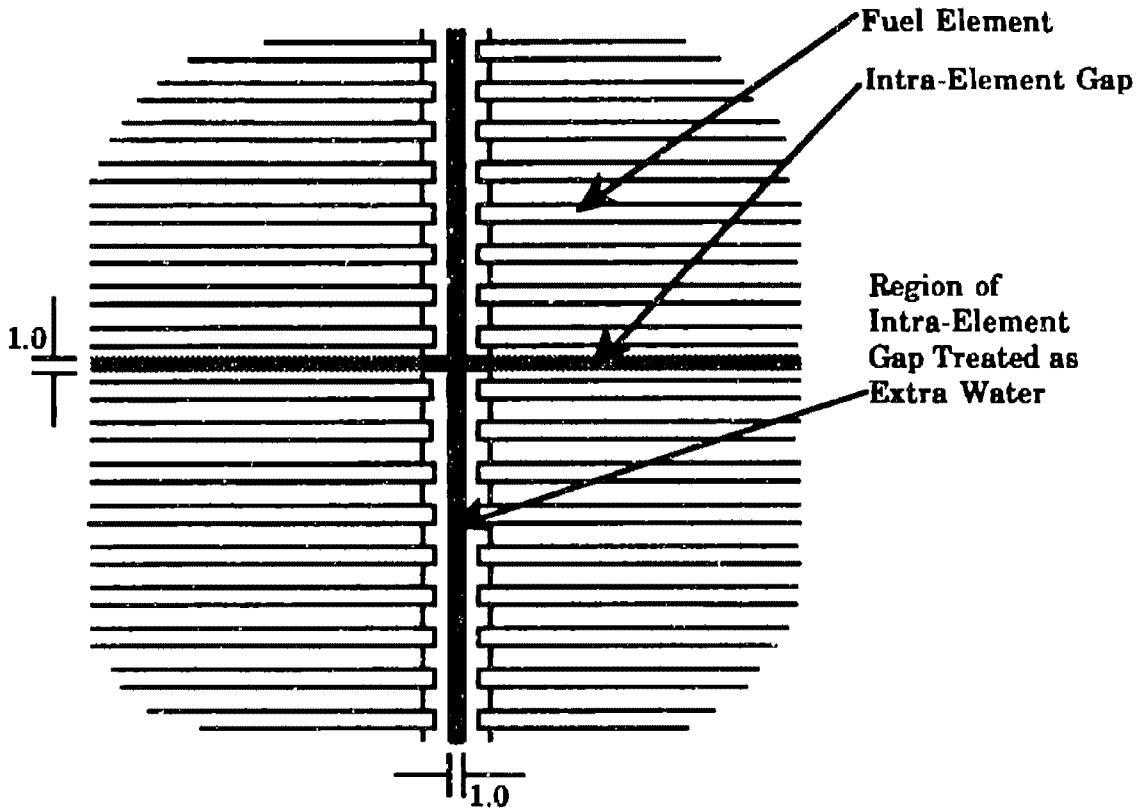


**Figure 4.8. Fuel element extra water.**

where

$s_1$  = Lattice pitch

$t_g$  = Intra-element water gap thickness

$t_w$  = Actual water channel thickness

$t'_w$  = Modified water channel zone thickness

The fuel zone thickness remains unchanged and is given by  $t_f$  which is the actual fuel meat thickness.

### **4.1.2.3 Treatment of the Burnable Poison Lump**

According to the earlier discussion, the thickness of the gadolinia lumps is a variable input design parameter for the cores utilizing 20% and 97.3% enriched uranium, Vol%(Gd<sub>2</sub>O<sub>3</sub>) in the fuel plate locations. This section describes the method used to model these variations in lump thickness.

#### **Cores (2.3.4.5)**

For reactor core designs 2,3,4 and 5 which employ a lumped gadolinia distribution, the lump thickness was used as a design variable (i.e., the lump thickness was varied for the iterative design calculations). Throughout these calculations, the sum thickness of the Gd<sub>2</sub>O<sub>3</sub> lump and associated cladding must be equal to the regular fuel plate thickness. For each lump thickness variation, the corresponding cladding thickness can be calculated by the following relation,

$$t_{lc} = 1/2 ( t_f + t'_c - t_l ) \quad (4.4)$$

where,

$t_{lc}$  = thickness of cladding for Gd<sub>2</sub>O<sub>3</sub> lump

$t_l$  = thickness of Gd<sub>2</sub>O<sub>3</sub> lump

The value of  $t_{lc}$  is input into EPRI-Cell by the parameter ZONECT.

#### 4.1.2.4 Composition Volume Percents in the Fuel Meat

For each reactor core design, the volume fraction (volume percent divided by 100) of the  $\text{UO}_2$  fuel and the Zr-4 structural material in the fuel meat must be determined and input into EPRI-Cell. As discussed earlier, the the volume percent ratio of  $\text{UO}_2$  to Zr -4 structural material in the fuel meat is a design variable for reactor cores 2,3,4 and 5 which utilize the lumped  $\text{Gd}_2\text{O}_3$  distribution. For reactor core 1, this ratio is fixed. The volume fraction of each composition is specified in the EPRI-Cell input file by the parameter  $\text{VOLFR}(K,L)$ , where K refers to the particular material composition and L specifies the particular zone. Note that for any changes of the number densities of the nuclides  $\text{U}^{235}$  and  $\text{U}^{238}$  or volume percent  $\text{UO}_2$  which bears these nuclides, the values of the resonance input parameters  $\text{Res}(4, \text{U}^{235})$  and  $\text{Res}(4, \text{U}^{238})$ , ( $\text{Res}(5, \text{U}^{235})$ ,  $\text{Res}(5, \text{U}^{238})$ ) must be recalculated. This is discussed in detail in Appendix E.

##### Core(1)

For reactor core design 1 which utilizes 7% enriched caramel type fuel, it is desirable for the  $\text{UO}_2$  volume fraction in the fuel meat to be as large as possible in order to maximize available reactivity. Thus for this core, the  $\text{Vol}\%_m(\text{UO}_2)$  in the fuel meat is not a design variable. In this case the  $\text{UO}_2$  is actually a mixture of  $\text{UO}_2$  and  $\text{Gd}_2\text{O}_3$ . The following equation is used to calculate the  $\text{UO}_2$  volume fraction,  $\text{Vol}_m(\text{UO}_2)$ , in the fuel meat of the original caramel fuel plate design.

$$\text{Vol}_m(\text{UO}_2) = \frac{4w_f^2}{(w_c + w_s) w_p} \quad (4.5)$$

where,

$w_c$  = caramel or platelet width

$w_s$  = spacing between platelets

The fixed  $UO_2$  volume percent in the fuel meat of the original caramel fuel plate  $Vol\%_m(UO_2)$  is calculated to be 84.44%.

The corresponding fixed Zr-4 volume percent,  $Vol_m(Zr-4)$ , in the fuel meat is determined by the volume fraction relation,

$$Vol_m(Zr-4) = 1 - Vol_m(UO_2) \quad (4.6)$$

where the resulting volume percent is calculated to be 15.56%

### Core(2)

As calculated above the maximum  $UO_2$  volume percent allowed for this study is 84.44% ( $Vol \times 100$ ), that of the original caramel fuel plate design. Since a uranium enrichment of 20% is used in this core and as will be shown in Chapter 5, the  $UO_2$  volume percent  $Vol\%_m(UO_2)$  in the fuel meat must be decreased in order to reduce the core excess reactivity to a controllable level. Thus, as discussed earlier, the  $UO_2$  volume percent in the fuel meat is a design variable. Since the optimum  $Vol\%_m(UO_2)$  for this design lies in the range,

$$84.44 \geq Vol\%_m(UO_2) \geq 50.0$$

a caramel fuel design was employed. As discussed in Chapter 3, fuel plates with fuel zone  $\text{UO}_2$  volume percents less than 50% will employ cermet fuel plate design. With each variation the corresponding Zr-4 volume percent in the fuel meat was calculated by equation 4.6. (The calculated fuel meat  $\text{Vol}\%_{\text{m}}\text{UO}_2$  for each core design is listed in Table 5.1).

A reduction in the  $\text{Vol}\%_{\text{m}}(\text{UO}_2)$  requires a reduction in the fuel platelet dimensions or caramels of the original design. This must be met with a corresponding increase in the thickness of the Zr-4 spacers, (Refer to Figure 3.1). Upon determination of the optimum  $\text{UO}_2$  volume percent, the caramel (platelet) and Zr-4 spacer widths are calculated by the following equations. Defining the caramel width to Zr-4 spacer width ratio as,

$$R_{\text{cs}} = \frac{w_{\text{c}}}{w_{\text{s}}} \quad (4.7)$$

Equation 4.5 can be written as,

$$V = \frac{4R_{\text{cs}}^2}{(R_{\text{cs}} + 1)w_{\text{p}}} \quad (4.8)$$

where  $V$  is the  $\text{UO}_2$  volume fraction,  $\text{Vol}_{\text{m}}(\text{UO}_2)$ . Rearranging Equation 4.8 yields,

$$R_{\text{cs}}^2 - \frac{1}{4}Vw_{\text{p}}R_{\text{cs}} - \frac{1}{4}Vw_{\text{p}} = 0 \quad (4.9)$$

Solving the above equation by the quadratic formula and rearranging yields

$$R_{\text{cs}} = \frac{1}{8}Vw_{\text{p}} + \sqrt{\left(\frac{1}{4}Vw_{\text{p}}\right)^2 - Vw_{\text{p}}} \quad (4.10)$$

Thus, solving Equation 4.7 for  $w_s$ ,

$$w_s = R_{cs}w_c \quad (4.11)$$

and substituting into the constraint equation,

$$w_p = 4w_c + 4w_s \quad (4.12)$$

and rearranging. The value of  $w_c$  is given by,

$$w_c = \frac{w_p}{4(1 + R_{cs})} \quad (4.13)$$

The value of  $w_s$  can be found by substituting the value of  $w_c$  into the constraint equation, Equation 4.11.

### Cores (3.4.5)

For reactor core designs 3,4,and 5 which are fueled with 97.3% enriched uranium (i.e., HEU), a low fuel meat  $UO_2$  volume percent is required to maintain controllable excess reactivity. Since the  $UO_2$  volume percents for these cores are less than 50% (this was initially assumed and later found to be true) a cermet fuel design is employed. The  $UO_2$  volume fraction was varied over the interval,

$$20.0 \leq \text{Vol}\%_m(UO_2) \leq 50.0$$

where 20% is the lower bound of the cermet  $\text{UO}_2$  volume percent, below which irradiation behavior can not be estimated (see Figure 3.1). The corresponding Zr-4 volume percents are determined by the volume fraction relation,

$$\text{Vol}_m(\text{Zr-4}) = 1 - \text{Vol}_m(\text{UO}_2). \quad (4.6)$$

#### 4.1.2.5 Number Densities

The nuclide number densities in each material composition  $\text{UO}_2$ ,  $\text{Gd}_2\text{O}_3$ , Zr-4 and  $\text{H}_2\text{O}$ , which are used in each reactor core design are specified in the EPRI-Cell input file via the input parameter  $\text{PUREDN}(J,K)$ . The values J and K specify the particular nuclide and material composition respectively. As stated in Section 4.1.2.1., for any changes of the number densities of the nuclides  $\text{U}^{235}$  and  $\text{U}^{238}$  or volume percent of  $\text{UO}_2$  which bears these nuclides, the values of the resonance input parameters  $\text{Res}(4, \text{U}^{235})$  and  $\text{Res}(4, \text{U}^{238})$ ,  $\text{Res}(5, \text{U}^{235})$ ,  $\text{Res}(5, \text{U}^{238})$  must be recalculated. This is discussed in detail in Appendix E.

#### Core (1)

As shown in Figure 4.3a, for reactor core design 1 the  $\text{Vol}\%_m(\text{UO}_2\text{-Gd}_2\text{O}_3 \text{ mixture})/\text{Vol}\%_m(\text{Zr-4 structural material})$  ratio in the fuel meat is constant. However, the fuel material consists of a mixture of  $\text{UO}_2$  and  $\text{Gd}_2\text{O}_3$  where the  $\text{UO}_2/\text{Gd}_2\text{O}_3$  ratio is a design variable. Thus with each variation of the  $\text{wt}\%\text{Gd}_2\text{O}_3$  in this mixture, the nuclide number densities in the fuel/burnable poison mixture ( $\text{UO}_2\text{-Gd}_2\text{O}_3$  mixture) must be

recalculated. In effect, the  $\text{UO}_2\text{-Gd}_2\text{O}_3$  mixture is treated as a single material composition in this case. The nuclide number densities in the Zr-4 structural material volume as well as in the cladding and coolant zones are constant.

#### Cores (2.3.4.5)

As shown in Figure 4.3b, reactor core designs 2,3,4 and 5, which utilize a lumped burnable poison distribution, the  $\text{Vol}\%_m(\text{UO}_2)/\text{Vol}\%_m(\text{Zr-4 structural material})$  ratio in the fuel meat is a design variable. The fuel consists of pure  $\text{UO}_2$  while the burnable poison lumps consist of pure  $\text{Gd}_2\text{O}_3$ . Thus the nuclide number densities in the  $\text{UO}_2$  fuel volume Zr-4 structural material volume, burnable poison lumps and cladding and coolant zones are constant.

The equations used to calculate the nuclide number densities for each material composition are described below for each composition. Also, the parameters used in each of these equations are defined as,

$N$  = Number density (atoms/cm<sup>3</sup>)

$V$  = Volume fraction  $\text{UO}_2$  compound or mixture of  $\text{UO}_2\text{-Gd}_2\text{O}_3$  compounds in the fuel meat

$M$  = Molecular weight (g/mole)

$f$  = Weight percent of uranium in the  $\text{UO}_2$  composition

$w$  = Weight percent  $\text{Gd}_2\text{O}_3$  in  $\text{UO}_2\text{-Gd}_2\text{O}_3$  mixture

$N_A$  = Avogadro's Number (atoms/mole)

$\rho$  = Material density (g/cm<sup>3</sup>)

## UO<sub>2</sub>-Gd<sub>2</sub>O<sub>3</sub>

For the UO<sub>2</sub> fuel of 7%, 20% and 97.3% enrichment which consists of a mixture of U<sup>235</sup> and U<sup>238</sup> atoms, the average molecular weight of the uranium atoms is given by the relation,

$$\frac{1}{M_{\text{ave}}} = \left[ \frac{(1 - e)}{M(\text{U}^{238})} + \frac{e}{M(\text{U}^{235})} \right] \quad (4.14)$$

The weight percent uranium in the UO<sub>2</sub> compound is then given by,

$$f = \frac{M_{\text{ave}}}{M_{\text{ave}} + 2M(\text{O})} \quad (4.15)$$

The number density of the nuclides U<sup>235</sup> and U<sup>238</sup> can then be determined by the following equations,

$$N(\text{U}^{235}) = \frac{(\rho)(1 - w)(f)(N_A)}{M(\text{U}^{235})(10^{24} \text{ barns/cm}^2)} \quad (4.16)$$

$$N(\text{U}^{238}) = \frac{(\rho)(1 - w)(f)(1 - e)(N_A)}{M(\text{U}^{238})(10^{24} \text{ barns/cm}^2)} \quad (4.17)$$

The term (1 - w) is the weight percent of UO<sub>2</sub> in the UO<sub>2</sub>-Gd<sub>2</sub>O<sub>3</sub> mixture and (f) is the weight percent of uranium in the UO<sub>2</sub> compound. For reactor cores 2,3,4 and 5 which do not utilize the lumped burnable poison (Gd<sub>2</sub>O<sub>3</sub>) distribution, (w) is set equal to zero.

The number density of the Gd<sub>2</sub>O<sub>3</sub> molecule is given by,

$$N(\text{Gd}_2\text{O}_3) = \frac{(\rho)(w)(N_A)}{M(\text{Gd}_2\text{O}_3)(10^{24}\text{barns/cm}^2)} \quad (4.18)$$

where  $M(\text{Gd}_2\text{O}_3)$  is the molecular weight of the Gd<sub>2</sub>O<sub>3</sub> molecule (See Table 2.7). The number densities of the nuclides Gd<sup>155</sup> and Gd<sup>157</sup> are the given by,

$$N(\text{Gd}^{155}) = \frac{a}{o}(\text{Gd}^{155})N(\text{Gd}_2\text{O}_3) \quad (4.19)$$

$$N(\text{Gd}^{157}) = \frac{a}{o}(\text{Gd}^{157})N(\text{Gd}_2\text{O}_3) \quad (4.20)$$

where  $a/o(\text{Gd}^{155})$  and  $a/o(\text{Gd}^{157})$  are the natural atomic abundances of the respective nuclides (See Table 2.6). Note that the other gadolinium isotopes, Gd<sup>154</sup>, Gd<sup>156</sup>, Gd<sup>158</sup> and Gd<sup>160</sup> must be treated as void. Upon specification of the isotope Gd<sup>155</sup>, EPRI-Cell automatically initializes Gd<sup>154</sup>, Gd<sup>156</sup> and Gd<sup>158</sup> in the naturally occurring proportions. This is discussed in Appendix E.

For the oxygen number density can now be determined by,

$$N(\text{O}) = \frac{(\rho)(1-w)(1-f)(N_A)}{M(\text{O})(10^{24}\text{barns/cm}^2)} + (1.5)N(\text{Gd}_2\text{O}_3) \quad (4.21)$$

where the first and second terms on the right-hand-side are the contributions from the UO<sub>2</sub> and Gd<sub>2</sub>O<sub>3</sub> compositions respectively. The term  $(1-w)$  is the weight percent UO<sub>2</sub> in the UO<sub>2</sub>-Gd<sub>2</sub>O<sub>3</sub> mixture and the term

(1 - f) is the weight percent oxygen in the UO<sub>2</sub> compound. For reactor cores 2,3,4 and 5 which do not utilize the lumped burnable poison (Gd<sub>2</sub>O<sub>3</sub>) distribution, (w) is set equal to zero. For the second term on the right-hand-side, the coefficient results since 1.5 oxygen atoms are present for every Gd<sub>2</sub>O<sub>3</sub> molecule.

### Zr-4

As stated in Section 4.1.2.1, the zircaloy-4 composition present in the fuel zones and cladding zones is treated as a single nuclide by EPRI-Cell. Thus this zone contains the nuclide Zr-4. The composition H<sub>2</sub>O contains the nuclides H and O.

$$N(\text{Zr-4}) = \frac{\rho(\text{Zr-4})(N_A)}{M(\text{Zr-4})(10^{24}\text{barns/cm}^2)} \quad (4.22)$$

where the associated Zr-4 properties are listed in Table 2.3. Thus N(Zr-4) is calculated to be 0.042518atoms/b-cm.

### H<sub>2</sub>O Coolant

The number density of the H<sub>2</sub>O molecule is given by,

$$N(\text{H}_2\text{O}) = \frac{\rho_{305^\circ\text{C}}(\text{H}_2\text{O})(N_A)}{M(\text{H}_2\text{O})(10^{24}\text{barns/cm}^2)} \quad (4.23)$$

where the associated H<sub>2</sub>O properties are listed in Table 2.8. Thus N(H<sub>2</sub>O) is calculated to be 0.02429atoms/b-cm. The number densities of the hydrogen and oxygen constituents are given by,

$$N(H) = 2N(H_2O) \quad (4.24)$$

$$N(O) = N(H_2O) \quad (4.25)$$

For all the calculational results given in this thesis, primarily Chapter 5, the value of  $\rho_{\text{room temp}}(H_2O) = 1.0\text{g/cm}^3$  was used. A correction to  $\rho_{305^\circ\text{C}}$  (i.e., lower H<sub>2</sub>O density in core) is discussed in Section 5.8. Thus N(H) and N(O) are 0.04840atoms/b-cm and 0.02420atoms/b-cm respectively, where  $\rho_{305^\circ\text{C}}(H_2O) = 0.74\text{g/cm}^3$ .

#### 4.1.2.6 Simplified Overall Core Calculation

As listed in Table 4.2 and discussed in Section 1.1, the total desired reactor core power, Q, is 50MW, on which all reactor core calculations are based. The reactor core power is specified by the EPRI-Cell input parameter POWR (Watts/cm of height). The value of POWR is given by the relation,

$$\text{POWR} = (q'''_{\text{ave,r}})(t_{\text{cell}})(t_{\text{unit}}) \quad (4.26)$$

where  $q'''_{\text{ave,r}}$  is the reactor core average power density. The cell thickness,  $t_{\text{cell}}$ , is determined by summing the thicknesses of the individual fuel cell zones used to represent the fuel element of the particular reactor core under consideration. The unit thickness,  $t_{\text{unit}}$ , is equal to 1cm and conserves dimensions. The reactor core average power density  $q'''_{\text{ave,r}}$  is given by the Equation 4.1,

$$q'''_{ave,r} = \frac{Q}{V_{core}} \quad (4.1)$$

where  $V_{core}$  is the reactor core volume. Since  $V_{core}$  is not known initially,  $q'''_{ave,r}$  can not be calculated and therefore must be guessed and is therefore a variable design parameter. According to Table 4.1, this guess is subject to the following constraints,

$$q'''_{ave,r} \geq 50\text{kW/L} \quad (4.27a)$$

$$q'''_{max} = \Omega_r q'''_{ave,r} \leq \begin{cases} 1000\text{kW/L} \\ 100\text{kW/L} \end{cases} \quad (4.27b)$$

where  $q'''_{max}$  is the maximum core power density and  $\Omega_r$ , which is defined below from Equation 1.2, is the power peaking factor for a finite cylindrical reflected reactor.

$$\Omega_r = \frac{q'''_{max}}{q'''_{ave,r}} \quad (4.28)$$

For a bare or unreflected cylindrical reactor, the power peaking factor is approximately 3.75. For a reflected reactor core, the power peaking factor is reduced by roughly 2/3.[7]

$$\Omega_r = \frac{2}{3} \frac{q'''_{max}}{q'''_{ave,u}} \quad (4.29)$$

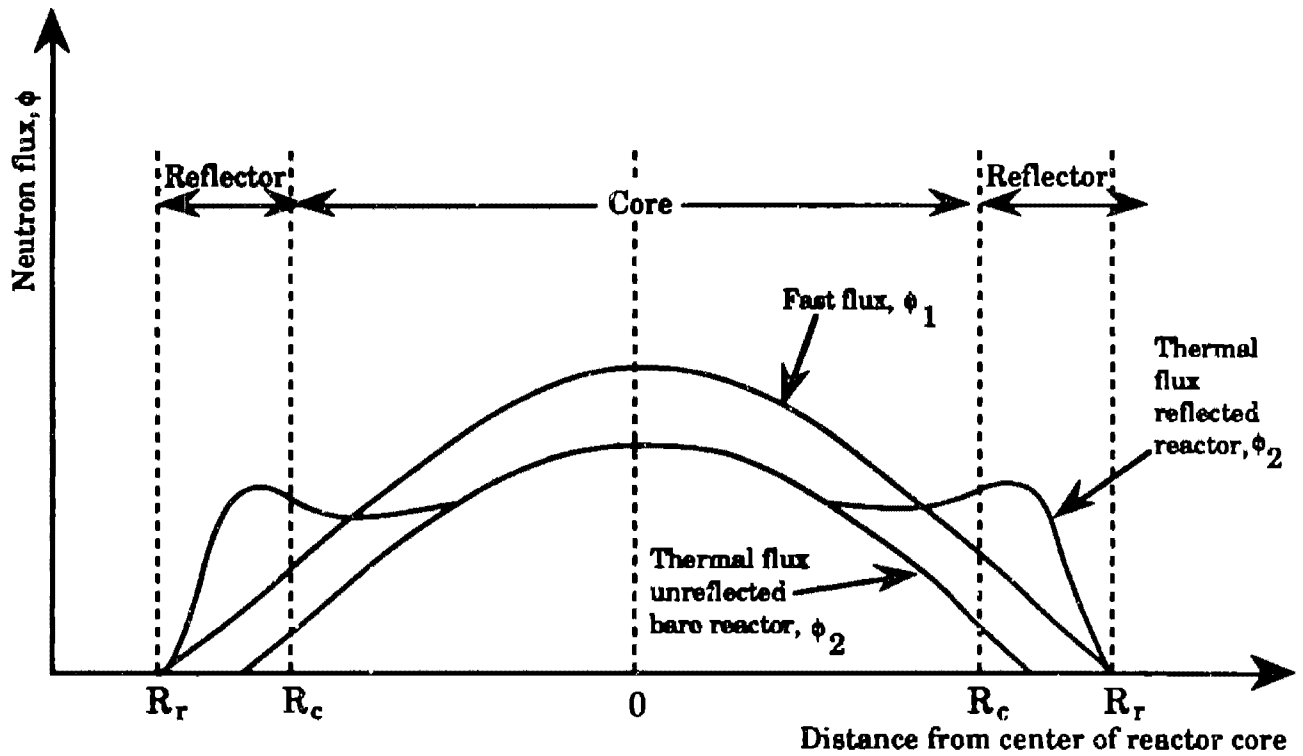


**Figure 4.9.** Thermal flux distribution for reflected reactor.

As illustrated in Figure 4.9, this is due to a buildup of thermal neutrons near the reflector/core interface which increases heat generation in the outer regions of the core. Thus as discussed earlier, the power peaking factor for the reflected reactor cores considered for this study is set at a reasonable 2.5. Combining Equations 4.28 and 4.29, the following approximate relation between  $q'''_{ave,r}$  and  $q'''_{ave,u}$  is obtained.

$$q'''_{ave,u} = \frac{2}{3} q'''_{ave,r} \quad (4.30)$$

As a check of Equation 4.26, the  $q'''_{ave,r}$  used to calculate the value of POWR should be equal to the  $q'''_{ave,r}$  calculated by EPRI-Cell which appears in the corresponding output file.

The volume in  $\text{cm}^3$  for the reflected reactor core for a particular total power  $Q$  (50MW) is given by rearranging Equation 4.1.

$$V_{\text{core},r} = \left( \frac{Q}{q'''_{\text{ave},r}} \right) \left( \frac{1}{1000} \frac{\text{MW}}{\text{kW}} \right) \left( \frac{1}{1000} \frac{\text{L}}{\text{cm}^3} \right) \quad (4.31)$$

As listed in Table 4.2, the height to radius ratio of the cylindrical reactors considered for this study is assumed to be,

$$\frac{H}{R} = 2.5 \quad (4.32)$$

as in the case of the reactor which powers the USS Savannah. The volume of a cylinder is given by,

$$V = \pi R^2 H \quad (4.33)$$

Substituting Equation 4.32 into 4.33 yields,

$$V_{\text{core},r} = 2.5\pi R_r^3 \quad (4.34)$$

for the reflected reactor cores of this study. Solving for  $R_r$  gives,

$$R_r = \sqrt[3]{\frac{V_r}{2.5\pi}} \quad (4.35)$$

The value of  $H_r$  is then given by rearranging Equation 4.32 to,

$$H_r = 2.5R_r \quad (4.36)$$

For a reactor core of finite dimensions, some neutrons are lost to leakage. The term used to account for this loss for a bare unreflected reactor core modeled in 1-D is known as the geometric buckling,  $B^2$ , which is a function of reactor geometry. The value of this term affects the value of  $k_{\text{eff}}$ . The geometric buckling,  $B^2$ , for an unreflected finite cylindrical reactor is given by,

$$B^2 = \left(\frac{2.405}{R_u}\right)^2 + \left(\frac{\pi}{H_u}\right)^2 \quad (4.37)$$

where  $R_u$  and  $H_u$  are the effective height and radius of the unreflected finite cylindrical reactor and taken for this approximation to be equal to the actual unreflected height and radius. For a constant total reactor power,  $Q$ ,  $R_u$  and  $H_u$  are larger than  $R_r$  and  $H_r$ . Thus, if the values for  $R_r$  and  $H_r$ , as derived from the guess of  $q'''_{\text{ave},r}$ , are used in Equation 4.37, the neutron leakage loss as represented by  $B^2$ , will be overestimated. Since the reactor cores considered for this study are reflected (i.e., surrounded by a water shroud), neutron leakage is reduced,  $q'''_{\text{ave}}$  is increased and the required reactor volume to produce a total power of 50MW decreases. Thus for the approximate comparative purposes of this study, it is assumed that the term  $B^2$ , as calculated for the unreflected finite cylindrical reactor also operating at a total power of 50MW, is representative of the neutron leakage of the 50MW reflected reactor. Both reflected and unreflected reactors have a height to radius ratio of 2.5. The volume of this unreflected counterpart is determined by substituting  $q'''_{\text{ave},u}$  as defined by Equation 4.30 into Equation 4.31. Thus,

$$V_{\text{core,u}} = \left( \frac{Q}{\frac{2}{3} q'''_{\text{ave,r}}} \right) \left( \frac{1}{1000} \frac{\text{MW}}{\text{kW}} \right) \left( \frac{1}{1000} \frac{\text{L}}{\text{cm}^3} \right) \quad (4.38)$$

From Equation 4.34,

$$V_{\text{core,u}} = 2.5\pi R_u^3 \quad (4.39)$$

Rearranging Equation 4.39 yields,

$$R_u = \sqrt[3]{\frac{V_u}{2.5\pi}} \quad (4.40)$$

Back substituting the value of  $R_u$  into Equation 4.36 for the unreflected reactor gives,

$$H_u = 2.5R_u \quad (4.41)$$

Substituting the values of  $R_u$  and  $H_u$  into Equation 4.37 yields  $B^2$  for the 50MW unreflected counterpart reactor which is assumed to represent the neutron leakage effects of the smaller 50MW reflected reactor. Thus, as discussed previously, a guess of  $q'''_{\text{ave,r}}$  is accompanied by a value of  $B^2$ . The value of  $B^2$  is specified in the EPRI-Cell input file by the by the input parameter BUCKLG. The calculated values for  $B^2$  are listed in Tables F.1 and F.2 of Appendix F. This approximate method is chosen to be consistent with the assumed (reasonable for small light water reactors, LWR's) power peaking factor of 2.5. It should be noted that the reflector savings (i.e., reduction in core height and radius) calculated by this method is not constant with variation in core volume as it is in reality. Appendix G

discusses a more accurate method to calculate the constant value of reflector savings or extrapolation length.

### **4.1.3 Reactor Core Design Procedure**

This section is intended to organize the core modeling steps discussed in Section 4.1.2 into a workable design procedure for each reactor core. An individual design procedure is described for reactor core 1 and for reactor cores 2,3,4 and 5.

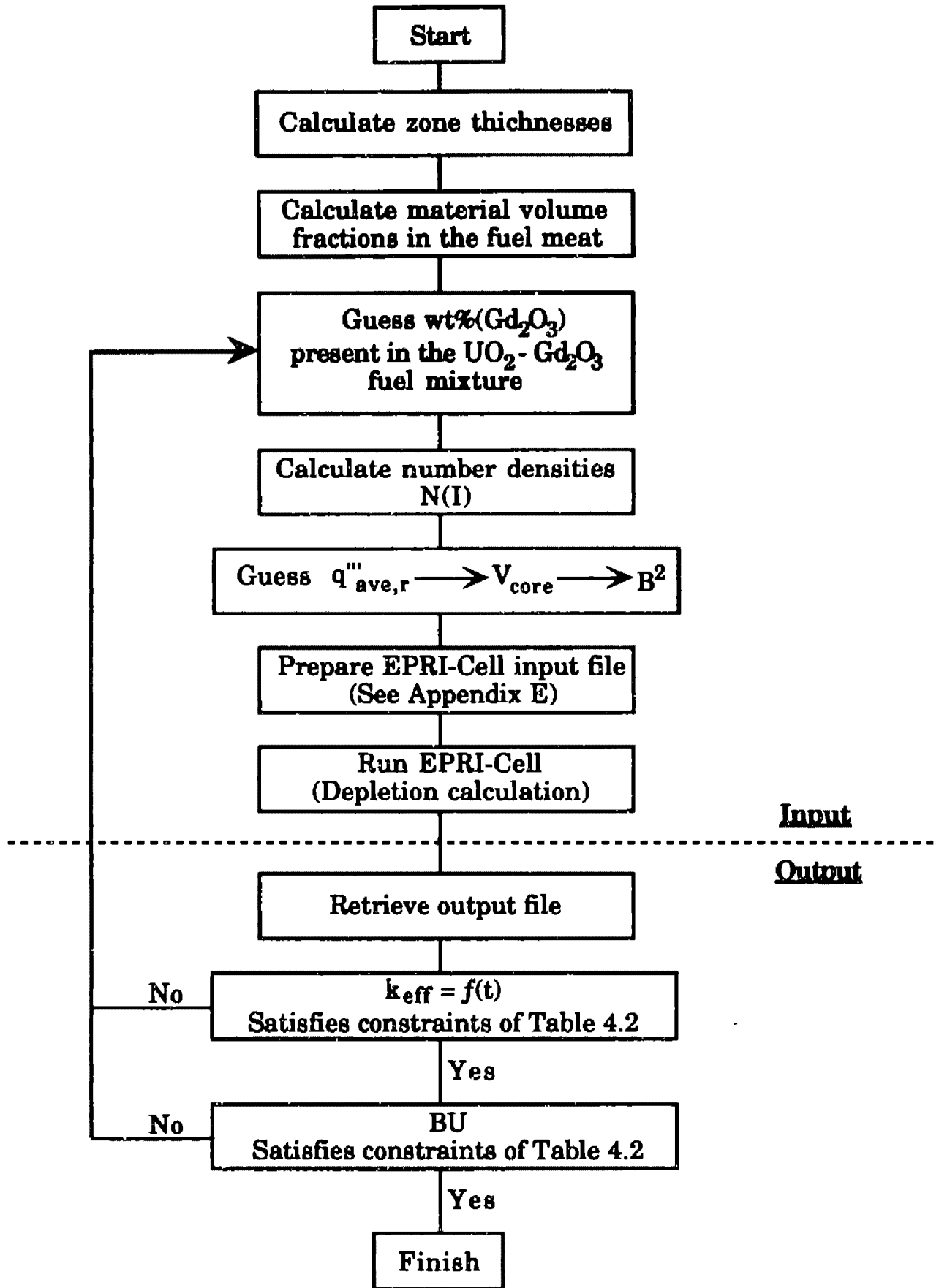
#### **Core (1)**

Figure 4.10 is a flow chart of the design procedure used to model reactor core 1. In order to model the fuel cell geometry, zone thicknesses are calculated according to Section 4.1.2.1 and 4.1.2.2. The material volume percents are calculated as discussed in Section 4.1.2.4. A value of the weight percent  $Gd_2O_3$   $wt\%(Gd_2O_3)$  present in the  $UO_2-Gd_2O_3$  mixture is guessed which typically ranges from 1-10%. With this value, the nuclide number densities within this mixture are calculated by the methods described in Section 4.1.2.5. As discussed in Section 4.1.2.6, a value for the average power density ( $q'''_{ave,r}$ ) is guessed, which also sets the core volume and dimensions by which the value of the neutron leakage term,  $B^2$ , is determined. This data is entered into an EPRI-Cell input file as outlined in Section E.2 of Appendix E, and used to run EPRI-Cell. The values of  $k_{eff}$  for each timestep,  $k = f(t)$ , and the value for burnup, BU, are obtained from the output file. If these values do not satisfy the constraints of Table 4.2, the values for  $wt\%(Gd_2O_3)$  and  $q'''_{ave,r}$  are adjusted in further EPRI-Cell runs

to yield  $k = f(t)$  and BU which satisfy these constraints. At this point, all reactor design parameters will lie in the design space of Figure 4.2.

#### Core (2,3,4,5)

Figure 4.11 illustrates the design procedure used to model reactor cores 2,3,4 and 5. All material number densities are calculated according to Section 4.1.2.4. The fuel cells are modeled as discussed in Section 4.1.2.1 and 4.1.2.2. A value for the thickness of the burnable poison ( $Gd_2O_3$ ) lump is guessed, and the corresponding poison plate cladding thickness is calculated as discussed in Section 4.1.2.3. The  $UO_2$  and Zr-4 volume percents in the fuel meat,  $Vol\%m(UO_2, Zr-4)$ , are guessed based on the discussion of Section 4.1.2.5. As described in Section 4.1.2.6, a value for  $q'''_{ave,r}$  is guessed, which sets the value of  $V_{core}$  by which the neutron leakage term  $B^2$  is calculated. This data is entered into EPRI-Cell files as outlined in Section E.2 of Appendix E and used to run EPRI-Cell. As with reactor core 1, the values of  $k_{eff}$  for each timestep,  $k = f(t)$ , and the value of BU are obtained from the output. The values for  $k = f(t)$  must satisfy the constraints of Table 4.2, while the value for BU must lie on or below the plot line of Figure 3.3. If these constraints are not satisfied, the burnable poison lump thickness,  $Vol\%m(UO_2, Zr-4)$  and  $q'''_{ave,r}$  are adjusted to yield new values for  $k = f(t)$  and BU. This procedure is repeated until the constraints are satisfied; at which all reactor design parameters will lie in the design space of Figure 4.2.



**Figure 4.10 . Design procedure for reactor core (1).**

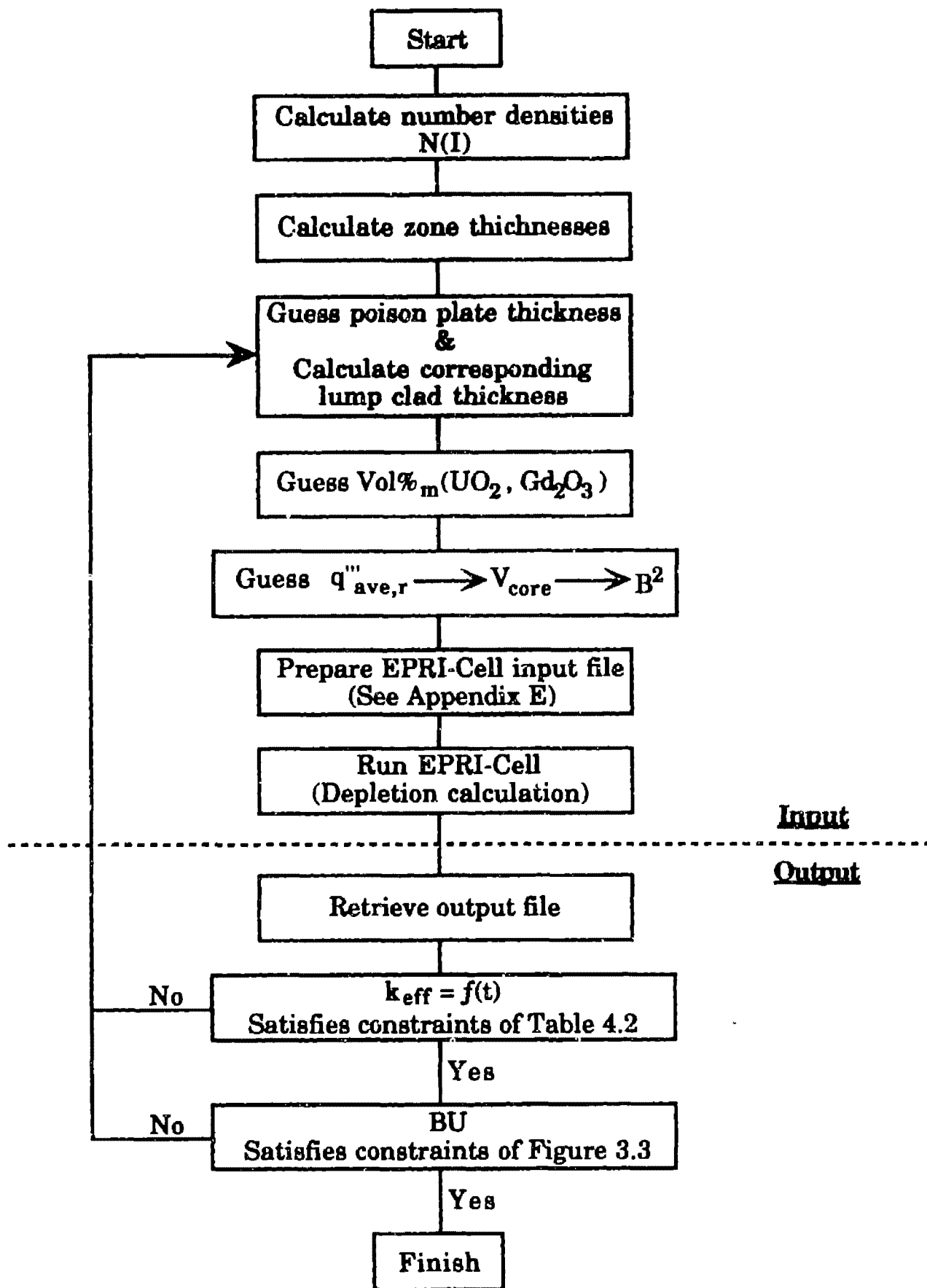


Figure 4.11. Design procedure for reactor cores (2,3,4,5).

#### 4.1.4 Whole Core Materials Calculations

Upon completion of the reactor design analysis outlined in Section 4.3, the net mass of a particular nuclide present in each core can be calculated for any depletion step. This calculation is performed using the Editcell Homogenized Concentrations of Nuclides for the particular depletion timestep listed in the EPRI-Cell output file (See Appendix E, Sections E.3 and E.4). The units of the Editcell Homogenized Concentrations of Nuclides or cell averaged number densities are atoms/barn-cm. The total mass of the particular nuclide present in the core is given by the following equation.

$$m(I) = \frac{N(I)M(I)V_{\text{core},r} \left( \frac{1 \text{ kg}}{1000 \text{ g}} \right) \left( 10^{24} \frac{\text{barns}}{\text{cm}^3} \right)}{N_A} \quad (4.42)$$

where,

$m(I)$  = Total mass of nuclide in core

$N(I)$  = Editcell homogenized concentration of particular  
nuclide, cell averaged number density  
(atoms/barn-cm)

$M(I)$  = Molecular weight of nuclide (grams/mole)

For additional information, the volume percent of  $\text{UO}_2$  and  $\text{Gd}_2\text{O}_3$  in each reactor core can be calculated.

### Core (1)

As described in Section 4.1.2.5., for reactor core 1, the ratio of the  $\text{UO}_2\text{-Gd}_2\text{O}_3$  mixture to the Zr-4 structural material is fixed. However, the  $\text{UO}_2/\text{Gd}_2\text{O}_3$  is a variable design parameter. Thus the wt% $\text{Gd}_2\text{O}_3$  in the  $\text{UO}_2\text{-Gd}_2\text{O}_3$  fuel mixture is known upon completion of the design procedure. The volume fraction  $\text{UO}_2$  within the  $\text{UO}_2\text{-Gd}_2\text{O}_3$  fuel mixture,  $\text{Vol}_f(\text{UO}_2)$ , is given by,

$$\text{Vol}_f(\text{UO}_2) = \frac{1}{1 + \frac{\rho_{\text{UO}_2}}{\rho_{\text{Gd}_2\text{O}_3}} \left( \frac{100}{1 - \text{wt}\% \text{Gd}_2\text{O}_3} - 1 \right)} \quad (4.43)$$

The corresponding volume fraction within this fuel mixture is given by,

$$\text{Vol}_f(\text{Gd}_2\text{O}_3) = 1 - \text{Vol}_f(\text{UO}_2) \quad (4.44)$$

The whole core volume fractions are given by the following equations,

$$\text{Vol}_c(\text{UO}_2) = \text{Vol}_f(\text{UO}_2) \text{Vol}_m(\text{fuel}) \left( \frac{t_f}{t_f + 2t'_c + t'_w} \right) \quad (4.45)$$

$$\text{Vol}_c(\text{Gd}_2\text{O}_3) = \text{Vol}_f(\text{Gd}_2\text{O}_3) \text{Vol}_m(\text{fuel}) \left( \frac{t_f}{t_f + 2t'_c + t'_w} \right) \quad (4.46)$$

where the subscript (c) denotes a whole core volume fraction.

### Cores (2.3.4.5)

For reactor cores 2,3,4 and 5 which utilize a lumped burnable poison distribution, the ratio of  $\text{UO}_2$  to Zr-4 structural material in the fuel meat and the thickness of the burnable poison ( $\text{Gd}_2\text{O}_3$ ) plate lumps are design variables. Thus, upon completion of the design procedure outline in Section 4.3, the  $\text{UO}_2$  volume fraction in the fuel meat and the burnable poison lump thickness are known. The whole core volume fractions for  $\text{UO}_2$  and  $\text{Gd}_2\text{O}_3$  are given by the following equations.

$$\text{Vol}_c(\text{UO}_2) = \text{Vol}_m(\text{UO}_2) \left( \frac{t_f}{t_f + 2t'_c + t'_w} \right) \left( \frac{N_f}{N_f + N_1} \right) \quad (4.47)$$

$$\text{Vol}_c(\text{Gd}_2\text{O}_3) = \left( \frac{t_b}{t_b + (t_f - t_b) + t'_w} \right) \left( \frac{N_1}{N_f + N_1} \right) \quad (4.48)$$

where,

$N_1$  = Number of burnable poison plate lumps in core

$N_f$  = Number of fuel plates in core

### 4.1.5 Safety Analysis

Following a transient that results in a reactor power increase, the fuel temperature will rise leading to an increase in the bulk coolant temperature. As the coolant water temperature increases, the density decreases. A fuel temperature increase or coolant density decrease is accompanied by positive or negative reactivity change (See Appendix C).

To estimate the reactivity change caused by an increase in fuel temperature, EPRI-Cell was run with the fuel temperature specified by the resonance data input parameter  $P_{res}(1,J)$  was decreased to 293°C room temperature (See Appendix E.) As stated in this appendix, the fuel operating temperature was set at 1000°C. For each reactor core, the reactivity change for a fuel temperature increase at B.O.C. and E.O.C. is given by the following equation,

$$\rho_T = \frac{k_{eff}(293^\circ\text{C}) - 1}{k_{eff}(293^\circ\text{C})} - \frac{k_{eff}(1000^\circ\text{C}) - 1}{k_{eff}(1000^\circ\text{C})} \quad (4.49)$$

where  $\rho_T$  is the fuel temperature reactivity change.

To estimate the reactivity change caused by a coolant density decrease, EPRI-Cell was run with the oxygen and hydrogen number density in the coolant zone decreased by 10%. As stated in Section 4.1.2.5., number densities are specified in the EPRI-Cell input files by the input parameter, PUREDN. For each reactor core, the reactivity change for a coolant density decrease of 10% at B.O.C. and E.O.C. is given by the following equation,

$$\rho_M = \frac{k_{eff}(\rho_{H_2O}100\%) - 1}{k_{eff}(\rho_{H_2O}100\%)} - \frac{k_{eff}(\rho_{H_2O}90\%) - 1}{k_{eff}(\rho_{H_2O}90\%)} \quad (4.50)$$

where  $\rho_M$  is the moderator density reactivity change and  $\rho_{H_2O}(100\%)$  was taken to be 1.0g/cm<sup>3</sup> for these  $k_{eff}$  calculations.

## 4.2 Thermal Hydraulic Analysis

As stated in Chapter 1, thermal-hydraulics considerations are assumed not to be limiting for the reactor designs modeled in this study. A simplified thermal-hydraulic analysis, however, has been included to verify that fuel element temperatures are within acceptable bounds and that the required coolant flow rates needed to remove heat are practical. Figure 4.12 illustrates the fuel plate and coolant channel geometry to which this analysis is applied. Below, each of the parameters used in the ensuing discussion are defined.

- $T_b$  = Bulk coolant temperature ( $^{\circ}\text{C}$ )
- $T_{in}$  = Reactor core inlet temperature ( $^{\circ}\text{C}$ )
- $T_{out}$  = Reactor core outlet temperature ( $^{\circ}\text{C}$ )
- $T_{co}$  = Cladding outer surface temperature ( $^{\circ}\text{C}$ )
- $T_{ci}$  = Cladding inner surface temperature ( $^{\circ}\text{C}$ )
- $T_{fs}$  = Fuel surface temperature ( $^{\circ}\text{C}$ )
- $T_{fc}$  = Maximum fuel center-line temperature ( $^{\circ}\text{C}$ )
- $h$  = Coolant heat transfer coefficient ( $\text{W}/\text{m}^2\cdot\text{K}$ )
- $k_w$  = Coolant water thermal conductivity ( $\text{W}/\text{m}\cdot\text{K}$ )
- $k_c$  = Clad thermal conductivity, assumed constant ( $\text{W}/\text{m}\cdot\text{K}$ )
- $k_f$  = Fuel thermal conductivity, assumed constant ( $\text{W}/\text{m}\cdot\text{K}$ )
- $k_p$  = Cermet fuel particle conductivity ( $\text{W}/\text{m}\cdot\text{K}$ )
- $k_m$  = Cermet matrix material conductivity ( $\text{W}/\text{m}\cdot\text{K}$ )
- $u$  = Coolant water dynamic viscosity ( $\mu\text{Pa}\cdot\text{S}$ )
- $c_p$  = Coolant water specific heat ( $\text{kJ}/\text{kg}\cdot\text{K}$ )
- $\rho$  = Coolant water density at operating conditions ( $\text{kg}/\text{m}^3$ )

- $w_p$  = Width of fuel plate (m)  
 $A_f$  = Fuel zone cross-sectional area (m<sup>2</sup>)  
 $A_w$  = Flow area of coolant channel (m<sup>2</sup>)  
 $P_h$  = Heated perimeter of coolant channel (m)  
 $P_w$  = Wetted perimeter of coolant channel (m)  
 $D_h$  = Hydraulic diameter of coolant channel (m)  
 $D_e$  = Equivalent diameter  
 $H$  = Height of reactor core (m)  
 $Re$  = Reynolds number (dimensionless)  
 $Pr$  = Prandtl number (dimensionless)  
 $Nu$  = Nusselt number (dimensionless)  
 $v$  = Coolant velocity (m/s<sup>2</sup>)

### Maximum Fuel Center-Line Temperature

The fuel maximum center-line temperature is determined by combining the heat transfer equations for the coolant bulk/cladding outer surface, cladding outer surface/inner surface, and fuel outer surface/fuel center-line interfaces. These equations are,

$$T_b = \frac{1}{2}(T_{in} + T_{out}) \quad (4.51)$$

$$T_{co} = \frac{q'''_{max,m} t_f}{h} + T_b \quad (4.52)$$

$$T_{ci} = T_{co} + \frac{q'''_{max,m} t_c t_f}{k_c} \quad (4.53)$$

$$T_{fc} = T_{fs} + \frac{q'''_{\max,m} t_f^2}{4k_f} \quad (4.54)$$

and are derived in Reference [7].

Combining Equations 4.51, 4.52, 4.53 and 4.54, and assuming perfect heat transfer across the fuel surface/cladding inner surface interface (i.e.,  $T_{ci} = T_{fs}$ ), the following equation for the maximum fuel temperature is obtained.

$$T_{fc} = q'''_{\max,m} \left[ \frac{t_f^2}{4k_f} + \frac{t_c t_f}{k_c} + \frac{t_f}{h} \right] + \frac{1}{2} (T_{in} + T_{out}) \quad (4.55)$$

The maximum power density in the fuel meat,  $q'''_{\max,m}$  is determined by the relation,

$$q'''_{\max,m} = \frac{q'''_{\max}}{\text{Vol}_c(\text{meat})} \quad (4.56)$$

where  $q'''_{\max}$  is determined by Equation 4.27b and represents the fuel cell averaged maximum power density. The value of the fuel meat volume fraction,  $\text{Vol}_c(\text{meat})$ , is given for reactor core 1 by,

$$\text{Vol}_c(\text{meat}) = \left( \frac{t_f}{t_f + 2t'_c + t'_w} \right) \quad (4.57)$$

while  $\text{Vol}_c(\text{meat})$  for reactor cores 2, 3, 4 and 5 is given by,

$$\text{Vol}_c(\text{meat}) = \left( \frac{t_f}{t_f + 2t'_c + t'_w} \right) \left( \frac{N_f}{N_f + N_l} \right) \quad (4.58)$$

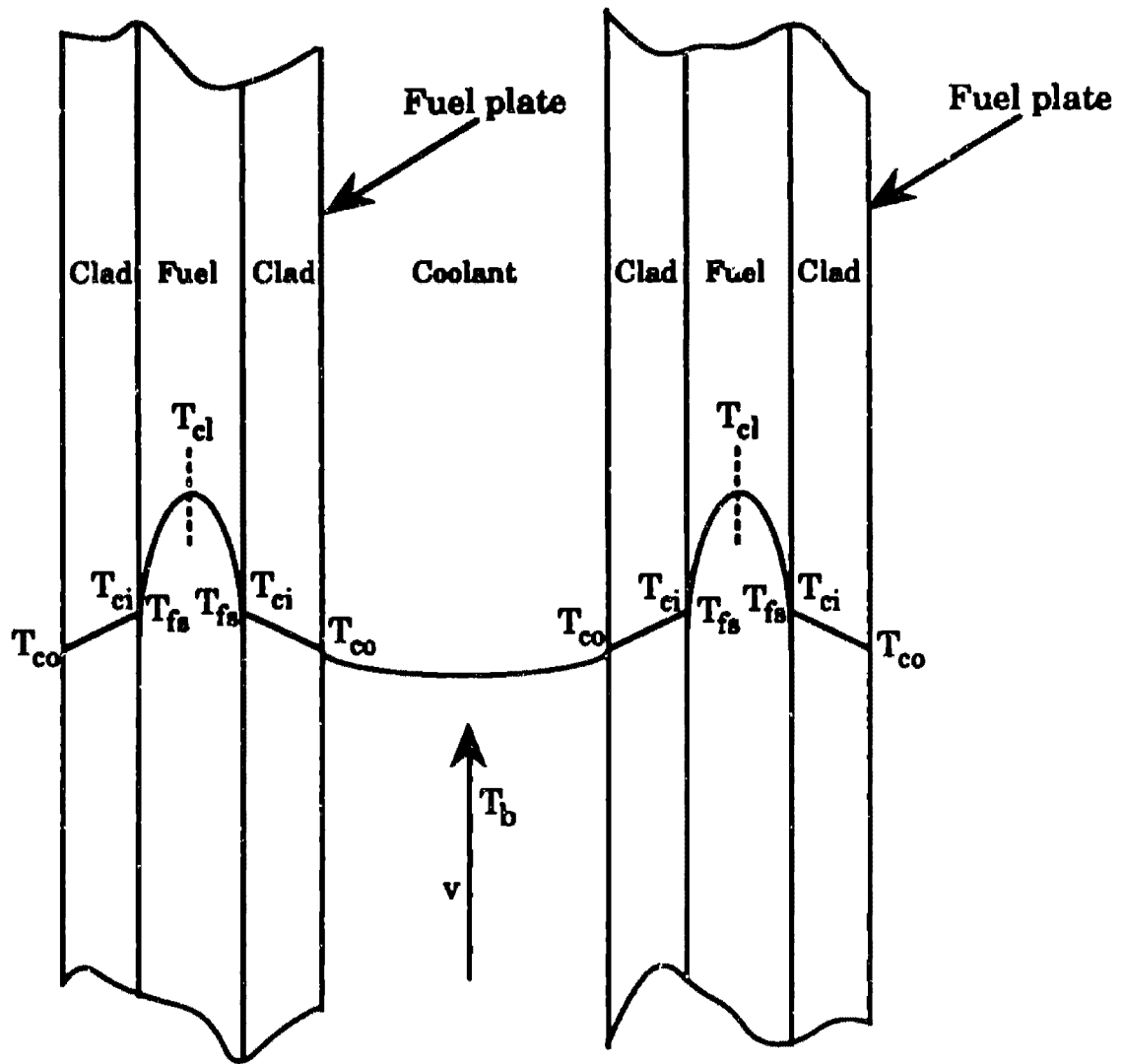


**Figure 4.12.** Fuel plate temperature profiles..

For reactor cores 1 and 2 which utilize caramel type fuel, the medium from fuel surface to fuel center-line is solid  $UO_2$  (i.e., through a fuel platelet as shown in Figure 3.1). Thus only the thermal conductivity of  $UO_2$  is needed. However, for reactor cores 3,4 and 5 which utilize a cermet type fuel, the medium from fuel surface to fuel center-line consists of  $UO_2$  particles and Zr-4 structural material. For this type of fuel, the net thermal conductivity can be estimated by the following correlation,

$$k_f = k_m \frac{1 - \left(1 - \frac{ak_p}{k_m}\right)b}{1 + (a-1)b} \quad (4.59)$$

where  $k_p$  and  $k_m$  are the thermal conductivities of the  $UO_2$  particles and Zr-4 structural material respectively.[18] The values of (a) and (b) are defined by the following relations.

$$a = \frac{3k_m}{2k_m + k_p} \quad (4.60)$$

$$b = \frac{\text{Vol}\%_m(UO_2)}{\text{Vol}\%_m(Zr-4) + \text{Vol}\%_m(UO_2)} \quad (4.61)$$

### Maximum Coolant Velocity

The maximum coolant velocity can be estimated by assuming the entrance to each fuel element is so orificed that the  $T_{out} - T_{in}$  is the same in every channel and hence the hottest channel need the highest coolant velocity. The hot channel is surrounded by the fuel plates which operate at the maximum linear power ( $q'_{max}$ ) of the reactor core. For the hot channel,

$$q'(z) = q'_{max,m} \cos\left(\frac{\pi z}{H}\right) \quad (4.62)$$

The linear heat generation rate is defined as,

$$q'_{max} = q'''_{max,m} t_f w_p \quad (4.63)$$

substituting Equation 4.63 into Equation 4.62 and integrating from  $H/2$  to  $-H/2$  yields,

$$q = \frac{2}{\pi} t_f w_p H q''_{\max, m} \quad (4.64)$$

where  $q$  is the total heat rate transferred to the coolant in the hot channel. The heat rate removed by the coolant is given by,

$$q = \dot{m} c_p \Delta T_{\text{Hot Channel}} = \dot{m} c_p (T_{\text{out}} - T_{\text{in}})_{\text{Hot Channel}} \quad (4.65)$$

From continuity,

$$\dot{m} = \rho A_w v \quad (4.66)$$

where,

$$A_w = t_w w_p \quad (4.67)$$

Substituting Equations 4.66 and 4.67 into 4.65 and rearranging yields the required maximum coolant velocity for the reactor core.

$$v = \frac{q}{\rho A_w c_p (T_{\text{out}} - T_{\text{in}})_{\text{Hot Channel}}} \quad (4.68)$$

### Coolant Heat Transfer Coefficient (h)

The heat transfer coefficient of the coolant water in the hot channel of each reactor core can be determined by use of the familiar Dittus-Boelter equation.

$$Nu = 0.023 Re^{0.8} Pr^{0.3} \quad (4.69)$$

where  $Nu$ ,  $Re$ , and  $Pr$  are the Nusselt, Reynolds and Prandtl numbers respectively which are defined below.

$$Nu = \frac{hD_h}{k} \quad (4.70)$$

$$Re = \frac{\rho v D_e}{u} \quad (4.71)$$

$$Pr = \frac{c_p u}{k} \quad (4.72)$$

Substituting Equations 4.70, 4.71 and 4.72 into Equation 4.69 and rearranging yields,

$$h = \left(\frac{k}{D_h}\right) 0.023 \left(\frac{\rho v D_e}{u}\right)^{0.8} \left(\frac{c_p u}{k}\right)^{0.3} \quad (4.73)$$

where  $(v)$  is the maximum coolant velocity and is determined by Equation 4.69. The term  $D_h$  is the hydraulic diameter of the coolant channel and is defined as,

$$D_h = \frac{4A_w}{P_h} \quad (4.74)$$

where the heated perimeter ( $P_h$ ) is given by,

$$P_h = 2w_p \quad (4.75)$$

The term  $D_e$  is the equivalent diameter of the coolant channel and is defined as,

$$D_e = \frac{4A_w}{P_w} \quad (4.76)$$

where the wetted perimeter ( $P_w$ ) is given by,

$$P_w = 2w_p + 2t_w \quad (4.77)$$

## **CHAPTER 5**

### **Results of the Analysis**

This chapter presents the results of the calculations described in Chapter 4 for each reactor core design. A detailed tabular summary of all calculated results is presented in Appendix F.

#### **5.1 Excess Reactivity Curves**

Figure 5.1 to 5.5 are plots of  $k_{eff} = f(t)$  for reactor cores 1,2,3,4 and 5 which are summarized in Table 4.1. each excess reactivity profile satisfies the constraint of Table 4.2.

$$1.04 \leq k_{eff} \leq 1.24$$

In Figures 5.1 to 5.5 the constraint boundaries are indicated by the horizontal dashed line.

The initial reactivity drop observed in Figures 5.2 to 5.5 represents the buildup of the strong neutron absorbing fission product  $Xe^{135}$ . Upon reaching the equilibrium  $Xe^{135}$  in the core, which occurs after about five days of full power operation, excess reactivity begins to increase. This is due to the higher neutron absorption cross-section of gadolinium compared to uranium resulting in faster depletion of the reactivity suppressing burnable poison. However, in Figure, 5.3, there remains a slight decrease in reactivity beyond the  $Xe^{135}$  equilibrium point up to about 150 days of operation. This can be attributed to the relatively thick  $Gd_2O_3$  plate lumps employed in this reactor core compared to those used in reactor cores 2,4

and 5. The thick lump provides sufficient self-shielding near B.O.C. such that the net uranium depletion is larger than the net  $Gd_2O_3$  depletion thus resulting in excess reactivity decrease.

The  $Xe^{135}$  buildup effect on excess reactivity is not observed in Figure 5.1 which represents reactor core 1. In this case, the uniformly distributed gadolinia depletes rapidly at B.O.C. (i.e., no self-shielding effects) causing an addition of positive reactivity which overrides the negative reactivity addition caused by the buildup of  $Xe^{135}$ .

During the core refueling lifetime, a peak in excess reactivity occurs as observed in Figures 5.1 to 5.5. At this point, positive reactivity addition due to  $Gd_2O_3$  depletion is equal to the negative reactivity addition due to uranium depletion. Since reactor core 1 utilizes a uniform  $Gd_2O_3$  distribution, this peak occur near B.O.C. while for reactor cores 2,3,4 and 5 which utilize a lumped  $Gd_2O_3$  distribution, it occurs near E.O.C.

The importance of the reduction of B.O.C. reactivity by the addition of the burnable poison  $Gd_2O_3$  is readily observed in Figure 5.1 (core 1) and Figure 5.3 (core 2) which utilize a uniform and a lumped  $Gd_2O_3$  distribution respectively. In these figures, the straight sections of the excess reactivity curves near E.O.C. are extrapolated to B.O.C. as illustrated by the sloped dashed line. For reactor core 1, this extrapolation yields a B.O.C.  $k_{eff}$  value of approximately 1.205 without B.O.C.  $Gd_2O_3$  reactivity control. By inspection of Figures 5.2 to 5.5,  $Xe^{135}$  buildup reduces B.O.C.  $k_{eff}$  by about 0.015. Combining this value with the extrapolation value yields a B.O.C.  $k_{eff}$  value of about 1.22. The reactivity peak with  $Gd_2O_3$  corresponds to a  $k_{eff}$  value of 1.8. Although the use of the  $Gd_2O_3$  burnable poison is not required in this case since the B.O.C.  $k_{eff}$  value remains less than 1.24, it has the desirable effect of reducing the required control swing,  $\Delta k_{eff}$ , from 1.24 to 1.8.

The necessity of the reduction of B.O.C. reactivity by the addition of the burnable poison  $Gd_2O_3$  is seen in Figure 5.3, the excess reactivity curve for reactor core 3. Extrapolating the E.O.C. straight section of the curve back to B.O.C. (illustrated by the sloped dashed line) yields a  $k_{eff}$  value above 1.28 (this extrapolation can also be done for reactor cores 2,4, and 5). A reactor core with such a large excess reactivity would be, for practical purposes, impossible to control. Thus the use of burnable poison to control B.O.C. excess reactivity is essential.

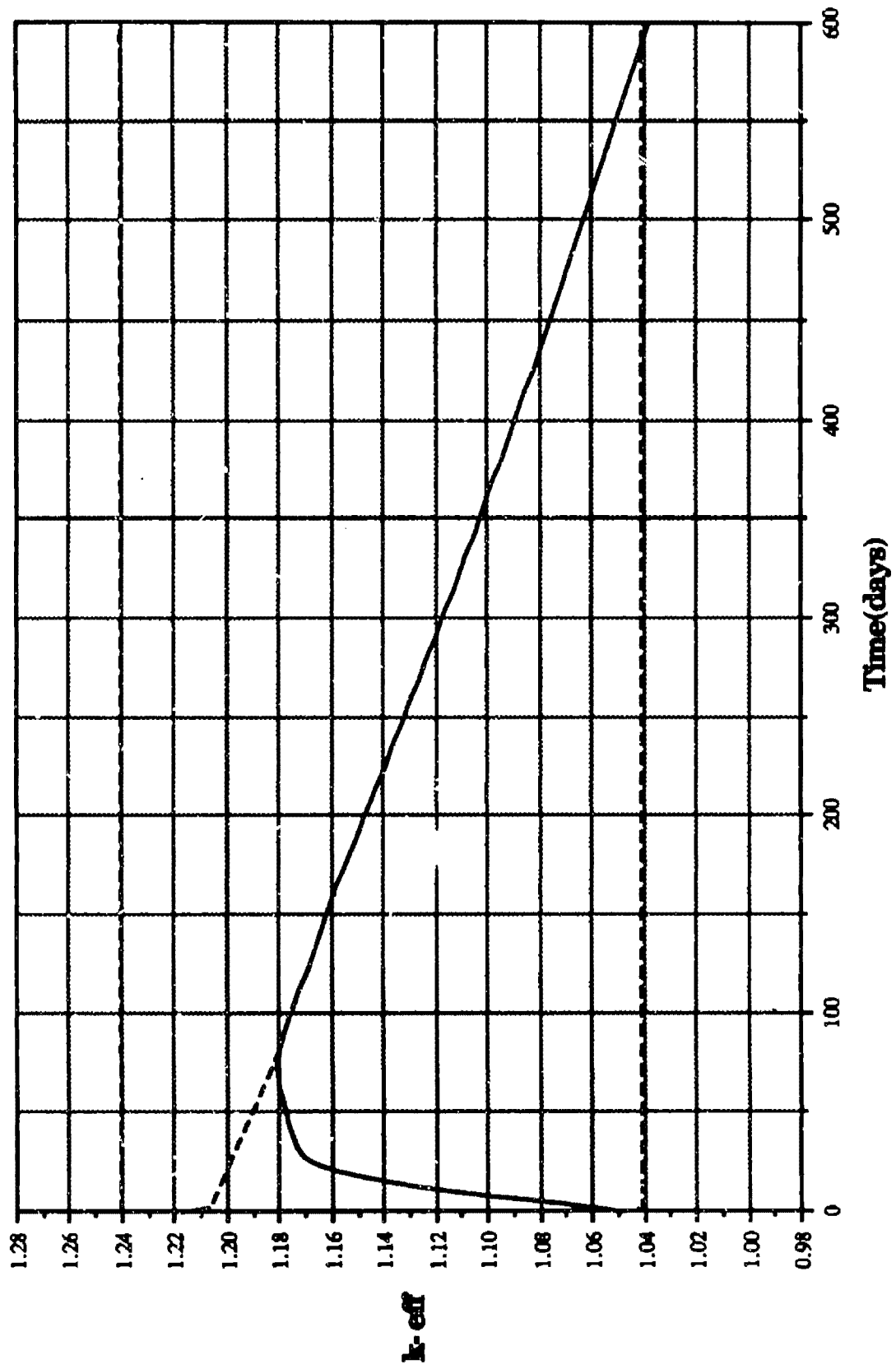
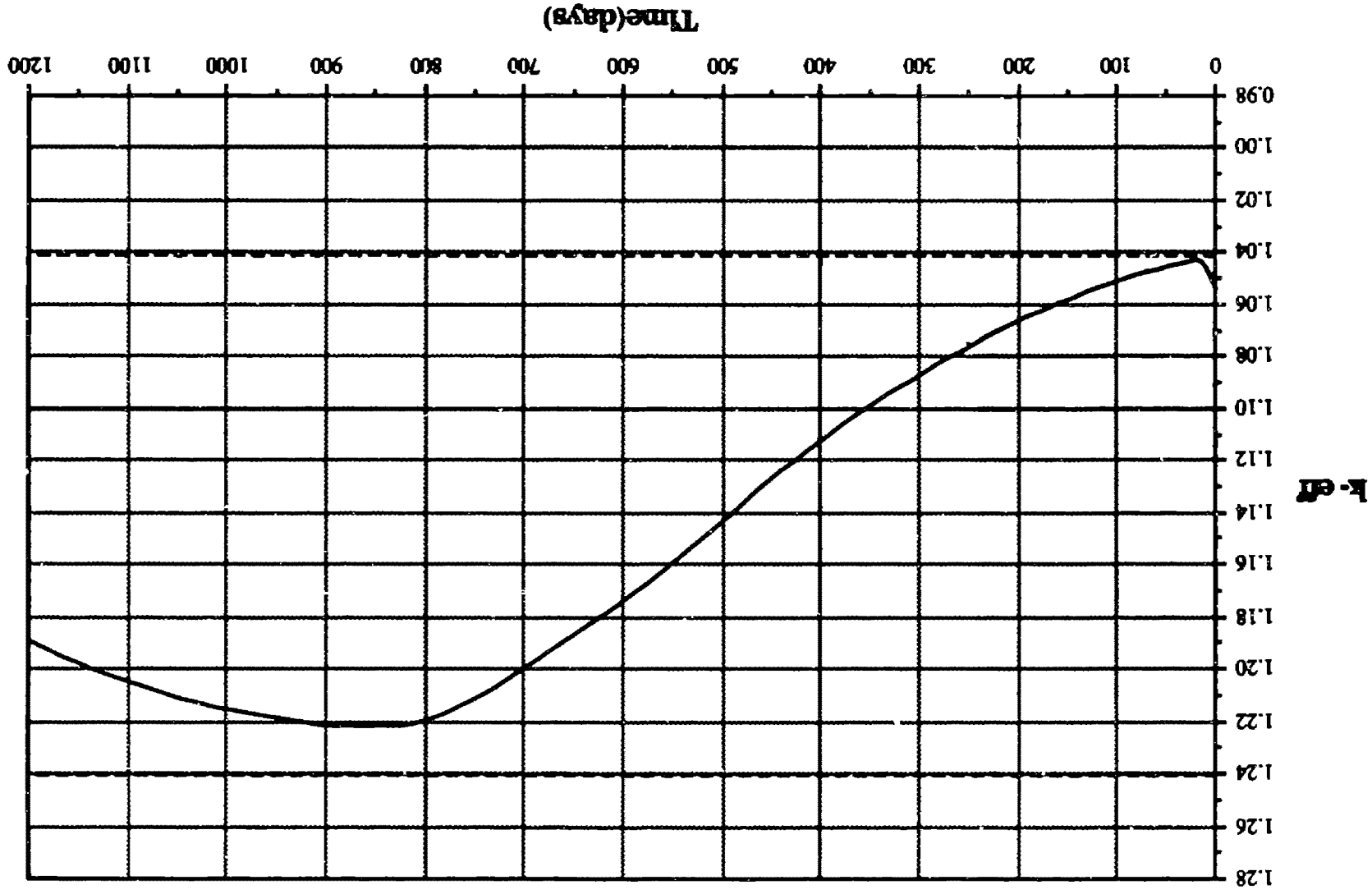


Figure 5.1. Reactor core (1), k-eff Vs. time.

Figure 5.2. Reactor core (2),  $k_{\text{eff}}$  Vs. time.



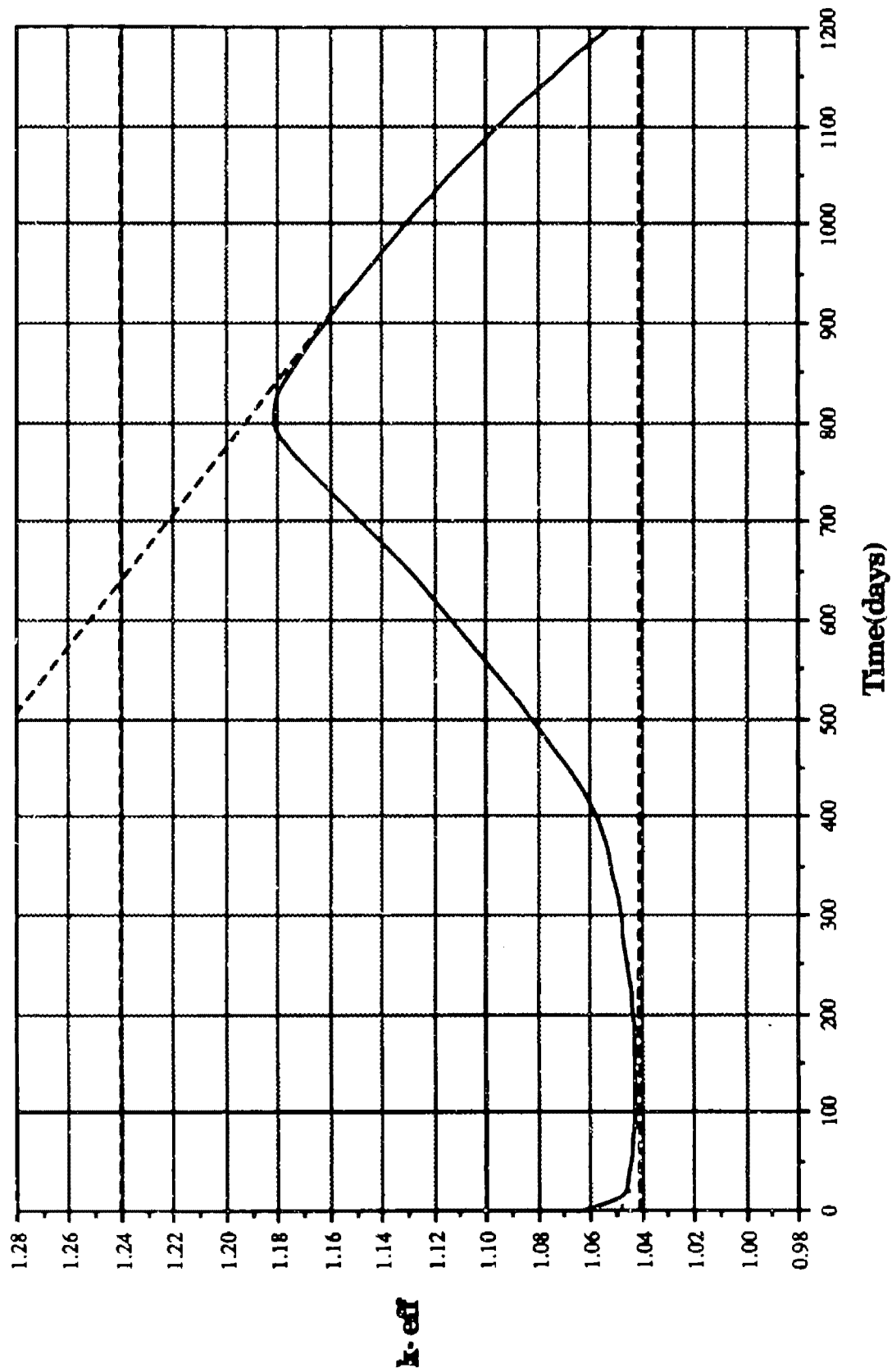


Figure 5.3. Reactor core (3),  $k_{eff}$  Vs. time.

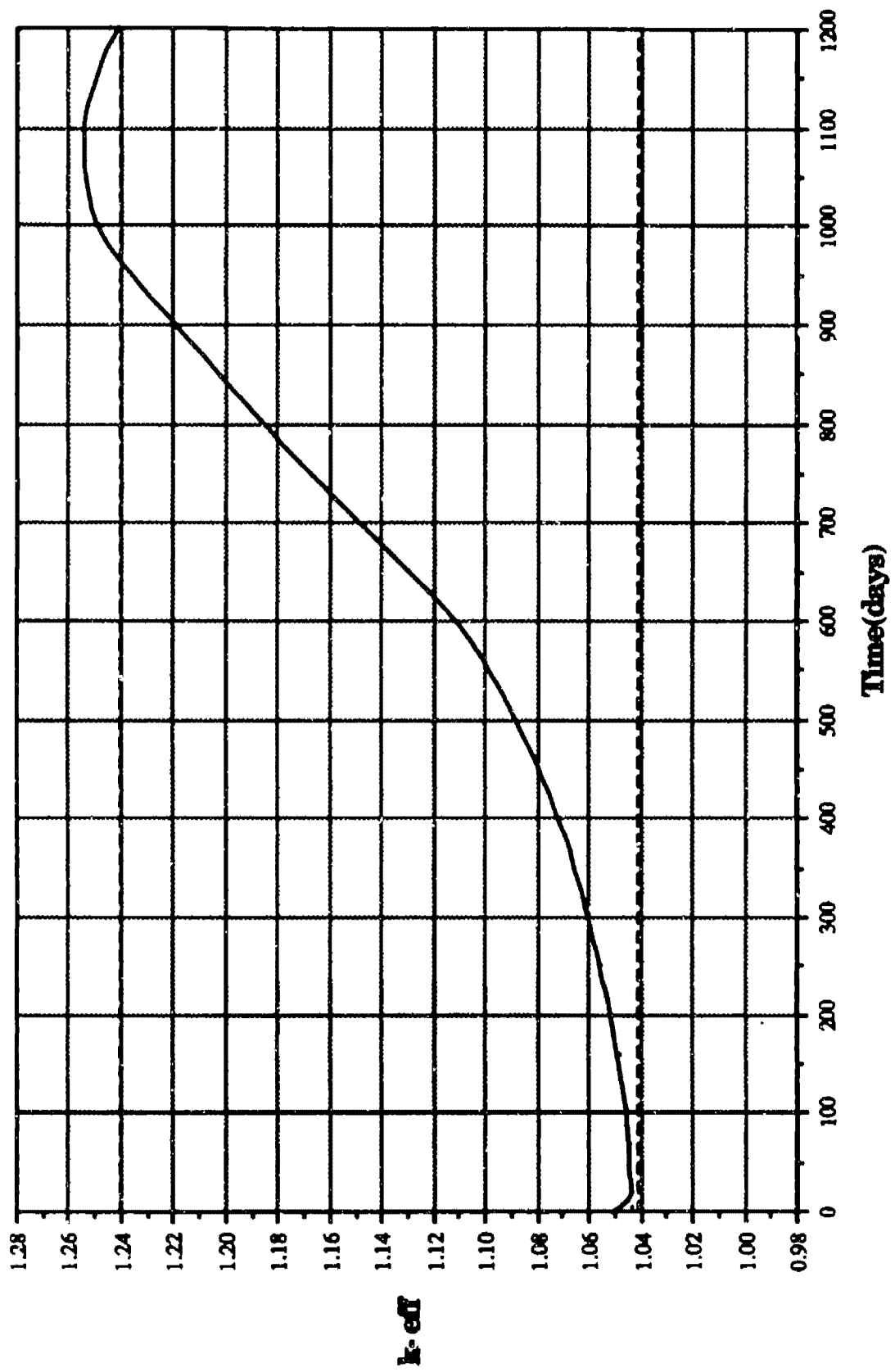


Figure 5.4. Reactor core (4),  $k_{\text{eff}}$  Vs. time.

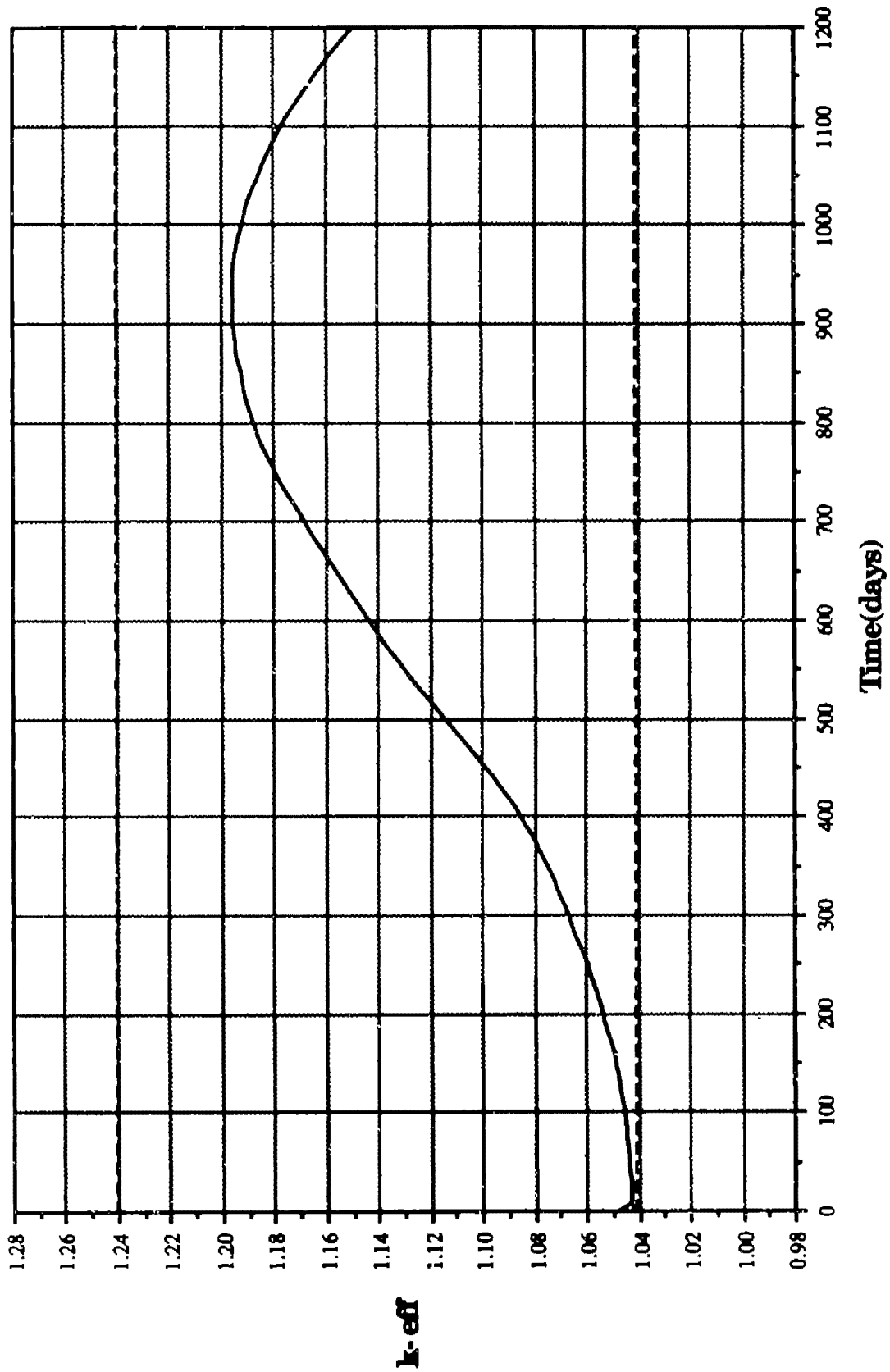


Figure 5.5. Reactor core (5),  $k_{\text{eff}}$  Vs. time.

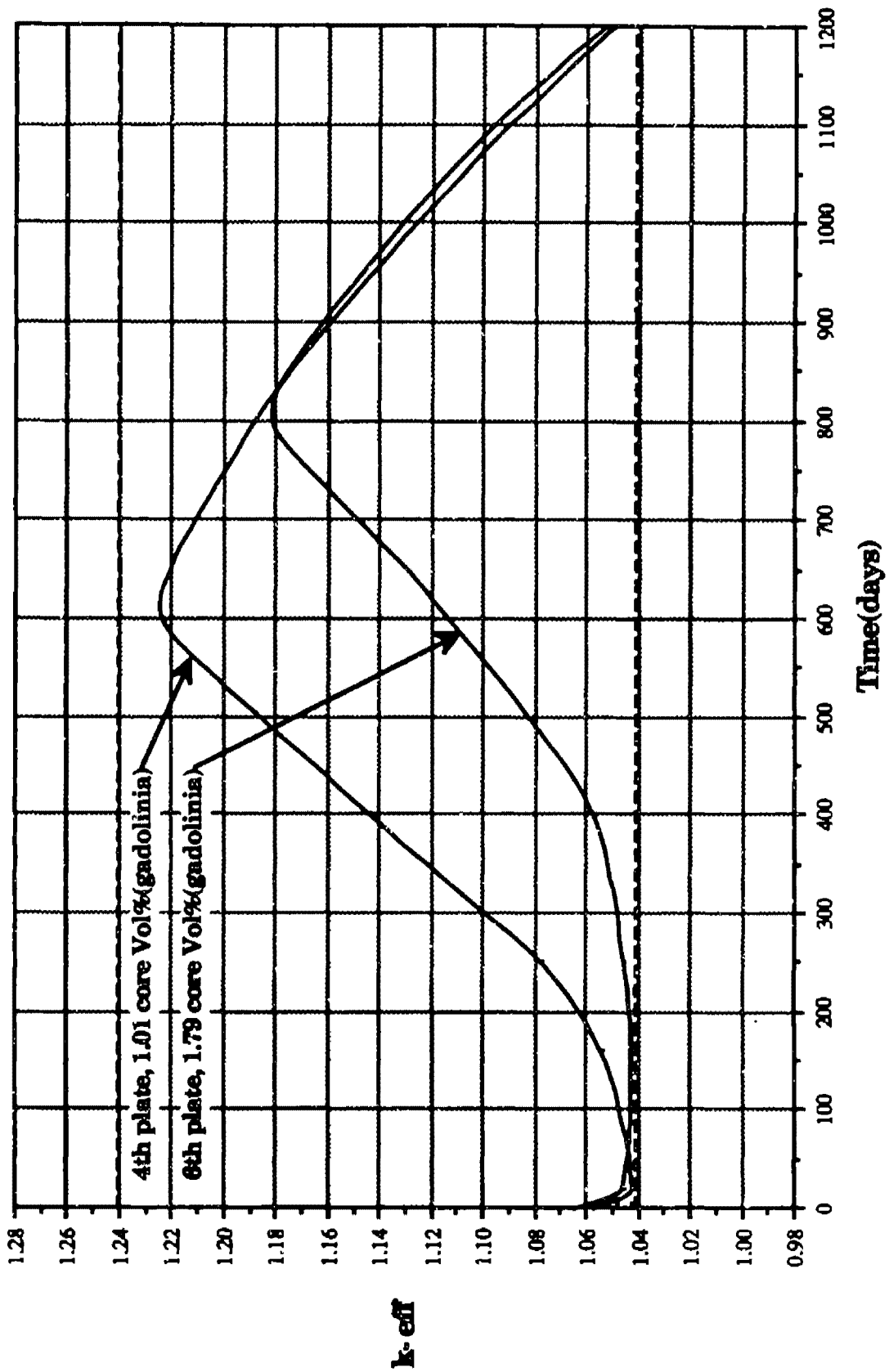


Figure 5.6. Effects of gadolinia distribution on  $k_{eff}$  Vs. time.

## 5.2 Potential for Excess Reactivity Curve Shape Adjustment

As discussed earlier, the excess reactivity profile for reactor core 4 (Figure 5.4) peaks at a value greater than 1.24 which does not satisfy the reactivity constraint. For this core which utilizes a lumped gadolinia distribution,  $Gd_2O_3$  plates were distributed in every sixth fuel plate location. The excess reactivity peaking effect for this core can be further suppressed by decreasing the number of  $Gd_2O_3$  lumps and increasing the thickness of the individual lumps (i.e., lumping  $Gd_2O_3$  into every 8th or 10th fuel plate location). Figure 5.6 illustrates the effect of changing the amount of lumping from every 4th fuel plate location to every fifth fuel plate location. The reactivity profiles of this figure are for the design of reactor core 3 utilizing the fuel cell designs of Figures 4.7a and 4.7b. (Note that the reactivity profile for reactor core 3 using the fuel cell of Figure 4.7b is also plotted in Figure 5.3). The change in the amount of lumping from every 4th to every 5th fuel plate location has two effects. First and most important, the reactivity peak is suppressed and also pushed closer to E.O.C. The increased self-shielding effect causes the net amount of burnable poison in the core to deplete more slowly. Second, the net amount of burnable poison in the core is increased without suppressing the B.O.C.  $k_{eff}$  value (excess reactivity) below the minimum allowed value of 1.04. (The value of 1.04 is set to allow for  $Xe^{135}$  override capability). As with the first effect, the increase in the net mass of  $Gd_2O_3$  is possible due to the increased self-shielding effect which results in a slower  $Gd_2O_3$  depletion rate. Thus with the conclusions derived from Figure 5.6, it is obvious that the reactivity peak of Figure 5.2 can be suppressed with increased lumping. For purposes of

this study, however, this was not possible due to the limit in the number of space point and zones that can be modeled by the EPRI-Cell code.

With a more sophisticated distribution or/and the use of other burnable poisons it may be possible to level the excess reactivity curve of Figures 5.1 to 5.5. In such a case, the rate of positive reactivity addition caused by  $Gd_2O_3$  depletion and the rate of negative reactivity addition caused by uranium depletion are equal throughout the refueling lifetime of the reactor core. This is what is done in an actual reactor.

### 5.3 Mechanical Burnup Results

The values for mechanical burnup as calculated by EPRI-Cell for each reactor core are in units of MWd/T. These burnup values are converted to units of atom percent (at%) by the equation,

$$BU(\text{at}\%) = BU\left(\frac{\text{MWd}}{\text{T}}\right) \left(\frac{1}{1 \times 10^6 \text{ g}}\right) \left(\frac{1}{0.948 \text{ MWd}}\right) \quad (5.1)$$

where the maximum possible burnup per unit mass of uranium is  $0.948\text{MWd/T}$ . [24] For each reactor core the calculated burnup values in units of MWd/T and at% are listed in Table 5.1.

For reactor core 1 which utilizes the caramel fuel design, a burnup of 28,290 MWd/T was obtained. As listed in Table 4.2, the mechanical limitations of this fuel design allow a maximum burnup of 60,000MWd/T. However, inspection of the excess reactivity curve for this core (Figure 5.1) shows that at E.O.C.  $k_{\text{eff}}$  has dropped to its minimum allowable value. Thus

the mechanically allowable burnup of 60,000MWd/T can not be obtained. The core refueling lifetime for this core (600FPD) is thus reactivity limited. Reactor core 2 also uses the caramel fuel design and is thus allowed a maximum burnup of 60,000MWd/T as listed in Table 4.2. A calculated burnup value of 62,120MWd/T was obtained. The excess reactivity curve for this core (Figure 5.2) shows an E.O.C. value of  $k_{eff} = 1.19$  where the minimum value for  $k_{eff}$  is 1.04. Thus the refueling lifetime for this core is not reactivity limited, rather it is limited by the structural mechanics of the fuel. As discussed in Section 3.1.1, internal fission gas pressure will cause fuel failure at a burnup greater than approximately 60,000MWd/T.

The maximum allowed burnup values for reactor cores 3,4 and 5 which utilize the cermet fuel design, are listed in Table 5.1. These values, in at%, have been estimated from Figure 3.3 by using the cermet  $Vol\%_m(UO_2)$  values also listed in Table 5.1. The calculated burnup values, in at%, for reactor cores 3,4 and 5 are below there respective maximum allowed burnup values in at% as required. As can be seen from the excess reactivity curves for reactor cores 3,4 and 5 (Figures 5.3 to 5.5), the E.O.C.  $k_{eff}$  values are above the minimum allowed  $k_{eff}$  value of 1.04. Thus as with reactor core 2, the refueling lifetimes of these reactor cores 3,4 and 5 are limited by the structural mechanical of the fuel.

**Table 5.1. Core burnup data.**

Reactor Core	Core 1	Core 2	Core 3	Core 4	Core 5
Burnup $\left[\frac{\text{MWd}}{\text{T}}\right]$	28290	62120	548570	336160	382700
Burnup (at%)	3.0	6.6	57.9	35.5	40.4
Burnup Limit	$60000 \frac{\text{MWd}}{\text{T}}$	$60000 \frac{\text{MWd}}{\text{T}}$	70 at%	42 at%	44 at%
Vol% $\text{UO}_2$	84	70	20	35	33

**Table 5.2. Safety coefficients of reactivity.**

Reactor Core	Core 1	Core 2	Core 3	Core 4	Core 5
Fuel Type	Caramel	Caramel	Cermet	Cermet	Cermet
B.O.C. $\Delta k_{\text{eff}}$ (fuel temp)	-0.027	-0.019	-0.0025	-0.00053	-0.00065
B.O.C. $\Delta k_{\text{eff}}$ (void)	-0.027	-0.021	-0.030	-0.017	-0.018
E.O.C. $\Delta k_{\text{eff}}$ (fuel temp)	-0.026	-0.022	-0.007	-0.0043	-0.0051
E.O.C. $\Delta k_{\text{eff}}$ (void)	-0.038	-0.028	-0.030	-0.025	-0.033

## **5.4 Reactor Safety Coefficients**

Table 5.2 summarizes the B.O.C. and E.O.C. temperature and void coefficients of reactivity for each reactor core design. As required, the values are negative in all cases. It can be seen that the B.O.C. and E.O.C. temperature coefficients of reactivity decrease with increase in uranium enrichment. This is due to the decrease in the  $U^{238}$  concentration. The effective neutron absorption cross-section of  $U^{238}$  increases with temperature by a phenomenon known as Doppler broadening. This is discussed in detail in Reference [7].

## **5.5 Reactor Core Volume and Power Density Results**

In Section 4.6, it was stated that the selection (guess) of the value of  $q'''_{ave,r}$  automatically set  $V_{core}$  by which the core height and radius can be determined. Table 5.3 summarizes the power maximum and average power densities and associated core dimensions for each reactor core. The core refueling times,  $t_{rf}$ , and fuel meat  $UO_2$  volume percents,  $Vol\%_m(UO_2)$  are also listed in Table 5.3.

Since the net  $U^{235}$  loading is larger for reactor core 2 which is fuel with 20% enriched uranium than for reactor core 3 which is fueled with 97.3% enriched uranium,  $V_{core}$  is larger for core 2 (667L) than for core 3 (265L). Both cores operate with the same refueling lifetime of 1200FPD.

Although the  $U^{235}$  loading is smaller for reactor core 1 which is fueled with 7% enriched uranium than for reactor core 2,  $V_{core}$  is smaller for core 1 (506L) than for core 2 (667L). This results since the refueling lifetime for

**Table 5.3. Core dimensions and power densities.**

Reactor Core	Core 1	Core 2	Core 3	Core 4	Core 5
Fuel Type	Caramel	Caramel	Cermet	Cermet	Cermet
Full Power Days	600	1200	1200	1200	1200
Diameter(m)	0.81	0.88	0.65	0.74	0.70
Height(m)	0.98	1.08	0.79	0.90	0.86
Volume(l)	506	667	265	385	333
$q'''_{avg,r}$ (kW/l)	99	75	189	131	150
$q'''_{max}$ (kW/l)	240	182	535	368	425

reactor core 1 is 600FPD while for reactor core 2 it is 1200FPD. Thus reactor core 1 consumes half as much uranium as reactor core 2.

For reactor cores 4 and 5 which are fueled with 97.3% enriched uranium and which also operate with refueling lifetimes of 1200FPD, the calculated values for  $V_{core}$  are 385L and 333L respectively. These values for  $V_{core}$  are larger than  $V_{core}$  for reactor core 3 which is also fueled with 97.3% enriched uranium and operated with a refueling lifetime of 1200FPD. The larger volumes of reactor cores 4 and 5 compared to core 3 is caused by the thinner fuel plates used by these cores. For a reactor core of constant uranium mass inventory, as the thickness of the fuel plates is decreased, a more homogeneous system is obtained. This results in a core reactivity decrease which, in this case, is compensated for by an increase in  $V_{core}$ . This topic is discussed in detail in Reference [25].

The associated reactor core dimensions range from 88cm to 65cm and 108cm to 79cm for the core diameters and heights respectively. This represents net differences of 29cm in height and 23cm in diameter.

Based on the calculated reactor core diameter values listed in Table 5.3, and the associated fuel element lattice cross-sectional areas listed in Table 3.2, the fuel element core grid layouts of Figure 5.7 were estimated. Figures 5.1a, 5.1b, 5.1c, 5.1d and 5.1e represent the estimated core grids for reactor cores 1, 2, 3, 4, and 5 respectively. Each square in the figures represents a fuel element

For reactor core 2 which is fueled with 20% enriched uranium, a mass of 193kg  $U^{235}$  is required while a mass of 106kg  $U^{235}$  is required for reactor core 3, where both operate with trf of 1200FPD. Reactor core 2 requires the larger  $U^{235}$  in order to provide sufficient positive reactivity in order to override the negative reactivity added by the increased  $U^{238}$  mass.

The calculated values of  $q''_{ave,r}$  for each reactor core satisfy the constraints listed in Table 4.2.

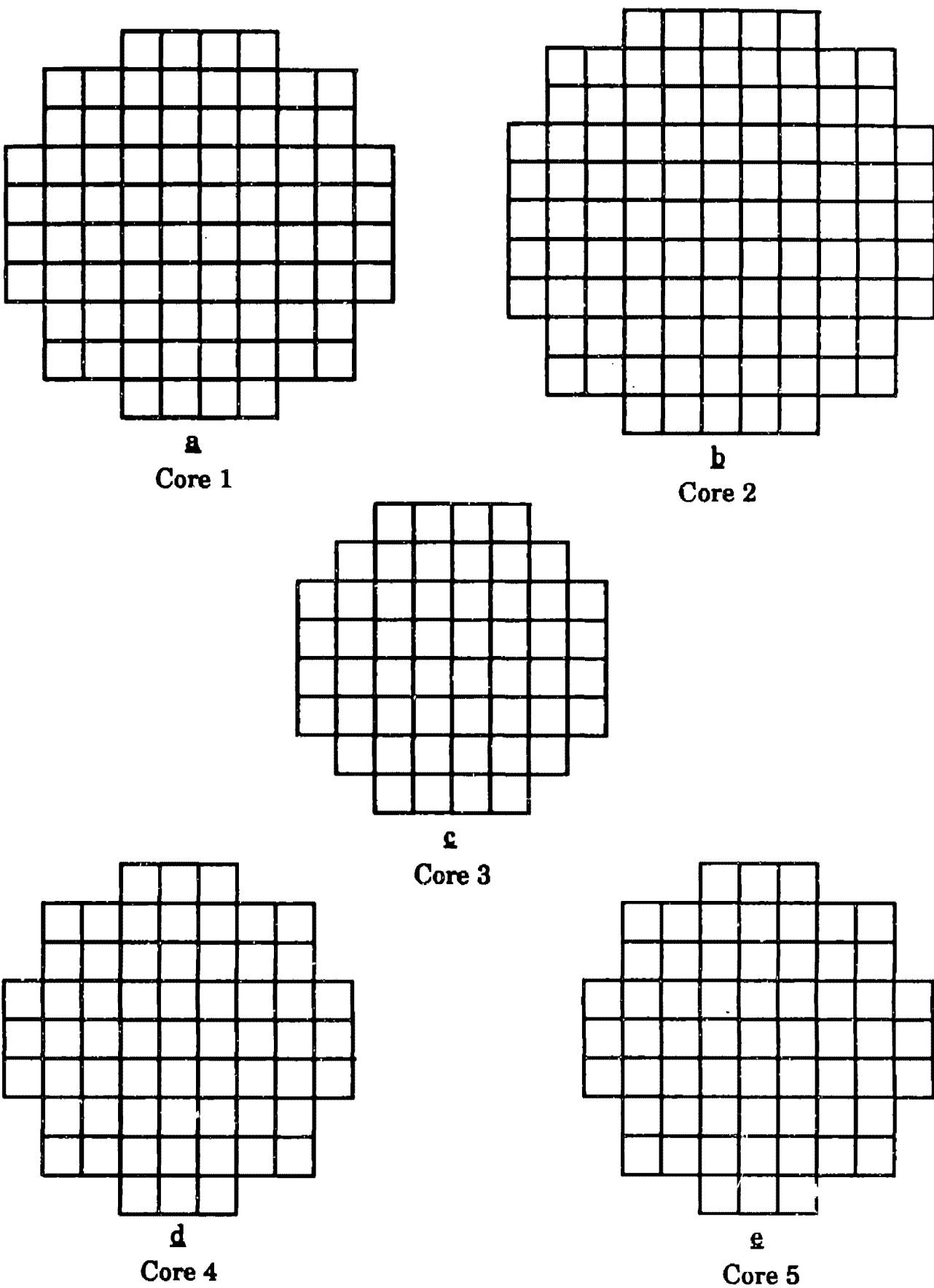


**Figure 5.7** Reactor core fuel element grids.

## **5.6 Thermal Hydraulic Results**

For each reactor core, the simplified thermal hydraulic analysis described in Section 4.2 was performed using the fuel cladding and coolant water properties of Tables 2.1, 2.3 and 2.8 respectively, the coolant water inlet and outlet temperatures listed in Section 1.2 and the fuel element dimensions for each core listed in Table 3.2. The results of these calculations are listed in Table 5.4.

The calculated values for the coolant water velocity range from 2.7m/s to 5.8m/s. The coolant velocity in the thin coolant channels of the Advanced Test Reactor (ATR) is 13.4m/s. Since the coolant channel thickness of reactor core 4 is of similar thickness and is thinner than the coolant channel design used by reactor cores 1, 2 and 3, the calculated coolant velocities for the reactor cores 1, 2, 3 and 4 are practical. The thickness of the channel used by reactor core 5 is 18% thinner than the channel used by reactor core 4. However, the coolant velocity required for this channel is 5.37m/s; 60% less than the coolant velocity which could be accommodated by the coolant channel of reactor core 4 as with the ATR. Thus it is reasonable to conclude that the coolant velocity of 5.37m/s calculated for reactor core 5 is practical.

For reactor cores 1, 2 and 3 which utilize the thick plate fuel design, the calculated fuel center-line temperatures,  $T_{fc}$ , range from 510°C to 530°C. This is well within acceptable bound since commercial reactor cores utilizing UO<sub>2</sub> fuel operate with center-line temperatures on the order of 2000°C.[7] For reactor core 3 which operates at a relatively high power density compared to reactor cores 1 and 2, the fuel center-line temperature is suppressed by the relatively high effective thermal

**Table 5.4. Thermal-hydraulic data.**

Reactor Core	Core 1	Core 2	Core 3	Core 4	Core 5
Vol% <sub>c</sub> (meat)	25.6	21.3	21.3	14.4	16.0
q''' <sub>max,m</sub> (kW/l)	939	855	2513	2550	2658
q(kW)	64.1	64.3	138.3	54.7	54.0
v(m/s)	2.7	2.7	5.8	4.4	5.4
h(W/m <sup>2</sup> -°K)	25763	25817	47680	44287	54229
k <sub>f</sub> (W/m-°K)	3.5	3.5	17.9	14.5	15.0
T <sub>fc</sub> (°C)	530	510	516	366	363

conductivity of the fuel meat. This high thermal conductivity results from the cermet fuel design where the volume percent in the fuel meat, Vol%<sub>m</sub>(Zr-4), of the relatively high thermal conductivity Zr-4 matrix material is greater than 50%.

For reference, the calculated values of Vol%<sub>c</sub>(meat), q'''<sub>max</sub>, h and k<sub>f</sub> are also listed in Table 5.4 for each reactor design.

## **5.7 Whole Core Materials**

Table 5.5 summarizes the whole core B.O.C. and E.O.C. materials data calculated by the methods described in Section 4.1.4. which have been calculated for reference purposes. The E.O.C. enrichment is the percentage of  $U^{235}$  which is contained in the total E.O.C. uranium mass (i.e, the sum of the E.O.C. masses of  $U^{235}$ ,  $U^{236}$  and  $U^{238}$ ).

Figures 5.8 to 5.12 are plots over the refueling lifetime of the plutonium mass contained in reactor cores 1, 2, 3, 4 and 5 respectively. Plutonium buildup results from the conversion of  $U^{238}$  to  $Pu^{239}$ , which in turn is converted to  $Pu^{240}$ ,  $Pu^{241}$  and  $Pu^{242}$ . Reactor core 1 which utilizes 7% enriched uranium contains less plutonium than reactor core 2 which is fueled with 20% enriched uranium since it has a refueling lifetime half that of core 2. For reactor core 3, Figure 5.10 indicates that the total mass of plutonium in the core decreases near E.O.C. This results since the  $U^{238}$  concentration has been depleted to an extent that  $Pu^{239}$  production is less than the consumption of  $Pu$  isotopes by fission or conversion to higher actinides.

**Table 5.5. Core materials data.**

Reactor Core	Core 1	Core 2	Core 3	Core 4	Core 5
$t_{rf}$ (years)	600	1200	1200	1200	1200
B.O.C. U <sup>235</sup> (kg)	74	195	106	174	153
B.O.C. U <sup>238</sup> (kg)	1049	783	3.0	4.9	4.3
B.O.C. enrichment (%)	7.0	20.0	97.3	97.3	97.3
Burnup(MWd/T)	28290	62120	548570	336160	382700
Burnup(at%)	3.0	6.6	57.9	35.5	40.4
E.O.C. U <sup>235</sup> (kg)	44	124	34	96	75
E.O.C. U <sup>238</sup> (kg)	5.7	14.2	14.0	—	16.7
E.O.C. U <sup>238</sup> (kg)	972	754	1.75	—	3.3
E.O.C. enrichment (%)	4.28	13.9	68.1	—	81.8
Pu total (kg)	8.9	11.5	0.26	0.44	0.46
Pu fissile (%)	83.5	85.6	75.6	94.5	84.5

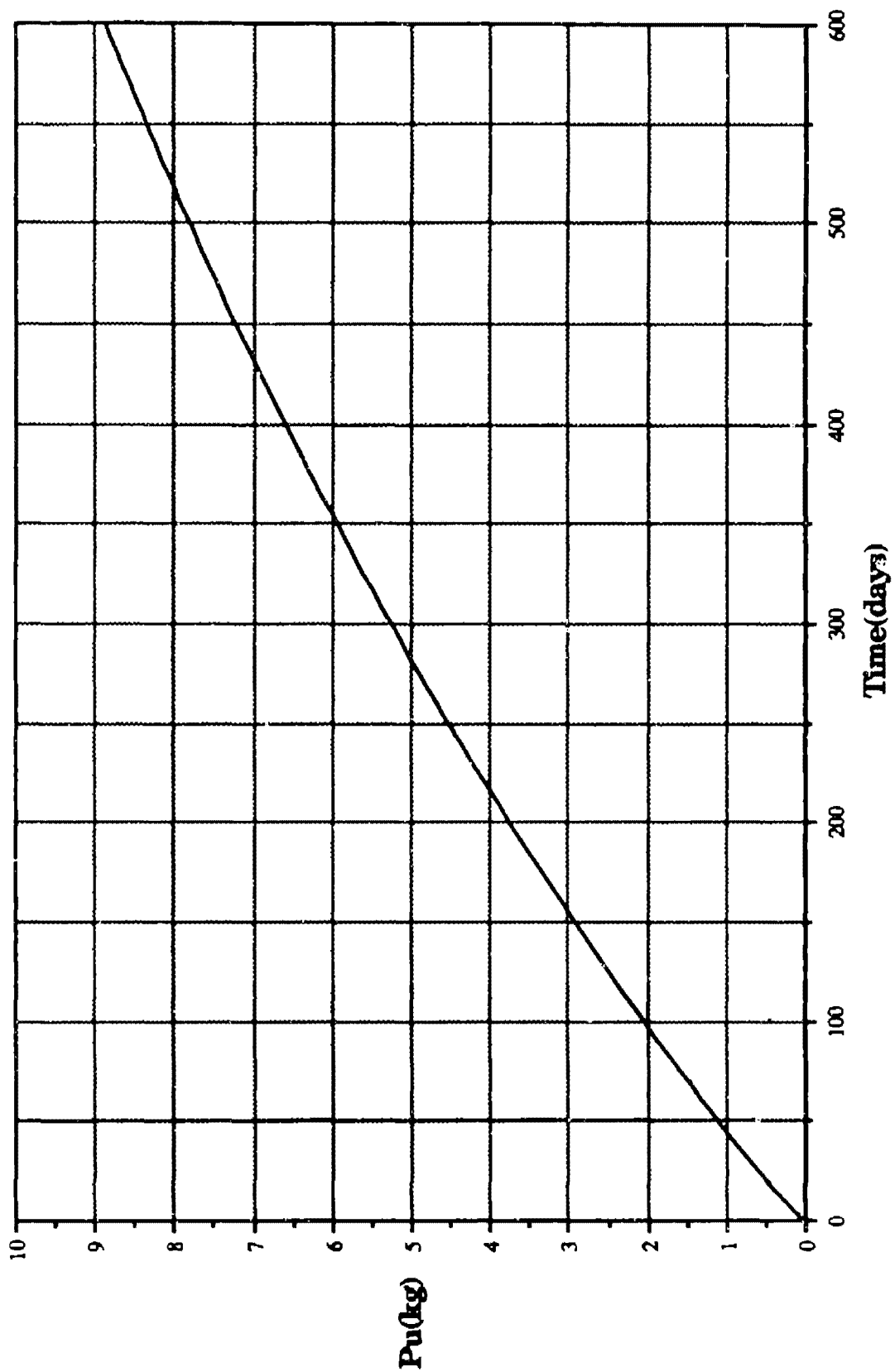


Figure 5.8. Reactor core (1), plutonium Vs. time.

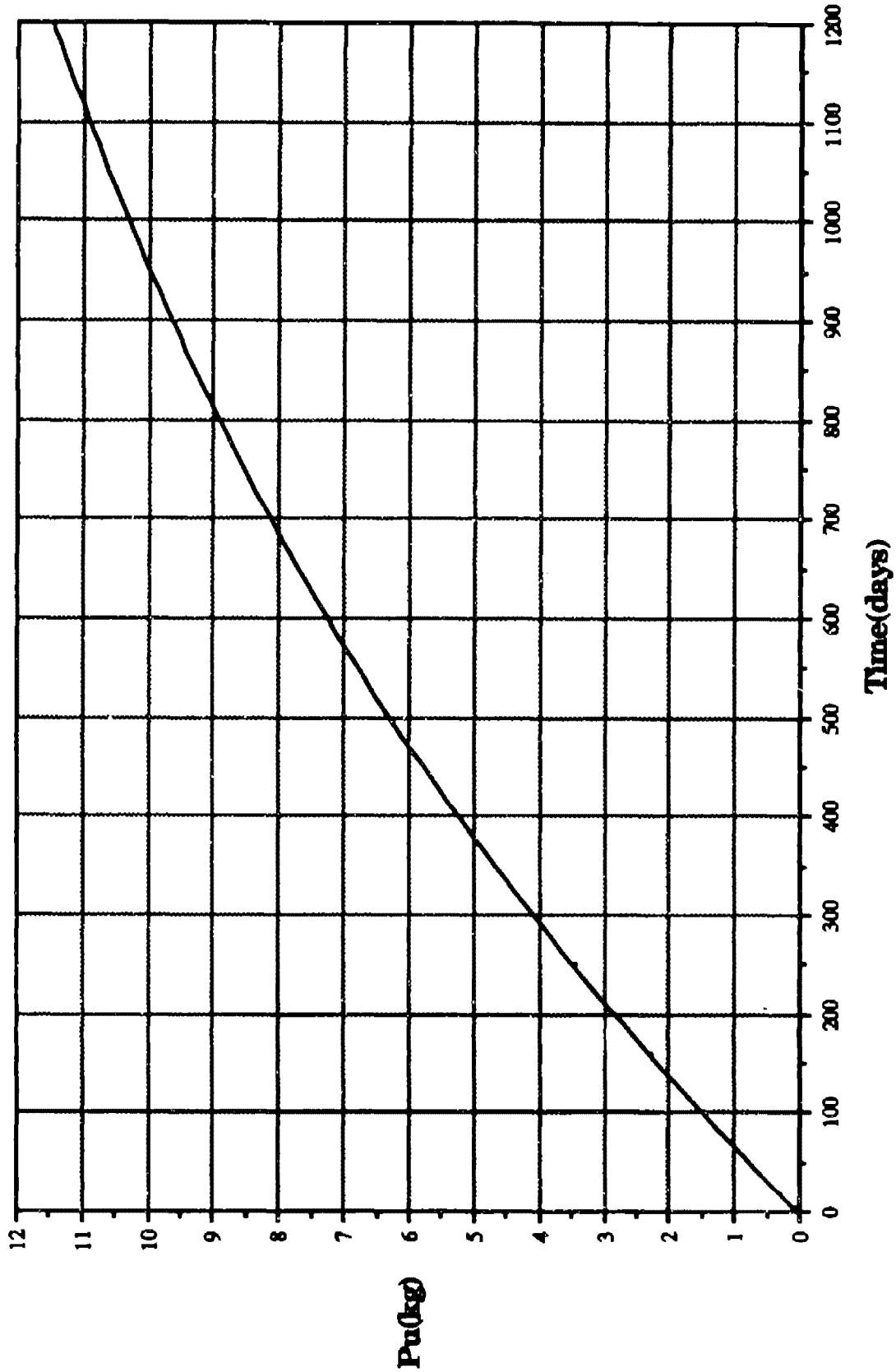
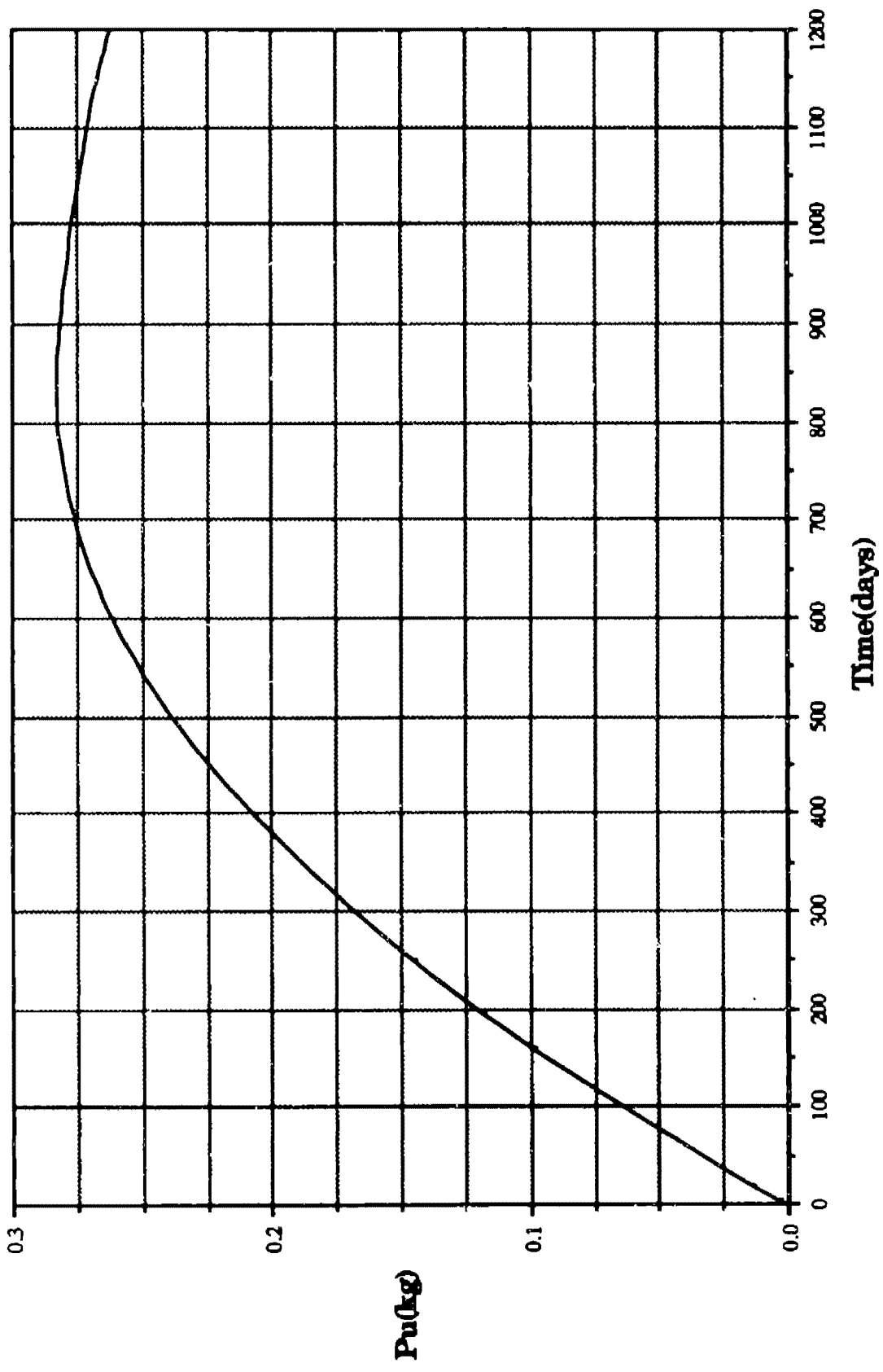


Figure 5.9. Reactor core (2), plutonium Vs. time.



**Figure 5.10. Reactor core (3), plutonium Vs. time.**

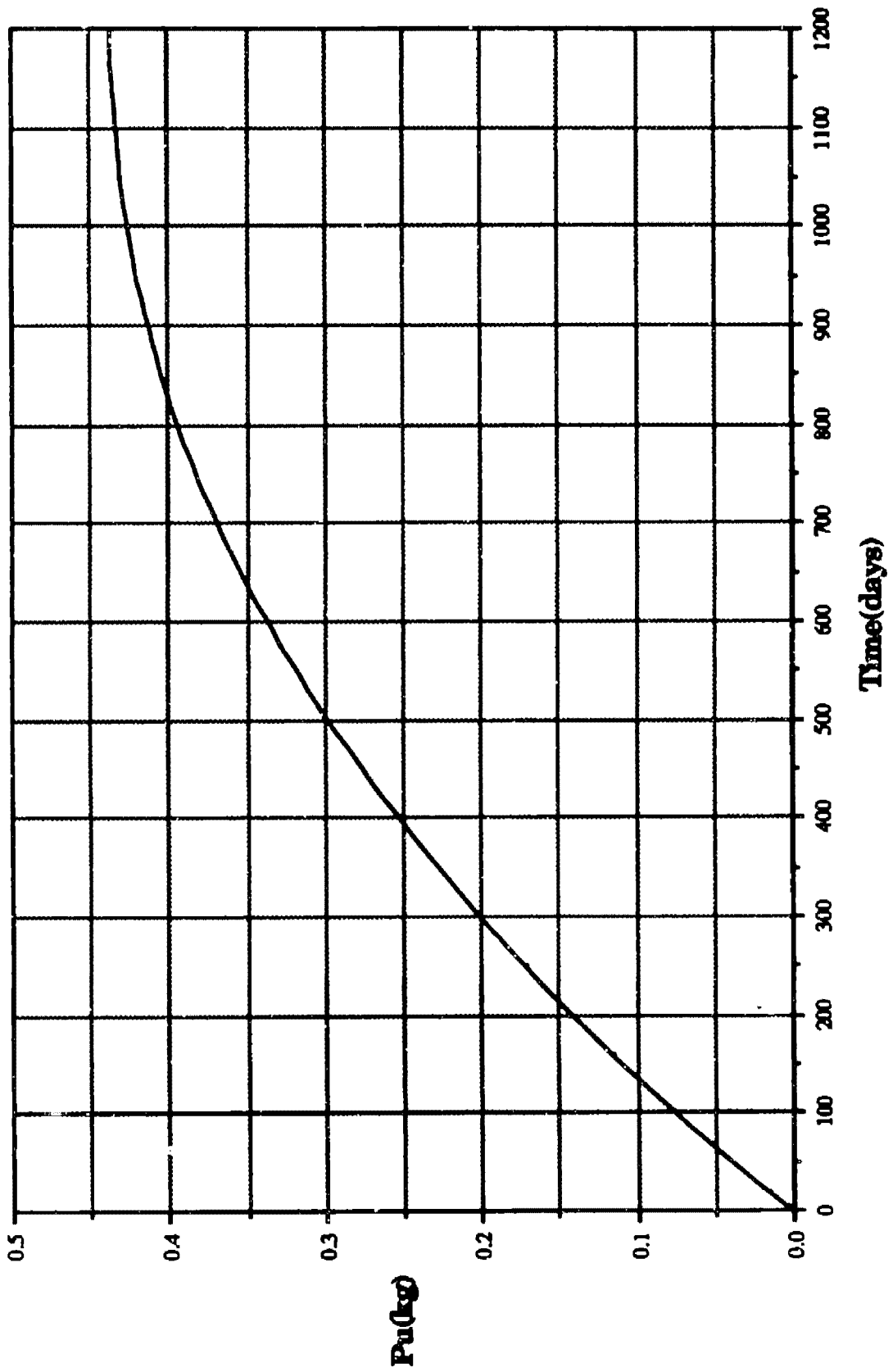


Figure 5.11. Reactor core (4), plutonium Vs. time.

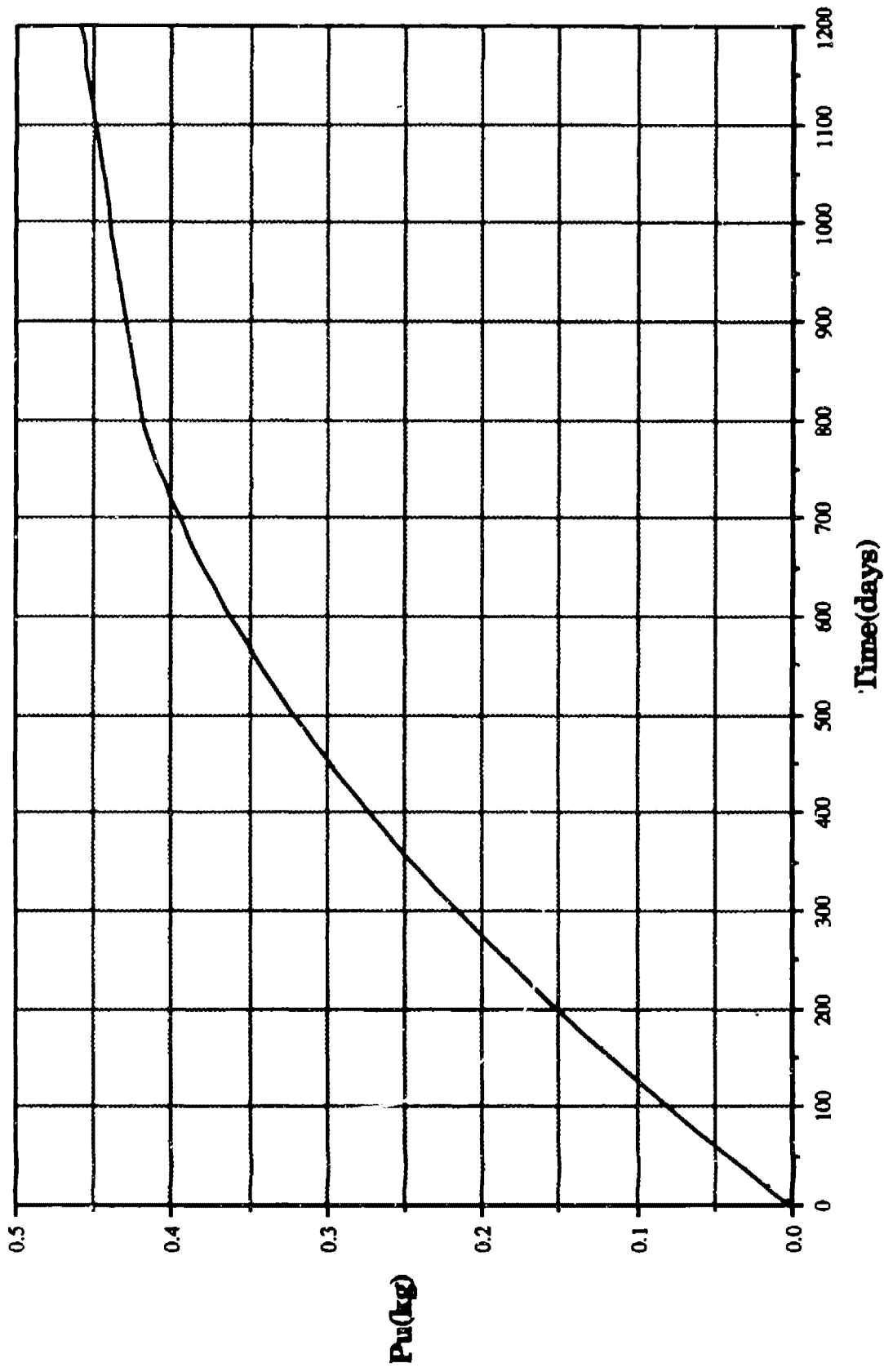


Figure 5.12. Reactor core (5), plutonium Vs. time.

## 5.8 Correction for Coolant Water Number Density Error

As discussed in Section 4.1.2.5, the hydrogen and oxygen number density values specified in the EPRI-Cell input files for all reactor core designs were calculated based on the density of water at room temperature rather than at the average reactor coolant temperature of 305°C. The density of water at room temperature (20°C) is 1g/cm<sup>3</sup> while at 305°C it is 0.74g/cm<sup>3</sup>. The Equations used to calculate the hydrogen and oxygen number densities are listed below.

The number density of the H<sub>2</sub>O molecule is given by,

$$N(\text{H}_2\text{O}) = \frac{\rho(\text{H}_2\text{O})(N_A)}{M(\text{H}_2\text{O})(10^{24}\text{barns/cm}^2)} \quad (4.23)$$

where the associated H<sub>2</sub>O properties are listed in Table 2.8. The number densities of the hydrogen and oxygen constituents are given by,

$$N(\text{H}) = 2N(\text{H}_2\text{O}) \quad (4.24)$$

$$N(\text{O}) = N(\text{H}_2\text{O}) \quad (4.25)$$

Thus at normal reactor operating conditions, the actual hydrogen and oxygen number densities are 26% less than the number densities that were used to model the reactor cores 1,2,3,4 and 5. As discussed in Chapter 3 and as shown by the moderator reactivity coefficients listed in Table 5.2, each reactor core is undermoderated. Thus the coolant water slowing down properties increase the thermal neutron population more the coolant water

neutron absorption properties decreases the thermal neutron population. Consequently, a decrease in coolant water density must be offset with an increase in  $V_{\text{core}}$  in order to maintain constant core excess reactivity with all other core materials volume fractions remaining unchanged. As a result, an increase in  $V_{\text{core}}$  for constant refueling time will result in a decrease in the values of  $q'''_{\text{ave,r}}$ ,  $B^2$  and  $BU$ . An increase in  $V_{\text{core}}$  will also cause an increase in the total mass of materials present in each core which are calculated by Equation 4.42.

In this section an estimated correction factor for  $V_{\text{core}}$ , which is applicable to each core considered for is study, is derived using an approximate 2-group diffusion analysis. The general multigroup neutron diffusion equation solved is,

$$D_g^k B^2 \phi_g + \Sigma_{tg}^k \phi_g = \sum_{g'=1}^G \frac{1}{\lambda} [\chi_{g'} \nu \Sigma_{fg'}^k \phi_{g'} + \Sigma_{gg'}^k \phi_{g'}] \quad (5.2)$$

where,

$$\Sigma_{tg}^k \phi_g = \Sigma_{ag}^k \phi_g + \sum_{g'=1}^G \Sigma_{g'g}^k \phi_{g'} \quad (5.3)$$

These Equations are described in great detail in Reference[25].

The terms used in Equations 5.2 and 5.3 are defined below.

$D_g$  = Neutron diffusion coefficient

$B^2$  = Geometric buckling

$\Sigma_{ag}$  = Neutron absorption cross-section

$\Sigma_{g'g}$  = Neutron scattering cross-section from group  $g$  to group  $g'$

$\Sigma_{gg'}$  = Neutron scattering cross-section from group  $g'$  to group  $g$

$\Sigma_{fg'}$  = Neutron fission cross-section in group  $g'$

$\nu$  = Average neutron yield per fission event

$\chi_g$  = Probability a fission neutron will be born in group  $g$

$\lambda$  = Eigenvalue to set the RHS and LHS of Equation 5.2 equal

$\phi_g$  = Neutron flux in group  $g$

$\kappa$  = Region of reactor core to which Equation 5.2 is applied

Solving Equation 5.2 for  $\lambda$  with  $\lambda = k_{eff}$  for two neutron energy groups yields,

$$k_{eff} = \frac{\nu \Sigma_{f2} \Sigma_{21}}{(D_1 B^2 + \Sigma_{a1} + \Sigma_{11})(D_2 B^2 + \Sigma_{a2})} + \frac{\nu \Sigma_{f1}}{(D_1 B^2 + \Sigma_{a1} + \Sigma_{11})} \quad (5.4)$$

For purposes of this analysis it is assumed that  $\Sigma_{12}$  (scattering from the thermal to the fast energy group) is equal to zero since it is sufficiently small. Also since most fission neutrons are born into the fast energy group, it is assumed that  $\chi_1 = 1$  and  $\chi_2 = 0$ . These considerations are further explained in Reference [Henry]. The diffusion coefficient  $D$  is defined by the following relation,

$$D_g = \frac{1}{3\Sigma_{trg}} \quad (5.5)$$

where,

$$\Sigma_{tr} = \text{Neutron transport cross-section}$$

Each macroscopic cross-section used in Equations 5.2 and 5.3 are the sum of the contributions of the macroscopic cross section of water and the macroscopic cross-section of all non-coolant materials present in the reactor. Thus  $\Sigma_{tr1}$ ,  $\Sigma_{tr2}$ ,  $\Sigma_{a1}$ ,  $\Sigma_{a2}$  and  $\Sigma_{21}$  are defined as,

$$\Sigma_{tr1} = \Sigma_{tr1}(m) + \Sigma_{tr1}(w) \quad (5.6a)$$

$$\Sigma_{tr2} = \Sigma_{tr2}(m) + \Sigma_{tr2}(w) \quad (5.6b)$$

$$\Sigma_{a1} = \Sigma_{a1}(m) + \Sigma_{a1}(w) \quad (5.6c)$$

$$\Sigma_{a2} = \Sigma_{a2}(m) + \Sigma_{a2}(w) \quad (5.6d)$$

$$\Sigma_{21} = \Sigma_{21}(m) + \Sigma_{21}(w) \quad (5.6e)$$

The parameter  $m$  refers to all non-coolant materials present in the reactor while  $(w)$  refers to the coolant water. For simplifying purposes of this analysis, it is assumed that  $\Sigma_{21}(m) = 0$  since it is small compared to  $\Sigma_{21}(w)$ . This concept is further discussed in Reference [25]. Substituting

Equations 5.6a and 5.6b into Equation 5.4 and Equations 5.6c, 5.6d and 5.6e into Equation 5.5 the following result is obtained.

$$\begin{aligned}
 k_{\text{eff}} = & \left( \frac{\nu \Sigma_{f2} \Sigma_{21}(w)}{\left[ (D_1(m) + D_1(w))B^2 + \Sigma_{a1}(m) + \Sigma_{a1}(w) + \Sigma_{21}(w) \right]} \right) \\
 & \times \left( \frac{1}{\left[ (D_2(m) + D_2(w))B^2 + \Sigma_{a2}(m) + \Sigma_{a2}(w) \right]} \right) \\
 & + \left( \frac{\nu \Sigma_{f1}}{\left[ (D_1(m) + D_1(w))B^2 + \Sigma_{a1}(m) + \Sigma_{a1}(w) + \Sigma_{21}(w) \right]} \right) \quad (5.7)
 \end{aligned}$$

The 2-group cross-section data used in this analysis is obtained from the 5-group cross-section data listed in the microscopic and macroscopic edits of the EPRI-Cell output file for timestep 1 of reactor core 3 which is listed in Appendix E. The first four cross-section groups are collapsed into 1 group (fast group) while the fifth group cross-section data remains constant (thermal group). For purposes of this simplified two group analysis, the 2-group energy structure described in Table 4.3 is employed. Thus the boundary between energy groups is 0.625eV.

To determine the 2-group macroscopic cross-sections for the H<sub>2</sub>O coolant water, the 5-group microscopic cross-sections for hydrogen and oxygen listed in the microscopic edit are used. The microscopic cross-sections used in the first four energy groups are collapsed into the fast energy group by flux weighting using the group fluxes listed in the macroscopic edit. For this purpose, the following equations are employed.

$$\sigma_{x1}(H) = \frac{\sum_{g=1}^4 \phi(g) \sigma_{x(g)}(H)}{\sum_{g=1}^4 \phi(g)} \quad (5.8)$$

$$\sigma_{x1}(O) = \frac{\sum_{g=1}^4 \phi(g) \sigma_{x(g)}(O)}{\sum_{g=1}^4 \phi(g)} \quad (5.9)$$

The subscripted numbers in parenthesis indicate the energy group of the cross-section as it is listed in the 5-energy group structure of the EPRI-Cell output file listed in Appendix E. The subscripted numbers not in parenthesis indicate the energy group of the new 2-group structure where 1 designates the fast group and 2 designates the thermal group. In each equation used in this analysis, the subscript,  $x$ , refer to any arbitrary cross-section.

The thermal group microscopic cross sections for hydrogen and oxygen are given by,

$$\sigma_{x2}(H) = \sigma_{x(5)}(H) \quad (5.10)$$

$$\sigma_{x2}(O) = \sigma_{x(5)}(O) \quad (5.11)$$

The core averaged macroscopic cross-sections for oxygen and hydrogen are then determined by the following equations.

$$\Sigma_{x1}(\text{H}_2\text{O}) = \text{Vol}_c(\sigma_{x1}(\text{H})N(\text{H}) + \sigma_{x1}(\text{O})N(\text{O})) \quad (5.12)$$

$$\Sigma_{x2}(\text{H}_2\text{O}) = \text{Vol}_c(\sigma_{x2}(\text{H})N(\text{H}) + \sigma_{x2}(\text{O})N(\text{O})) \quad (5.13)$$

where the hydrogen and oxygen number densities,  $N(\text{H})$  and  $N(\text{O})$ , are listed in the zone homogenized number densities of the EPRI-Cell output file of Section E.4. The multiplying factor  $\text{Vol}_c(\text{H}_2\text{O})$ , which is the  $\text{H}_2\text{O}$  volume fraction (volume percent divided by 100) in the core, must be included since the microscopic cross-sections are not core averaged. The core  $\text{H}_2\text{O}$  volume fraction is given by,

$$\text{Vol}\%_c(\text{H}_2\text{O}) = \frac{t'_w}{t_f + 2t'_c + t'_w} (100) \quad (5.14)$$

To determine the 2-group macroscopic cross-sections representing all noncoolant materials present in the core, the 2-group core homogenized cross section representing all materials present in the core are first determined. For this purpose, the 5-group macroscopic cross-section data listed in the macroscopic edit of the EPRI-Cell output file listed in Section E.4 is used. The macroscopic cross-sections used in the first four energy groups are collapsed into the fast energy group by flux weighting using the group fluxes also listed in the macroscopic edit. The following equation is used for this calculation.

$$\Sigma_{x1} = \frac{\sum_{g=1}^4 \phi(g) \Sigma_{x1}(g)}{\sum_{g=1}^4 \phi(g)} \quad (5.15)$$

The thermal group macroscopic cross sections are given by the relation,

$$\Sigma_{x2} = \Sigma_{x(5)} \quad (5.16)$$

The thermal group value for  $\nu\Sigma_{f2}$  is given by,

$$\nu\Sigma_{f2} = \nu\Sigma_{f(5)} \quad (5.17)$$

Thus the 2-group core averaged macroscopic cross-sections representing all noncoolant materials are given by the following equations.

$$\Sigma_{x1(m)} = \Sigma_{x1} - \Sigma_{x1}(\text{H}_2\text{O}) \quad (5.18)$$

$$\Sigma_{x2(m)} = \Sigma_{x2} - \Sigma_{x2}(\text{H}_2\text{O}) \quad (5.19)$$

The values of  $\Sigma_{21}$  can not be calculated directly from the cross-section data listed in the EPRI-Cell output file. The scattering cross-sections listed include ingroup scattering according to the following equation.

$$\Sigma_{s1} = \Sigma_{21} + \Sigma_{11} \quad (5.20)$$

The macroscopic removal cross-section is defined as,

$$\Sigma_{r1} = \Sigma_{t1} - \Sigma_{11} \quad (5.21)$$

which is used to determine  $\Sigma_{11}$ . Substituting this value into Equation 5.20,  $\Sigma_{21}$  is determined by,

$$\Sigma_{21} = \Sigma_{e1} - \Sigma_{11} \quad (5.22)$$

For Equation 5.7 the value of  $B^2$  remains to be determined. Since the values for  $V_{core}$  calculated for this study range from 264.6L to 666.7L as listed in Table 5.3, an intermediate value for  $V_{core}$  was chosen in order to calculate the value of  $B^2$  for use in Equation 5.7. The value of  $B_2$  is then determined by Equation 4.37.

$$B^2 = \left(\frac{2405}{R}\right)^2 + \left(\frac{\pi}{H}\right)^2 \quad (4.37)$$

where

$$R = \sqrt[3]{\frac{V}{2.5\pi}} \quad (4.35)$$

and

$$H = 2.5R \quad (4.36)$$

The data calculated using the techniques described above and the associated values are listed below.

$$\begin{aligned}\Sigma_{a1}(m) &= 0.0145\text{cm}^{-1} \\ \Sigma_{a1}(w) &= 0.00017\text{cm}^{-1} \\ \Sigma_{a2}(m) &= 0.3642\text{cm}^{-1} \\ \Sigma_{a2}(w) &= 0.00547\text{cm}^{-1} \\ \Sigma_{tr1}(m) &= 0.1367\text{cm}^{-1} \\ \Sigma_{tr1}(w) &= 0.1872\text{cm}^{-1} \\ \Sigma_{tr2}(m) &= 0.3436\text{cm}^{-1} \\ \Sigma_{tr2}(w) &= 0.7572\text{cm}^{-1} \\ D_1(m) &= 2.483\text{cm} \\ D_1(w) &= 1.781\text{cm} \\ D_2(m) &= 0.9700\text{cm} \\ D_2(w) &= 0.4402\text{cm} \\ v\Sigma_{f1} &= 0.0187\text{cm}^{-1} \\ v\Sigma_{f2} &= 0.4876\text{cm}^{-1} \\ \Sigma_{t1}(w) &= 0.45393\text{cm}^{-1} \\ \Sigma_{s1}(w) &= 0.46149\text{cm}^{-1} \\ \Sigma_{r1}(w) &= 0.07071\text{cm}^{-1} \\ \Sigma_{11}(w) &= 0.38322\text{cm}^{-1} \\ \Sigma_{21}(w) &= 0.07827\text{cm}^{-1} \\ B^2 &= 0.00533\text{cm}^{-2}\end{aligned}$$

The values listed above are substituted into Equation 5.7 and used to calculate a value for  $k_{\text{eff}}$  which is calculated to be  $k_{\text{eff}} = 1.036$ .

To determine the effect of a reduction in coolant density on  $V_{\text{core}}$ , Equation 5.7 is rewritten as,

$$\begin{aligned}
 k_{\text{eff}} = & \left( \frac{v \Sigma_{f2} f_w \Sigma_{21}(w)}{[(D_1(m) + f_w D_1(w)) f_B B^2 + \Sigma_{a1}(m) + f_w \Sigma_{a1}(w) + f_w \Sigma_{21}(w)]} \right) \\
 & \times \left( \frac{1}{[(D_2(m) + f_w D_2(w)) f_B B^2 + \Sigma_{a2}(m) + f_w \Sigma_{a2}(w)]} \right) \\
 & + \left( \frac{v \Sigma_{f1}}{[(D_1(m) + f_w D_1(w)) f_B B^2 + \Sigma_{a1}(m) + f_w \Sigma_{a1}(w) + f_w \Sigma_{21}(w)]} \right) \quad (5.23)
 \end{aligned}$$

where,

$f_w$  = Fraction by which  $\rho(\text{H}_2\text{O})$  must be decreased

$f_B$  = Fraction by which  $B^2$  must be decreased in response to  $f_w$

Substituting a value for  $f_w = 0.75$  into Equation 5.23 along with the calculated values for the other parameters Equation 5.23 is solved via iteration for  $f_B$ . The parameter  $f_B$  is the approximate fraction by which the geometric buckling of each reactor core must be decreased in order to maintain constant reactivity. As evident from Equations 4.36 and 4.37,  $f_B$  is proportional to the inverse square of  $f_R$  (fraction by which the core radius must be increased) by the following relation,

$$f_B = \frac{1}{(f_R)^2} \quad (5.24)$$

Solving Equation 5.24 for  $f_R$  yields,

$$f_R = \sqrt{\frac{1}{f_B}} \quad (5.25)$$

By Equation 4.35 the correction multiplier,  $f_V$ , for  $V_{\text{core}}$  is given by,

$$f_V = (f_R)^3 \quad (5.26)$$

The parameter  $f_V$  is the volume correction multiplier. By Equation 4.1, the correction multiplier,  $f_q$ , for  $q'''_{\text{ave},r}$  and  $q'''_{\text{max}}$  is given by,

$$f_q = \frac{1}{f_V} \quad (5.27)$$

Since mechanical burnup is proportional to  $q'''_{\text{ave},r}$ , the burnup correction multiplier is given by,

$$f_{\text{BU}} = f_q \quad (5.28)$$

The correction multiplier,  $f_m$ , for the net core material masses which are listed in Table 5.4 is given by,

$$f_m = f_V \quad (5.29)$$

The values for the approximate correction factors are listed in Table 5.6.

**Table 5.6. Approximate correction multipliers.**

$f_B$	0.90
$f_R$	1.05
$f_H$	1.05
$f_V$	1.17
$f_q$	0.85
$f_{BU}$	0.85
$f_m$	1.17

## **CHAPTER 6**

### **Conclusion and Recommendations**

#### **6.1 Conclusion**

As stated earlier, it is known that modern U.S. are fueled with very highly enriched uranium; greater than 90%. In this study, a reactor core using plate type fuel elements fueled with 97.3% enriched uranium which operates with a refueling lifetime of 1200FPD, was modeled. The safety coefficients of reactivity and thermal hydraulics results calculated are acceptable.

The French have proved that the use of LEU (i.e., approximately 7% enriched uranium) as a nuclear submarine fuel is feasible. In this study a reactor core using plate type fuel elements fueled with 7% enriched uranium was modeled. However, it was not possible for this core to maintain criticality beyond a refueling lifetime of approximately 600FPD. Also for this case, the safety coefficient of reactivity and thermal hydraulics are acceptable. The volume of this core is roughly twice the size of the core fueled with 97.35 enriched uranium. This corresponds to a 17cm and 20cm increase in diameter and height respectively (these dimensions are corrected using correction factors of Table 5.6) .

A reactor core using plate type fuel elements fueled with 20% enriched uranium which operates with a refueling lifetime of 1200FPD, was modeled. The safety coefficient of reactivity and thermal hydraulics differ very little compared to the core fueled with 97.3% enriched uranium. As discussed in Chapter 1, low enriched uranium, LEU, is internationally regarded to be uranium with enrichment in the range 0% - 20%. Thus it is

demonstrated that a reactor core using LEU and with operating performance similar to the 97.3% enriched core, can be designed. The core fuel with 20% enriched uranium is, however, about two and one half times larger than the core fueled with 97.3% enriched uranium. This corresponds to a 24cm and 30cm increase in diameter and height respectively (these dimensions are corrected using correction factors of Table 5.6). Thus as maintained in Chapter 1, these dimensional increases are sufficiently small that they can easily be compensated for by the use of an integral reactor design.

## **6.2 Recommendations for Future Work**

For each reactor core modeled in this study using one dimensional calculations, a more detailed analysis can be done which accounts for spatial dependence of fuel depletion, control rod motion and startup, shutdown and transient behavior.

The DIF3D code developed by Argonne National Laboratory can be used to model, with 3-D diffusion theory, the steady-state behavior of each reactor core. DIF3D solves multigroup diffusion theory eigenvalue, adjoint, fixed source and criticality (concentration search) problems in 1-, 2- and 3-space dimensions for for orthogonal (rectangular and cylindrical), triangular and hexagonal geometries.[26] The reactor core fuel element grids illustrated in Figure 5,1 and dimensions of Table 3.2 can be used in preparation of a DIF3D input file. The core heights listed in Table 5.5 can also be used. (Note that these dimensions must be corrected using the correction factors listed in Table 5.6). The EPRI-Cell input files used for this study are set up to produce 5-group cross-section data in ISOTXS data sets (see Appendix E) which can be input directly into DIF3D.

To model the time dependant aspects of the fuel cycle of each reactor core, the REBUS-3 fuel cycle analysis code, also developed by Argonne National Laboratory, can be used. As in the above case the corrected dimensional data described above can be used in preparation of a REBUS-3 input file. There are four types of search procedures that may be carried out in order to satisfy user supplied constraints.[27]

- 1) **Adjustment of the reactor refueling lifetime in order to achieve a specified E.O.C. fuel burnup.**
- 2) **Adjustment of the B.O.C. uranium enrichment in order to achieve a specified E.O.C.  $k_{eff}$  at any specified point during the refueling lifetime.**
- 3) **Adjustment of the burnable poison density (i.e., coolant water boron concentration) in order to maintain a specified value of  $k_{eff}$  throughout the reactor refueling lifetime.**
- 4) **Adjustment of the reactor refueling lifetime to achieve a specified value of  $k_{eff}$  at E.O.C.**

Also, for REBUS-3, the 5-group cross-section data listed in the ISOTXS data sets can be input directly.

For thermal hydraulic transient analysis, the PARET code developed by the Phillips Petroleum Company, can be used. PARET is a digital computer program designed for use in predicting the course and consequences of nondestructive reactivity accidents in small reactor cores. This code couples neutronics and thermal hydraulics and uses point kinetics, 1-D hydrodynamics and 1-D heat transfer.[28]

## **References**

- [1] Cochran, Thomas B., Arkin, William M., Norris, Robert S., Hoenig, Milton M., Nuclear Weapons Data Book, Volume II, U.S. Nuclear Warhead Production, Ballinger Publishing Company, Cambridge, Massachusetts, 1987.
- [2] Girard, Yves, Technicatome of France, Presentation at the Conference on The Implication of the Aquisition of Nuclear-Powered Submarines (SSN) by Non-Nuclear Weapons States, MIT, March 27 - 28, 1989.
- [3] Nuclear Theft: Risks and Safeguards, A Report to the Energy Policy Project of the Ford Foundation, Manson Willrich, Theodore B. Taylor, Ballinger Publishing Company, Cambridge, Mass, 1974, Pg. 228.
- [4] An Analysis of Air Independent Power Plants for Adaption to Conventional Submarines; Prepared for the Department of National Defense, DMEE-6, GasTops Ltd., GTL-7-47-TR.1, Gloucester, July, 1987.
- [5] Fact Sheet, Rubis/Trafalgar Class SSN's, Canadian National Defense, Ottawa, Ontario.
- [6] Freidman, Norman, Submarine Design and Development, Naval Institute Press, Annapolis, Maryland, 1984.

- [7] **Lamarsh, John R., Introduction to Nuclear Engineering (2nd Edition), Addison-Wesley publishing Company, Reading, Massachusetts, 1983.**
- [8] **Wings Magazine, Canadian Submarine Acquisition Program (CASAP), Nuclear Propulsion, Thomas Lynch, April 1988, Pgs 64-68.**
- [9] **EPRI-CELL Code Description, Prepared by: Nuclear Associates International Corporation, 6003 Executive Boulevard, Rockville, Md, 20852, Prepared for: Electric Power Research Institute, 3412 Hillview Avenue, Palo Alto, Ca, 94304, October 29, 1975.**
- [10] **Personal Communication**
- [11] **Directory of Nuclear Reactors, Research and Test Reactors, Vol. V, International Atomic Energy Agency, Vienna, 1964, Pg 107.**
- [12] **Research Reactor Core Conversion From the Use of Highly Enriched Uranium to the Use of Low Enriched Uranium Fuels Guidebook, A Technical Document Issued by the International Atomic Energy Agency, Vienna, 1980.**

- [13] Barnier, M., Baylot, J.P., Osiris, A MTR Adopted and Well Fitted to LEU Utilization, Qualification and Development, Experimental Reactors Department, Saclay Nuclear Center, France, As Presented in, JAERI-M 80-073, Proceedings of the International Meeting on Reduced Enrichment for Research and Test Reactors, October 24-27, 1983, Tokai, Japan, May 1984.
- [14] Reactors of the World, Second Series, Simmons-Boardman Publishing Corporation, New York.
- [15] Robertson, J.A.L., Irradiation Effects in Nuclear Fuels, Atomic Energy of Canada, Ltd., American Nuclear Society, Gordon and Breach, N.Y., 1969.
- [16] Frost, Brian T., Nuclear Fuel Elements, (Argonne National Laboratory), Pergamon Press, N.Y., 1982.
- [17] Kaufman, Albert F., Nuclear Reactor Fuel Elements, Metallurgy and Fabrication, John Wiley & Sons, N.Y., 1962.
- [18] Tong, L.S., Weisman, J., Thermal Analysis of Pressurized Water Reactors, 2nd Edition, American Nuclear Society, LaGrange Park, Illinois, 1979.

- [19] Copeland, G.L., Hobbs, R.W., Hofman, G.L., Snelgrove, J.L.,  
Performance of Low-Enriched  $U_3Si_2$  - Aluminum Dispersion Fuel in  
the Oak Ridge Research Reactor, Argonne National Laboratory,  
ANL/RERTR/TM-10, October, 1987.
- [20] Finnieston, H.M., Howe, J.P., Progress in Nuclear Energy, Series V,  
Metallurgy and Fuels, Pergamon Press, N.Y., 1955.
- [21] Travelli, A., Seminar Presented at M.I.T., The Reduced Enrichment  
Reactor Program, March, 1989.
- [22] Class Notes, Course 22.70, Nuclear Materials, Massachusetts  
Institute of Technology, Spring 1989.
- [23] Rahn, Frank J., Adamantiades, Achilles G., Kenton, John E.,  
Braun, Chaim, (of the Electric Power Research of California), A  
Guide to Nuclear Power Technology, A resource for Decision  
Making, John Wiley & Sons, N.Y., 1984, Pg 437.
- [24] Benedict, Manson, Pigford, Thomas H., Levi, Hans Wolfgang,  
Nuclear Chemical Engineering, McGraw Hill Book Company, New  
York, 1981.
- [25] Henry, Allan F., Nuclear-Reactor Analysis, MIT Press, Cambridge,  
Massachusetts, 1975.

- [26] ANL-82-64, DIF3D: A Code to Solve One-, Two-, and Three-Dimensional Diffusion Theory Problems, K.L. Derstine, Applied Physics Division, Argonne National Laboratory, 9700 South Cass Avenue, Argonne Illinois, 60439, April, 1984, Prepared for the U.S. Department of Energy.
- [27] ANL-83-2, A User's Guide for the REBUS-3 Fuel Cycle Analysis Capability, B.J. Toppel, Applied Physics Division, Argonne National Laboratory, 9700 South Cass Avenue, Argonne Illinois, 60439, March, 1983, Prepared for the U.S. Department of Energy.
- [28] PARCET - A Program for the Analysis of Reactor Transients, C.F. Obenchain, Phillips Petroleum Company, Atomic Energy Division, Contract AT(10-1)-205, Idaho Operations Office, U.S. Atomic Energy Commission, (IDO-17282, AEC Research and Development Report, Reactor Technology, Issued: January 1969).
- [29] Desjardins, Marie France, Rauf, Tariq, Opening Pandora's Box, Nuclear Powered Submarines and the Spread of Nuclear Weapons, Aurora Papers 8, The Canadian Center for Arms Control and Disarmament, June, 1988.
- [30] Desjardins, Marie France, Rauf, Tariq, Canada's Nuclear Submarine Program: A New Proliferation Concern, Arms Control Today, December, 1988,

- [31] **Nero, Anthony B. Jr., A Guidebook to Nuclear Reactors, Fuel Cycles, The Issues of Nuclear Power, University of California Press, Los Angeles, 1979.**
- [32] **India Gets Soviet Nuclear-Powered Sub, The Washington Post, Wednesday, January 6, 1988, Pg A8.**
- [33] **Manchanda, Rita, (New Delhi), Nuclear Ambitions: Soviet Submarine Deal Comes to Surface, Far Eastern Review, Defence Section, December 24, 1987.**
- [34] **Plutonium, Power and Politics, International Arrangements for the Disposition of Spent Fuel, Gene I. Rochlin, University of California Press, Los Angeles, 1979.**

## **Appendix A**

### **Non-Proliferation Treaty and Foreign Nuclear Objectives**

Modern day concerns are not only with the continued diffusion of information related to the design of nuclear weapons, but also with the increasing availability of the technology to produce weapons usable materials. To date there are five "official" nuclear weapons states (NWS), the U.S., the U.S.S.R., the U.K., France and China. However, Israel, South Africa and Pakistan are widely believed to have the capability to produce nuclear weapons, while India detonated a peaceful nuclear explosion (PNE) in 1974.

Relatively early on in the nuclear age, pressure began to develop for an international agreement to thwart both the vertical and especially the horizontal proliferation of nuclear weapons. (Horizontal proliferation refers to an increase in the number of states possessing nuclear weapons, while vertical proliferation refers to the growth in the nuclear arsenals of the five nuclear weapons states.)

Consequently, in June 1958, Ireland submitted to the UN General Assembly, a resolution requesting the establishment of a committee to study the dangers inherent in the further dissemination of nuclear weapons. This resolution did not deal specifically with horizontal proliferation; however it recognized the possibility that an increase in the number of nuclear weapons states may occur. Following mounting concern by the international community, the title Non-Proliferation of Nuclear Weapons was adopted in 1965 by the UN General Assembly in a resolution calling on the Eighteen Nation Disarmament Committee (ENDC) to lay the foundation for such a treaty. After intense negotiations between

the US and the USSR, final drafts of a treaty were submitted at the UN.[29] Upon further revisions by the ENDC the Non-Proliferation of Nuclear Weapons Treaty was signed in June 1968. A central element of the Treaty is a system of safeguards to be administered by the Vienna based International Atomic Energy Agency (IAEA), which was established in 1957. The objective of the safeguards system is to verify that nuclear materials used for peaceful activities in NNWS is not diverted to the production of nuclear weapons.

Since it entered into force in March of 1970, 135 nations have signed the treaty, including three of the five nuclear weapons states. France and China refused to sign, along with a number of NNWS such as Argentina, Brazil, India, Israel, Pakistan and South Africa. This brings to light an inherent weakness in the non-proliferation regime; not all of the significant NNWS are members.[30] This was further demonstrated by the indigenous acquisition of a nuclear explosive by India in 1974 as evidenced by its so called "peaceful nuclear explosion". In its attainment of a nuclear explosive capability, India set a precedent; none of the other NWS had reached this status via commercial nuclear development, rather the converse is true: commercial nuclear development was based, in part, on previous military work.[31] Since India is not an NPT signatory, it could claim to have violated neither the Treaty's prohibition of all nuclear explosive devices or explosive use of nuclear material supplied by other nations. However, Canada did claim that India violated its pledge not use a Canadian supplied research reactor to produce the plutonium for the PNE.

Another perceived weakness of the NPT is the nonrequirement of safeguards for nuclear material used for maritime nuclear propulsion, including its military application. This was intended by the Treaty's

drafters. In the 1960s, several NATO members, including Italy and the Netherlands, were actively considering the acquisition of nuclear powered ships and demanded an exclusion for nuclear propulsion.[29] As a result, it is permissible under Paragraph 14 of the IAEA model safeguards agreement INFCIRCL153 - 10 to withdraw from IAEA safeguards, nuclear fuel when it is used in non-explosive military applications such as fuel for submarine reactors.[30] The NPT only assigns the IAEA the obligation of applying safeguards to nuclear materials in use for peaceful activities such as that used in research or commercial reactors. However, to date, no NNWS has availed itself to this exemption to the rule that all nuclear material in NPT NNWS is subjected to safeguards.

To date, only the five members of the official nuclear weapons club have developed the technology to build nuclear powered submarines (SSNs). However, in December 1987, India "leased" an SSN of the Charlie class from the Soviet Union, making it the first ever NNWS to operate this type of submarine.[32] The NPT and associated IAEA system of safeguards did not prohibit this transfer on either the part of the Soviets or India.[33] A related development occurred in June 1987, when Canada, a long time supporter of non-proliferation, announced plans to acquire a fleet on 10-12 SSNs\*. Since Canada has impeccable non-proliferation credentials, there was little concern that it would utilize the safeguards exemption to divert enriched uranium for weapons. However, some analysts thought that it would set an unfortunate precedent in this regard. However, Canada sought to allay these concerns by declaring that it would enter into a bilateral monitoring arrangement with its supplier to cover the period during which the material is not subject to IAEA safeguards\*.

Another problem is that states such as Brazil may seek to justify the

**development of an indigenous uranium enrichment capability by the requirement for enriched uranium for nuclear submarine reactor fuel. The potential for nuclear weapons development exists if such a capability were achieved.**

- **In April 1989, Canada has since cancelled its SSN acquisition program due to budgetary constraints.**

## **Appendix B**

### **Nuclear Materials Criticality**

Naturally occurring uranium exists in the following isotopes,  $U^{234}$ ,  $U^{235}$  and  $U^{238}$  where for our purposes,  $U^{234}$  is negligible. The enrichment of natural uranium or  $U^{Nat}$  is 0.711% where enrichment is defined as,

$$\epsilon = \frac{\text{mass of fissile material}}{\text{mass of fissile material} + \text{mass of fissionable material}} \quad (\text{B.1})$$

or for this case,

$$\epsilon = \frac{\text{mass } (U^{235})}{\text{mass } (U^{235}) + \text{mass } (U^{238})} \quad (\text{B.2})$$

Fissile isotopes ( $U^{233}$ ,  $U^{235}$ ,  $Pu^{239}$ ,  $Pu^{241}$ ) have a large fission cross-section at thermal neutron energies (i.e., 500b at 0.025eV), while fissionable isotopes such as  $Pu^{241}$  and  $U^{238}$  have a very low cross-section at such energies. In fact, the fission cross-section of  $U^{238}$  is essentially zero below a neutron energy of 1MeV.

The principal fissile isotopes used in nuclear weapons are  $U^{235}$  and  $Pu^{239}$ . Weapons grade uranium and plutonium contain greater than 90% of these isotopes respectively. The actual amounts required for weapons use depend on the details of a number of factors which are not available to the general public. However, it is known that the critical mass (minimum mass required for criticality based on prompt neutrons) of the fissile metal as a reflected sphere is roughly 5kg for  $Pu^{239}$ , and 18kg for  $U^{235}$ . A possible reflector in this case is beryllium.

About 8kg of typical LWR plutonium constitutes a critical mass when fabricated into a reflected sphere.[31] Use of an oxide reduces the fissile atom density and increases the critical mass by approximately 50%. Such quantities of these materials are not very large; i.e., a 4kg sphere of plutonium is smaller than a baseball.[1]

When the concentration or enrichment of  $U^{235}$  drops below 20%, the reflected critical mass becomes prohibitively high, becoming infinite below about 6%. For  $Pu^{239}$ , the reflected critical mass is 20kg at 0% fissile content. This is illustrated in Figure B.1. Bare unreflected critical masses are a factor of three to four times higher.[34].

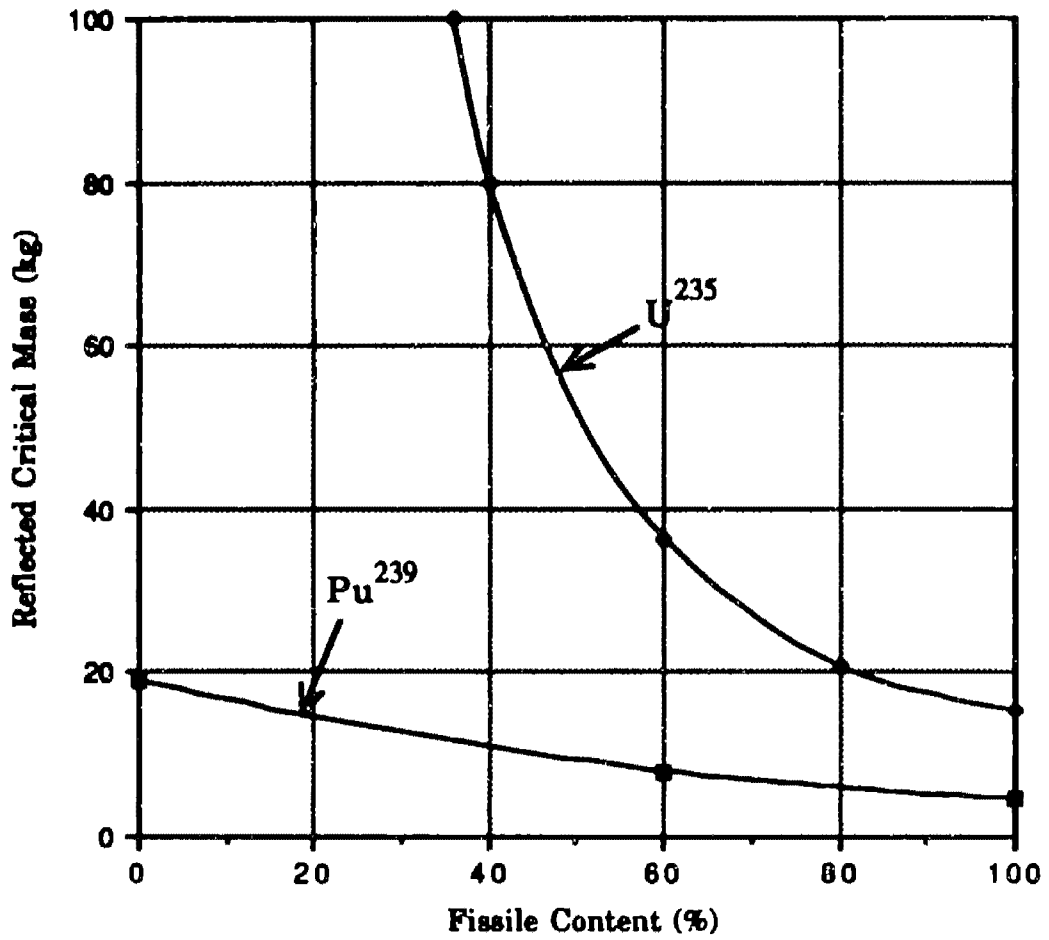


**Figure B.1.** Reflected critical masses of uranium and plutonium Vs. isotopic mix.[34]

## **Appendix C**

### **Reactivity Considerations**

The nuclear fission chain reaction can be described quantitatively in terms of the neutron multiplication factor ( $k$ ). This is defined as the ratio of the number of fissions (or fission neutrons) in one generation to the number of fissions (or fission neutrons) in the preceding generation.

$$k = \frac{\text{number of fissions in one generation}}{\text{number of fissions in preceding generation}} \quad (\text{C.1})$$

If  $k$  is equal to 1, the reactor is said to be critical and is operating in a steady state. If  $k$  is greater than or less than 1, the reactor is said to be supercritical and subcritical respectively. The infinite multiplication factor,  $k_{\text{inf}}$ , is used to describe a reactor of infinite dimensions (i.e., no neutron leakage from the reactor surface). The effective multiplication factor,  $k_{\text{eff}}$ , is used to describe a reactor of finite dimensions (i.e., accounts for neutron leakage).

The neutron multiplication factor is used to define a term known as reactivity,  $\rho$ .

$$\rho = \frac{k_{\text{eff}} - 1}{k_{\text{eff}}} \quad (\text{C.2})$$

If a reactor is critical,  $k_{\text{eff}}$  is equal to 1 and the reactivity is equal to 0. If  $k_{\text{eff}}$  were reduced, for example, by the insertion of a neutron absorber into the reactor, the reactivity would be negative. Thus the insertion of a neutron absorber or control rod corresponds to the insertion of negative reactivity. A

**positive reactivity insertion corresponds to the a change that increases the neutron population such as replacing a fuel element with one containing uranium fuel of a higher enrichment. There are many other changes that can take place in a reactor that correspond to the insertion of negative reactivity or positive reactivity.**

## Appendix D

### Fuel Burnup Considerations

For a reactor operating at a thermal power of P megawatts (MW) and with a recoverable energy per fission, the rate at which fissions occur per second in the entire reactor is,

$$\begin{aligned} \text{Fission rate} &= P \text{ MW} \times \frac{10^6 \text{ joules}}{\text{MW-sec}} \times \frac{\text{fission}}{200 \text{ MeV}} \times \frac{\text{MeV}}{1.60 \times 10^{-13} \text{ joule}} \times \frac{86,400 \text{ sec}}{\text{day}} \\ &= 2.70 \times 10^{21} P \text{ fissions/day.} \end{aligned} \quad (\text{D.1})$$

This can be converted to grams per day fissioned, which is also called the burnup rate.

$$\begin{aligned} \text{Burnup rate} &= \frac{2.70 \times 10^{21} P \text{ fissions}}{\text{day}} \times \frac{6.023 \times 10^{23} \text{ atoms}}{\text{mole}} \times \frac{\text{mole}}{235 \text{ grams } ^{235}\text{U}} \\ &= 1.05 P \text{ grams fissioned/day.} \end{aligned} \quad (\text{D.2})$$

Thus 1 g/day of  $\text{U}^{235}$  is fissioned for every megawatt of reactor thermal operating power. Equation D.2 neglects the effects of radiative capture in  $\text{U}^{235}$ . The total neutron absorption rate in the uranium,  $(1 + \alpha)$ , is given by the ratio of the microscopic absorption cross section to the microscopic fission cross-section,

$$(1 + \alpha) = \frac{\sigma_a}{\sigma_f} \quad (\text{D.3})$$

From Equations D.1 and D.3 it follows that,

$$\text{Consumption rate} = 1.05(1 + \alpha)P \text{ g/day.} \quad (\text{D.4})$$

Since the value of  $\alpha$  at thermal energies is 0.169, from Equation D.4,  $\text{U}^{235}$  is consumed at a rate of 1.23g/day for every megawatt of reactor thermal operating power. The consumption rate however does not represent the amount of heavy metal destroyed.

Since a reactor operating at 1MW for 1 day fissions 1.05 grams of  $\text{U}^{235}$ ,

$$\frac{1\text{MWd}}{1.05 \text{ g}} \times \frac{10^6 \text{ g}}{\text{t}} = 950,000\text{MWd/t}$$

is the maximum theoretical burnup attainable.[7]

## **Appendix E**

### **EPRI-CELL Input/Output Description**

This appendix is divided into four sections that together describe the EPRI-Cell input/output data and process. These sections include an input description as presented by the EPRI-Cell user's manual, a discussion of the input data required to satisfy the input parameters needed to perform the calculations, description and interpretation of the EPRI-Cell output, and a sample EPRI-Cell output file.

#### **E.1 Input Description**

The following is a description, according to the EPRI-Cell user's manual, of the input information such as titles, variables and calculation/edit controls needed to run the EPRI-Cell code and produce the desired output in a suitable form. Each input item is numbered for later reference.

All input, with the exception of title cards, uses the standard NAMELIST input routine. For the general input option, data are entered in the namelist title of INFREE.

#### **Titles**

Alphanumeric titles for EPRI-Cell must precede all other input cards. The content of title cards are as follows:

- (1) CARD 1            This is a case title, which may use 80 columns and be in any format.
- (2) CARD 2            Four character name for each composition K in increasing order. (20A4 format)
- (3) CARD 3            Four character name for each region in increasing order. (10A4 format)
- (4) CARD 4            Four character name for each zone L in increasing order. (10A4 format)

## Nuclides and Number Densities

The NAMELIST input required to describe the initial number densities are listed below.

- (5) NCOM            Number of Compositions in the cell.  
(6) ID              Number of nuclides in the problem (max=25).
- (7) NUCLID(J)    ZAS I.D. for each nuclide present in the problem, entered in increasing order. The ZAS I.D. for an isotope is determined from:
- $$\text{ZAS I.D.} = Z*10000 + A*10 + S$$
- where Z = Atomic Number  
A = Atomic Weight  
S = Any I.D. from 0 to 9 to distinguish different sources of cross-section sets for the same isotope.
- Table 3.3 of the EPRI-Cell user's manual lists the nuclides in the GAM/THERMOS library. Also, an attached memo by E. M. Pennington, April 4, 1984, lists the ZAS I.D.'s of the nuclides in the EPRI-Cell library. Note that for depletion calculations, nuclides 999999 and 999998 (fission products are lumped into these dummy nuclides) must be included in this list as well as the isotopes of plutonium, Xe<sup>135</sup> and Sm<sup>149</sup> (as 10<sup>-20</sup> if zero).
- (8) TEMPID(J)    Temperature I.D. for scattering kernel of each nuclide. Allowable values of ZAS I.D. and temperature I.D. for the current library are listed in Table 3.3 of the EPRI-Cell user's manual. (°K)
- (9) PUREDN(J,K) Pure number density of nuclide J in composition K. (atoms/barn-cm)
- (10) VOLFRK(K,L) Volume fraction of composition K in zone L.  
(DEFAULT=400\*0.0)
- (11) DENFRK(K,L) Density fraction of composition K in zone L.  
(DEFAULT=400\*1.0)

## Calculation and Edit Controls

Optional calculational paths and edits are specified via the input array OPTION(I). In general, if OPTION(I)=1, the option is selected and if it is entered as 0 it is not selected. The default values are zero unless specified.

- (12) OPTION(1)    Not Used (N.U.)  
(13) OPTION(2)    N.U.  
(14) OPTION(3)    Group dependent buckling will be used. Array AL2(J) also required as input.  
(15) OPTION(4)    Heavy scatterer present.

- (16) OPTTON(5) Resonance overlap correction applied. Appropriate for mixed oxide fuel only.
- (17) OPTTON(6) Equal volume space points within each zone.
- (18) OPTTON(7) Buckling search: With this option, group constants edited reflect converged buckling. Note that options 7 and 3 may not be selected simultaneously.
- (19) OPTTON(8) Analytic isotropic boundary condition.
- (20) OPTTON(9) N.U.
- (21) OPTTON(10) N.U.
- (22) OPTTON(11) Edit fast and thermal microgroup cross-sections.
- (23) OPTTON(12) Edit fast and thermal microgroup fluxes (thermal fluxes are  $\phi\Delta u$ ).
- (24) OPTTON(13) CINDER number densities printed for each depletable point (intended only as debug output). Note that only main chain  $Xe^{135}$  and  $Sm^{149}$  are printed.
- (25) OPTTON(14) Short libraries are supplied.
- (26) OPTTON(15) Heterogeneous fast effect correction applied. Use only if the three innermost zones are fuel, clad and moderator.
- (27) OPTTON(16) If OPTTON(16)=N is entered, macroscopic conventional 5 group cross-sections are punched in PDQ format for table set N. If OPTTON(16)=-N, the same cross-sections are punched except the thermal group is MND. ( $1 \leq N \leq 99$ )
- (28) OPTTON(17) Enter OPTTON(17)=2,3 or 4 indicating the number of collapsed broad groups to be edited. Table 3.2 of the EPRI-Cell user's manual defines the energy breakpoints for the standard collapsed edits. Set=5 for standard 5 group edit.
- (29) OPTTON(18) If OPTTON(18)=1, the collapsed macroscopic cross-sections will be punched for input to PDQ. OPTTON(16) and OPTTON(17) must be set also.
- (30) OPTTON(19) N.U.
- (31) OPTTON(20) If OPTTON(20)=6, is entered, an  $S_n$  - compatible broadgroup edit will be done in the standard 5 group structure. Note that this option has not been thoroughly evaluated.
- (32) OPTTON(21) N.U.
- (33) OPTTON(22) N.U.
- (34) OPTTON(23) N.U.

(35) OPTION(24) Enter 0 if timestep lengths input in MWD/TONNE, or 1 if input in hours.

(36) OPTION(25) —

### Other Parameters Controlling the Calculation

(37) NTS Number of GAM/THERMOS calculations. (max=30, DEFAULT=1)

(38) TIMSTP(N) Duration in hours for timestep N for CINDER calculation. (max=29, DEFAULT=100.0, 400.0, 1500.0, 26\*2000.0)

(39) POWR Power in Watts/cm of height. (DEFAULT=1.0)

(40) RELPWR(N) Relative power of timestep N. (DEFAULT=30\*1.0; use 1.0E-7 for a zero power timestep)

(41) BUCKLG Total buckling in  $\text{cm}^{-2}$ . This is the group independent buckling when OPTION(3)=0. When OPTION(3)=1, see below.

(42) AL2(J) Group dependent buckling for 68 fast groups. Use when OPTION(3)=1, in which case BUCKLG is used as a single value of buckling for the thermal group.

(43) THERMG Number of groups in thermal calculation (DEFAULT=35 for the current library).

(44) ISPEC Index of fission spectrum (9 for  $\text{UO}_2$  or 10 for  $\text{MO}_2$  is recommended). (DEFAULT=9)

(45) PHITYP Enter 1.0 for P-1 or 0.0 for B-1 fast calculation.

(46) IEDIT(L) Edit indicator for each zone L. Each zone L whose edit indicator is 1 is included in the "edit cell". Extra zones in a supercell calculation supercell calculation, IEDIT for the extra region should be 0. For a supercell edit, IEDIT for the extra region should be 1.

(47) LBG(I) First fine group in broad fast group I. The standard 5 group structure is obtained by inputting LBG=1,11,31,63. (DEFAULTS)

(48) ISGT(I) The thermal broad group for each fine thermal group. The standard 5 group structure is obtained by inputting ISGT=21\*5, 14\*5. (DEFAULTS)

(49) DSIRDK Value of  $k_{\text{eff}}$  sought if this is a search run. (DEFAULT=1.0)

(50) EPSILN Convergence criteria for search calculations. (DEFAULT=0.0001)

- (51) TEMP(L)      Temperature (°K): If a nuclide is entered whose thermal cross-sections are determined from doppler-broadened resonance parameters, (e.g., Pu<sup>240</sup>, Gd<sup>155</sup>), TEMP(1) is required. TEMP(3), required for the 5 or collapsed group edits, is the moderator temperature (utilized in the generation of the MND diffusion coefficient).

### Geometry Data

The input required to describe the general geometry is listed below.

- (52) NGEOM      Set this equal to 1 to invoke slab geometry. Absence of this flag invokes the standard cylindrical geometry.
- (53) ZONEPT(I)    Number of space points in zone I.
- (54) ZONETK(I)    Thickness of zone I in cm.
- (55) ZONECT(I)    Depletion indicator for zone I. Use 1 if zone I is depletable or zero if zone I is not depletable.
- (56) XTREG        Region number or scattering ring, if any. This signals the code that region number "XTREG" has no physical significance and is not to be included in the thermal flux normalization, etc. (DEFAULT=0)

### Resonance Data

The resonance treatment in EPRI-Cell is based on equivalence relations which employ tables of groupwise resonance integrals as a function of temperature and excess potential scattering cross-sections. In the current library, U<sup>235</sup>, U<sup>238</sup>, Pu<sup>239</sup> and Pu<sup>240</sup> have resonance data. If a nuclide is requested in the cell calculation and no resonance data are entered, then the infinite dilute cross-sections are used. Therefore, entries for Pu<sup>239</sup> and Pu<sup>240</sup> should be made for depletion calculations even though initial atom densities are 10<sup>-20</sup>. The input describing the resonance data is as follows:

- (57) NUCRE        Number of nuclides for which resonance data are entered.
- (58) IDRES(J)     ZAS I.D. number of nuclides for which resonance calculations are to be done. For each of the nuclides listed in IDRES(J), five input values are required.
- (59) RES(1,J)     Resonance temperature in °K for the J<sup>th</sup> resonance nuclide.
- (60) RES(2,J)     The mean chord length  $L_{ave}$ , for the absorbing lump where the J<sup>th</sup> nuclide exists. For the fuel cell problem,

$$L_{ave} = \frac{4V}{S} \quad (E.1)$$

where,

- V = Volume of fuel (i.e., material between cladding plates).  
S = Surface area of fuel.

- (61) RES(3,J) The Dancoff factor, C, for the interaction between lumps containing the J<sup>th</sup> resonance nuclide.
- (62) RES(4,J) The excess potential scattering cross-section in absorbing lump for the J<sup>th</sup> resonance nuclide. This value is calculated from,

$$RES(4,J) = \frac{1}{N_J} \sum_{I \neq J} N_I \lambda_I \sigma_{pI} \quad (E.2)$$

where  $N_J$  is the number density of the J<sup>th</sup> resonance nuclide in the absorbing lump. The summation over I includes all nuclides in the absorbing lump except the J<sup>th</sup> resonance nuclides.

The values in the summation are,

- $N_I$  = Number densities of the isotopes in the lump.
- $\lambda_I$  = Intermediate resonance parameter  $\lambda$  for isotope I.
- $\sigma_{pI}$  = Potential scattering for isotope I.

Recommended values for  $\lambda$  and  $\sigma_p$  are listed in Table 3.4 of the EPRI-Celi user's manual.

- (63) RES(5,J) Number density of the J<sup>th</sup> resonance nuclide in the absorbing lump where,

$$\text{Number density} = \text{PUREDN} * \text{VOLFR} * \text{DENFR} \quad (E.3)$$

### Grain Heterogeneity Data

The correction for grain heterogeneity will be applied if the following data are entered as non-zero values.

- (64) NUMGRN Composition number of the grain particles. (DEFAULT=0)
- (65) GRAIND Grain diameter in cm.

### Factors for Depletion

The following correction factor may be adjusted to adjust depletion results, if required.

- (66) DEPNF Depletion normalization factor applied in GAM/THERMOS to both  $\Sigma_{a3/4}$  and  $\Sigma_{a4/4}$  from CINDER.

## Variables Used to Designate an ISOTXS Data Set

An ISOTXS data set must be created in order to allow the input of the EPRI-Cell generated data into DIF3D. (DIF3D is a code used to solve one, two and three dimensional diffusion theory problems)

- (67) ISOSTP(N)      Flag for generation of ISOTXS cross-sections for timestep N.  
=0 (DEFAULT) Exclude cross-sections for this timestep.  
=1 Include cross-sections for this timestep. Combine the epithermal and thermal fission products into one fission product.  
=2 Include cross-section for this timestep. Leave the epithermal and thermal fission products as separate lumped fission products.
- (68) ISOCS            Flag to describe how the epithermal and thermal fission product cross-sections are to be calculated in the ISOTXS data set.  
=0 (DEFAULT) Write the pseudo cross-sections. These are the same cross-sections that are printed in the EPRI-Cell output. These pseudo cross-sections when multiplied by the homogenized concentrations printed in EPRI-Cell give "true" macroscopic cross-sections.  
=1 Write the "real" cross-sections. These cross-sections are the pseudo cross-sections multiplied by the homogenized concentrations divided by the total fission source per unit volume. The ECDATA file generated by the EPRI-Cell contains the pseudo lumped fission product cross-sections, homogenized concentrations, and total fission source per unit volume.
- (69) OLDISO            Flag for the existence of ISOTXS data set.  
=0 (DEFAULT) ISOTXS is a new data set.  
=1 ISOTXS is an old data set. Add cross-sections to this set.
- (70) NTHBG            Number of broad groups in the thermal region. (DEFAULT=2)
- (71) NFSBG            Number of broad groups in fast region. (DEFAULT=3)
- (72) HISONM(J)        User supplied isotope name to designate the isotope in the ISOTXS data set. Isotope names must be in the same order as the ZAS nuclide I.D.'s specified in the NUCLID array. (DEFAULT=names specified in the THERMOS library). Blank name designates that isotope will not be written into the ISOTXS data set for any time step.

N.U. - Not Used

## **E.2 Variables Used in the Calculations of this Study**

In order to use EPRI-Cell to accomplish the objectives of this study, not all of the input items 1 through 72 listed above were required. The following section is a list of the of the input items used. Also included are comments on the data supplied or method of obtaining the data to satisfy each of the input items used. Default values of variables are automatically invoked by the EPRI-Cell code when the variable is not used in an input file.

<u>Item</u>	<u>No.</u>	<u>Input Data Description</u>
CARD1	(1)	Title of case, (reactor power, type of fuel, number of fuel plates in the fuel element, uranium enrichment, weight percent (wt%) gadolinia present in the fuel)
CARD2	(2)	Four character name for each composition, in increasing order, in fuel cell to be modeled.  GAD = Gadolinia ZR4 = Zircaloy - 4 H2O = Water UO2 = Uranium dioxide fuel  Note, forth character is entered as a blank
CARD3	(3)	Four character name for each region, in increasing order, in the fuel cell to be modeled.  FUEL = Fuel region of UO <sub>2</sub> and structural zircaloy - 4 with or without Gd <sub>2</sub> O <sub>3</sub> . CLAD = Clad region consisting only of zircaloy - 4. MOD = Coolant region consisting only of H <sub>2</sub> O. POIS = Lumped burnable poison region consisting only of Gd <sub>2</sub> O <sub>3</sub> .
CARD4	(4)	Four character name for each zone L, in increasing order, in increasing order.  FUEL = Fuel zone of UO <sub>2</sub> and structural zircaloy - 4 with or without Gd <sub>2</sub> O <sub>3</sub> . CLAD = Clad zone consisting only of zircaloy - 4. MOD = Coolant zone consisting only of H <sub>2</sub> O. POIS = Lumped burnable poison zone consisting only of Gd <sub>2</sub> O <sub>3</sub> .

- NGEOM (52) Set equal to 1 to invoke slab geometry (i.e., plate type fuel).
- NCOM (5) Set at 4, (i.e., four compositions in the fuel element, GAD, ZR4, H2O AND UO2)
- ID (6) Set at 17 for the nuclides present in the fuel element.
- NUCLID(J) (7) The ZAS I.D. of the 17 nuclides or lumped nuclides present in the fuel element. Each nuclide and its ZAS I.D. are listed below. Note that the higher actinides have been neglected for purposes of this study.

<u>Nuclide</u>	<u>ZAS I.D.</u>	
Zircaloy - 4	4040	Zircaloy - 4 is treated as a single nuclide by EPRI-Cell.
Hydrogen	10010	Treats all hydrogen isotopes in natural proportions.
Boron	50100	Treats all boron isotopes in natural proportions. The input files were set up with the capability to model borated coolant. However, this burnable poison (chemical shim) was not considered in this study. Thus its concentration in the input number density arrays was zeroed by entering a number density of $10^{-20}$ atoms/barn-cm.
Oxygen	80160	Treats all oxygen isotopes in natural proportions.
Xenon	541350	Treats Xe <sup>135</sup> . This isotope, either as a fission product or a product of fission product decay is not included in the fission product lumps.
Samarium	621490	Treats Sm <sup>149</sup> . This isotope, either as a fission product or a product of fission product decay is not included in the fission product lumps.

Gd <sup>155</sup>	641550	Treats the isotope Gd <sup>155</sup> . Entering Gd <sup>155</sup> initializes Gd <sup>154</sup> , Gd <sup>156</sup> , Gd <sup>158</sup> and Gd <sup>159</sup> in the CINDER calculation in the naturally occurring proportions. Thus only the number densities of the isotopes Gd <sup>155</sup> and Gd <sup>157</sup> are entered in the input files, while the remaining gadolinium isotopes are treated as a void by the user.
Gd <sup>157</sup>	641570	Treats the isotope Gd <sup>157</sup> .
U <sup>235</sup>	922354	Treats the isotope U <sup>235</sup> .
U <sup>236</sup>	922361	Treats the isotope U <sup>236</sup> .
U <sup>238</sup>	922384	Treats the isotope U <sup>238</sup> .
Pu <sup>239</sup>	942394	Treats the isotope Pu <sup>239</sup> .
Pu <sup>240</sup>	942402	Treats the isotope Pu <sup>240</sup> .
Pu <sup>241</sup>	942411	Treats the isotope Pu <sup>241</sup> .
Pu <sup>242</sup>	942421	Treats the isotope Pu <sup>242</sup> .
F.P.1	999998	This is a dummy isotope for treatment of the lumped epithermal absorption effects of fission products. (1b. from 0.625ev to 5530 ev)
F.P.2	999999	This is a dummy isotope for treatment of the lumped thermal absorption effects of fission products. (1b. at 2200m/sec) (1/v from 0 to 0.625ev)

HISONM(J) (72) Each input file was set up for the generation of the ISOTXS data set so as to allow the option of running DIF3D for a particular case in the event a more detailed calculation was deemed necessary. Thus an entry for HISONM was required for each nuclide in order to designate its existence in the ISOTXS data set. The abbreviation or HISONM chosen for each each of the 17 nuclides, in order of increasing ZAS I.D. are, ZR, H, B, O, XE, SM, G155, G157, U35, U36, U38, P39, P40, P41, P42, FP1 and FP2.

TEMPID(J)	(8)	The values of for this parameter were selected from TABLE 3.3 of the EPRI-Cell user's manual based on an estimated average coolant temperature of 300°C for the coolant, 380°C for the cladding and 700°C for the fuel. These numbers need not be refined since the current EPRI-Cell library contains roughly 3 to 7 temperatures at which microscopic cross-section sets are available. The cross-section sets at the temperatures closest to those specified above for coolant, cladding and fuel were selected.
OLDISO	(69)	Set at 0 in order to generate a new ISOTXS data set after each EPRI-Cell run.
ISOTSP(N)	(67)	Set at 1 for each timestep in order that the cross-sections for each timestep be included in the ISOTXS data set. A value of 1 results in the epithermal and thermal fission products being combined into one fission product.
NTHBG	(70)	Default taken resulting in two broad groups in the thermal region.
NFSBG	(71)	Default taken resulting in three broad groups in the fast region.
ISOCS	(68)	Set at 1 by the direction of Reference [10].
PURED(N,J,K)	(9)	Design variable which specifies the number densities of each nuclide in each composition. The number densities in each fuel zone must be changed with each design calculation. Number densities in the moderator zone are changed in order to calculate the coolant void coefficient of reactivity for a particular reactor core. The calculation of these values is discussed in Section 4.1.2.5. These values are read into an array by the EPRI-Cell code. Array locations not receiving an entry are set at 0 by default.
VOLFRC(K,L)	(10)	Design variable which specifies the volume fractions of each composition in each zone of the cell and which must be changed with each calculation. The calculation of these values is discussed in Section 4.1.2.4. These values are read into an array by the EPRI-Cell code. Array locations not receiving an entry are set at 0 by default.
OPTION(6)	(17)	Set at one resulting in the space points of a particular zone being set at equal thickness. The number of space points is designated by the input parameter ZONEPT(I) where I is the zone number in the cell.
OPTION(8)	(19)	Set at 1 to invoke the analytic isotropic boundary condition.
OPTION(17)	(28)	Set=5 for the standard 5 group edit in the EPRI-Cell output. Thus five collapsed broad groups will be edited.

OPTION(24)	(35)	Set=1 in order to permit time steps to be entered in MWD/Tonne.
OPTION(25)	(36)	—
NTS	(37)	The number of depletion calculations (GAM/THERMOS calculations) that will be performed by EPRI-Cell is equal to NTS-1. For each run, EPRI-Cell automatically performs an initial undepleted cell calculation. For the LEU case to be run at 600 FPD (full power days), NTS was set equal to 9 resulting in 8 depletion calculations. For the HEU cases to be run at 1200FPD, NTS was set equal to 12 resulting in 11 depletion calculations.
TIMSTP	(38)	<p>Although NTS-1 intervals or timesteps exist between depletion calculations, NTS intervals must be specified in the EPRI-Cell input file. The last timestep is not used by EPRI-Cell.</p> <p>For both the 600FPD LEU cases and the 1200 FPD HEU cases run for this study, depletion calculations were performed at the following times (in days) extending over the operating life of the reactor cores.</p> <p>( 0-1-4-20-70-160-250-400-600-800-1000-1200 )</p> <p>The initial undepleted cell calculation is performed at time=0 in the above sequence. Depletion calculations are spaced close together at the beginning of core life in order to account for xenon buildup. The above sequence results in the following timestep values (in hours).</p> <p>(24.0,72.0,384.0,1200.0,2*2160.0,3600.0,5*4800.0,)</p>
POWR	(39)	<p>Design variable specifying the reactor core power density in Watts/cm of height. Its use is discussed in Section 4.1.2.6. This value is calculated by the following equation,</p> $\text{POWR} = (q'''_{\text{ave,r}})(t_{\text{cell}})(t_{\text{unit}}) \quad (\text{E.4})$ <p>where <math>q'''_{\text{ave,r}}</math> is the desired reactor average power density in kW/L or W/cm and the cell thickness is the sum thickness of the zones specified by the parameter ZONE'TK(I) in cm.</p>
BUCKLG	(41)	Design variable specifying the reactor core geometric buckling. Its use in this study is discussed in Section 4.1.2.6 (See Appemdix F).
ISPEC	(44)	Set=9 to invoke a UO <sub>2</sub> fission neutron energy spectrum.
PHITYP	(45)	Set=0 to invoke transport theory calculation.
IEDIT(L)	(49)	Set=1 for for each zone to be modeled in order that data calculated for each zone appear in the output file.

- TEMP(L) (51) Set=293 for each zone by the direction of Reference [10].
- ZONEPT (53) The EPRI-Cell code has the capability to handle 60 space points or intervals. However, on the IBM 3033 computer used for this study, cases run with greater than 50 space points resulted in run time errors. Thus the number of space points was kept to 50 or below. In order to permit the modeling of a maximum number of fuel plate and coolant channels into one cell, space points specified in each of these zones was kept to a minimum. For fuel plates, 3 space points were specified; thus approximating the self shielding effect. For burnable poison plates consisting of solid lumped gadolinium, 7 space points were specified in order to model the desired self shielding effect. The number of space points in the cladding and moderator (coolant channels) were set at 1 and 2 respectively.
- ZONETK (54) Design variable specifying the thickness of each zone; fuel cladding, moderator and also burnable poison.
- ZONECT (55) Set=1 for fuel and burnable poison zones since they are depletable. Set=0 for cladding and moderator zones since they are none depletable.
- NUCRE (57) Set=7 since 7 nuclides are present in the fuel element for which resonance data are entered.
- IDRES(J) (58) The 7 nuclides and corresponding ZAS I.D. for which resonance data are entered are listed below.

<u>Nuclide</u>	<u>ZAS I.D.</u>	
U <sup>235</sup>	922354	Treats the isotope U <sup>235</sup> .
U <sup>236</sup>	922361	Treats the isotope U <sup>236</sup> .
U <sup>238</sup>	922384	Treats the isotope U <sup>238</sup> .
Pu <sup>239</sup>	942394	Treats the isotope Pu <sup>239</sup> .
Pu <sup>240</sup>	942402	Treats the isotope Pu <sup>240</sup> .
Pu <sup>241</sup>	942411	Treats the isotope Pu <sup>241</sup> .
Pu <sup>242</sup>	942421	Treats the isotope Pu <sup>242</sup> .

- RES(1,J) (59) The nuclides for which resonance data are entered are present in the fuel zone of which the average temperature was estimated to be roughly 700°C. Thus RES(1,J) was set equal to 1000°K.

- RES(2,J) (60) The mean chord length, specified by RES(2,J), was calculated by Equation E.1 to be 0.29cm and 0.1cm for the thick plate and thin plate reactor designs respectively.
- RES(3,J) (61)
- RES(4,J) (62) This variable must be changed in response to a change in the design variables PURED<sub>N</sub>(J,K) and/or VOLFR<sub>C</sub>(K,L). This is discussed in Sections 4.1.2.4. and 4.1.2.5. The intermediate resonance parameter  $\lambda_1$ , was set equal to 1.0 at the direction of Reference [10]. Below,  $\sigma_p$  as determined from Table 3.4 of the EPRI-Cell user's manual, is listed for each nuclide present in the fuel zone.

<u>Nuclide</u>	<u>Potential Scattering (<math>\sigma_p</math>)</u>
Zircaloy - 4	6.216 [10]
Oxygen	3.748
Gd <sub>2</sub> O <sub>3</sub>	0.727 [10]
U <sup>235</sup>	11.500
U <sup>236</sup>	10.995
U <sup>238</sup>	10.599
Pu <sup>239</sup>	10.200
Pu <sup>240</sup>	10.599
Pu <sup>241</sup>	10.939
Pu <sup>242</sup>	10.694

As stated in Section 4.1.2.4, the parameter RES(4,<sup>235</sup>) and RES(4,U<sup>238</sup>) must be changed with each calculation involving a change in the UO<sub>2</sub>/Gd<sub>2</sub>O<sub>3</sub> ratio in the fuel zone (fuel meat) or a change in the volume fraction of fuel material in the fuel zone. For the fuel element designs of this study, these parameters are calculated by the following equations,

$$\text{RES}(4, \text{U}^{235}) = \frac{\text{Vol}\%(\text{UO}_2) [N^{38} \sigma_p^{35} + N^O \sigma_p^O + N^G \sigma_p^G] + (1 - \text{Vol}\%(\text{UO}_2)) N^{234} \sigma_p^{234}}{\text{Vol}\%(\text{UO}_2) N^{38}} \quad (\text{E.5})$$

$$\text{RES}(4, \text{U}^{238}) = \frac{\text{Vol}\%(\text{UO}_2) [N^{38} \sigma_p^{35} + N^O \sigma_p^O + N^G \sigma_p^G] + (1 - \text{Vol}\%(\text{UO}_2)) N^{234} \sigma_p^{234}}{\text{Vol}\%(\text{UO}_2) N^{35}} \quad (\text{E.6})$$

Also for each change that requires a recalculation of RES(4,J), RES(5, U<sup>235</sup>) and RES(5, U<sup>238</sup>) must also be recalculated. These parameters are calculated by the following equations,

$$\text{RES}(5, \text{U}^{235}) = \text{Vol}\%(\text{UO}_2) N^{35} \quad (\text{E.7})$$

$$\text{RES}(5, \text{U}^{238}) = \text{Vol}\%(\text{UO}_2) N^{38} \quad (\text{E.8})$$

RES(5,J)      (63)      By Equation E.3, this variable must be changed in response to a change in the design variables PUREDN(J,K) and/or VOLFRFC(K,L). This is discussed in Section 4.1.2.4 and 4.1.2.5.

### **E.3 EPRI-Cell Output Description and Interpretation**

Each section of the EPRI-Cell output file is described below. The sections are numbered for future reference.

- (1) Echo back of input case or sample EPRI-Cell input file.

#### **Processed Input Data Listings**

- (2) ZAS and TEMPID of each nuclide
- (3) Geometry edit containing the interval radii of the each space point in the modeled cell along with its respective zone number, region number, depletion indicator and edit indicator.
- (3) Pure Number Density arrays specified by PUREDN(J,K).
- (4) Volume Fractions for each zone as specified by VOLFRC(K,L).
- (5) Density Factors for each zone as specified by DENFRC(K,L). Note that in this study, this input parameter has not been used.

#### **Beginning of Calculation (Edited for Each Timestep)**

- (6) Homogenized Number Densities of nuclides by region.
- (7) Homogenized Concentrations of nuclides for the Super Cell and the Edit Cell.
- (8) Non-Lattice fraction printed.
- (9) Two Group High Cut Off Macroscopic Cross-Sections and  $k_{eff}$  for two group Super Cell.
- (10) Microscopic Cross-Section edit.
- (11) Macroscopic Cross-Sections,  $k_{eff}$ , and  $k_{inf}$ .
- (12) Fractional Neutron Balance edit.

#### **E.4 Sample EPRI-Cell Output File**

This appendix contains two sample time steps printed with the EPRI-Cell output file for the thick plate 97.3% enriched HEU case. The edit for timestep 1 contains the data for the initial undepleted fuel cell calculation, while the edit for timestep 2 contains the data for the second depletion calculation. Also included are the preceding input echo back and processed input data listings.



ZONE1X(1)=0.0725,0.05755,0.26990,0.05755,0.1450,0.05755,0.26990,0.05755,0.1450,0.05755,0.26990,0.05755,0.09680,0.06650,0.09680,0.26990,0.05755,0.1450,0.05755  
 0.26990,0.05755,0.1450,0.05755,0.26990,0.05755,0.0725,  
 ZONECT(1)=1,3=0,1,3=0,1,3=0,1,3=0,1,3=0,1,3=0,1,  
 NUCRE=7  
 IDRES(1)=922354,922361,922384,942394,942402,942411,942421,  
 RES(1,1)=1000.0,0.29,0.43598,54.75925,4.52095-3,  
 RES(1,2)=1000.0,0.29,0.43598,3.864409E+19,1.0E-20,  
 RES(1,3)=1000.0,0.29,0.43598,2407.73454,1.23868-4,  
 RES(1,4)=1000.0,0.29,0.43598,3.864409E+19,1.0E-20,  
 RES(1,5)=1000.0,0.29,0.43598,3.864409E+19,1.0E-20,  
 RES(1,6)=1000.0,0.29,0.43598,3.864409E+19,1.0E-20,  
 RES(1,7)=1000.0,0.29,0.43598,3.864409E+19,1.0E-20,  
 \$END

IMPT10-1000: SLAB GEOMETRY

ECINFO-9000: \*\*\*\* ECDATA\*\*\*\*  
 NONDEP-INDEX OF LAST NONDEPLETABLE ISOTOPE IN IDS LIST IS 4  
 IDEPFI-INDEX OF FIRST DEPLETABLE ISOTOPE IN IDS LIST IS 5  
 IDEPL-INDEX OF LAST DEPLETABLE ISOTOPE IN IDS LIST IS 15  
 IBORON-INDEX OF DEPLETABLE BORON ISOTOPE IN IDS LIST IS 3  
 IFUEL-TOTAL NUMBER OF FUEL ISOTOPE IN IDS LIST IS 7  
 IFSPRO-NUMBER OF DUMMY FISSION PRODUCT ISOTOPE IN IDS LIST IS 2  
 ISO-NUMBER OF DEPLETABLE GAN/THERMOS ISOTOPE FOUND IS 13

TIME TO PROCESS INPUT

\*\*\*\*\*CPU EXECUTION TIME= 3.71290-01 SEC.

\*\*\*\*\*PERIPHERAL PROCESSOR TIME= 0.0 SEC.

FTAPE-0200: NUCLEIDE 922354 HAS RESONANCE DATA PRESENT IN LIBRARY.  
 FTAPE-0200: NUCLEIDE 922361 HAS RESONANCE DATA PRESENT IN LIBRARY.  
 FTAPE-0200: NUCLEIDE 922384 HAS RESONANCE DATA PRESENT IN LIBRARY.  
 FTAPE-0200: NUCLEIDE 942394 HAS RESONANCE DATA PRESENT IN LIBRARY.  
 FTAPE-0200: NUCLEIDE 942402 HAS RESONANCE DATA PRESENT IN LIBRARY.  
 FTAPE-0200: NUCLEIDE 942411 HAS RESONANCE DATA PRESENT IN LIBRARY.  
 FTAPE-0200: NUCLEIDE 942421 HAS RESONANCE DATA PRESENT IN LIBRARY.

SHORT LIBRARIES CREATED ON FILES FAST AND THERM CONTAINING THE FOLLOWING 17 NUCLEIDES/TEMPERATURES -

4040/ 631	10010/ 578	50100/ 591	50160/ 591	541350/ 293	621490/ 293	641550/ 0
641570/ 0	922354/ 886	922361/ 886	922384/ 886	942394/ 886	942402/ 886	942411/ 886
942421/ 886	999990/ 0	999999/ 0				

SPACE POINT	INNER	MIDDLE	INTERVAL RADIUS (CHI)	ZONE NUMBER	REGION NUMBER	DEPLETION INDICATOR	EDIT INDICATOR
1	0.0	0.0	0.02417	1	1	1	1
2	0.02417	0.04833	0.07250	1	2	1	1
3	0.07250	0.10127	0.13005	2	3	0	1
4	0.13005	0.19752	0.26500	3	4	0	1
5	0.26500	0.33248	0.39995	3	4	0	1
6	0.39995	0.42873	0.45750	4	5	0	1
7	0.45750	0.48167	0.50583	5	6	1	1
8	0.50583	0.53000	0.55417	5	7	1	1
9	0.55417	0.57833	0.60250	5	8	1	1
10	0.60250	0.63127	0.66005	6	9	0	1
11	0.66005	0.72752	0.79500	7	10	0	1
12	0.79500	0.86248	0.92995	7	10	0	1
13	0.92995	0.95873	0.98750	8	11	0	1
14	0.98750	1.01167	1.03583	9	12	1	1
15	1.03583	1.06000	1.08417	9	13	1	1
16	1.08417	1.10833	1.13250	9	14	1	1
17	1.13250	1.16127	1.19005	10	15	0	1
18	1.19005	1.25752	1.32500	11	16	0	1
19	1.32500	1.39248	1.45995	11	16	0	1
20	1.45995	1.50833	1.55675	12	17	0	1
21	1.55675	1.56150	1.56625	13	16	1	1
22	1.56625	1.57100	1.57575	13	19	1	1
23	1.57575	1.58050	1.58525	13	20	1	1
24	1.58525	1.59000	1.59475	13	21	1	1
25	1.59475	1.59950	1.60425	13	22	1	1
26	1.60425	1.60900	1.61375	13	23	1	1
27	1.61375	1.61850	1.62325	13	24	1	1

28	1.62325	1.67165	1.72005	14	25	0	1
29	1.72005	1.78753	1.85500	15	26	0	1
30	1.85500	1.92248	1.98995	15	26	0	1
31	1.98995	2.01873	2.04750	16	27	0	1
32	2.04750	2.07167	2.09583	17	28	1	1
33	2.09583	2.12000	2.14417	17	29	1	1
34	2.14417	2.16833	2.19250	17	30	1	1
35	2.19250	2.22125	2.25000	18	31	0	1
36	2.25000	2.31748	2.38495	19	32	0	1
37	2.38495	2.45243	2.51990	19	32	0	1
38	2.51990	2.54868	2.57745	20	33	0	1
39	2.57745	2.60162	2.62578	21	34	1	1
40	2.62578	2.64995	2.67412	21	35	1	1
41	2.67412	2.69828	2.72245	21	36	1	1
42	2.72245	2.75123	2.78000	22	37	0	1
43	2.78000	2.84748	2.91495	23	38	0	1
44	2.91495	2.98243	3.04990	23	38	0	1
45	3.04990	3.07868	3.10745	24	39	0	1
46	3.10745	3.12558	3.14370	25	40	1	1
47	3.14370	3.16183	3.17995	25	41	1	1

PURE NUMBER DENSITIES

ID.	NUCL	NAME	COMP	NUMBER	1	2	3	4	UO2
4040	ZIRC4			1.000000D-20	4.251800D-02	0.0	0.0	1.000000D-20	
10010	HYDROGEN			1.000000D-20	0.0	6.686103D-02	1.000000D-20	1.000000D-20	
50100	BORON-10			1.000000D-20	0.0	1.000000D-20	1.000000D-20	1.000000D-20	
80160	OXYGEN-1			1.904100D-02	0.0	3.343051D-02	4.644820D-02	1.000000D-20	
541350	XE1354			1.000000D-20	0.0	0.0	0.0	1.000000D-20	
621490	SM1494			1.000000D-20	0.0	0.0	0.0	1.000000D-20	
641550	60-155			1.878710D-03	0.0	0.0	0.0	1.000000D-20	
641570	60-157			1.986610D-03	0.0	0.0	0.0	1.000000D-20	
922354	U-235S			1.000000D-20	0.0	0.0	0.0	2.260480D-02	
922361	U-236S			1.000000D-20	0.0	0.0	0.0	1.000000D-20	
922384	U-238S			1.000000D-20	0.0	0.0	0.0	6.193421D-04	
942394	PU2394			1.000000D-20	0.0	0.0	0.0	1.000000D-20	
942402	PU240S			1.000000D-20	0.0	0.0	0.0	1.000000D-20	
942411	PU241S			1.000000D-20	0.0	0.0	0.0	1.000000D-20	
942421	PU242S			1.000000D-20	0.0	0.0	0.0	1.000000D-20	
999998	F.P. EPI			1.000000D-20	0.0	0.0	0.0	1.000000D-20	
999999	F.P. THE			1.000000D-20	0.0	0.0	0.0	1.000000D-20	

VOLUME FRACTIONS

NUMB	MTRL	ZONE							
		NAME	FUEL	CLAD	MOD	CLAD	FUEL	CLAD	MOD
		NUMBER	1	2	3	4	5	6	7
1	GAD		0.0	0.0	0.0	0.0	0.0	0.0	0.0
2	ZR4		8.000000D-01	1.000000D+00	0.0	1.000000D+00	8.000000D-01	1.000000D+00	0.0
3	H2O		0.0	0.0	1.000000D+00	0.0	0.0	0.0	1.000000D+00
4	UO2		2.000000D-01	0.0	0.0	0.0	2.000000D-01	0.0	0.0



* ZONE *		* NAME *		* MOD *		* FUEL *		* CLAD *		* MOD *		* CLAD *	
* MTRL *	* NUMBER *	* NAME *	* MOD *	* FUEL *	* CLAD *	* MOD *	* CLAD *	* MOD *	* CLAD *	* MOD *	* CLAD *	* MOD *	* CLAD *
1	6AD	0.0	0.0	0.0	0.0	0.0	0.0	0.0	0.0	0.0	0.0	0.0	0.0
2	ZR4	0.0	1.0000000+00	8.0000000-01	1.0000000+00	0.0	0.0	1.0000000+00	8.0000000-01	1.0000000+00	0.0	0.0	0.0
3	H2O	1.0000000+00	0.0	0.0	0.0	1.0000000+00	0.0	0.0	0.0	0.0	0.0	0.0	2.0000000-01
4	UO2	0.0	0.0	2.0000000-01	0.0	0.0	0.0	0.0	0.0	0.0	0.0	0.0	0.0

		* ZONE			
		* NAME			
* MTRL	* NUMBER	* 22	* 23	* 24	* 25
NUMB	NAME				
1	6AD	0.0	0.0	0.0	0.0
2	ZR4	1.0000000+00	0.0	1.0000000+00	8.0000000-01
3	H2O	0.0	1.0000000+00	0.0	0.0
4	UO2	0.0	0.0	0.0	2.0000000-01

DENSITY FACTORS

* ZONE		*****						
* HTR	* NAME	* FUEL	* CLAD	* MOD	* CLAD	* FUEL	* CLAD	* MOD
* NUPB	* NUMBER	1	2	3	4	5	6	7
1	5A0	1.000000D+00						
2	ZR4	1.000000D+00						
3	H2O	1.000000D+00						
4	WR2	1.000000D+00						

		ZONE													
		NAME	CLAD	FUEL	CLAD	MDD	CLAD	FOIS	CLAD						
NUMB	NAME	8	9	10	11	12	13	14							
1	EAD	1.0000000+00	1.0000000+00	1.0000000+00	1.0000000+00	1.0000000+00	1.0000000+00	1.0000000+00	1.0000000+00	1.0000000+00	1.0000000+00	1.0000000+00	1.0000000+00	1.0000000+00	
2	ZR4	1.0000000+00	1.0000000+00	1.0000000+00	1.0000000+00	1.0000000+00	1.0000000+00	1.0000000+00	1.0000000+00	1.0000000+00	1.0000000+00	1.0000000+00	1.0000000+00	1.0000000+00	
3	H2O	1.0000000+00	1.0000000+00	1.0000000+00	1.0000000+00	1.0000000+00	1.0000000+00	1.0000000+00	1.0000000+00	1.0000000+00	1.0000000+00	1.0000000+00	1.0000000+00	1.0000000+00	
4	UC2	1.0000000+00	1.0000000+00	1.0000000+00	1.0000000+00	1.0000000+00	1.0000000+00	1.0000000+00	1.0000000+00	1.0000000+00	1.0000000+00	1.0000000+00	1.0000000+00	1.0000000+00	



		ZONE			
		NAME			
HTRL	NUMBER	22	23	24	25
NUMB	NAME				
1	E3D	1.000000+00	1.000000+00	1.000000+00	1.000000+00
2	ZR4	1.000000+00	1.000000+00	1.000000+00	1.000000+00
3	H2D	1.000000+00	1.000000+00	1.000000+00	1.000000+00
4	U02	1.000000+00	1.000000+00	1.000000+00	1.000000+00

BEGIN TIMESTEP 1

REGION HOMOGENIZED NUMBER DENSITIES

ID.	NUCL	NAME	REG.	NUMBER	1	2	3	4	5	6	7
4040	ZIRC4			3.4014400-02	3.4014400-02	3.4014400-02	4.2518000-02	0.0	4.2518000-02	3.4014400-02	3.4014400-02
10010	HYDROGEN			2.0000000-21	2.0000000-21	2.0000000-21	0.0	6.6861030-02	0.0	2.0000000-21	2.0000000-21
50100	BORON-10			2.0000000-21	2.0000000-21	2.0000000-21	0.0	1.0000000-20	0.0	2.0000000-21	2.0000000-21
80160	OXYGEN-1			9.2896400-03	9.2896400-03	9.2896400-03	0.0	3.3430510-02	0.0	9.2896400-03	9.2896400-03
541350	XE1354			2.0000000-21	2.0000000-21	2.0000000-21	0.0	0.0	0.0	2.0000000-21	2.0000000-21
621490	SM1494			2.0000000-21	2.0000000-21	2.0000000-21	0.0	0.0	0.0	2.0000000-21	2.0000000-21
641550	60-155			2.0000000-21	2.0000000-21	2.0000000-21	0.0	0.0	0.0	2.0000000-21	2.0000000-21
641570	60-157			2.0000000-21	2.0000000-21	2.0000000-21	0.0	0.0	0.0	2.0000000-21	2.0000000-21
922354	U-235S			4.5209600-03	4.5209600-03	4.5209600-03	0.0	0.0	0.0	4.5209600-03	4.5209600-03
922361	U-236S			2.0000000-21	2.0000000-21	2.0000000-21	0.0	0.0	0.0	2.0000000-21	2.0000000-21
922384	U-238S			1.2386840-04	1.2386840-04	1.2386840-04	0.0	0.0	0.0	1.2386840-04	1.2386840-04
942394	PU2394			2.0000000-21	2.0000000-21	2.0000000-21	0.0	0.0	0.0	2.0000000-21	2.0000000-21
942402	PU240S			2.0000000-21	2.0000000-21	2.0000000-21	0.0	0.0	0.0	2.0000000-21	2.0000000-21
942411	PU241S			2.0000000-21	2.0000000-21	2.0000000-21	0.0	0.0	0.0	2.0000000-21	2.0000000-21
942421	PU242S			2.0000000-21	2.0000000-21	2.0000000-21	0.0	0.0	0.0	2.0000000-21	2.0000000-21
999998	F.P. EPI			2.0000000-21	2.0000000-21	2.0000000-21	0.0	0.0	0.0	2.0000000-21	2.0000000-21
999999	F.P. THE			2.0000000-21	2.0000000-21	2.0000000-21	0.0	0.0	0.0	2.0000000-21	2.0000000-21

ID.	NUCL	REG.	NAME	NUMBER	FUEL	CLAD	MOO	CLAD	FUEL	FUEL	FUEL	FUEL
					8	9	10	11	12	13	14	
4040	ZIRC4			4.2518000-02	0.0	4.2518000-02	0.0	4.2518000-02	3.4014400-02	3.4014400-02	3.4014400-02	3.4014400-02
10010	HYDROGEN			2.0000000-21	0.0	2.0000000-21	6.6861030-02	0.0	2.0000000-21	2.0000000-21	2.0000000-21	2.0000000-21
50100	BORON-10			1.9936570-21	0.0	1.9936570-21	1.0000000-20	0.0	1.9939850-21	1.9942400-21	1.9941740-21	1.9941740-21
80160	OXYGEN-1			9.2896400-03	0.0	9.2896400-03	3.3430510-02	0.0	9.2896400-03	9.2896400-03	9.2896400-03	9.2896400-03
541350	XE1354			3.8203060-08	0.0	3.8203060-08	0.0	0.0	3.7621560-08	3.7013250-08	3.7244150-08	3.7244150-08
621490	SM1494			2.1176300-08	0.0	2.1176300-08	0.0	0.0	2.0249320-08	1.9504010-08	1.9703840-08	1.9703840-08
641550	60-155			3.9378890-13	0.0	3.9378890-13	0.0	0.0	3.7604370-13	3.6193800-13	3.6566190-13	3.6566190-13
641570	60-157			5.5058390-11	0.0	5.5058390-11	0.0	0.0	5.2655910-11	5.0746860-11	5.1251100-11	5.1251100-11
922354	U-2359			4.5180110-03	0.0	4.5180110-03	0.0	0.0	4.5181320-03	4.5182290-03	4.5182030-03	4.5182030-03
922361	U-236S			6.9486020-07	0.0	6.9486020-07	0.0	0.0	6.7603220-07	6.6127530-07	6.6511520-07	6.6511520-07
922384	U-238S			1.2383990-04	0.0	1.2383990-04	0.0	0.0	1.2383990-04	1.2383990-04	1.2383990-04	1.2383990-04
942394	PU2394			2.8045200-08	0.0	2.8045200-08	0.0	0.0	2.8032180-08	2.8021960-08	2.8024660-08	2.8024660-08
942402	PU240S			1.1451030-11	0.0	1.1451030-11	0.0	0.0	1.0892880-11	1.0470010-11	1.0588160-11	1.0588160-11
942411	PU241S			2.1249220-14	0.0	2.1249220-14	0.0	0.0	2.0312870-14	1.9322800-14	1.9790360-14	1.9790360-14
942421	PU2429			1.9992360-21	0.0	1.9992360-21	0.0	0.0	1.9991890-21	1.9991550-21	1.9991630-21	1.9991630-21
999998	F.P. EPI			3.8857190-05	0.0	3.8857190-05	0.0	0.0	3.7082670-05	3.5686640-05	3.6055530-05	3.6055530-05
999999	F.P. THE			2.8975040-04	0.0	2.8975040-04	0.0	0.0	2.7663950-04	2.6621060-04	2.6896420-04	2.6896420-04

REG.

ID.	NUCL	NAME	CLAD	MOO	CLAD	POIS	18	19	20	POIS
	NUMBER	15	16	17	18	19	20	21		
4040	ZIRC4	4.2518000-02	0.0	4.2518000-02	1.0000000-20	1.0000000-20	1.0000000-20	1.0000000-20	1.0000000-20	1.0000000-20
10010	HYDROSEN	0.0	6.6861030-02	0.0	1.0000000-20	1.0000000-20	1.0000000-20	1.0000000-20	1.0000000-20	1.0000000-20
50100	BORON-10	0.0	1.0000000-20	0.0	9.9798050-21	9.9818450-21	9.9823530-21	9.9824870-21	9.9824870-21	9.9824870-21
80160	OXYGEN-1	0.0	3.3430510-02	0.0	1.9041000-02	1.9041000-02	1.9041000-02	1.9041000-02	1.9041000-02	1.9041000-02
541350	XE1354	0.0	0.0	0.0	5.0709420-25	4.7370600-25	4.5891560-25	4.5452070-25	4.5452070-25	4.5452070-25
621490	SM1494	0.0	0.0	0.0	2.5237200-25	2.2692730-25	2.1852090-25	2.1613940-25	2.1613940-25	2.1613940-25
641550	60-155	0.0	0.0	0.0	1.8736920-03	1.8757390-03	1.8759690-03	1.8760200-03	1.8760200-03	1.8760200-03
641570	60-157	0.0	0.0	0.0	1.9713470-03	1.9808860-03	1.9819620-03	1.9822010-03	1.9822010-03	1.9822010-03
922354	U-2359	0.0	0.0	0.0	9.9953760-21	9.9957030-21	9.9957850-21	9.9958060-21	9.9958060-21	9.9958060-21
922361	U-2369	0.0	0.0	0.0	9.9983240-21	9.9982730-21	9.9982620-21	9.9982590-21	9.9982590-21	9.9982590-21
922384	U-2389	0.0	0.0	0.0	9.9977080-21	9.9977090-21	9.9977100-21	9.9977100-21	9.9977100-21	9.9977100-21
942394	Pu2394	0.0	0.0	0.0	9.9874870-21	9.9891030-21	9.9896970-21	9.9898690-21	9.9898690-21	9.9898690-21
942402	Pu240S	0.0	0.0	0.0	9.9479540-21	9.9476110-21	9.9474560-21	9.9474110-21	9.9474110-21	9.9474110-21
942411	Pu241S	0.0	0.0	0.0	1.0044690-20	1.0045730-20	1.0046060-20	1.0046160-20	1.0046160-20	1.0046160-20
942421	Pu242S	0.0	0.0	0.0	9.9946740-21	9.9943450-21	9.9942350-21	9.9942040-21	9.9942040-21	9.9942040-21
999998	F.P. EPI	0.0	0.0	0.0	6.0865780-05	2.7224380-05	2.3434690-05	2.2592280-05	2.2592280-05	2.2592280-05
999999	F.P. THE	0.0	0.0	0.0	7.9603250-05	3.4209990-05	2.9094910-05	2.7958230-05	2.7958230-05	2.7958230-05

ID.	NUCL NAME	REG.							
		NAME	POIS	POIS	POIS	CLAD	MOD	CLAD	FUEL
		NUMBER	22	23	24	25	26	27	28
4040	ZIRC4		1.000000D-20	1.000000D-20	1.000000D-20	4.251800D-02	0.0	4.251800D-02	3.401440D-02
10010	HYDROGEN		1.000000D-20	1.000000D-20	1.000000D-20	0.0	6.686103D-02	0.0	2.000000D-21
50100	BORON-10		9.982353D-21	9.981845D-21	9.979805D-21	0.0	1.000000D-20	0.0	1.994174D-21
80160	OXYGEN-1		1.904100D-02	1.904100D-02	1.904100D-02	0.0	3.343051D-02	0.0	9.289640D-03
541350	XE1354		4.589159D-25	4.737072D-25	5.070957D-25	0.0	0.0	0.0	3.724421D-08
621490	SM1494		2.185211D-25	2.269280D-25	2.523729D-25	0.0	0.0	0.0	1.970391D-08
641550	GD-155		1.875969D-03	1.875739D-03	1.873692D-03	0.0	0.0	0.0	3.656642D-13
641570	GD-157		1.981962D-03	1.980886D-03	1.971347D-03	0.0	0.0	0.0	5.125138D-11
922354	U-235S		9.995784D-21	9.995703D-21	9.995376D-21	0.0	0.0	0.0	4.518203D-03
922361	U-236S		9.998262D-21	9.998275D-21	9.998324D-21	0.0	0.0	0.0	6.651175D-07
922386	U-238S		9.997710D-21	9.997709D-21	9.997708D-21	0.0	0.0	0.0	1.238399D-04
942394	PU2394		9.989697D-21	9.989103D-21	9.987487D-21	0.0	0.0	0.0	2.802473D-08
942402	PU240S		9.947456D-21	9.947611D-21	9.947953D-21	0.0	0.0	0.0	1.058825D-11
942411	PU241S		1.004607D-20	1.004573D-20	1.004469D-20	0.0	0.0	0.0	1.979011D-14
942421	PU242S		9.994235D-21	9.994345D-21	9.994674D-21	0.0	0.0	0.0	1.999163D-21
999998	F.P. EPI		2.343471D-05	2.722446D-05	6.086603D-05	0.0	0.0	0.0	3.605568D-05
999999	F.P. THE		2.909493D-05	3.421009D-05	7.960358D-05	0.0	0.0	0.0	2.689653D-04

REG.

ID.	NUCL	NAME	FUEL	29	FUEL	30	FUEL	31	CLAD	32	MOD	CLAD	33	FUEL	34	FUEL	35
4040	ZIRC4		3.4014400-02	3.4014400-02	4.2518000-02	0.0	4.2518000-02	0.0	4.2518000-02	0.0	6.6861030-02	0.0	4.2518000-02	3.4014400-02	3.4014400-02	3.4014400-02	3.4014400-02
10010	HYDROGEN		2.0000000-21	2.0000000-21	0.0	0.0	0.0	0.0	0.0	0.0	1.0000000-20	0.0	0.0	2.0000000-21	2.0000000-21	2.0000000-21	2.0000000-21
50100	GORON-10		1.9942400-21	1.9939850-21	0.0	0.0	0.0	0.0	0.0	0.0	1.0000000-20	0.0	0.0	1.9936570-21	1.9938020-21	1.9938020-21	1.9938020-21
80160	OXYGEN-1		9.2896400-03	9.2896400-03	0.0	0.0	0.0	0.0	0.0	0.0	3.3430510-02	0.0	0.0	9.2896400-03	9.2896400-03	9.2896400-03	9.2896400-03
541350	XE1354		3.7013300-08	3.7621690-08	0.0	0.0	0.0	0.0	0.0	0.0	0.0	0.0	0.0	3.8203080-08	3.7837780-08	3.7837780-08	3.7837780-08
621490	SM1494		1.9504090-08	2.0249470-08	0.0	0.0	0.0	0.0	0.0	0.0	0.0	0.0	0.0	2.1176340-08	2.0746820-08	2.0746820-08	2.0746820-08
641550	60-155		3.6194060-13	3.7604810-13	0.0	0.0	0.0	0.0	0.0	0.0	0.0	0.0	0.0	3.9379160-13	3.8568500-13	3.8568500-13	3.8568500-13
641570	60-157		5.0747180-11	5.2656450-11	0.0	0.0	0.0	0.0	0.0	0.0	0.0	0.0	0.0	5.5058690-11	5.3967050-11	5.3967050-11	5.3967050-11
922354	U-235S		4.5182290-03	4.5181320-03	0.0	0.0	0.0	0.0	0.0	0.0	0.0	0.0	0.0	4.5180110-03	4.5180660-03	4.5180660-03	4.5180660-03
922361	U-236S		6.6127800-07	6.7603650-07	0.0	0.0	0.0	0.0	0.0	0.0	0.0	0.0	0.0	6.9486250-07	6.8644110-07	6.8644110-07	6.8644110-07
922384	U-238S		1.2383990-04	1.2383990-04	0.0	0.0	0.0	0.0	0.0	0.0	0.0	0.0	0.0	1.2383990-04	1.2383990-04	1.2383990-04	1.2383990-04
942394	FU2394		2.8022060-08	2.8032290-08	0.0	0.0	0.0	0.0	0.0	0.0	0.0	0.0	0.0	2.8045330-08	2.8039480-08	2.8039480-08	2.8039480-08
942402	FU240S		1.0470110-11	1.0893040-11	0.0	0.0	0.0	0.0	0.0	0.0	0.0	0.0	0.0	1.1451090-11	1.1214450-11	1.1214450-11	1.1214450-11
942411	FU241S		1.9322670-14	2.0312830-14	0.0	0.0	0.0	0.0	0.0	0.0	0.0	0.0	0.0	2.1248870-14	2.0563040-14	2.0563040-14	2.0563040-14
942421	FU242S		1.9991550-21	1.9991890-21	0.0	0.0	0.0	0.0	0.0	0.0	0.0	0.0	0.0	1.9992360-21	1.9992180-21	1.9992180-21	1.9992180-21
999998	F.P. EPI		3.5686800-05	3.7082970-05	0.0	0.0	0.0	0.0	0.0	0.0	0.0	0.0	0.0	3.8837310-05	3.8034040-05	3.8034040-05	3.8034040-05
999999	F.P. THE		2.6621190-04	2.7664180-04	0.0	0.0	0.0	0.0	0.0	0.0	0.0	0.0	0.0	2.8975130-04	2.8375220-04	2.8375220-04	2.8375220-04

REG.

ID.	NUCL	NAME	FUEL	CLAD	MOO	CLAD	FUEL	FUEL
	NUMBER	NUMBER	36	37	38	39	40	41
6040	ZIRC4	3.4014400-02	4.2518000-02	0.0	4.2518000-02	3.4014400-02	3.4014400-02	3.4014400-02
10010	HYDROGEN	2.0000000-21	0.0	6.6861030-02	0.0	2.0000000-21	2.0000000-21	2.0000000-21
50100	BORON-10	1.9935860-21	0.0	1.0000000-20	0.0	1.9934500-21	1.9936640-21	1.9936640-21
80160	OXYGEN-1	9.2896400-03	0.0	3.3430510-02	0.0	9.2896400-03	9.2896400-03	9.2896400-03
541350	XE1354	3.8325180-08	0.0	0.0	0.0	3.8573580-08	3.8083720-08	3.8083720-08
621490	SM1494	2.1378820-08	0.0	0.0	0.0	2.1767010-08	2.1136890-08	2.1136890-08
641550	60-155	3.9766320-13	0.0	0.0	0.0	4.0508310-13	3.9314990-13	3.9314990-13
641570	60-157	5.5580210-11	0.0	0.0	0.0	5.6580350-11	5.4976170-11	5.4976170-11
922354	U-235S	4.5179840-03	0.0	0.0	0.0	4.5179330-03	4.5180150-03	4.5180150-03
922361	U-236S	6.9893590-07	0.0	0.0	0.0	7.0676360-07	6.9434050-07	6.9434050-07
922384	U-238S	1.2383990-04	0.0	0.0	0.0	1.2383990-04	1.2383990-04	1.2383990-04
942394	PU2394	2.8048180-08	0.0	0.0	0.0	2.8053630-08	2.8044990-08	2.8044990-08
942402	PU240S	1.1561670-11	0.0	0.0	0.0	1.1785720-11	1.1443300-11	1.1443300-11
942411	PU241S	2.1443340-14	0.0	0.0	0.0	2.1896110-14	2.0977250-14	2.0977250-14
942421	PU242S	1.9992460-21	0.0	0.0	0.0	1.9992650-21	1.9992370-21	1.9992370-21
999998	F.P. EPI	3.9220540-05	0.0	0.0	0.0	3.9954910-05	3.8772350-05	3.8772350-05
999999	F.P. THE	2.9261490-04	0.0	0.0	0.0	2.9810170-04	2.8926900-04	2.8926900-04

ZONE HOMOGENIZED NUMBER DENSITIES

ID.	NAUCL	ZONE NAME	FUEL	CLAD	MOO	CLAD	FUEL	CLAD	MOO
	NUMBER	1	2	3	4	5	6	7	
4040	ZIRC4	3.4014400-02	4.2518000-02	0.0	4.2518000-02	3.4014400-02	4.2518000-02	0.0	0.0
10010	HYDROGEN	2.0060000-21	0.0	6.6861030-02	0.0	2.0000000-21	0.0	6.6861030-02	0.0
50100	BORON-10	1.9935570-21	0.0	1.0000000-20	0.0	1.9936620-21	0.0	1.0000000-20	0.0
80160	OXYGEN-1	9.2896400-03	0.0	3.3430510-02	0.0	9.2896400-03	0.0	3.3430510-02	0.0
541350	XE1354	3.8329870-08	0.0	0.0	0.0	3.8121970-08	0.0	0.0	0.0
621490	SM1494	2.1452280-08	0.0	0.0	0.0	2.1100580-08	0.0	0.0	0.0
641550	60-155	3.9911980-13	0.0	0.0	0.0	3.9237640-13	0.0	0.0	0.0
641570	60-157	5.5778970-11	0.0	0.0	0.0	5.4868260-11	0.0	0.0	0.0
922354	U-2359	4.5179740-03	0.0	0.0	0.0	4.5180200-03	0.0	0.0	0.0
922361	U-2369	7.0055470-07	0.0	0.0	0.0	6.9341020-07	0.0	0.0	0.0
922384	U-2389	1.2383990-04	0.0	0.0	0.0	1.2383990-04	0.0	0.0	0.0
942394	FU2394	2.804910-08	0.0	0.0	0.0	2.8044160-08	0.0	0.0	0.0
942402	FU2409	1.1614590-11	0.0	0.0	0.0	1.1408970-11	0.0	0.0	0.0
942411	FU2419	2.1437700-14	0.0	0.0	0.0	2.1085330-14	0.0	0.0	0.0
942421	FU2429	1.9992510-21	0.0	0.0	0.0	1.9992330-21	0.0	0.0	0.0
999998	F.P. EPI	3.9364170-05	0.0	0.0	0.0	3.8697120-05	0.0	0.0	0.0
999999	F.P. THE	2.9368930-04	0.0	0.0	0.0	2.8870480-04	0.0	0.0	0.0

ID.	NUCL	NAME	NUMBER	CLAD	FUEL	CLAD	MOD	CLAD	POIS	CLAD
			8	10	9	4.2518000-02	11	12	13	14
4040	ZIRC4		4.2518000-02	3.4014400-02	4.2518000-02	0.0	4.2518000-02	1.0000000-20	4.2518000-02	4.2518000-02
10010	HYDROGEN		0.0	2.0000000-21	0.0	6.6861030-02	0.0	1.0000000-20	0.0	0.0
50100	BORON-10		0.0	1.9941330-21	0.0	1.0000000-20	0.0	9.9814990-21	0.0	0.0
80160	OXYGEN-1		0.0	9.2896400-03	0.0	3.3430510-02	0.0	1.9041000-02	0.0	0.0
541350	XE1354		0.0	3.7292990-08	0.0	0.0	0.0	4.7627930-25	0.0	0.0
621490	SM1494		0.0	1.9819050-08	0.0	0.0	0.0	2.3025450-25	0.0	0.0
641550	60-155		0.0	3.6788120-13	0.0	0.0	0.0	1.8752600-03	0.0	0.0
541570	60-157		0.0	5.1551290-11	0.0	0.0	0.0	1.9786560-03	0.0	0.0
922354	U-235S		0.0	4.5181880-03	0.0	0.0	0.0	9.9956480-21	0.0	0.0
922361	U-236S		0.0	6.6747420-07	0.0	0.0	0.0	9.9982830-21	0.0	0.0
922384	U-238S		0.0	1.2383990-04	0.0	0.0	0.0	9.9977090-21	0.0	0.0
942394	PU2394		0.0	2.8026270-08	0.0	0.0	0.0	9.9889210-21	0.0	0.0
942402	PU240S		0.0	1.0650350-11	0.0	0.0	0.0	9.9476360-21	0.0	0.0
942411	PU241S		0.0	1.9808680-14	0.0	0.0	0.0	1.0045590-20	0.0	0.0
942421	PU242S		0.0	1.9991690-21	0.0	0.0	0.0	9.9943870-21	0.0	0.0
999998	F.P. EPI		0.0	3.6274950-05	0.0	0.0	0.0	3.5091760-05	0.0	0.0
999999	F.P. THE		0.0	2.7060480-04	0.0	0.0	0.0	4.4825000-05	0.0	0.0

ID.	NUCL NAME	ZONE							
		NUMBER	15	16	FUEL 17	CLAD 18	MOD 19	CLAD 20	21
4040	ZIRC4	0.0	4.2518000-02	3.4014400-02	4.2518000-02	0.0	4.2518000-02	3.4014400-02	
10010	HYDROGEN	6.6861030-02	0.0	2.0000000-21	0.0	6.6861030-02	0.0	2.0000000-21	
50100	BORON-10	1.0000000-20	0.0	1.9941330-21	0.0	1.0000000-20	0.0	1.9936820-21	
80160	OXYGEN-1	3.3430510-02	0.0	9.2896400-03	0.0	3.3430510-02	0.0	9.2896400-03	
541350	XE1354	0.0	0.0	3.7293070-08	0.0	0.0	0.0	3.8122010-08	
621490	SM1494	0.0	0.0	1.9819160-08	0.0	0.0	0.0	2.1100670-08	
641550	GD-155	0.0	0.0	3.6788430-13	0.0	0.0	0.0	3.9237990-13	
641570	GD-157	0.0	0.0	5.1551670-11	0.0	0.0	0.0	5.4868650-11	
922354	U-235S	0.0	0.0	4.5181880-03	0.0	0.0	0.0	4.5180200-03	
922361	U-236S	0.0	0.0	6.6747730-07	0.0	0.0	0.0	6.9341320-07	
922384	U-238S	0.0	0.0	1.2383990-04	0.0	0.0	0.0	1.2383990-04	
942394	PU2394	0.0	0.0	2.8026360-08	0.0	0.0	0.0	2.8044330-08	
942402	PU240S	0.0	0.0	1.0650470-11	0.0	0.0	0.0	1.1409070-11	
942411	PU241S	0.0	0.0	1.9808540-14	0.0	0.0	0.0	2.1035080-14	
942421	PU242S	0.0	0.0	1.9991690-21	0.0	0.0	0.0	1.9992330-21	
999998	F.P. EPI	0.0	0.0	3.6275150-05	0.0	0.0	0.0	3.8697300-05	
999999	F.P. THE	0.0	0.0	2.7060630-04	0.0	0.0	0.0	2.8870610-04	

ID.	NUCL	NAME	ZONE	NUMBER	22	23	24	25
4040	ZIRCA			4.2518000-02	0.0	4.2518000-02	3.4014400-02	
10010	HYDROGEN			0.0	6.6861030-02	0.0	2.0000000-21	
50100	BORON-10			0.0	1.0000000-20	0.0	1.9935570-21	
80160	OXYGEN-1			0.0	3.3430510-02	0.0	9.2896400-03	
541350	XE1354			0.0	0.0	0.0	3.8328650-08	
621490	SM1494			0.0	0.0	0.0	2.1451950-08	
641550	60-155			0.0	0.0	0.0	3.9911650-13	
641570	60-157			0.0	0.0	0.0	5.5778260-11	
922354	U-2359			0.0	0.0	0.0	4.5179740-03	
922361	U-236S			0.0	0.0	0.0	7.055210-07	
922384	U-238S			0.0	0.0	0.0	1.2383990-04	
942394	FU2394			0.0	0.0	0.0	2.8049310-08	
942402	FU240S			0.0	0.0	0.0	1.1614510-11	
942411	FU241S			0.0	0.0	0.0	2.1436680-14	
942421	FU242S			0.0	0.0	0.0	1.9992510-21	
999998	F.P. EPI			0.0	0.0	0.0	3.9363630-05	
999999	F.P. THE			0.0	0.0	0.0	2.9368530-04	

NUCLIDE	HOMOGENIZED CONCENTRATIONS		
	ID.	NAME	EDIT CELL
	3040	ZIRCA	1.8037680-02
	10010	HYDROGEN	3.4049200-02
	50100	BORON-10	5.7558460-21
	80160	OXYGEN-1	1.9540740-02
	541350	XE135A	8.6253220-09
	621490	SM149A	4.7099090-09
	641950	SO-155	3.9215970-05
	641570	SO-157	4.1378220-05
	922354	U-235S	1.0300810-03
	922361	U-236S	1.5605200-07
	922364	U-238S	2.8234380-05
	942394	PLU239A	6.3924260-09
	942402	PLU240S	2.5413430-12
	942411	PLU241S	4.7068650-15
	942421	PLU242S	6.6480750-22
	999998	F.P. EPI	9.3659700-06
	999999	F.P. THE	6.5336150-05

\*\*\*\*\*CPU EXECUTION TIME= 9.88010-01 SEC.

\*\*\*\*\*PERIPHERAL PROCESSOR TIME= 0.0 SEC.  
SLAB GEOMETRY

TRHM50-0290: THERMAL FLUX CONVERGED IN 76 ITERATIONS TO 1.1930661D-08

GAH100-0350: RESONANCE DATA FOR NUCLID 922354 HAS BEEN PROCESSED

GAH100-0350: RESONANCE DATA FOR NUCLID 922361 HAS BEEN PROCESSED

GAH100-0350: RESONANCE DATA FOR NUCLID 922384 HAS BEEN PROCESSED

GAH100-0350: RESONANCE DATA FOR NUCLID 942394 HAS BEEN PROCESSED

GAH100-0350: RESONANCE DATA FOR NUCLID 942402 HAS BEEN PROCESSED

GAH100-0350: RESONANCE DATA FOR NUCLID 942411 HAS BEEN PROCESSED

GAH100-0350: RESONANCE DATA FOR NUCLID 942421 HAS BEEN PROCESSED

GAH100-0280: 1.0 - INITIAL DANCING FACTOR = 0.5640198D+00 ( 1.0 - RES(3,K) )

TWO GROUP HIGH CUT OFF MACROSCOPIC CROSS SECTIONS

GROUP	ABSORPTION	CAPTURE	FISSION	MJ+FISSION	MU	TOTAL
1	1.338850-02	6.763700-03	6.624780-03	1.616710-02	2.440390+00	5.806840-01
2	2.506940-01	1.094010-01	1.412930-01	3.417600-01	2.418800+00	1.014580+00

GROUP	DIFF. COEF.	TRANSPORT	SCATTERING	REMOVAL	P-1 SCATTERING	P-1 REMOVAL
1	1.201160+00	2.775100-01	5.500750-01	1.722070-02	5.936940-01	1.285410-02
2	4.171020-01	7.991650-01	7.638850-01	9.0	0.0	0.0

2-GROUP SUPERCELL K-EFF = 1.0646230+00

NORM10-1000: TOTAL POWER = 6.01010500+02 (WATTS/CM) FAST FRACTION = 0.41013 THERMAL FRACTION = 0.58987

TIME FOR 6AM-THERMOS FLUX CALCULATION

\*\*\*\*\*CPU EXECUTION TIME= 3.84430+01 SEC.

\*\*\*\*\*PERIPHERAL PROCESSOR TIME= 0.0 SEC.



MICROSCOPIC EDIT

NUCLIDE-ZIRCA

GRP	ABSORPTION	FISSION	SCATTERING	TOTAL	MU-FISSION	TRANSPORT	REMOVAL	N-2-H	KAPPA FISSION	IRT
1	0.0	0.0	4.97570+00	4.97570+00	0.0	4.454420+00	4.415600-01	7.845700-05	0.0	6.348710-02
2	1.065570-03	0.0	8.063650+00	8.063650+00	0.0	7.779380+00	2.203960-02	0.0	0.0	3.539940-02
3	1.538140-01	0.0	6.736820+00	6.890640+00	0.0	6.855780+00	1.153470-02	0.0	0.0	1.848620-02
4	4.170080-02	0.0	6.314830+00	6.354330+00	0.0	6.309700+00	1.386100-01	0.0	0.0	1.273750-01
5	8.134050-02	0.0	6.060000+00	6.141380+00	0.0	6.093830+00	0.0	0.0	0.0	0.0

NUCLIDE-HYDROGEN

GRP	ABSORPTION	FISSION	SCATTERING	TOTAL	MU-FISSION	TRANSPORT	REMOVAL	N-2-H	KAPPA FISSION	IRT
1	3.487450-05	0.0	3.042160+00	3.042160+00	0.0	1.706770+00	1.663750+00	0.0	0.0	2.034190+00
2	1.458370-04	0.0	1.109170+01	1.109190+01	0.0	3.291660+00	2.133290+00	0.0	0.0	2.134330+00
3	7.702320-03	0.0	2.833540+01	2.834370+01	0.0	5.992200+00	1.884700+00	0.0	0.0	2.475330+00
4	5.191420-02	0.0	8.938650+00	8.990570+00	0.0	9.283600+00	8.938650+00	0.0	0.0	1.768280+01
5	1.510160-01	0.0	2.143710+01	2.158810+01	0.0	1.898780+01	0.0	0.0	0.0	0.0

NUCLIDE-BORON-10

GRP	ABSORPTION	FISSION	SCATTERING	TOTAL	MU-FISSION	TRANSPORT	REMOVAL	N-2-H	KAPPA FISSION	IRT
1	2.922760-01	0.0	1.819570+00	2.107840+00	0.0	1.759510+00	3.002210-01	0.0	0.0	1.349450-01
2	2.089970-00	0.0	2.990380+00	5.680350+00	0.0	4.689000+00	4.264580-02	0.0	0.0	1.127800-01
3	8.369390+01	0.0	2.099110+00	9.879400+01	0.0	8.892590+01	3.353620-02	0.0	0.0	4.945530-02
4	5.973260-02	0.0	2.024950+00	5.993510+02	0.0	5.841500+02	3.810470-01	0.0	0.0	3.508950-01
5	1.673820-03	0.0	2.131680+00	1.675950+03	0.0	1.340180+03	0.0	0.0	0.0	0.0

NUCLIDE-OXYGEN-1

GRP	ABSORPTION	FISSION	SCATTERING	TOTAL	MU-FISSION	TRANSPORT	REMOVAL	N-2-H	KAPPA FISSION	IRT
1	8.064900-03	0.0	2.476300+00	2.484370+00	0.0	2.016670+00	3.110770-01	0.0	0.0	1.198810-01
2	0.0	0.0	3.907760+00	3.907760+00	0.0	3.578670+00	4.723790-02	0.0	0.0	9.452640-02
3	6.170110-04	0.0	3.680810+00	3.688820+00	0.0	3.540460+00	3.860000-02	0.0	0.0	5.576890-02
4	2.815780-05	0.0	3.800540+00	3.800660+00	0.0	3.640840+00	4.596760-01	0.0	0.0	4.224160-01
5	7.940890-05	0.0	3.995710+00	3.995790+00	0.0	3.819230+00	0.0	0.0	0.0	0.0

NUCLIDE-XE1354

GRP	ABSORPTION	FISSION	SCATTERING	TOTAL	MU-FISSION	TRANSPORT	REMOVAL	N-2-H	KAPPA FISSION	IRT
1	5.636290-04	0.0	5.939190+04	5.939200+00	0.0	3.343800+00	5.423340-01	0.0	0.0	3.539730-02
2	3.183690-03	0.0	6.331030+00	6.334220+00	0.0	4.856230+00	1.731110-02	0.0	0.0	1.886650-02
3	2.107870-01	0.0	4.361250+01	6.669120+01	0.0	6.290020+01	8.744440-01	0.0	0.0	8.122830-02
4	3.411340+03	0.0	2.431620+03	5.842960+03	0.0	3.469180+03	3.623110+01	0.0	0.0	3.329440+01
5	6.112700+05	0.0	1.250920+05	7.363620+05	0.0	8.868980+04	0.0	0.0	0.0	0.0

HELIUM-SH1494

GRP	ABSORPTION	FISSION	SCATTERING	TOTAL	MU-FISSION	TRANSPORT	REMOVAL	N-2-H	KAPPA FISSION	IRT
1	5.423460-02	0.0	6.708300+00	6.762610+00	0.0	4.311030+00	1.132550+00	1.150270-02	0.0	3.622520-02
2	9.262840-01	0.0	9.048210+00	9.974500+00	0.0	9.372980+00	2.718220-02	0.0	0.0	2.443020-02
3	9.702360-01	0.0	6.273030+01	1.597540+02	0.0	1.577920+02	1.249650-02	0.0	0.0	1.058570-01

4	1.889250+03	0.0	3.464470+01	1.923900+03	0.0	1.606030+02	4.677040-01	0.0	0.0	4.297930-01
5	1.90670+04	0.0	1.598160+02	1.916650+04	0.0	1.748870+03	0.0	0.0	0.0	0.0

NUCLIDE-60-153

GRP	ABSORPTION	FISSION	SCATTERING	TOTAL	MU-FISSION	TRANSPORT	REMOVAL	M-2-H	KAPPA FISSION	IRT
1	2.228690-01	0.0	6.521380+00	6.744250+00	0.0	4.450370+00	1.636370+00	0.0	0.0	3.382070-02
2	1.785240+00	0.0	8.457720+00	1.024200+01	0.0	8.392970+00	1.869350-02	0.0	0.0	2.193140-02
3	1.304240+02	0.0	1.197260+01	1.423960+02	0.0	1.378730+02	3.539850-04	0.0	0.0	1.940360-02
4	3.146410+01	0.0	0.0	3.146410+01	0.0	1.764720+01	0.0	0.0	0.0	0.0
5	5.646100+02	0.0	0.0	5.646100+02	0.0	3.542510+02	0.0	0.0	0.0	0.0

NUCLIDE-60-157

GRP	ABSORPTION	FISSION	SCATTERING	TOTAL	MU-FISSION	TRANSPORT	REMOVAL	M-2-H	KAPPA FISSION	IRT
1	7.501820-01	0.0	6.518930+00	7.269170+00	0.0	4.961660+00	1.635710+00	0.0	0.0	3.337740-02
2	3.948700+00	0.0	8.318830+00	1.226750+01	0.0	1.027700+01	1.829250-02	0.0	0.0	2.129650-02
3	8.483160+01	0.0	1.508980+01	9.992080+01	0.0	9.864420+01	5.702810-03	0.0	0.0	2.414410-02
4	1.303930+02	0.0	0.0	1.303930+02	0.0	7.283840+01	0.0	0.0	0.0	0.0
5	2.463190+03	0.0	0.0	2.463190+03	0.0	1.501790+03	0.0	0.0	0.0	0.0

NUCLIDE-U-235S

GRP	ABSORPTION	FISSION	SCATTERING	TOTAL	MU-FISSION	TRANSPORT	REMOVAL	M-2-H	KAPPA FISSION	IRT
1	3.01560+00	1.236400+00	5.088640+00	7.190000+00	1.955640+00	4.718440+00	7.536700-01	8.106350-03	3.946890-11	2.015870-02
2	2.092540+00	1.632760+00	8.821150+00	1.091370+01	3.991650+00	9.244660+00	1.113440-02	0.0	5.248910-11	1.509880-02
3	3.159520+01	2.026280+01	1.217440+01	4.376970+01	4.901230+01	4.329500+01	8.528950-03	0.0	6.663830-10	1.302400-02
4	5.367540+01	4.557030+01	1.185480+01	6.553020+01	1.102250+02	5.262810+01	1.014570-01	0.0	1.459860-09	9.323320-02
5	2.313960+02	1.955550+02	1.163840+01	2.428340+02	4.730080+02	1.875130+02	0.0	0.0	6.353610-09	0.0

NUCLIDE-U-238S

GRP	ABSORPTION	FISSION	SCATTERING	TOTAL	MU-FISSION	TRANSPORT	REMOVAL	M-2-H	KAPPA FISSION	IRT
1	4.712570-01	7.168070-01	6.683820+00	7.554270+00	1.955640+00	5.072570+00	1.588380+00	7.900070-03	2.266650-11	2.278130-02
2	4.579140-01	7.844820-03	1.096260+01	1.142050+01	1.939690-02	9.881840+00	1.444280-02	0.0	2.498810-13	1.868490-02
3	3.304600+01	0.0	2.431670+01	5.816270+01	0.0	5.737000+01	6.247120-03	0.0	0.0	2.590370-02
4	1.009420+00	0.0	8.693870+00	9.703296+00	0.0	9.678020+00	7.409000-02	0.0	0.0	6.808450-02
5	1.595860+00	0.0	6.993920+00	8.589760+00	0.0	8.513030+00	0.0	0.0	0.0	0.0

NUCLIDE-U-238S

GRP	ABSORPTION	FISSION	SCATTERING	TOTAL	MU-FISSION	TRANSPORT	REMOVAL	M-2-H	KAPPA FISSION	IRT
1	4.200540-01	3.618830-01	6.906630+00	7.336650+00	1.009560+00	4.885450+00	1.386210+00	1.622170-02	1.172050-11	2.334560-02
2	2.508130-01	3.630860-04	1.083910+01	1.109710+01	8.797390-04	9.308930+00	1.462070-02	0.0	1.174680-14	1.831910-02
3	2.709240+01	7.885550-05	2.935190+01	5.644400+01	1.829150-04	5.548400+01	6.113870-03	0.0	2.592220-15	3.100470-02
4	5.085750-01	3.962820-08	8.454160+00	8.962740+00	9.191760-08	8.937260+00	7.144180-02	0.0	1.274000-18	6.565090-02
5	1.054500+00	0.0	8.157040+00	9.211540+00	0.0	9.181500+00	0.0	0.0	0.0	0.0

NUCLIDE-PU2394

GRP	ABSORPTION	FISSION	SCATTERING	TOTAL	MU-FISSION	TRANSPORT	REMOVAL	M-2-H	KAPPA FISSION	IRT
1	1.856570+00	1.644720+00	5.476710+00	7.333270+00	5.911010+00	5.024420+00	8.208710-01	3.380850-03	6.033600-11	1.843500-02
2	1.973340+00	1.624560+00	8.668290+00	1.064160+01	4.728450+00	9.004930+00	1.674980-02	0.0	5.356300-11	1.458900-02
3	4.182470+01	2.364020+01	1.313330+01	5.495800+01	6.792600+01	5.428220+01	6.867420-03	0.0	8.003570-10	1.581490-02

4 5.29993+01 3.81680+01 9.35615+00 6.20540+01 1.09673+02 5.31947+01 8.04170+02 0.0 1.25383+09 7.38986+02  
 5 1.11116+03 6.85838+02 7.68756+00 1.11885+03 1.97062+03 5.48375+02 0.0 2.28994+08 0.0

NUCLIDE-PU2403

GRP	ABSORPTION	FISSION	SCATTERING	TOTAL	MU-FISSION	TRANSPORT	REMOVAL	H-2-H	KAPPA FISSIION	IRT
1	1.65383+00	1.59299+00	5.54644+00	7.20027+00	5.11122+00	4.93437+00	7.64841+01	1.36786+03	1.55230+11	1.85920+02
2	6.53860+01	2.63180+01	1.02412+01	1.03951+01	7.76000+01	9.01883+00	1.43172+02	0.0	8.59116+12	1.71646+02
3	1.81932+01	2.12870+01	2.51471+01	4.33483+01	6.18918+01	4.32402+01	2.02158+02	0.0	7.13235+12	2.63421+02
4	6.44095+03	1.22928+00	3.08180+01	6.47176+03	3.52779+03	3.66291+02	2.56259+01	0.0	5.99515+11	2.37326+01
5	1.46039+02	2.87572+02	2.47917+01	1.70331+02	8.24414+02	1.61678+02	0.0	0.0	9.49133+13	0.0

NUCLIDE-PU2415

GRP	ABSORPTION	FISSION	SCATTERING	TOTAL	MU-FISSION	TRANSPORT	REMOVAL	H-2-H	KAPPA FISSIION	IRT
1	1.74606+00	1.65453+00	5.87206+00	7.61820+00	5.39472+00	4.91848+00	8.47174+01	2.27282+02	5.50047+11	1.94025+02
2	4.95655+00	2.10124+00	9.51359+00	1.19701+01	6.22371+00	9.54814+00	1.20152+02	0.0	7.04178+11	1.58794+02
3	6.64829+01	5.43546+01	1.25480+01	7.90237+01	1.59385+02	7.77967+01	6.08190+03	0.0	1.87080+09	1.30826+02
4	3.58334+01	3.02866+01	9.48849+00	4.53280+01	9.05666+01	4.39718+01	7.91878+02	0.0	1.03138+09	7.27691+02
5	6.77930+02	4.91974+02	7.63330+00	6.85563+02	1.44261+03	2.84662+02	0.0	0.0	1.66994+08	0.0

NUCLIDE-PU2429

GRP	ABSORPTION	FISSION	SCATTERING	TOTAL	MU-FISSION	TRANSPORT	REMOVAL	H-2-H	KAPPA FISSIION	IRT
1	1.51040+00	1.47167+00	5.65110+00	7.16150+00	4.64990+00	4.65981+00	6.59170+01	5.69090+03	4.75972+11	1.87739+02
2	4.17090+01	1.68898+01	1.07620+01	1.11790+01	4.87976+01	9.13559+00	1.72980+02	0.0	5.50820+12	1.76750+02
3	9.29787+01	0.0	3.35743+01	1.26530+02	0.0	1.21510+02	2.98939+03	0.0	0.0	3.48553+02
4	9.22350+00	0.0	4.45916+00	1.36828+01	0.0	1.28478+01	3.70349+02	0.0	0.0	3.40326+02
5	6.45577+00	0.0	3.58717+00	1.00429+01	0.0	9.94358+00	0.0	0.0	0.0	0.0

NUCLIDE-F.P. EPI

GRP	ABSORPTION	FISSION	SCATTERING	TOTAL	MU-FISSION	TRANSPORT	REMOVAL	H-2-H	KAPPA FISSIION	IRT
1	0.0	0.0	0.0	0.0	0.0	0.0	0.0	0.0	0.0	0.0
2	0.0	0.0	0.0	0.0	0.0	0.0	0.0	0.0	0.0	0.0
3	1.00000+00	0.0	0.0	1.00167+00	0.0	1.00167+00	0.0	0.0	0.0	0.0
4	9.78977+01	0.0	0.0	9.78977+01	0.0	9.78977+01	0.0	0.0	0.0	0.0
5	0.0	0.0	0.0	0.0	0.0	0.0	0.0	0.0	0.0	0.0

NUCLIDE-F.P. THE

GRP	ABSORPTION	FISSION	SCATTERING	TOTAL	MU-FISSION	TRANSPORT	REMOVAL	H-2-H	KAPPA FISSIION	IRT
1	0.0	0.0	0.0	0.0	0.0	0.0	0.0	0.0	0.0	0.0
2	0.0	0.0	0.0	0.0	0.0	0.0	0.0	0.0	0.0	0.0
3	0.0	0.0	0.0	0.0	0.0	0.0	0.0	0.0	0.0	0.0
4	0.0	0.0	0.0	0.0	0.0	0.0	0.0	0.0	0.0	0.0
5	2.99233+01	0.0	0.0	2.99233+01	0.0	2.75718+01	0.0	0.0	0.0	0.0

MACROSCOPIC EDIT

GRP	ABSORPTION	FISSION	SCATTERING	TOTAL	MU-FISSION	TRANSPORT	REMOVAL	N-2-M	KAPPA FISSIOM	IRT
1	1.552040-03	1.284620-03	2.485130-01	2.500660-01	3.486520-03	1.832490-01	7.164090-02	1.022880-05	4.101830-14	7.241420-02
2	2.622480-03	1.682950-03	6.095960-01	6.119730-01	4.114370-03	3.328400-01	7.397100-02	0.0	5.408220-14	7.517570-02
3	4.501670-02	2.888560-02	9.004770-01	9.454940-01	5.051880-02	4.525830-01	6.518170-02	0.0	6.867840-13	8.572920-02
4	6.451330-02	4.697110-02	5.049840-01	5.694970-01	1.134140-01	5.592740-01	5.810390-01	0.0	1.506740-12	6.127300-01
5	3.696650-01	2.015660-01	9.293240-01	1.298990+00	4.875470-01	1.100910+00	0.0	0.0	6.548910-12	0.0

GRP	DIF. COEFF	CHI	FLOX	CURRENT	BUCKLING
1	1.819820+00	7.304590-01	1.778950+14	1.969420+13	5.355660-03
2	1.001360+00	2.611570-01	1.450340+14	1.062840+13	5.355660-03
3	7.365120-01	1.775350-04	9.640630+13	5.888470+12	5.355660-03
4	5.960170-01	0.0	9.485340+12	4.137270+11	5.355660-03
5	3.027780-01	0.0	1.484400+13	3.289130+11	5.355660-03

K-EFF. = 1.06440  
 K-INF. = 1.29359

M9D

ABSORPTION	MU-FISSION	DIFFUSION CONST	KAPPA FISSIOM	AVG. CELL VELOCITY
8.9301700-01	1.1777910+00	1.4745910-01	1.5820520-11	2.4157490+00

SPECTRAL REDUCTION FACTOR = 8.055940-01

FRACTIONAL NEUTRON BALANCE

SUMMARY TABLE  
(NORMALIZED TO ONE NEUTRON LOSS)

NUCLIDE	DENSITY(KG/L)	ABSORPTIONS	FISSIONS	PRODUCTIONS	FRACTIONAL POWER
4040 ZIRCA	2.732180+00	2.218670-02	0.0	2.520640-05	0.0
10010 HYDROGEN	5.697900-02	8.964410-03	0.0	0.0	0.0
50100 BORON-10	0.0	1.705360-17	0.0	0.0	0.0
80160 OXYGEN-1	5.191200-01	1.406480-03	0.0	0.0	0.0
541350 XE135A	0.0	4.574360-16	0.0	1.362670-22	0.0
621490 SM149A	0.0	1.553700-17	0.0	0.0	0.0
641550 G0-155	1.010630-02	6.312730-02	0.0	0.0	0.0
641570 G0-157	1.082520-02	1.457890-01	0.0	0.0	0.0
92235A U-235S	4.022720-01	5.748720-01	4.383260-01	1.064200+00	9.997950-01
922361 U-236S	0.0	1.707050-19	4.303200-21	1.181920-20	9.533600-21
92238A U-238S	1.116270-02	5.688890-03	9.114440-05	2.623790-04	2.050380-04
94239A PU239A	0.0	1.077160-18	6.643840-19	1.913070-18	1.556150-18
942402 PU240S	0.0	3.278100-18	1.207720-20	4.060610-20	2.954630-20
942411 PU241S	0.0	8.661450-19	6.643750-19	1.952090-18	1.586930-18
942421 PU242S	0.0	4.620890-19	9.952490-21	3.115610-20	2.257330-20
999998 F.P. EPI	0.0	5.207780-21	0.0	0.0	0.0
999999 F.P. THE	0.0	2.230970-22	0.0	0.0	0.0
		TOTAL	TOTAL	TOTAL	TOTAL
		8.220350-01	4.384170-01	1.064490+00	4.539580-11

INFINITE MULTIPLICATION FACTOR = 1.294940+00  
 EFFECTIVE MULTIPLICATION FACTOR = 1.064490+00  
 NET FRACTIONAL LEAKAGE = 1.779650-01  
 INSTANTANEOUS CONVERSION RATIO = 9.737380-03  
 CUMULATIVE CONVERSION RATIO = 9.737380-03  
 ENRICHMENT ( KG FISSIONABLE / KG HEAVY METAL LOADED ) = 9.730000-01  
 CURRENT HEAVY METAL INVENTORY (KG/L) = 4.134350-01

TIME FOR MICROSCOPIC AND MACROSCOPIC X-SECTION CALCULATION

\*\*\*\*\*CPU EXECUTION TIME= 3.12570+00 SEC.

\*\*\*\*\*PERIPHERAL PROCESSOR TIME= 0.0 SEC.

3 2 1.00000-20

DATA FOR ISOTXS DATA SET

MAXIMUM ENERGY BOUNDARY  
 1.00000E+07 8.20850E+05 5.53084E+03 1.85539E+00 6.24933E-01 2.53000E-04

DATA FOR FAST GROUPS

GROUP	FLUX	CURRENT	CHI
1	1.178950+14	1.569420+13	7.38659E-01
2	1.450340+14	1.062840+13	2.61157E-01
3	9.440630+13	5.088470+12	1.77535E-04

DATA FOR FIVE GROUP SET

GROUP	FLUX	CURRENT	CHI
1	1.178950+14	1.569420+13	7.38659E-01
2	1.450340+14	1.062840+13	2.61157E-01
3	9.440630+13	5.088470+12	1.77535E-04
4	9.485340+12	4.137270+11	0.0
5	1.484400+13	3.289130+11	0.0

THERMAL BROAD GROUP FLUX  
 GROUP FLUX

4	9.483340+12
5	1.484400+13

247

NUCLIDE	4040	ZIRCA					
	ABSORPTION	FISSION	NU-FISSION	TOTAL	SCATTERING	TRANSPORT	N,ZN
1	0.0	0.0	0.0	4.975745E+00	4.975474E+00	4.454416E+00	7.845642E-05
2	1.065566E-03	0.0	0.0	8.064700E+00	8.063615E+00	7.779364E+00	0.0
3	1.538141E-01	0.0	0.0	6.890603E+00	6.725227E+00	6.855721E+00	0.0
4	4.169944E-02	0.0	0.0	6.356193E+00	6.314487E+00	6.309714E+00	0.0
5	8.137912E-02	0.0	0.0	6.141153E+00	6.059780E+00	6.093845E+00	0.0

NUCLIDE	10010	HYDROGEN					
	ABSORPTION	FISSION	NU-FISSION	TOTAL	SCATTERING	TRANSPORT	N,ZN
1	3.487447E-05	0.0	0.0	3.042158E+00	3.041825E+00	1.706779E+00	0.0
2	1.458372E-04	0.0	0.0	1.109184E+01	1.109024E+01	3.291684E+00	0.0
3	7.702313E-03	0.0	0.0	2.034303E+01	1.845004E+01	5.992243E+00	0.0
4	3.191391E-02	0.0	0.0	2.990492E+00	8.938573E+00	8.898370E+00	0.0
5	1.510102E-01	0.0	0.0	2.158721E+01	2.143634E+01	1.750105E+01	0.0

NUCLIDE	50100	BORON-10					
	ABSORPTION	FISSION	NU-FISSION	TOTAL	SCATTERING	TRANSPORT	N,ZN

1	2.922734E-01	0.0	0.0	2.107843E+00	1.815559E+00	1.759506E+00	0.0
2	2.089967E+00	0.0	0.0	5.080335E+00	2.990339E+00	4.688978E+00	0.0
3	8.569577E+01	0.0	0.0	9.075388E+01	2.064565E+00	8.882571E+01	0.0
4	5.973057E+02	0.0	0.0	5.993293E+02	2.024877E+00	5.841589E+02	0.0
5	1.673638E+03	0.0	0.0	1.675780E+03	2.131626E+00	1.340166E+03	0.0

NUCLIDE	80160	OXYGEN-1					
	ABSORPTION	FISSION	NU-FISSION	TOTAL	SCATTERING	TRANSPORT	N,ZH
1	8.964896E-03	0.0	0.0	2.484367E+00	2.476286E+00	2.016669E+00	0.0
2	0.0	0.0	0.0	3.907743E+00	3.907716E+00	3.578650E+00	0.0
3	6.170098E-06	0.0	0.0	3.688807E+00	3.650174E+00	3.540458E+00	0.0
4	2.815739E-05	0.0	0.0	3.800448E+00	3.800428E+00	3.640844E+00	0.0
5	7.940455E-05	0.0	0.0	3.995543E+00	3.995465E+00	3.819239E+00	0.0

NUCLIDE	541350	XE1354					
	ABSORPTION	FISSION	NU-FISSION	TOTAL	SCATTERING	TRANSPORT	N,ZH
1	5.636287E-04	0.0	0.0	5.939711E+00	5.938928E+00	3.343795E+00	0.0
2	3.183687E-03	0.0	0.0	6.334201E+00	6.339994E+00	4.856222E+00	0.0
3	2.107887E+01	0.0	0.0	6.469113E+01	4.273799E+01	6.290012E+01	0.0
4	3.411228E+03	0.0	0.0	5.842855E+03	2.431511E+03	3.469179E+03	0.0
5	6.112501E+05	0.0	0.0	7.363422E+05	1.250896E+05	8.868975E+04	0.0

NUCLIDE	621490	SM1494					
	ABSORPTION	FISSION	NU-FISSION	TOTAL	SCATTERING	TRANSPORT	N,ZH
1	5.423860E-02	0.0	0.0	6.762609E+00	6.708177E+00	4.311028E+00	1.150249E-02
2	9.262826E-07	0.0	0.0	9.974479E+00	9.048049E+00	9.372883E+00	0.0
3	9.762362E+01	0.0	0.0	1.597538E+02	6.271718E+01	1.577917E+02	0.0
4	1.889148E+03	0.0	0.0	1.923790E+03	3.464429E+01	1.604032E+02	0.0
5	1.900563E+04	0.0	0.0	1.916533E+04	1.598114E+02	1.748874E+03	0.0

NUCLIDE	641550	GD-155					
	ABSORPTION	FISSION	NU-FISSION	TOTAL	SCATTERING	TRANSPORT	N,ZH
1	2.228682E-01	0.0	0.0	6.744245E+00	6.521081E+00	4.450369E+00	0.0
2	1.784242E+00	0.0	0.0	1.024194E+01	8.457505E+00	8.392955E+00	0.0
3	1.504234E+02	0.0	0.0	1.423959E+02	1.197219E+01	1.378723E+02	0.0
4	3.146393E+01	0.0	0.0	3.146393E+01	0.0	1.764722E+01	0.0
5	5.646084E+02	0.0	0.0	5.646084E+02	0.0	3.942510E+02	0.0

NUCLIDE	641570	GD-157					
	ABSORPTION	FISSION	NU-FISSION	TOTAL	SCATTERING	TRANSPORT	N,ZH

NUCLIDE	922354	U-2359	FISSION	MU-FISSION	TOTAL	SCATTERING	TRANSPORT	N,ZH
1	7.501813E-01	0.0	0.0	0.0	7.269103E+00	6.518631E+00	4.961655E+00	0.0
2	3.948697E+00	0.0	0.0	0.0	1.226752E+01	8.518611E+00	1.027695E+01	0.0
3	6.683078E+01	0.0	0.0	0.0	9.992046E+01	1.508404E+01	9.866374E+01	0.0
4	1.303907E+02	0.0	0.0	0.0	1.303907E+02	0.0	7.283646E+01	0.0
5	2.463168E+03	0.0	0.0	0.0	2.463168E+03	6.0	1.501792E+03	0.0

NUCLIDE	922361	U-2369	FISSION	MU-FISSION	TOTAL	SCATTERING	TRANSPORT	N,ZH
1	1.101358E+00	1.236396E+00	3.354881E+00	3.354881E+00	7.189999E+00	5.888403E+00	4.718434E+00	8.106329E-03
2	2.092538E+00	1.632753E+00	3.991638E+00	1.091347E+01	1.091347E+01	8.820953E+00	9.246446E+00	0.0
3	3.159320E+01	2.026274E+01	4.901222E+01	4.376949E+01	4.376949E+01	1.216363E+01	4.329478E+01	0.0
4	5.367374E+01	4.556876E+01	1.102220E+02	6.552771E+01	6.552771E+01	1.185463E+01	5.262810E+01	0.0
5	2.315933E+02	1.955521E+02	4.729868E+02	2.428315E+02	2.428315E+02	1.143624E+01	1.875132E+02	0.0

NUCLIDE	922384	U-2389	FISSION	MU-FISSION	TOTAL	SCATTERING	TRANSPORT	N,ZH
1	8.712566E-01	7.168064E-01	1.955640E+00	1.955640E+00	7.584249E+00	6.682793E+00	5.072564E+00	7.900055E-03
2	4.579128E-01	7.844300E-03	1.939690E-02	1.939690E-02	1.142049E+01	1.096256E+01	9.881828E+00	0.0
3	3.354592E+01	0.0	0.0	0.0	5.816245E+01	2.431036E+01	5.734904E+01	0.0
4	1.009398E+00	0.0	0.0	0.0	9.702876E+00	8.693457E+00	9.678026E+00	0.0
5	1.595837E+00	0.0	0.0	0.0	8.589522E+00	6.993679E+00	8.513052E+00	0.0

NUCLIDE	922394	PU2394	FISSION	MU-FISSION	TOTAL	SCATTERING	TRANSPORT	N,ZH
1	4.240936E-01	3.618521E-01	1.009558E+00	1.009558E+00	7.330680E+00	6.906349E+00	4.805934E+00	1.622087E-02
2	2.500126E-01	3.638859E-04	8.797338E-04	8.797338E-04	1.109706E+01	1.083895E+01	9.308914E+00	0.0
3	2.709241E+01	7.835494E-05	1.829144E-04	5.644417E+01	2.934572E+01	2.934572E+01	5.548390E+01	0.0
4	5.085632E-01	3.962761E-08	9.191666E-08	8.962522E+00	8.962522E+00	8.453961E+00	8.937264E+00	0.0
5	1.054480E+00	0.0	0.0	9.211272E+00	9.211272E+00	8.156778E+00	9.181513E+00	0.0

NUCLIDE	942394	PU2409	FISSION	MU-FISSION	TOTAL	SCATTERING	TRANSPORT	N,ZH
1	1.856567E+00	1.644716E+00	5.911003E+00	5.911003E+00	7.332666E+00	5.476454E+00	5.024418E+00	3.350827E-03
2	1.973336E+00	1.624360E+00	4.728443E+00	1.044162E+01	1.044162E+01	8.668097E+00	9.004920E+00	0.0
3	4.162463E+01	2.364020E+01	6.792575E+01	5.495704E+01	5.495704E+01	1.312639E+01	5.428218E+01	0.0
4	5.249789E+01	3.018931E+01	1.896665E+02	6.205335E+01	6.205335E+01	9.555768E+00	5.319478E+01	0.0
5	1.111117E+03	6.858079E+02	1.970565E+03	1.118806E+03	1.118806E+03	7.687310E+00	5.483755E+02	0.0

NUCLIDE	942402	PU2409	FISSION	MU-FISSION	TOTAL	SCATTERING	TRANSPORT	N,ZH
1	1.856567E+00	1.644716E+00	5.911003E+00	5.911003E+00	7.332666E+00	5.476454E+00	5.024418E+00	3.350827E-03
2	1.973336E+00	1.624360E+00	4.728443E+00	1.044162E+01	1.044162E+01	8.668097E+00	9.004920E+00	0.0
3	4.162463E+01	2.364020E+01	6.792575E+01	5.495704E+01	5.495704E+01	1.312639E+01	5.428218E+01	0.0
4	5.249789E+01	3.018931E+01	1.896665E+02	6.205335E+01	6.205335E+01	9.555768E+00	5.319478E+01	0.0
5	1.111117E+03	6.858079E+02	1.970565E+03	1.118806E+03	1.118806E+03	7.687310E+00	5.483755E+02	0.0

NUCLIDE	942411	FU2419	FISSION	MU-FISSION	TOTAL	SCATTERING	TRANSPORT	N,ZH
1	1.63832E+00	1.592993E+00	5.111212E+00	7.290263E+00	5.546205E+00	4.934373E+00	1.367854E-03	0.0
2	6.539450E-01	2.631868E-01	7.760066E-01	1.039504E+01	1.024110E+01	9.018314E+00	0.0	0.0
3	1.819315E+01	2.128484E-02	6.109162E-01	4.334026E+01	2.512482E+01	4.324019E+01	0.0	0.0
4	0.440844E+03	1.229259E+00	3.527590E+00	6.471660E+03	3.081753E+01	3.062910E+02	0.0	0.0
5	1.466546E+02	2.872626E-02	8.244020E-02	1.708261E+02	2.479141E+01	1.616778E+02	0.0	0.0

NUCLIDE	942421	FU2423	FISSION	MU-FISSION	TOTAL	SCATTERING	TRANSPORT	N,ZH
1	1.746062E+00	1.654544E+00	5.394718E+00	7.618115E+00	5.871815E+00	4.918678E+00	2.272792E-02	0.0
2	2.456546E+00	2.101233E+00	6.223689E+00	1.197813E+01	9.513423E+00	9.548129E+00	0.0	0.0
3	6.648276E+01	5.435446E+01	1.593844E+02	7.982345E+01	1.253459E+01	7.779645E+01	0.0	0.0
4	3.583289E+01	3.088618E+01	9.836288E+01	4.532138E+01	9.488069E+00	4.397189E+01	0.0	0.0
5	6.778370E+02	4.919639E+02	1.442550E+03	6.855188E+02	7.632773E+00	2.846621E+02	0.0	0.0

NUCLIDE	942421	FU2423	FISSION	MU-FISSION	TOTAL	SCATTERING	TRANSPORT	N,ZH
1	1.510457E+00	1.471666E+00	4.645576E+00	7.161549E+00	5.650849E+00	4.655806E+00	5.890973E-03	0.0
2	4.170580E-01	1.688967E-01	4.879752E-01	1.117980E+01	1.076268E+01	9.135578E+00	0.0	0.0
3	9.297867E+01	0.0	0.0	1.265530E+02	3.357129E+01	1.215104E+02	0.0	0.0
4	9.223278E+00	0.0	0.0	1.368234E+01	4.459041E+00	1.284783E+01	0.0	0.0
5	6.455503E+00	0.0	0.0	1.004265E+01	3.587018E+00	9.943600E+00	0.0	0.0

NUCLIDE	999998	F.P. EPI	FISSION	MU-FISSION	TOTAL	SCATTERING	TRANSPORT	N,ZH
1	0.0	0.0	0.0	0.0	0.0	0.0	0.0	0.0
2	0.0	0.0	0.0	0.0	0.0	0.0	0.0	0.0
3	1.650000E+01	0.0	0.0	1.450000E+01	0.0	1.450000E+01	0.0	0.0
4	1.425000E+01	0.0	0.0	1.425000E+01	0.0	1.425000E+01	0.0	0.0
5	0.0	0.0	0.0	0.0	0.0	0.0	0.0	0.0

NUCLIDE	999999	F.P. THE	FISSION	MU-FISSION	TOTAL	SCATTERING	TRANSPORT	N,ZH
1	0.0	0.0	0.0	0.0	0.0	0.0	0.0	0.0
2	0.0	0.0	0.0	0.0	0.0	0.0	0.0	0.0
3	0.0	0.0	0.0	0.0	0.0	0.0	0.0	0.0
4	0.0	0.0	0.0	0.0	0.0	0.0	0.0	0.0
5	5.000000E+01	0.0	0.0	5.000000E+01	6.0	5.000000E+01	0.0	0.0

## **Appendix F**

### **Tabular Summary of Calculated Results**

This appendix summarizes in detail all calculated results for this study. Table F.1 summarizes the design results for reactor cores 1, 2 and 3. Table F.2 summarizes the design results for reactor cores 4 and 5. In these tables, isotopic number densities in the fuel for the uranium and plutonium nuclides at B.O.C. and E.O.C. are listed.

**Table F.1. Summary of calculated results (thick plate design).**

	LEU		HEU
	7%	20%	97.3%
Initial Fuel enrichment	7%	20%	97.3%
Fuel type	Caramel	Caramel	(UO <sub>2</sub> /Zr Cermet)
Full power days at 50 MWth	600	1,200	1,200
Fuel volume percent in core	25.55%	21.29%	21.29%
UO <sub>2</sub> volume percent in fuel	84.44%	70.0%	20.0%
UO <sub>2</sub> loading in core(g/cm <sup>3</sup> )	2.095	1.449	0.413
Gd <sub>2</sub> O <sub>3</sub> distribution	Uniform	(Lumped every 7th plate)	
Gd <sub>2</sub> O <sub>3</sub> in the fuel (wt%)	0.101	0	0
Gd <sub>2</sub> O <sub>3</sub> volume percent in core	0.136	0.770	1.793
Lump thickness(cm)	0	0.0245	0.0665
<b><u>Core Size</u></b>			
Diameter (m)	0.81	0.88	0.65
Height (m)	0.98	1.08	0.79
Volume (liters)	506.1	666.7	264.6
Buckling (cm <sup>-3</sup> )	3.4754x10 <sup>-3</sup>	2.8921x10 <sup>-3</sup>	5.3557x10 <sup>-3</sup>
q''' <sub>avg</sub> (kw/liter)	99	75	189
q''' <sub>max</sub> (kw/liter)	240	182	535
Burnup (MWD/T)	28290	62120	548570
Burnup (at%)	3.0	6.6	57.9
<b><u>Beginning of Core Life (BOC)</u></b>			
U-235 number density (a/cm <sup>3</sup> )*	1.4430x10 <sup>21</sup>	3.2563x10 <sup>21</sup>	4.5210x10 <sup>21</sup>
U-235 content (kg)	74.2	193.3	106.4
U-238 number density (a/cm <sup>3</sup> )*	1.8020x10 <sup>22</sup>	1.2861x10 <sup>22</sup>	1.2387x10 <sup>20</sup>
U-238 content (kg)	1049	783	3.0
Pu <sup>total</sup> content (kg)	0	0	0
Δk <sub>fuel temp</sub> (T <sub>fuel</sub> 293°K - 1000°K)	-0.027	-0.019	-0.0025
Δk <sub>void</sub> (ρ(water) decrease 10%)	-0.027	-0.021	-0.030

### End of Core Life (EOL)

Final Fuel Enrichment	4.3	13.9	68.1
U-235 number density (a/cm <sup>3</sup> )*	8.9016x10 <sup>20</sup>	2.0931x10 <sup>21</sup>	1.4282x10 <sup>21</sup>
U-235 content (kg)	43.7	124.2	33.6
U-236 number density (a/cm <sup>3</sup> )*	1.0482x10 <sup>20</sup>	2.3891x10 <sup>20</sup>	5.9040x10 <sup>20</sup>
U-236 content (kg)	5.7	14.2	14.0
U-238 number density (a/cm <sup>3</sup> )*	1.7752x10 <sup>22</sup>	1.2554x10 <sup>22</sup>	9.1914x10 <sup>19</sup>
U-238 content (kg)	972	754	1.75
Pu-239 number density (a/cm <sup>3</sup> )*	1.2042x10 <sup>20</sup>	1.4453x10 <sup>20</sup>	5.6331x10 <sup>18</sup>
Pu-240 number density (a/cm <sup>3</sup> )*	2.4873x10 <sup>19</sup>	2.5580x10 <sup>19</sup>	1.5063x10 <sup>18</sup>
Pu-241 number density (a/cm <sup>3</sup> )*	1.4070x10 <sup>19</sup>	1.7663x10 <sup>19</sup>	2.6001x10 <sup>18</sup>
Pu-242 number density (a/cm <sup>3</sup> )*	1.6359x10 <sup>18</sup>	1.7679x10 <sup>18</sup>	9.9400x10 <sup>17</sup>
Pu-239 content (kg)	6.62	8.72	0.135
Pu-240 content (kg)	1.37	1.55	0.036
Pu-241 content (kg)	0.78	1.08	0.063
Pu-242 content (kg)	0.09	0.18	0.024
Pu <sup>total</sup> content (kg)	8.86	11.45	0.262
$\Delta k_{\text{fuel temp}} (T_{\text{fuel}} 293^{\circ}\text{K} - 1000^{\circ}\text{K})$	-0.026	-0.022	-0.007
$\Delta k_{\text{void}} (\rho(\text{water}) \text{ decrease } 10\%)$	-0.038	-0.028	-0.030

\* - The isotopic number densities listed are for the fuel meat and are not averaged over the core.

**Table F.2. Summary of calculated results (ATR type, thin plate design).**

	HEU (Regular Channel)	HEU (Thin Channel)
Fuel enrichment	97.3%	97.3%
Fuel type	(UO <sub>2</sub> /Zr Cermet)	(UO <sub>2</sub> /Zr Cermet)
Full power days at 50 MWth	1,200	1,200
Fuel volume percent in core	14.34%	15.72%
UO <sub>2</sub> volume percent in fuel	35.0%	33.0%
UO <sub>2</sub> loading in core(g/cm <sup>3</sup> )	0.464	0.470
Gd <sub>2</sub> O <sub>3</sub> distribution	(Lumped every 7th plate)	
Gd <sub>2</sub> O <sub>3</sub> in the fuel (wt%)	0	0
Gd <sub>2</sub> O <sub>3</sub> volume percent in core	2.24	1.34
Lump thickness(cm)	0.03910	0.0285
<u>Core Size</u>		
Diameter (m)	0.74	0.70
Height (m)	0.90	0.86
Volume (liters)	384.6	333.3
Buckling (cm <sup>-3</sup> )	4.1732x10 <sup>-3</sup>	4.5909x10 <sup>-3</sup>
q''' <sub>avg</sub> (kw/liter)	131	150
q''' <sub>max</sub> (kw/liter)	368	425
Burnup (MWD/T)	336160	382700
Burnup (at%)	35.5	40.4
<u>Beginning of Core Life (BOC)</u>		
U-235 number density (a/cm <sup>3</sup> )*	8.0704x10 <sup>21</sup>	7.4598x10 <sup>21</sup>
U-235 content (kg)	173.7	152.5
U-238 number density (a/cm <sup>3</sup> )*	—	2.0438x10 <sup>20</sup>
U-238 content (kg)	4.9	4.3
Pu <sup>total</sup> content (kg)	0	0
$\Delta k_{\text{fuel temp}}$ (T <sub>fuel</sub> 293°K - 1000°K)	-0.00053	-0.00065
$\Delta k_{\text{void}}$ ( $\rho$ (water) decrease 10%)	-0.017	-0.018

### End of Core Life (EOC)

Final Fuel Enrichment	—	81.8
U-235 number density (a/cm <sup>3</sup> )*	4.4455x10 <sup>21</sup>	3.6650x10 <sup>21</sup>
U-235 content (kg)	95.66	74.9
U-236 number density (a/cm <sup>3</sup> )*	—	8.1154x10 <sup>20</sup>
U-236 content (kg)	—	16.7
U-238 number density (a/cm <sup>3</sup> )*	—	1.6026x10 <sup>20</sup>
U-238 content (kg)	—	3.3
Pu-239 number density (a/cm <sup>3</sup> )*	1.5055x10 <sup>19</sup>	1.4138x10 <sup>19</sup>
Pu-240 number density (a/cm <sup>3</sup> )*	2.7132x10 <sup>18</sup>	2.6677x10 <sup>18</sup>
Pu-241 number density (a/cm <sup>3</sup> )*	3.8509x10 <sup>17</sup>	4.3772x10 <sup>18</sup>
Pu-242 number density (a/cm <sup>3</sup> )*	5.4273x10 <sup>18</sup>	7.5292x10 <sup>17</sup>
Pu-239 content (kg)	0.330	0.294
Pu-240 content (kg)	0.012	0.056
Pu-241 content (kg)	0.085	0.092
Pu-242 content (kg)	0.012	0.016
P <sub>U</sub> <sup>total</sup> content (kg)	0.437	0.457
$\Delta k_{\text{fuel temp}}$ (T <sub>fuel</sub> 293°K - 1000°K)	-0.0043	-0.0051
$\Delta k_{\text{void}}$ ( $\rho(\text{water})$ decrease 10%)	-0.025	-0.033

\* - The isotopic number densities listed are for the fuel meat and are not averaged over the core.

## **Appendix G**

### **Improved Reflector Savings Calculation Method**

As stated in Section 4.1.2.6, the method used to account for the reduction in critical mass due to reflection (i.e., dimensional reduction or reflector savings) is an approximation that is reasonable for small light water reactors. The reflector savings calculated by this method varies with core volume. In reality, reflector savings is constant as core volume changes. For water moderated and reflected systems, the following empirical formula may be used to obtain the reflector savings or extrapolation length.[7]

$$\delta = 7.2 + 0.10(M^2_T - 40) \quad (\text{G.1})$$

where

$\delta$  = Reflector savings (cm)

$M^2_T$  = Thermal neutron migration area in the core (cm<sup>2</sup>)

The thermal neutron migration area is defined as,

$$M^2_T = L^2_T + \tau_T \quad (\text{G.2})$$

where

$L^2_T$  = Thermal neutron diffusion area in the core (cm<sup>2</sup>)

$\tau$  = Neutron age (cm<sup>2</sup>)

For water,  $\tau$  is  $27\text{cm}^2$ . The thermal neutron diffusion area is defined as,

$$L^2_T = (1 - f)L^2_{TM} \quad (\text{G.3})$$

where

$L^2_{TM}$  = Thermal neutron diffusion area of the water moderator ( $\text{cm}^2$ )

$f$  = Thermal utilization

For water,  $L^2_{TM}$  is  $8.1\text{cm}^2$ . The thermal utilization is defined as,

$$f = \frac{Z}{Z + 1} \quad (\text{G.4})$$

The parameter,  $Z$ , is given by,

$$Z = \frac{N_F \bar{\sigma}_{aF}}{N_M \bar{\sigma}_{aM}} \quad (\text{G.5})$$

where the subscripts F and M refers to the fuel and moderator respectively.

As in earlier discussion,  $N$  and  $\sigma$  refer to atom number density and

microscopic neutron absorption cross-section respectively.